UNCLASSIFIED

AD NUMBER

ADB049493

NEW LIMITATION CHANGE

TO

Approved for public release, distribution unlimited

FROM

Distribution authorized to U.S. Gov't. agencies only; Test and Evaluation; Aug 1979. Other requests shall be referred to Air Force Flight Dynamic Laboraatory, Attn: FB, Wright-Patterson AFB, OH 45433.

AUTHORITY

AFWL ltr, 30 May 1985

THIS PAGE IS UNCLASSIFIED

AD B049492

AUTHORITY: AFWAL ltr, 30 May 85

AFFDL-TR-79-3111
VOLUME I

LEVEL II

STOL AIRCRAFT STRUCTURAL VIBRATION PREDICTION METHOD

VOLUME I
PREDICTION PROCEDURE AND AIRCRAFT PARAMETRIC STUDIES

AD B049493

Boeing Aerospace Company
Boeing Military Airplane Development
P.O. Box 3999, Seattle, Wa. 98124

AUGUST 1979

DTIC
ELECTE
AUG 7 1980
S D
A

FINAL REPORT FOR PERIOD AUGUST 1977 - AUGUST 1979

Distribution limited to U.S. Government agencies only; test and evaluation; statement applied in August 1979. Other requests for this document must be referred to AF Flight Dynamic Laboratory (FB), Wright-Patterson AFB, Ohio 45433

AIR FORCE FLIGHT DYNAMICS LABORATORY (AFFDL/FBG)
AIR FORCE SYSTEM COMMAND
WRIGHT PATTERSON AFB, OHIO 45433

80 8 4 030

NOTICE

When Government drawings, specifications, or other data are used for any purpose other than in connection with a definitely related Government procurement operation, the United States Government thereby incurs no responsibility nor any obligation whatsoever; and the fact that the government may have formulated, furnished, or in any way supplied the said drawings, specifications, or other data, is not to be regarded by implication or otherwise as in any manner licensing the holder or any other person or corporation, or conveying any rights or permission to manufacture, use, or sell any patented invention that may in any way be related thereto.

This technical report has been reviewed and is approved for publication.

Jerome Pearson
JEROME PEARSON
Project Engineer

Ralph N. Bingman
RALPH N. BINGMAN
Technical Manager

FOR THE COMMANDER:

Ralph L. Kuster
RALPH L. KUSTER, JR., Colonel, USAF
Chief, Structures and Dynamics Division

"If your address has changed, if you wish to be removed from our mailing list, or if the addressee is no longer employed by your organization please notify AFFDL/FB, W-P AFB, OH 45433 to help us maintain a current mailing list".

Copies of this report should not be returned unless return is required by security considerations, contractual obligations, or notice on a specific document.

AIR FORCE/56780/23 July 1980 — 180

UNCLASSIFIED

SECURITY CLASSIFICATION OF THIS PAGE (When Data Entered)

12 299

19 REPORT DOCUMENTATION PAGE

READ INSTRUCTIONS BEFORE COMPLETING FORM

1. REPORT NUMBER 18 AFFDL TR-79-3111 - VOL-1	2. GOVT ACCESSION NO. AD-B049493L
3. RECIPIENT'S CATALOG NUMBER	
4. TITLE (and Subtitle) Volume I 6 STOL Aircraft Structural Vibration Prediction Method. Volume I. Prediction Procedure and Aircraft Parametric Studies.	5. TYPE OF REPORT & PERIOD COVERED 9 FINAL REPORT. Aug 77 — Aug 79
	6. PERFORMING ORG. REPORT NUMBER
7. AUTHOR(s) 10 C. S. Doherty L. M. Butzel	8. CONTRACT OR GRANT NUMBER(s) 15 F33615-77-C-3035
9. PERFORMING ORGANIZATION NAME AND ADDRESS BOEING AEROSPACE COMPANY BOEING MILITARY AIRPLANE DEVELOPMENT P.O. BOX 3999, SEATTLE, WA 98124	10. PROGRAM ELEMENT, PROJECT, TASK AREA & WORK UNIT NUMBERS Project 2401 Task 240104 W. O. 24010407
11. CONTROLLING OFFICE NAME AND ADDRESS AIR FORCE FLIGHT DYNAMICS LABORATORY (AFFDL/FBG) AIR FORCE SYSTEMS COMMAND WRIGHT PATTERSON AFB, OHIO 45433	12. REPORT DATE 11 Augu[redacted]979 13. NUMBER OF PAGES 290
14. MONITORING AGENCY NAME & ADDRESS (if different from Controlling Office) 16 2401 17 04	15. SECURITY CLASS. (of this report) UNCLASSIFIED 15a. DECLASSIFICATION/DOWNGRADING SCHEDULE

16. DISTRIBUTION STATEMENT (of this Report)

Distribution limited to U.S. Government agencies only; test and evaluation; statement applied in AUG 79. Other requests for this document must be referred to AF Flight Dynamic Laboratory (FB) Wright-Patterson AFB, Ohio 45433

17. DISTRIBUTION STATEMENT (of the abstract entered in Block 20, if different from Report)

622017

18. SUPPLEMENTARY NOTES

This report consists of two volumes. Volume II contains the Appendices.

19. KEY WORDS (Continue on reverse side if necessary and identify by block number)

STRUCTURAL VIBRATION, UPPER SURFACE BLOWN FLAPS, SHORT TAKE OFF AND LANDING AIRCRAFT, VIBRATION AND ACOUSTIC PREDICTION TECHNIQUES

20. ABSTRACT (Continue on reverse side if necessary and identify by block number)

A structural vibration response prediction method was developed for STOL type aircraft. The method was developed to significantly improve environmental prediction methods that have been used in the past. A mathematically rigorous spectral analysis approach was developed that simulated the structure with a finite element model which used correlated and calculated acoustic input data for a forcing function.

DD FORM 1 JAN 73 1473 EDITION OF 1 NOV 65 IS OBSOLETE

UNCLASSIFIED

SECURITY CLASSIFICATION OF THIS PAGE (When Data Entered)

410258 Gm

The structural vibration predictions adequately described the operating levels and spectral frequency content of chosen locations on two STOL aircraft. Comparisons of predicted and measured data show that the method developed may be used for a precise way to predict complex structural response to jet engine excitation.

The development of prediction method for determination of external acoustic levels for STOL aircraft was accomplished in a concise manner. The method is described in detail with successful comparisons of actual measurements to predictions.

The method is seen to give good results and represents a significant improvement in acoustic prediction methods for STOL aircraft.

FOREWORD

This report was prepared by the Boeing Aerospace Company, Military Airplane Development Division, Seattle, Washington, for the Air Force Flight Dynamics Laboratory, Air Force Systems Command, Wright-Patterson Air Force Base, Ohio, under Contract F33615-77-C-3035. This research was conducted under Project 2401 and Task 240104, "Vibration Prediction and Control, Measurement and Analysis." Mr. Jerome Pearson (AFFDL/FBG) was project engineer.

This report entitled, "STOL Aircraft Structural Vibration Prediction Method," has been divided into two volumes, Volume I is entitled, "Prediction Procedure and Aircraft Parameteric Studies", and Volume II is entitled, "Acoustic Prediction Details and Additional Plots For Small STOL Aircraft."

The performance period for this project was August 1977 through August 1979.

Overall cognizance of the project including technical method development and application was carried out by the Structural Dynamics Group of the Boeing Military Airplane Division. Key personnel associated with this program were as follows:

B. F. Dotson	Program Manager
C. S. Doherty	Technical Leader
L. M. Butzel	Acoustics Staff
C. D. Larkins	Structural Dynamics Staff
S. J. Nanevicz	Structural Dynamics Staff

Acknowledgements are given to Mr. Leo Butzel as co-author of the report who largely was responsible for development of the ribbon external acoustic prediction method. Mr. C. D. Larkins helped in the early stages of the report with timely suggestions for interpolating and extrapolating the pressure data to each panel of the finite element structural math model. Mr. Stan Nanevicz did the lion's share of the finite element modeling analyses and performed the response calculations using the Random Harmonic Analysis Program, TEV156. Valuable aid and comments were received from both Mr. Hussein Nijim and Mr. Gautam Sen Gupta on methods to simulate fuselage structure for acoustic response predictions. Thanks are also due Diane Ellis for the considerable work of typing, and to Kristi Pepper for the graphics layout and assembly of the final document.

This report was submitted by the authors in August 1979 for publication as an AFFDL Technical Report.

TABLE OF CONTENTS

TABLE OF CONTENTS (Continued)

SUMMARY

Structural response predictions have been made for two important areas of a short-takeoff-and-landing (STOL) aircraft. The method was developed to significantly improve environmental predictions compared to those used in the past. A mathematically rigorous spectral analysis approach was developed that simulated the structure with a finite-element model which used correlated and calculated acoustic input data for the forcing function.

The structural vibration analyses were successful in predicting operating levels and describing the frequency content of responses at selected locations on the structure. Comparisons of predicted and measured data show that the method developed and described here may be used to predict complex structural response to jet engine excitation.

A method was also developed for the prediction of the external acoustic environment of STOL aircraft with upper-surface-blown (USB) flaps. The method is described in detail, and comparisons are given between predicted and actual measurements. The method gives good results and represents a significant improvement over previous acoustic prediction methods.

SECTION I
INTRODUCTION

1.1 Program Objectives

The first objective of the program was to use available data of the vibration and acoustic characteristics on Short Takeoff and Landing (STOL) aircraft to predict the resulting aircraft structural vibration levels.

A second objective was to develop a method of predicting the external acoustic levels for a STOL aircraft and to use these predictions as inputs to the structural vibration analysis program.

The two areas chosen for detailed study of both objectives were the wing/flap structure and the fuselage section adjacent to the wing root, upper surface.

Use of the methods developed will provide environmental vibration predictions in all areas of STOL type aircraft.

Additionally, parametric studies were made of STOL aircraft from 50,000 lb to 1,000,000 lbs for structural vibration prediction levels. These values were compared to the vibration criteria of MIL-STD 810 C.

1.2 Program Definition

Phase I of the STOL Program was divided into 10 tasks. These include:

Task 1	Program Definition
Task 2	Method Development - Flap Structures
Task 3	Apply YC-14 USB Flap Data
Task 4	Comparison to Flap Data Tests
Task 5	Discrepancies and Refinement of Flap Prediction
Task 6	Fuselage Structure Method Development
Task 7	Apply YC-14 Fuselage Data
Task 8	Comparison to Fuselage Data Tests

Task 9	Discrepancies and Refinement of Fuselage Predictions
Task 10	Acoustic Field Prediction Development

Phase II was divided into four tasks. These include:

Task 11	Parametric Studies of Vibration Response
Task 12	Noise Field Parametric Predictions
Task 13	Compare Predictions to Estimated Test Specs
Task 14	Report Preparation

PHASE I - DEVELOP PREDICTION METHOD

SECTION II

TECHNICAL ANALYSIS METHOD DEVELOPMENT

The technical analysis for Phase I consisted of three parts: 1) eigenvalue analysis of a finite element structural model, 2) definition of the acoustic environment, and 3) random harmonic analysis. The data flow for the analysis appears in Figure 1.

For the finite element models used in the analysis, two USB flap models and three fuselage models were developed. These are described in greater detail in Sections III and IV. Inputs to the finite element analysis included model geometry and degrees of freedom of an array of nodes; definition of a system of structural elements, fixity of each element, section properties, material properties and assumed structural damping values. The Structural Analysis Program, SAP IV, (Reference 1), written for the CDC 6600 computer, was used for the finite element model eigenvalue analysis. Outputs included modal frequencies and modal displacements at each node location. The acoustic environment used for the analysis in Phase I was based on available test data which consisted of power spectral density plots of sound pressure vs frequency at several microphone locations. A scheme was devised for interpolating and extrapolating the data to each panel. This interpolation scheme is discussed in Section III. The interpolation was accomplished through a simple computer program which generated output data in the complex matrix format required for subsequent analyses. Real and imaginary parts of each matrix element were generated, with one matrix being generated for each input frequency. The matrix size is equal to the number of panels. The diagonal elements (real) are values of power spectral density at each panel. The off-diagonal terms, representing cross-spectral density terms, were included in the first set of calculations for the USB flap response and compared to the results from calculations where the off-diagonal terms were set equal to zero. The results differed by only 10%, so subsequent computations were made using only the diagonal elements.

For the structural response analysis, it was necessary to know the modal displacements at the centroids of each panel. A simple computer program was written to interpolate the mode shapes from the finite element analysis. This interpolation consisted of simple arithmetic averaging of the modal displacement at each of the four corners of a panel.

The modal data and the acoustic environment data were input to the Random Harmonic Analysis Program (TEV 156, Reference 2). Also input were values of generalized stiffness, structural damping, modal displacements at output stations (corresponding to accelerometer locations for which test data are available), and a list of frequencies at which output data were desired. Details of the solution technique employed appear in Reference 2. Briefly, the program solves Equation 1 of Reference 2 which, when modified for this application is:

$$\left[M_1\right]\left\{q\right\} + \left[M_3\right]\left\{\ddot{q}\right\} + i2\,\zeta\left[M_1\right]\left\{q\right\} = \left[C_3\right]\left\{P\right\} \qquad (1)$$

where $[M_1]$ = Generalized stiffness matrix (size m x m)
$[M_3]$ = Generalized inertia matrix (size m x m)
$[C_3]$ = $[\phi]^T[A]$ = Forcing function matrix (size m x n)
$[\phi]$ = Matrix of modal dispalcements (size n x m)
$[A]$ = Matrix of panel areas (size n x n)
$\{q\}$ = Matrix of generalized coordinates (size m x 1)
$\{\ddot{q}\}$ = Matrix of generalized accelerations (size m x 1)
ζ = Structural damping coefficient

$\{p\}$ = matrix of panel pressures (size n x 1)
m = Number of modes
n = Number of panels

The load equations follow the same format as the equations of motion.

$$\left\{\ddot{Z}\right\} = \left[\bar{M}_3\right]\left\{\ddot{q}\right\} \qquad (2)$$

where $\{\ddot{Z}\}$ = Matrix of accelerations at output stations (size k x 1)
k = Number of output stations

$[\bar{M}_3]$ = $(1/g)\left[\phi_A\right]$ = Matrix of coefficients (size K x m)
g = Gravitational acceleration
$[\phi_A]$ = Matrix of modal displacements at output stations (size k x m)

The program performs Laplace transformations on Equations 1 and 2, resulting in,

$$\left[\left[M_1\right] (1+ 2i\zeta) + s^2\left[M_3\right] \right]\left\{\bar{q}\right\} = \left[C_3\right]\left\{L(P)\right\} \tag{3}$$

$$\left\{L(\ddot{Z})\right\} = s^2 \left[\bar{M}_3\right]\left\{\bar{q}\right\} \tag{4}$$

where: s = Laplace operator
$\left\{\bar{q}\right\}$ = Laplace transformed coordinate matrix
$\left\{L(P)\right\}$ = Laplace transform of panel pressures
$\left\{L(\ddot{Z})\right\}$ = Laplace transform of output accelerations

Generalized coordinate and load frequency response functions are obtained by solving Equations 3 and 4.

The program then employs the technique of generalized harmonic analysis, viz.,

$$\Phi_o(\omega) = \lfloor T \rfloor \left[CPSD\right] \left\{T\right\} \tag{5}$$

where: $\Phi_o(\omega)$ = Output power spectrum at a specific station at frequency
$\lfloor T \rfloor$ = Row matrix of output frequency response to a sinusoidal force of frequency ω acting at the i^{th} excitation point (size 1 x n)
$\left\{T\right\}$ = Transpose of T
$\left[CPSD\right]$ = Matrix of cross-power spectral densities at frequency ω (size n x n)

Equation (5) is solved for each frequency of interest and for each output station. The root-mean-square response is obtained by the expression:

$$\bar{A} = \left[\int_0^\infty \Phi_o(\omega)\, d\omega\right]^{1/2}$$

SECTION III

FLAP STRUCTURE VIBRATION PREDICTION

This section of the study is limited to the YC-14 aircraft USB flap structure, since significant amounts of ground and flight test data were available for comparisons.

Both vibration and acoustic data were obtained from ground and flight tests. These data were recorded simultaneously for several conditions to enable correlation studies to be made of the acoustic input and the structural response. The flap area received the highest input energy on the aircraft and thus determination of the structural response in this area was of paramount interest.

3.1 USB Flap Model Development

The first Upper Surface Blowing (USB) flap model was considered as two separate panels (plates); the main USB flap and the aft USB flap.

To solve the frequency determination of plates, an approximate solution, using the Rayleigh principle, was used with the Warburton Method (Reference 3) where the coefficients in the frequency equation were given for several different boundary conditions.

Calculations were made for a plate simulating the YC-14 main USB flap. The initial boundary condition used was condition 15 on page 375 of Reference 3 where the forward edge was assumed to be fixed.

The comparison of calculated and experimental frequencies indicated a large discrepancy between use of Warburton's prediction for a flap aspect ratio of 1.716 and 1.225, i.e., ratios of span to chord dimension of main and aft USB flaps.

In reviewing the frequency data of both the YC-14 airplane main and aft flaps, it was noted that the frequency of both were nearly identical. This fact clearly leads us to believe the two flaps act very nearly as a single unit. With this in mind, the decision was made to calculate Warburton's frequency predictions using the combined flap assembly as a single unit, where the aspect ratio was .2941.

The frequency comparisons indicated a good first approximation but not sufficiently accurate to warrant use of this model for response calculations using acoustic excitation of the flap. In the interest of a more rigorous math model and an overall calculation method, the decision was made to build a finite element model. With such a model, the details of the structure could be more accurately described and response of given locations compared to the flight test data

Two finite element USB flap models were then used in the development. Model I was a simple plate finite element model and was found to lack some definition. As a result, a more detailed model was formulated in Model II and provided more detailed results.

3.2 Finite Element USB Flap Model I—Definition

Model I was fashioned after the plate model that was studied earlier with the Warburton calculations. This model was formulated as drawn in Figure 2. The dimensions for the model nodal points were selected as shown in Figure 3.

Model I was then input to the SAP IV program with the input format as given in the print-out of the data card image of Figure 4. The print-out of the frequencies for the first 10 modes was listed in Figure 5. This data was plotted for comparison to test data in Figure 6.

Model I was formulated after the mass was matched to the actual flap weight of 837 pounds. The Warburton calculations had the dimensions,

L	=	204 in.	(length)
w	=	60 in.	(width)
t_o	=	.94 in.	(thickness)
ρ_o	=	$\frac{0.1}{386}$ lb/in^2	(Mass density)

Thus, $W_o = L w t_o \rho_o = 1150.56$ lbs.

or, $\frac{W}{W_o} = \frac{837}{1150.86} = .7275$, was the correction factor for mass.

The SAP IV run, using Warburtons thickness as a first input, gave a frequency ratio from experiment of 7.64 as seen in the experimental data, i.e.,

$$\left(\frac{f}{f_o}\right)^2 = (7.64)^2 = 58.3$$

from this then $\frac{K/W}{Ko/Wo} = \left(\frac{f}{f_o}\right)^2 = 58.3$

$$\frac{K}{Ko} = 58.3\ (.7275) = 42.41$$

Now, for a plate, $\frac{K}{K_o} = \left(\frac{t}{t_o}\right)^3 = 42.41$

or $\frac{t}{t_o} = 3.49$

from which t = 3.49 (.94) = 3.28 inches.

Then, to calculate the correct mass density of the plate, we see,

$$\frac{W}{Wo} = \frac{\rho t}{\rho o\, t_o}$$

$$= \left(\frac{W}{Wo}\ \frac{t_o}{t}\right)\rho o = \left(\frac{.7275}{3.49}\right)\left(\frac{.1}{3.86}\right) = 5.4 \times 10^{-5}\ \text{slugs/in}^3$$

These values of thickness and mass density were then used as input to the finite element program, SAP IV. The resulting model frequencies are shown in Figure 5 for the first ten modes. Comparison with measured values is shown in Figure 6.

Modal plots have been generated from these SAP IV runs, using the tabulated data as shown in Figure 7. The actual mode shape plots were obtained from this tabulation and are shown in Figure 8 thru 13. It can be seen that the modal definitions are reasonable for the density of the data points taken. This model was thus felt to represent, in a realistic manner, the USB flap and warranted the application of an input excitation for harmonic analysis.

3.3 Harmonic Analysis of Model 1

The USB flap response power spectrum for surface element g due to the pressure excitation forces on all surface elements is of the form:

$$\Phi_q(\omega) = \sum_i \sum_j \Phi_{ij}(\omega)\, T_{iq}(\omega)\, T_{jq}(\omega^*) = \lfloor T^* \rfloor \left[CPSD \right] \lfloor T \rfloor \quad (6)$$

where

$\Phi_q(\omega)$ = Response power spectrum for element q

$\Phi_{ij}(\omega)$ = Cross-power spectra (CPSD) of the excitation forces on elements i and j

$T_{iq}(\omega)$ = Output frequency response at element q to a unit force acting at the i^{th} element.

The excitation points were determined by dividing the USB flap upper surface into 16 panels of equal area as was shown in Figure 14 with a given pressure acting over each panel. The power spectra and cross-power spectra for the pressures acting on the panels were extrapolated from the data that was obtained from the four acoustic sensors located as shown in Figure 14. The extrapolation of the data for each panel for which there were no measured data was accomplished using the following formulas:

<u>Measured Data</u>

$\Phi_{10,\,10}$; $\Phi_{11,\,11}$; $\Phi_{13,\,13}$; $\Phi_{14,\,14}$; $\Phi_{10,\,14}$; $\Phi_{11,\,14}$; $\Phi_{13,\,14}$

<u>Extrapolation Formula</u>

$\Phi_{9,\,9} = \Phi_{10,\,10}$

$\Phi_{12,\,12} = \Phi_{13,\,13}$

$\Phi_{15,\,15} = \Phi_{16,\,16} = \Phi_{14,\,14}$

$\Phi_{i,i} = \Phi_{(i+8)(i+8)}$, where $i=1, \ldots 8$

$\Phi_{i,(i+1)} = \Phi_{13,14}$, where $i=1, \ldots 7$ and $i=9, \ldots 15$

$\Phi_{i,(i+2)} = \Phi_{11,14}$, where $i+1, \ldots 6$ and $i=9, \ldots 14$

$\Phi_{i,(i+3)} = \Phi_{11,14}$, where $i=1, \ldots 5$ and $i=9, \ldots 13$

$\Phi_{i,(i+4)} = \Phi_{10,14}$, where $i=1, \ldots 4$ and $i=9, \ldots 12$

$\Phi_{i,(i+7)} = \Phi_{13,14}$, where $i=2, \ldots 8$

$\Phi_{i,(i+8)} = \Phi_{13,14}$, where $i=1, \ldots 8$

$\Phi_{i,(i+9)} = \Phi_{13,14}$, where $i=1, \ldots 7$

A map of the upper triangle of the CPSD matrix is shown in Figure 15. The lower part of the triangle is the complex conjugate of the upper triangle.

The equations of motion and load equations were based on modes calculated in SAP IV.

Equations of Motion

$$\left[M_1\right] q + \left[M_3\right]\left\{\ddot{q}\right\} + i2\zeta\left[M_1\right]\left\{q\right\} = \left[C_3\right]\left\{P\right\} \tag{7}$$

where $\left[M_1\right]$ = Generalized stiffness matrix (size m x m)

$\left[M_3\right]$ = Generalized inertia matrix (size m x m)

$\left[C_3\right]$ = $\left[\phi\right]^T\left[A\right]$ = Forcing function matrix (size m x n)

$\left[\phi\right]$ = Matrix of modal dispalcements (size n x m)

$\left[A\right]$ = Matrix of panel areas (size n x n)

$\left\{q\right\}$ = Matrix of generalized coordinates (size m x 1)

$\left\{\ddot{q}\right\}$ = Matrix of generalized accelerations (size m x 1)

ζ = Structural damping coefficient

$\left\{p\right\}$ = matrix of panel pressures (size n x 1)

m = Number of modes

n = Number of panels

An example of a portion of the output spectrum values for the three accelerometer positions are shown on the computer printout sheet in Figure 16. These results have been tabulated and converted from G^2/RAD/sec to G^2/Hz as shown in Figure 17.

The solutions were for YC-14 flight condition where the test conditions were; altitude 7,620 feet, speed 216 ft/sec, N_1 of 3,098 RPM, and USB flap setting of 40 degrees.

The resulting RMS accelerations for the three accelerometer locations were as follows, tabulated below:

ACCELEROMETER NO.	DENSE CPSD MATRIX $g = .03$ (G_{RMS})	DENSE CPSD MATRIX $g = .01$ (G_{RMS})	DIAGONAL CPSD MATRIX $g = .03$ (G_{RMS})
1421	1.82	3.02	1.67
1417	2.93	4.82	2.55
1428	1.58	2.58	1.18

LOAD EQUATIONS

$$[T] = \frac{1}{386}[\Phi_o][\bar{\bar{q}}]S^2 \qquad (8)$$

$[T]$ = frequency responses for acceleration

$[\Phi_o]$ = matrix of modal values at accelerometer locations

$[\bar{\bar{q}}]$ = The matrix of generalized coordinates, each column representing the response to a unit pressure acting on one of the excitation panels.

Procedure

At each frequency, the dynamic analysis computer program solves for the response, $[T]$, and performs the calculations as shown in Equation (8). Each output spectrum is integrated over the specified frequency range (26 to 195 Hz) to obtain the RMS value of the accelerometer response. The cross-power spectra were enriched by extrapolating the measured data as described in the list of extrapolation formulas given previously. The basic equations of motion using the generated modal values from the SAP IV finite element program yielded the generalized coordinates of the response to a unit pressure

acting on the excitation panels. Once the response coordinates were obtained the frequency responses could be determined as indicated in Equation (8).

3.4 Comparison of Model I and Test Data

The following experimental values were obtained for the frequency range used in the calculations (26-195 Hz):

Acceleration No.	G_{RMS}
1421	1.59
1417	1.20
1428	0.40

Several points must be discussed before any general conclusions can be drawn. Model I does not contain the hard points of flap actuation attachment, where the accelerometers were located. Neither does this math model simulate the heavy spars in the flaps where those attachment points are located. From this lack of simulated tie-down or hard points, we would expect the calculated results to lack definition.

The initial comparisons for the USB flap setting of 40° were for three accelerometer locations where calculations for $g = .03$ were used with the "dense" cross-power spectral density (CPSD) matrix. Calculations for these accelerometers using the diagonal CPSD matrix gave results that were within 10% of the results from the "dense" CPSD matrix. Thus, only the diagonal CPSD matrix was used for subsequent comparisons.

The response values for the YC-14 USB flap were calculated for additional damping values of .06, .09, .12 and .15; see Figure 18. The total damping value for the USB flap of 0.15 represents the best match. This value would include structural damping as well as aerodynamic damping.

The response values for the three USB flap accelerometers for an assumed structural damping value of $g = .15$ are shown in Figures 19, 20, and 21.

3.5 Finite Element USB Flap Model II—Definition

The results from the Model I were encouraging but did indicate a better model was needed for more detailed response predictions. Thus, Model II was formulated and much of the actual USB flap structure was simulated including the attachment points of the two hydraulic actuators at node points 40-73 and 45-74 of Figure 22. Details of this model appear in Figures 23 through 25. The refinements incorporated into Model II which did not exist in Model I, include the following: (1) The number of nodes has been increased by a factor of nearly 3; (2) Actual geometry is better represented; (3) Spars, ribs, leading edges, and trailing edges are represented as beam elements; (4) Hinges are free to rotate; (5) Actuators are simulated by truss elements (6) Actual material properties are used in the simulation of the various structural components.

The finite element model includes 78 nodes, 74 of which are on the flap and 4 of which represent actuator attachment points. Structural elements include 64 beams, 59 plates, and two truss elements. Although the skin thickness and material vary over the flap, a constant equivalent aluminum plate thickness was used in the model. Since the flap is actually a three-dimensional structure, it was necessary to use equivalent plate thickness as described previously for Model I. Using the SAP IV program, following an initial eigenvalue analysis and mode shape inspection, a procedure similar to that described previously was employed to obtain a frequency match.

The list of the first 13 natural modes of the USB flap is given in Figure 26. These mode shapes resulting from the finite element analysis have been plotted in Figures 27 thru 39 and illustrate the complexity of the USB flap vibrational response thru a frequency of approximately 300 Hz.

3.6 Harmonic Analysis of Model II (78 Node Model)

The harmonic analysis of the USB flap, Model II was made using the acoustic excitation measured by the four acoustic microphones, M35, M37, M40 and M41, as shown in Figure 40 as the input forcing function. This acoustic data for the four microphones is given in

Figures 41 through 44. These data were obtained from the YC-14 in a STOL condition, altitude 7620 feet, speed 216 ft/sec and a USB flap angle of 40°. The diagonal CPSD was used for the input excitation and the data interpolated to cover the entire model. The Random Harmonic Analysis was then used with the USB flap finite element Model II simulation to determine the response values for the three locations corresponding to accelerometers No. 1417, 1421 and 1428 shown with asterisks in Figure 45. The resultant response predictions have been tabulated in Figure 46 for three different assumed damping values. A sample page from the computer print-out for the accelerometer response prediction with g = .06 is given in Figure 47.

3.7 Comparison of Predictions for Model II With Test Data

The predictions for G = .15 for all three accelerometer locations have been plotted in Figures 48, 49 and 50. The actual test data from three accelerometers that were located on hard structure where actuators were attached are also shown. The detailed structure at these locations was not completely simulated but the results show levels that were very representative of the high environment associated with this area. The frequency content also is noted to be indicative of the frequency range in the higher environment.

SECTION IV

FUSELAGE STRUCTURE VIBRATION PREDICITON

4.1 Fuselage Finite Element Model Development

The fuselage area of interest is shown in Figure 51. The primary considerations in the finite element structural modeling were: (1) The need to cover a broad frequency range (25 - 1000 cps); (2) Computer resource limitations; (3) Computation costs. It was determined that a single finite element model would not be adequate for the entire frequency range. Three models were developed, one for the low frequency range (25 to 100 cps), one for the intermediate range (100 to 200 cps), and one for the high frequency range (above 200 cps). Figures 52 through 54 show the nodal grids of each model relative to the actual fuselage structure.

Details of each model appear in Figures 55 through 67. For the low-frequency-range model, nodes were located at the intersections of every third frame and every fourth stringer as shown in Figure 52.

A finer nodal grid was selected for the intermediate-frequency-range model as shown in Figure 53. Nodes were located at the intersections of each frame and stringer. Additional nodes were located on each stringer at points midway between frames. The nodal density was 24 times that of the low-frequency-range model.

The high-frequency-range model was represented by a nodal grid as shown in Figure 54. The central portion of the model employed a finer grid than the outer portion to give better definition in area of measurements. Nodes were placed at each frame/stringer intersection. Additionally, in the streamwise direction, seven rows of nodes were placed equally spaced between successive frames. Nodes were placed midway between stringers in the outer portions of the model and three equally spaced rows of nodes between stringers in the central portion. In the outer portions, the grid density was 8 times that of the intermediate-frequency-range model and 192 times that of the low-frequency-range model. In the central portion, the grid density was 16 times that of the intermediate model and 384 times that of the low-frequency-range model, giving much increased definition for determination of the higher frequency modes.

Nodes, coordinates, and structural elements for the low frequency range Model I are shown in Figures 55 through 58. The complete model simulates a half-cylinder section of the fuselage spanning 16 frames. Employing the grid described previously, the model consists of 66 nodes. Between each successive set of stringer nodes is a beam element with four times the cross-sectional area and four times the moment of inertia of a stringer. Between each successive set of nodes in a tangential direction is a beam element with three times the section properties of each frame. The total number of beam elements is 116. Plate elements, 55 in number, are located between each set of 4 adjacent nodes. Element material and section properties appear in Figure 67. With the exception of nodes 1-6 and nodes 61-66, each node was given two translational degrees of freedom, Y and Z, and three rotational degrees of freedom. Symmetrical boundary conditions were imposed on nodes 1-6 and nodes 61-66, i.e., these nodes were constrained from displacement in the Z direction and from rotation about the X and Y axes. The corner nodes, 1, 6, 61, and 66 were constrained from any translational or rotational motion.

Nodes, coordinates, and structural elements for the intermediate frequency range Model II are shown in Figures 59 through 62. The model simulates a section of fuselage defined by four frames and five stringers. The model includes 35 nodes. Beam elements with section properties equal to those of the actual structure are located at the stringer and frame locations. Plate elements are also included. Material and section properties appear in Figure 67. Each node was given two rotational degrees of freedom, about the X and Y axes. All but the corner nodes, 1, 7, 29, and 35, were given a Z translational degree of freedom.

Details of the high frequency range Model III are given in Figures 63 through 66. The model includes 81 nodes, 48 beams, and 64 plates. The degrees of freedom were the same as for the intermediate frequency range model, i.e., Z translation and X and Y rotation for all but the corner nodes (1, 9, 73, and 81) which were constrained from Z translation.

The above descriptions have been given to indicate the degree of detail that would be used to cover given frequency ranges.

4.2 Low Frequency Fuselage Model I

The SAP IV finite element program was used to predict the lower frequencies of interest of the Fuselage Model I. A tabulation of the first 20 frequencies has been listed in Figure 68. The mode shape of the center portion of the model have been plotted and serve to indicate the response of such a structure nearly free of the end constraints. In this case, the model was supported with the four extreme corners clamped. These node points were 1, 6, 61 and 66 as seen in Figure 55. The mode shapes of the center portion, defined by node points 19, 24,43, and 48 have been plotted in Figures 69, 70, 71 and 72.

The acoustic excitation for this portion of the fuselage was available only at a limited number of transducer locations. Microphones M6, M13, M16, M18 and M20 were used and interpolation and extrapolation were necessary so as to cover the entire model. The locations of the microphones have been shown in Figure 73. The condition chosen for the response study was for maximum engine thrust during ground run-up. The acoustic data was plotted in Figures 74, 75, and 76. The summary of the acoustic data was listed in Figure 77 with extrapolated data for two microphones M18 and M20.

The acoustic PSD data was then used to excite the low frequency fuselage model of Figure 52 and the response from the Harmonic Dynamic Analysis Program was obtained at locations on the finite element model corresponding to locations where actual accelerometers were located in the YC-14 airplane. The accelerometers were located as shown in Figure 73.

The calculated responses of the low-frequency fuselage model have been plotted at corresponding locations on the model for the accelerometer locations of A58 (stringer), A59 (body frame) and A61 (skin, center of panel) and compared to the PSD data from the actual accelerometer responses. These comparisons have been plotted in Figures 78, 79, and 80.

4.3 Mid - Frequency Fuselage Model II

The mid-frequency fuselage Model II was shown in Figure 53. The eigenvalues for the first 8 modes are shown in Figure 81 and cover a frequency range from 60 to 350 hz. The model was pinned at the four corners at node points 1, 7, 29 and 35. The mode shapes have been plotted in Figures 82 thru 89. The acoustic excitation of the model was again obtained from extrapolated data from microphones M6, M13, M16, and M20. The same Flight Test Condition was used to calculate model response. The orientation of the Mid-Frequency Fuselage Model II in relation to the low-frequency fuselage Model I is shown in Figure 90. In addition, the location of the microphones and response measuring accelerometers are shown in this same Figure 90.

The response of the fuselage local section Model II has been plotted also in Figures 78, 79, and 80 for the three accelerometer locations.

4.4 High Frequency Fuselage Model III

The High-Frequency Fuselage Model III was shown in Figure 54. The detail node positions have been defined in Figure 63, the coordinates in Figure 64 , the beam elements in Figure 65 and the plate elements in Figure 66. The SAP IV program gave the first 20 frequencies from 269 to 987 Hz as listed in Figure 91. The mode shapes have been plotted in Figures 92 thru 95.

The acoustic excitation was the same as for the previous models with the Harmonic Analysis results of the response predictions for the stringer (A58) and the skin (A61) as shown in Figures 96 and 97.

SECTION V

ACOUSTIC FIELD PREDICTION METHOD

5.1 Introduction

A procedure for estimating fluctuating pressures, hereafter referred to as noise, on STOL aircraft is presented in this section. The procedure is mainly concerned with predictions aft of the nozzle exit plane and in direct view of the engine exhaust flow stream, in region A of Figure 98. An approach to extending the procedure to indirect points, in Region B, is also provided.

The procedure yields 1/3 octave band spectrum estimates associated with five propulsion/flap noise sources and with turbulent boundary layer (TBL) activity.

The total noise is then taken to be the (power) sum of the separate source spectra. A typical (low speed/high power) situation is suggested in Figure 99.

The general range of application of this procedure is summarized in Figure 100, and is discussed in Sections 5.2-5.4.

Methods for modifying or supplementing the 1/3 octave band estimate procedure to yield power spectral density estimates are discussed briefly in Section 5.5. Finally, comparisons between measured and estimated 1/3 octave band noise spectra are presented in Section 5.6.

Within the context of the present contract, (i) the exterior surface noise is taken to be the principal function governing airframe vibration, and (ii) exterior surface noise is considered to be known no better than is the airframe vibration. Exterior surface noise estimation hence becomes a part of the general overall problem of estimating airframe structure vibration given airplane configuration and structure details and given engine and airplane operating parameter values. Hence, within the context of Phase I of the present contract, noise estimation is considered as independent of the vibration estimation problem in which the noise environment is known, and vice versa. Development of the vibration prediction procedure is thus broken into two independent parts, (i)

vibration response prediction given the noise excitation, and (ii) noise excitation prediction given the airplane/engine/flap configuration and operating status. The focus in this section is on the latter prediction procedure.

The procedure presented has resulted from support provided both under the present contract and under recently completed NASA contract NAS2-9328 (Reference 5). YC-14 data--which was the prime data used in the development of the noise estimation procedure presented herein--was analyzed and a general characterization for the YC-14 airplane developed. This characterization was then generalized and formalized into a prediction procedure applicable to any USB STOL airplane. Without question the motivation and support of both contracts has been essential, and without support provided under both, the development of the procedure presented herein would not have been possible.

5.2 Scope

The present procedure provides 1/3 octave band estimates of fluctuating pressures on USB STOL aircraft surfaces primarily aft of the nozzle exit plane, and in direct view of (most of) the engine exhaust field.

The estimate for a typical field point P in Figure 101 is taken to depend primarily on the characteristics of the jet flow field closest to P. For the purposes of the estimate, a ribbon idealization of the flow field is employed. The procedure is specifically oriented to points strongly scrubbed by the exhaust flow stream, as well as points up to about 5 (hydraulic) nozzle diameters away from the flow boundary, and up to about 10 diameters downstream of the nozzle. The procedure is most applicable for cold secondary, dual flow nozzles (with bypass ratios between 2 and 6 and aspect ratios less than about 5) where the bottom lip is integral with the wing top surface.

The procedure yields 1/3 octave band spectrum estimates for each of the following:

- Jet mixing noise in the presence of a scrubbed wing/flap system with or without vortex generators
- Near-nozzle noise
- Trailing-edge noise
- Noise associated with (partial) separation of the exhaust flow from flaps

- Turbulent boundary layer noise
- Exhaust shock noise

A summary flow diagram for the overall procedure is present in Figure 102. Note that turbomachinery noise (for both inlet and exhaust) is not included in this estimation procedure.

5.3 Estimation Procedure Development

As noted in Section 5.2, the prime source of data drawn upon has been that for the YC-14, and which is summarized and discussed in Reference 5.

The most obvious characteristics of all the static and low-speed YC-14 data was (a) the simple, single-peaked, gently rolling-off spectrum shape of the noise for all points close to or scrubbed by the jet mixing region of the exhaust flow field, and (b) the inverse ratio between the spectral levels and their distance from where the flow field roughly seemed to be. The general shape of noise spectra is illustrated in Figure 103. The dependence on distance away from the flow field is illustrated in the same figure, and also in Figure 104 & 105, in which the position of the flow field (as reflected in the position of the USB flaps) is changing. The effect of forward velocity is illustrated in Figure 106, and suggests a reduction in peak spectral level and an increase in the frequency of the peak level with increasing forward velocity.

On the basis of observations as these, a flow field idealization model and a jet mixing noise model were developed. These models together yielded fuselage field point to flow boundary separation distances, and noise levels consistent with the smoothed behavior of much of the YC-14 ground (and some low-speed flight) surface noise data.

Estimate procedures for the remaining noise source components addressed in the overall procedure were then built up to account for the most obvious deviations of the data from the estimated jet mixing noise component. The exhaust shock noise component was based on correction of distinctive deviations (re. the other components) observed during high-speed/high-altitude (cruise) operations.

The effort summarized in the above three paragraphs is discussed in detail in Reference 5. In particular, extensive discussions of the characterization of the flow field, jet mixing noise, trailing edge noise, exhaust shock noise and turbulent boundary layer noise are to be found there.

5.4 Estimation Procedure

Computational aspects of the estimation procedure are divided into 9 sections, and which are presented in detail in Appendix A of Volume II. These sections are:

Appendix A Section	Subject Addressed
3.1	Characterization of the Flow Ribbon
3.2	Geometry Computations
3.3	Jet Mixing Noise
3.4	Near-Nozzle Noise
3.5	Trailing-Edge Noise
3.6	Separation Noise
3.7	Turbulent Boundary Layer Noise
3.8	Exhaust Shock Noise
3.9	Estimation for Indirect Field Points

Briefly, the parameters used to characterize the flow field (ribbon) idealization*, shown in Figure 107, are its maximum width, W^*, (or W^*_{DOOR}), its skew angle, θ^*, and its trail-off angle, θ'. These are computed in Section 3.1. The geometric factors which enter into these computations are:

*The specific idealization is as follows: The flow exits the nozzle with a width equal to the nozzle exit width, flush with the wing surface. The ribbon spreads linearly in width with position downstream of the nozzle exit plane until it reaches the beginning of the strongly curved portion of the flap. Thereafter its width remains constant, and its direction of flow (as viewed from above) parallel to the engine centerline. It initially remains attached to the strongly curved portion of the flap, turning to the angle θ', at which point it separates from the flap and continues on a straight course at the elevation angle θ'.

- o nozzle side lip angles
- o nozzle top lip (kickdown) and bottom angles
- o wing surface inclination angle
- o nozzle width, height and effective exit area
- o skew angle of nozzle exit plane
- o distance from nozzle exit plane to start of strongly curved portion of flap system
- o size of nozzle side door opening (if present)

In addition, the following operational parameters enter into the computations:

- o static flow turning angle of the propulsion/flap system at the specific flap setting considered
- o airplane speed
- o engine exhaust mixed jet velocity

The coordinates of the field point, P, at which the noise estimates are sought, are next computed (Section 3.2) in terms of (see Figure 101)

δ = minimum distance of P from ribbon

S = downstream coordinate of P as measured along ribbon

Information required for these include (in addition to those flow ribbon parameters from Section 3.1):

- o Coordinates of the field point P
- o Coordinates of fixed reference point P_o on the nozzle exit plane (see Figure 3 of Vol. II, Appendix A)

The values of these two coordinates, when normalized by D_H, where

$$D_H = \sqrt{\frac{4}{\pi} A_{EFF}} ,$$

and

A_{EFF} = effective area of engine nozzle exit plane (including effect of both primary and fan flows),

along with the values of parameters listed in Figure 108, are then used to compute the estimates of the various noise components:

- o jet mixing noise (Section 3.3)
- o near-nozzle noise (Section 3.4)
- o trailing edge noise (Section 3.5)
- o separation noise (Section 3.6)
- o exhaust shock noise (Section 3.8)

In the case of turbulent boundary layer (TBL) noise, δ and S are not required, but rather (see Section 3.9)

$\bar{X}$ = boundary layer growth length along the airframe surface to the field point,

Operational parameters required are

$\bar{V}$ = representative flow velocity along boundary layer growth path
$\bar{\rho}$ = representative flow density of fluid along boundary layer growth path,

rather than those given in Figure 108.

Each noise component is characterized in terms of

- o a generalized spectrum shape
- o spectrum shape peak level, SPL_{pk}
- o frequency at which the peak level occurs, f_{pk}, as suggested in Figure 109. In the case of jet mixing noise a modification of the generalized spectrum shape is introduced if vortex generators are deployed into the flow (see Section 3.3).

All generalized spectrum shapes a... essentially based on measured 1/3 octave band data. As an example the data shown previously in Figure 103 for measurement points 3, 4, 7, 13 and 14 was in part used to define the generalized spectrum shape for jet mixing noise.

Peak level computations generally combine conceptual scaling rules for velocity and density effects with empirically observed effects of the dimensionless distance of the field point away from the flow ribbon, δ/D_H, and downstream of the nozzle exit plane, S/D_H. The general form used for SPL_{pk} is

$$SPL_{pk} = 10 \text{ Log}\left(\frac{\rho^2_{rep}}{\rho_o^2}\right) + 10 \text{ Log}\left[F\left(\frac{V_{rep}}{V_o}\right)\right]$$

$$+\Delta_1(\delta/D_H)+\Delta_2(S/D_H)+SPL^o_{pk},$$

in which

$$\rho_{rep} = \begin{cases} \bar{\rho}\text{ ; for TBL noise} \\ \rho_j\text{ ; for all other noise components,} \end{cases}$$

and

$\bar{\rho}$ = representative fluid density for TBL

ρ_j = engine mixed exhaust jet density

ρ_o = reference density at which SPL^o_{pk} is defined.

With regard to the second term

$$F\left(\frac{V_{rep}}{V_o}\right) = \begin{cases} \left(\frac{V_j - V_A}{V_o}\right)^4\text{; for jet mixing noise} \\ \left(\frac{V_j}{V_o}\right)^4\text{ ; for near nozzle noise and separation noise} \\ \left(\frac{V_j - V_A}{V_o}\right)^4\left(\frac{V_j + V_A}{2C}\right)\text{; for trailing edge noise} \\ \left(\frac{V}{V_o}\right)^4\text{ ; for TBL noise} \end{cases}$$

$$\left[\left[\sqrt{\left(\frac{V_j}{C_j}\right)^2 - 1}\right]^4 = \beta^4 \text{ ; for shock noise}\right.$$

where

V_j	=	engine mixed exhaust jet velocity
V_A	=	airplane velocity
V_o	=	reference velocity at which SPL^o_{pk} is evaluated
C_j	=	engine mixed exhaust sound speed
$\bar{V}$	=	representative velocity for TBL activity

The third and fourth terms in the general expression for SPL_{pk}, i.e., Δ_1 and Δ_2, are empirically determined relations for the effect of δ/D_H and S/D_H on peak level. Recall that D_H is the engine exhaust nozzle hydraulic diameter. Note that in the case of TBL, terms of the form of Δ_1 and Δ_2 do not appear, as suggested previously.

Finally the fifth term in the general expression for SPL_{pk}, is the reference peak spectrum level at the reference conditions of $\rho_{rep} = \rho_o$, $V_{ref} = V_o$, and at $\delta/D_H = o$, and usually at $S/D_H = 3$.

The computation of f_{pk}, i.e., the frequency at which the peak spectral level occurs, is typically a blend of empirical relations for the effect of δ/D_H and S/D_H, and scaling rules based on the size of and speed at which eddies closest to the field point are generated or are convected past the field point. A general form is

$$f_{pk} = f^o_{pk}\left(\frac{V_{ref}}{\ell_{ref}}\right) x \alpha \left(\frac{V_A}{V_j}\right) x \; C(\delta/D_H),$$

where

$$f^o_{pk}\left(\frac{V_{ref}}{\ell_{ref}}\right) = \begin{cases} \dfrac{1.8\, V_j/D_H}{S/D_H + 3} \text{ ; for jet mixing and shock noise} \\ \\ 3.6\, V_j/D_H \text{; for near nozzle noise} \end{cases}$$

$$
\left\{
\begin{array}{l}
\dfrac{1.8\ V_j/D_H}{S_{TE}/D_H + 3}\ ;\ \text{for trailing edge noise} \\[2ex]
\dfrac{1}{4}\ V_j/\delta_{TE};\ \text{for separation noise} \\[2ex]
\dfrac{1}{2}\ \bar{V}/\delta_{BL};\ \text{for TBL noise}
\end{array}
\right.
$$

and in which V_J, S, D_H and $\bar{V}$ are as defined previously, and

S_{TE} = distance from nozzle exit to flap trailing edge as measured along the flow ribbon

δ_{TE} = distance between flow ribbon and flap trailing edge

δ_{TB} = thickness of TBL at field point

For the second term in the general expression for f_{pk}

$$
\alpha\left(\frac{V_A}{V_J}\right) = \left\{
\begin{array}{ll}
\left(\dfrac{J_J + V_A}{V_J - V_A}\right)\left(\dfrac{V_J + V_A}{2\,V_J}\right) & ;\ \text{for jet mixing, trailing edge and shock noise} \\[2ex]
1 & ;\ \text{for all other noise components}
\end{array}
\right.
$$

The third term in the general expression for f_{pk}, namely $C(\delta/_{DH})$, is empirical in nature accounting for frequency changes (typically increasing) associated with increasing distance between field point and the flow ribbon point of closest approach.

5.5 Application to Narrow Band Noise Estimation

The procedure referred to in Section 5.4 and in Appendix A of Volume II was developed using 1/3 octave band acoustic data, and hence was itself posed in 1/3 octave band terms. However, for purposes of structural vibration estimation, a power spectral density estimate is required rather than a 1/3 octave band format.

Limited examination of power spectral density data (corresponding to the 1/3 octave band data used in the prediction method development) shows these to be in general smooth curves free of distinctive (narrow band) peaks. Hence the 1/3 octave band procedure can in principal be quite simply extended to predict exterior surface noise field power spectral density:

(a) For each source component generalized 1/3 octave band spectrum shape curve denoted as spl(f), determine a generalized power spectral density shape curve, denoted by psd(f), such that

$$I(f_i) - \int_{2^{-1/6} f_i}^{2^{1/6} f_i} psd(f)df = 0$$

where

$$I(f_i) = 10^{spl(f_i)/10},$$

and f_i is the i th 1/3 octave band center frequency.

(b) determine the location of the frequency of the peak of the generalized psd shape curve with respect to the peak of the generalized spl shape curve.

The determination of a psd function yielding a desired set of $I(f_i)$ values at $f = f_i$ $(i=1,2,\ldots,n)$, requires one to assume a form for the psd function (containing undetermined coefficients). Values for these coefficients are then chosen to make the right hand side of the equation relating $I(f_i)$ and psd(f) as close to zero at $f=f_i$ $(i=1,2,\ldots,n)$ as desired.

As example, a simple form for a psd function is

$$\mathrm{psd}(f) = \begin{cases} c_1 & ; \; 2^{-1/6} f_1 \leq f < 2^{1/6} f_1 \\ c_2 & ; \; 2^{-1/6} f_2 \leq f < 2^{1/6} f_2 \\ \vdots & \quad \vdots \\ c_n & ; \; 2^{-1/6} f_n \leq f < 2^{1/6} f_n \end{cases}$$

In this case the C_i's are given simply by

$$c_i = \left(\frac{1}{2^{1/6} - 2^{-1/6}}\right) \frac{I(f_i)}{f_i}$$

This format is in fact used in Section VI, except that it is applied external to the estimate procedure, rather than within it.

5.6 Comparisons of Measured vs Estimated Acoustic Data

Comparisons are presented between measurements and estimates generated with the procedure summarized in the previous section and presented fully in Appendix A of Volume II. Four sets of YC-14 measurement points/flight conditions are considered:

Set 1: At five flap measurement points all at the same STOL approach condition.

Set 2: At nine fuselage measurement points at the same brake release condition.

Set 3: During various phases of a take-off, covering brake release to climbout, at one fuselage location.

Set 4: At various extensions of the USB flaps at two fuselage locations.

Values of geometry parameters for the YC-14 used in arriving at these estimates are listed in Figure 110. Measurement point locations coordinates are summarized in Figure 111. A general diagram showing the location of these and other YC-14 measurement points appears in Figure 40, presented previously in Section 3.6. Values of operating parameters for the 10 ground and flight conditions examined are shown in Figure 112.

Finally, a measurement-point/flight-condition cross reference list is presented in Figure 113.

With regard to each of the resultant estimates presented in each of Figures 114 - 139, the measured value curve is indicated by solid circular symbols, the curve of (total) estimated noise by solid up-side-down triangular symbols. The remaining open symbols indicate values of various noise components, as noted on the lower part of each figure. Note also that the lower part of each figure provides a brief indication of the operating status of the airplane, and under "NOTES" the location of the measurement point and the name of the flight condition. With regard to these, the following abbreviations are used.

ALT = airplane altitude

SPEED = airplane speed

N1 = engine fan shaft rotational speed

VMIX = engine mixed primary and fan exhaust velocity

USBFA = USB flap angle

Under Notes:

BS = body station location of measurement point

WL = water line location of measurement point

BL = butt line location of measurement point

VG = vortex generator

The above selection of measurement point/flight conditions spans a reasonably broad scope of the STOL airplane low speed operations. Note that this selection covers an overall acoustic level variation of about 30 dB (i.e., 128 to 159 dB) and a 10 to 1 frequency range within which the peak spectral level falls (i.e., 40 to 400 Hz). Figures 114-127 give an indication of the prediction procedure ability to assess correctly the effect of measurement point location relative to the engine exhaust stream on acoustic levels. Figures 127-131 indicate directly the procedure's ability to handle forward velocity effects, while Figures 132-139, USB flap position effects.

Since a portion of the data exhibited in these figures was used in the development of generalized spectrum shapes, reference levels, etc., appearing in the prediction procedure, the comparisons shown indicate primarily the self consistency of the procedure. Based on comparisons presented, and the range of locations and operating conditions covered, it is felt that the procedure is to first order highly self consistent. Improved self consistency could be achieved with further evaluation of YC-14 and other (as for example QSRA) data. However, such an effort is felt to be beyond the scope of the present program.

PHASE II PARAMETRIC STUDIES

Analytical techniques and computer programs used in Phase I were extended for use in Phase II of the program. These extensions were used to explore the variation of environmental vibration and acoustic levels in STOL type aircraft smaller and larger than the medium STOL airplane studied in Phase I. The technical analysis of Phase II consisted of three parts: (1) development and eigenvalue analysis of finite element structural models, (2) definition of the acoustic environment, and (3) random harmonic analyses. The USB flap structure and fuselage structure near the wing root were the two areas studied for parametric effects. These studies follow in Sections 6.0, 7.0 and 8.0.

SECTION VI

FLAP STRUCTURE VIBRATION PREDICTION–PARAMETRIC STUDIES

6.1 Small STOL - QSRA USB Flap

The QSRA airplane was chosen to represent the small scale STOL. Since we had some experience with modification of the airplane for NASA, we had access to structural details and could use this data in our structural representations.

The QSRA USB flap structural representation was derived from the structure shown in Figures 140, 141, and 142. The upper skin material was .071" AL 301.

The finite element models of the QSRA flap were developed, as shown in Figure 143, with 31 node points. The coordinates for the nodes were assigned as shown in Figure 144. The beam elements were determined as shown in Figure 145 and the plate elements are given in Figure 146. This model was then input to the Structural Analysis Program (SAP IV) to obtain the mode shapes and frequencies of the QSRA flap. It is to be noted that the response of the six locations are on the flap structure and would not include the attachment point (which is assumed rigid in this analysis and would have no motion).

The first 20 frequencies were calculated and are listed in Figure 147. The mode shapes are shown in Figures 148 through 157.

The acoustic input was determined from the data as described in the acoustic parametric prediction Section VIII of this report. The excitation points of the flap were determined by dividing the USB flap upper surface into 20 panels as shown previously in Figure 146 with a given pressure acting over each panel. The power spectra and cross-power spectra for the pressures acting on the panels were extrapolated from the data that were given for the six locations. The acoustic data have been given in Section VIII in the discussion of the fluctuating pressure estimates for the 50,000 lb STOL airplane. The extrapolation of this data for all the panels was accomplished using the extrapolation technique used for the YC-14 predictions. The frequency responses for six arbitrarily chosen locations on the flap used the dynamic analysis computer program as was used in the YC-14 calculation in Phase I. The locations chosen are shown in Figure 158 as points

1 through 6. Structural response results have been obtained for g = .06, .09, .12 and .15. Results of g = .09 are shown in the plots of Figures 159 through 161 for locations 1, 3, and 5, for the airplane condition, STOL approach, N_1 = 85%, 50° USB flaps.

A comparison with flight data for the QSRA flap is given in Figure 162. Location 1 was taken as the point for comparison to the accelerometer that was mounted on the flap actuator (A13V).

6.2 Large STOL - USB Flap

To formulate a design for the large STOL airplane flap we follow the scaling chart listed below:

	SMALL	LARGE
WT	50,000 lbs	1,000,000 lbs
SPAN	100 ft	270 ft
THRUST	20,000 lbs	400,000 lbs

The linear scale factor of large STOL airplane to small STOL airplane is 2.7. If we scaled the QSRA flap accordingly, the large STOL airplane flap would have a chord of 130 inches and span of 190 inches.

The design of the large STOL flap would differ only slightly from the QSRA for purposes of this study. The details of design are shown in Figures 163, and 164 with the values of the components listed in Figure 164. Figure 165 indicates the 6 locations chosen for the analyses solutions.

The large STOL USB flap model was input to the SAP IV program with node points as shown in Figure 166, the coordinates as shown in Figure 167 the plate elements as shown in Figure 168 and the structural component values as shown in Figure 169.

The output from the SAP IV program is listed in Figure 170 for the first 20 Modes. The mode shapes are shown in the following Figures 171 through 177.

The acoustic input was obtained as detailed in Section 8.4. The response plots of the large STOL USB flap model to the STOL condition of 50° flap setting and 85% power are shown in Figures 178 through 189.

We see the response of the large USB flap has lower frequency content than the QSRA flap with the response of the 64 Hz mode and the second and third modes clearly seen in the response plots. The energy content of the large USB flap is also seen in the 150-300 frequency region,as would be expected.

SECTION VII

FUSELAGE STRUCTURE VIBRATION PREDICTION—PARAMETRIC STUDIES

7.1 Small STOL - QSRA Fuselage

The QSRA fuselage model was chosen to represent the upper fuselage from the top surface of the wing to airplane center line. The area chosen can be seen in Figure 190 and 191. Several models were constructed, one being a 16 node model, where response calculations were made. However, for better accuracy, a larger model was finally selected as shown in Figure 192 that had 77 nodes. The coordinates for this model were selected as given in Figure 193 with the beam and plate elements given in Figure 194 and 195. The actual stringer used in the QSRA airplane are shown in drawings of Figure 196 and 197 which were included in the model calculations. Figure 198 summarizes the structural values used in the QSRA fuselage model.

The results of the calculation of SAP IV with the Beam-Plate QSRA fuselage model of 70 nodes is listed in Figure 199 for the first 20 modes. The shapes of the lower modes have been drawn in Figures 200 through 209.

The model was then excited by the acoustic input described in Section 8.3 for the locations shown and for a damping value of .09. The results are shown in Figures 210, 211 and 212.

The fuselage model represented the upper fuselage structure from airplane structure, body station 345 to 450 and WL 198 to 209. The QSRA accelerometers that would correspond to this region are:

A5V, <u>A6L</u>	BS 400 Side Frame/Stringer Junction
A7V, <u>A8L</u>	BS 500 Ceiling Longeron

A comparison with flight data for the QSRA fuselage is given in Figure 213 where location 7 of the math model is compared to accelerometer A66 which was mounted in the QSRA airplane at BS 400 on a side frame-stringer junction. The levels show satisfactory agreement. Location 1 was also compared to test data and indicates the

test data to be lower than predicted up to approximately 70 Hz. (Figure 214). This area is somewhat out of the direct impingement area and could be responsible for some error in the assumed excitation or the model.

7.2 Large STOL - Fuselage

The fuselage model was scaled up from the QSRA data with length, area and mass factors proportional to 2.5, $(2.5)^2$, and $(2.5)^3$. The scaled structural values were input to the SAP IV program for modal frequencies listed in Figure 215 and plotted for mode shapes shown in Figure 216 through 221.

The acoustic input was then determined as given in Section VIII and the structural response for the stringer frame locations are given in Figures 222, 223 and 224.

SECTION VIII

NOISE FIELD PARAMETRIC PREDICTION

This section discusses fuselage and flap surface noise predictions which were generated to provide an excitation input source to the vibration analyses of "small" and "large" STOL airplanes discussed in Sections VI and VII. The selected airplane geometries, operating conditions, field point locations and necessary scale factor relations for dimensions and operating parameter values are set forth. An example noise prediction tabulation and plot for the small airplane are presented and discussed. Their relation to the prediction procedure of Section VI is discussed. The simple manner in which the estimates for the small airplane can be applied to the large airplane are stated.

8.1 STOL Airplane Prediction Parameters

The basic airplane geometries for which flap and fuselage surface noise levels have been generated (and which have previously been discussed in Sections VI and VII are:

- o A four-engine, 50,000 lb gross weight airplane - the QSRA configuration/design is used.
- o A four-engine, 1,000,000 lb gross weight airplane - a scaled version of the QSRA is used for simplicity.

The two operating conditions for each are chosen as:

- o Brake release (100% rated thrust)
  - Airplane speed (V_A) = 0
  - Engine mixed jet velocity (V_J) = 870 ft/sec
  - USB flaps at 0^o (fully retracted)
- o STOL operation (85% rated thrust)
  - Airplane speed = 110 ft/sec (65 knots)
  - Airplane altitude (ALT) = 6500 ft
  - Engine mixed jet velocity = 680 ft/sec
  - USB flaps extended to 50^o

Fixed vortex generators are assumed for both airplanes at both operating conditions, following the scheme actually used for QSRA.

Figures 225 — 230 in the present section describe the 50,000 lb QSRA type airplane, and the field points at which estimates have been made. Geometric data shown in these figures is based on QSRA drawings, primarily Boeing Dwg. 340-000003.

The 1,000,000 lb gross weight airplane was taken to be a scaled up version of the above 50,000 lb airplane, with its dimensions proportional to the cube root of the ratio of the gross weights. Hence all dimensions of the QSRA airplane apply to the 1,000,000 lb airplane upon multiplying by a scale factor SF, of

$$SF = \sqrt[3]{1{,}000{,}000/50{,}000} = 2.71$$

A second assumption made is that the engines of the 1,000,000 lb airplane are exact scaled replicas of those of the 50,000 lb airplane, and all have the same engine cycle, by-pass ratio, etc.

Under these assumptions it is further assumed that engine mixed jet velocity, airplane speed and USB flap angle are the same for both airplanes at brake release at 100% rated thrust, and at STOL operation at 85% rated thrust.

8.2 Prediction Method

The method described in Section V was used to generate the estimates for the small STOL airplane, as well as providing the simple guidelines needed to apply these to the large STOL airplane.

Through Boeing in-house support, a computerized version of the current procedure has been developed for the CDC system. This program USBEST(3), generates tabulated spectral value lists by noise component and in total, as well as plotting files. Via an existing computer plotting program constructed as a part of a 1976-1977 AFFDL/NASA contract effort to measure YC-14 cabin noise, graphs of the estimates can also be generated. These programs have been used to generate all estimates appearing in this report.

An example of a computer tabulation and corresponding computer plot are shown in Figures 231 and 232, respectively.

The one principle difference between the computerized version of the noise prediction procedure and that presented in Appendix A of Volume II is the definition of zones. Within the program, and on the output tabulation forms (e.g., Figure 231) the following definitions are applied:

Zone 0: All points above the upper wing surface which are forward of the engine nozzle exit plane.

Zone 1: All points above or on the wing upper surface which have S values between O and L_W.

Zone 2: All points above or on the wing upper surface which have S values between L_W and S'.

Zone 3: All points above or on the wing upper surface with an S value greater than S', and all points with an S value greater than S_{TE}.

Zone 4: All points with an S value less than S_{TE} and which are below the wing lower surface.

The definitions of S, S' and S_{TE} used above are the same as those used in Appendix A of Volume II.

Symbols and abbreviations appearing on the tabulation and plot forms of Figures 231 and 232 generally follow or are mnemonics for those used in Appendix A of Volume II. For instance, with regard to Figure 231:

ALT = airplane altitude
VA = airplane forward speed
VJ = engine mixed (primary and fan) exhaust flow velocity
VGS = vortex generators
R/RO = ratio of at altitude air density to sea level air density
THETAS = θ_s, per Appendix A of Volume II
THETAP = θ', per Appendix A of Volume II
EX = "exit"
TE = "trailing edge"
DELTA = δ, per Appendix A of Volume II

Abbreviations for noise components include:

- MIX = jet mixing noise
- NN = near nozzle noise
- TE = trailing edge noise
- SEP = separation noise
- TBL = turbulent boundary layer noise
- SUM = noise associated with power sum of all above noise components

8.3 Fluctuating Pressure Estimates - Small STOL

A complete set of tabulations and plots for the 8 flap and wing field points and the 9 body field points are included as Appendix B of Volume II. A summary of overall levels at each field point at each of the two conditions considered (brake release and STOL operation) is shown in Figure 233.

Note in this figure that separate estimates due to the inboard pair of engines alone and due to the outboard pair of engines alone are included: The estimate procedure is designed for, and is based on, data from airplanes with two symmetrically placed engines, as the YC-14. Hence treatment of a four-engine airplane must be handled indirectly, i.e., two-engines at a time. To this end it is assumed that for noise purposes the contributions from each pair of engines can be treated independently, and then summed on a power basis to obtain total noise. (Measured QSRA does exist for evaluating this assumption at least for noise on the fuselage, but such a check has not been made. See for instance Boeing Document D6-47118, "QSRA Flight Test-Noise," J. E. Sommers and A. J. Bohn, 14 Dec. 1978.) The values in Figure 233 and in the Appendix tabulations and plots (see Volume II) indicate that under this assumption, the contribution of the outboard engine pair never contributes more to the total (summed) noise on the fuselage or inboard flaps than 3 dB and in most cases less than 1 dB.

8.4 Fluctuating Pressure Estimates - Large STOL

Because of the very special relationships imposed between the two "paper" STOL airplanes which are considered, i.e.,

- o They are geometrically similar with each dimension of the large airplane being 2.71 times the corresponding dimension of the small airplane.

- o The operating parameter values are exactly the same for both at brake release, and then again at the STOL operation considered,

the spectral estimates for the small airplane can be extended with but small error to the large airplane. Specifically,

- o overall levels and spectral levels for large airplane = overall and spectral levels for small airplane

- o Frequencies (and frequency scales) for large airplane = (dimensional scale factor)$^{-1}$ x frequencies (and frequency scales) for small airplane.

That is, the spectra for the large airplane are those for the small airplane upon dividing the frequency scale (of the small airplane spectra) by the dimensional scale factor, being 2.71 for the two airplanes considered here.

These simple spectral relationships arise from the interaction of the similar geometries and identical operating condition values for the two airplanes considered with the following properties of the noise estimation method summarized in Section V and described in detail in Appendix A of Volume II.

- o All component noise levels depend upon the <u>ratio</u> of field point distance to nozzle hydraulic diameter, which for the airplanes under study are the same for both (see in particular Section 5.4).

- o Beyond this all levels depend in addition on airplane and engine operating parameter values (i.e., airplane altitude and speed, engine mixed exhaust velocity, sound speed, and density, and USB flap angle), and which for the airplanes under study are the same for both (see in particular Section 5.4).

- With the exception of TBL noise, characteristic frequencies scale inversely with engine hydraulic diameter, which for these two airplanes are related by the scale factor of 2.71.

In the case of TBL noise, the characteristic frequencies scale inversely to boundary layer thickness which for the two airplanes considered here go as (geometric scale factor)$^{.8}$ = $(2.71)^{.8} = 2.2$. At brake release where the airplane speed is essentially 0, this effect is negligible. At the STOL operation condition the TBL noise component is small compared to the jet mixing noise component so that again the non-simple scaling effect for TBL has a negligible effect on the total noise. (See in particular Section A.4.7 of Appendix A of Volume II.)

The manner chosen for relating the geometries and operating statuses of different weight airplanes in this study leads to probably the most concise relationship possible between surface noise fields for different airplanes. To first order the scaling approaches employed seem quite reasonable. Hence, to first order, surface noise levels would be expected to remain about the same for airplanes of different size, (but with the same number of engines of the same by-pass ratio), while the characteristic frequency of the noise would become lower with increasing airplane size.

A detailed examination of differences in missions, aerodynamic and propulsive performance of airplanes of differing weight would undoubtably lead to less simple geometric and operations relations. In turn, these would lead to less easily describable differences in the surface noise fields. However, within the limitations of the noise prediction procedure which has been developed in the present study, such differences in geometry and operations should be addressable directly, and without difficulty.

SECTION IX

ENVIRONMENTAL VIBRATION PREDICTION COMPARISONS

Comparison of the applicable military standards was made here to indicate the impact of the predicted vibration levels in STOL aircraft. Four pages of MIL-STD 810 C showing the predicted levels for this type aircraft are shown in Figures 234 through 237. Figure 238 upper curve indicates the levels in MIL-STD 810 C for 1 HR test and the lower curve, the actual environment based upon a 20,000 hour life as specified in test factor from Reference 4, Shock and Vibration Handbook, p. 24-24.

The plot of the STOL responses, Figure 239, compared to the MIL-STD 810 C levels show the lower frequencies of the large STOL airplane to be of some concern since this energy can be transmitted into primary structure at these frequencies. The levels shown for the small STOL in Figure 240 will have considerable attenuation as we move from the stringer frame locations down to heavier frame support structure where equipment would be located, but MIL-STD 810 C still would appear to be somewhat inadequate for the smaller STOL aircraft in the frequency range from 125 to 300 Hertz.

REFERENCES

1. SAP IV, "Application Users Manuals", Boeing Computer Services, Inc., 10208-013. July 1975

2. "Random Harmonic Analysis Program, 6221 (TEV 156)," Volume I: Engineering and Usage, R. D. Miller and M. L. Graham. Boeing D6-44466, 1 May 1979.

3. G. B. Warburton, "The Vibration of Rectangular Plates," Department of Mechanical Engineering, University of Nottingham, England, 1967.

4. C. M. Harris and C. E. Crede, "Shock and Vibration Handbook." McGraw-Hill, Inc. 1961.

5. L. M. Butzel, A. J. Bohn, R. Armstrong & J. B. Reed, "Noise Environment of Wing, Fuselage and Cabin Interior of a USB STOL Airplane," NASA CR-159053, July 1979.

6. M. Harper-Bourne & M. J. Fisher, "The Noise from Shock Waves in Supersonic Jets," AGARD CP-131, 1973.

7. H. K. Tanna, P. D. Dean & R. H. Borrin, "The Generation and Radiation of Supersonic Jet Noise", Vol IV, "Shock-Associated Noise Data," Air Force Aero Propulsion Laboratory Technical Report AFAPL-TR-76-75, September, 1976.

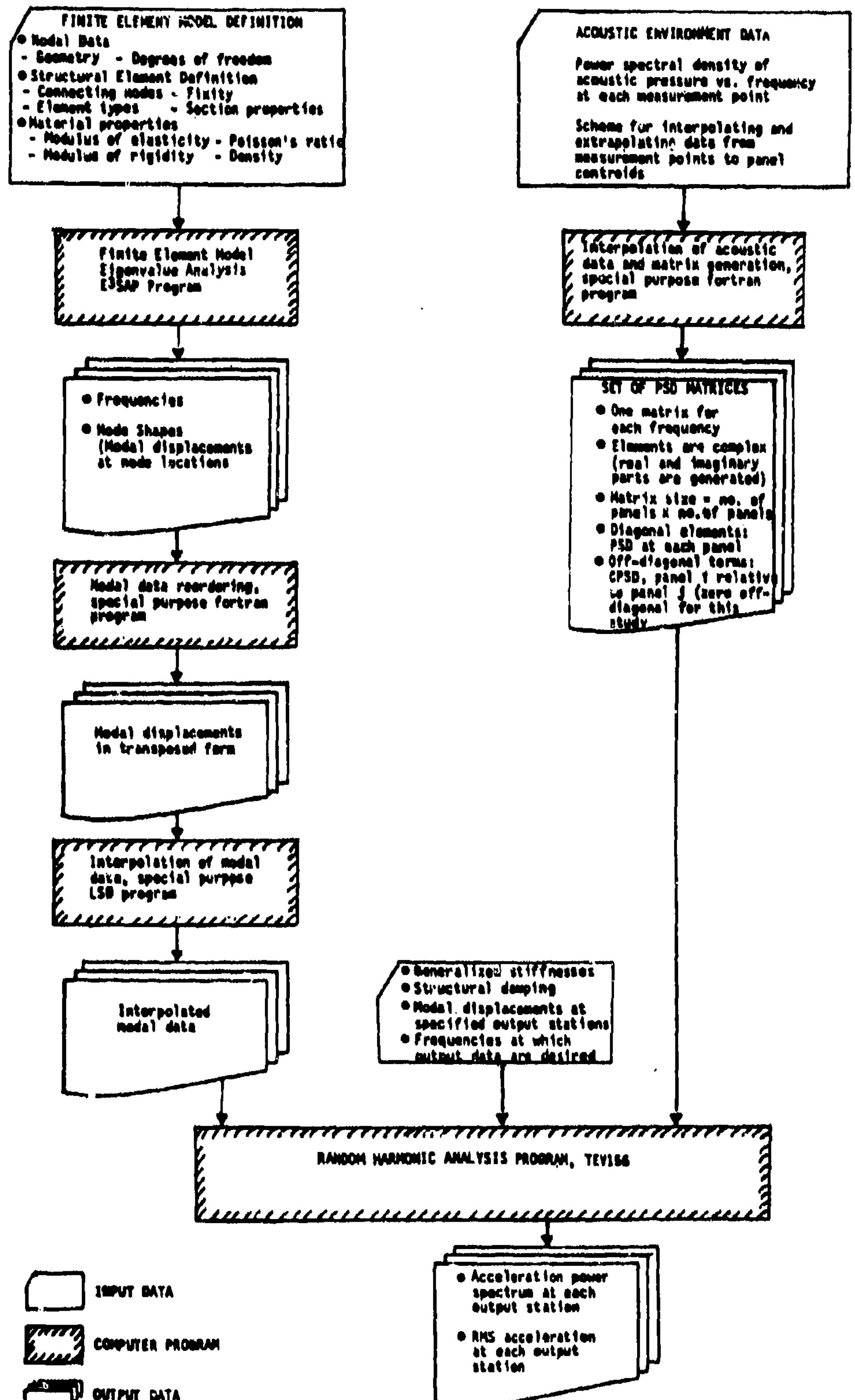

Figure 1. Harmonic Analysis Data Flow Diagram

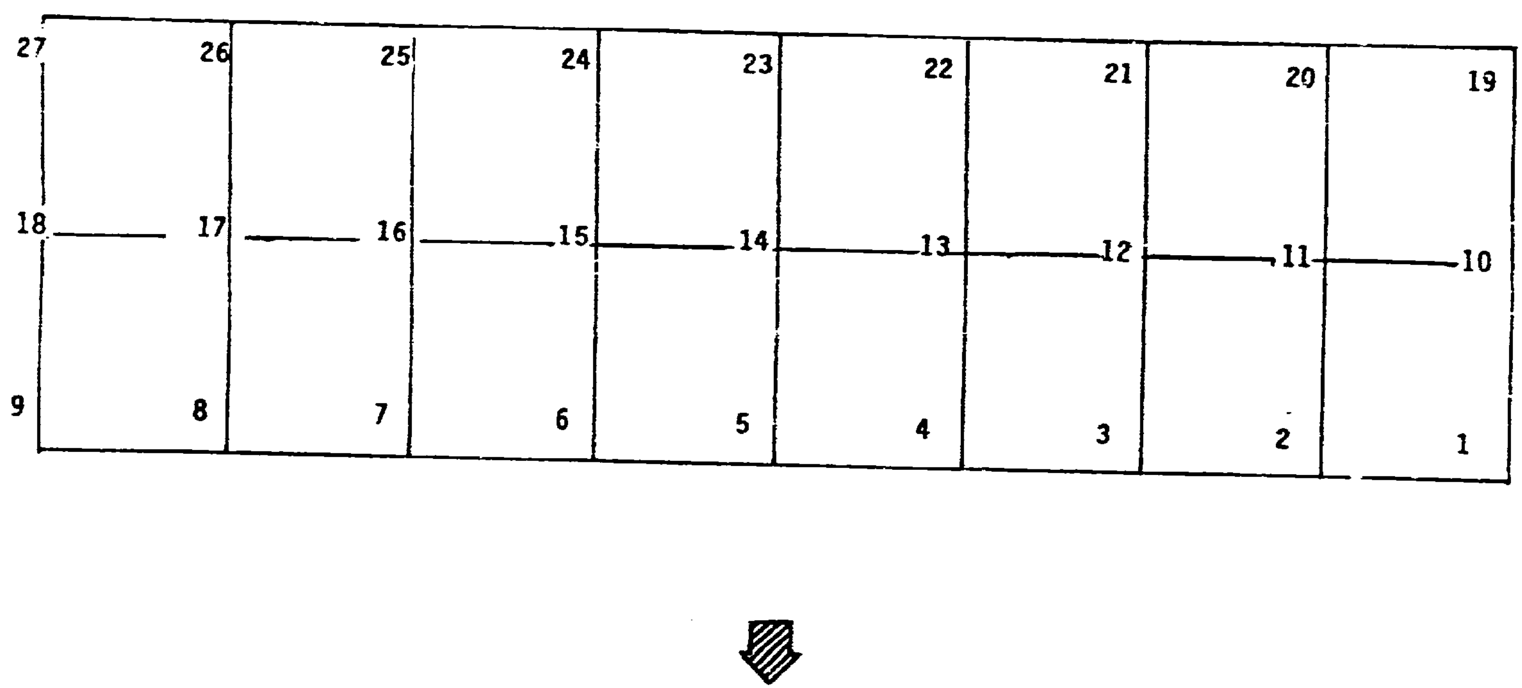

Figure 2. YC-14 USB Flap Simulation for the EKS-SAP IV

NODE	X	Y
1	-30	-102.0
2		-76.5
3		-51.0
4		-25.5
5		0.0
6		25.5
7		51.0
8		76.5
9		102.0
10	0	-102.0
11		-76.5
12		-51.0
13		-25.5
14		0.0
15		25.5
16		51.0
17		76.5
18		102.0
19	+30	-102.0
20		-76.5
21		-51.0
22		-25.5
23		0.0
24		25.5
25		51.0
26		76.5
27		102.0

Note: Measurements in inches

Figure 3. Coordinates for Nodes in YC-14 USB Flap Simulation

```
                                                                                              DATE 01/24/76 TIME 12 25
                                        D A T A   C A R D   I M A G E
CARD             1         2         3         4         5         6         7         8
 NO     12345678901234567890123456789012345678901234567890123456789012345678901234567890

  1-    THIN  SHELL ELEMENT 27 NODES
  2-       27    1        10    3                   0    1
  3-        1    1    1    0    0    0    1   -30.0   -102.0        0.0
  4-        2    1    1    0    0    0    1   -30.0    -76.5         .0
  5-        3    1    1    1    0    1    1   -30.0    -51.0        0.0
  6-        4    1    1    0    0    0    1   -30.0    -25.5         .0
  7-        5    1    1    0    0    0    1   -30.0      0.0         .0
  8-        6    1    1    0    0    0    1   -30.0     25.5         .0
  9-        7    1    1    1    0    1    1   -30.0     51.0        0.0
 10-        8    1    1    0    0    0    1   -30.0     76.5         .0
 11-        9    1    1    0    0    0    1   -30.0    102.0        0.0
 12-       10    1    1    0    0    0    1     0.0   -102.0        0.0
 13-       11    1    1    0    0    0    1      .0    -76.5         .0
 14-       12    1    1    0    0    0    1      .0    -51.0         .0
 15-       13    1    1    0    0    0    1      .0    -25.5         .0
 16-       14    1    1    0    0    0    1      .0      0.0         .0
 17-       15    1    1    0    0    0    1      .0     25.5         .0
 18-       16    1    1    0    0    0    1      .0     51.0         .0
 19-       17    1    1    0    0    0    1      .0     76.5         .0
 20-       18    1    1    0    0    0    1      .0    102.0         .0
 21-       19    1    1    0    0    0    1    30.0   -102.0        0.0
 22-       20    1    1    0    0    0    1    30.0    -76.5        0.0
 23-       21    1    1    0    0    0    1    30.0    -51.0        0.0
 24-       22    1    1    0    0    0    1    30.0    -25.5        0.0
 25-       23    1    1    0    0    0    1    30.0      0.0        0.0
 26-       24    1    1    0    0    0    1    30.0     25.5        0.0
 27-       25    1    1    0    0    0    1    30.0     51.0        0.0
 28-       26    1    1    0    0    0    1    30.0     76.5        0.0
 29-       27    1    1    0    0    0    1    30.0    102.0        0.0
 30-        6   16    1    0
 31-            1                          5.40E-5
 32-      1.0E+7       2.5E+6      0.0      1.0E+7    0.0        4.0E+6
 33-      1.0          0.0         0.0      0.0
 34-     1.0           0.0         0.0      0.0
 35-      0.0          0.0         0.0      0.0
 36-      0.0          0.0         0.0      0.0
 37-      0.0          0.0         0.0      0.0
 38-        1    1   10   11    2           1    1    3.28
 39-        2    2   11   12    3           1    1    3.28
 40-        3    3   12   13    4           1    1    3.28
 41-        4    4   13   14    5           1    1    3.28
 42-        5    5   14   15    6           1    1    3.28
 43-        6    6   15   16    7           1    1    3.28
 44-        7    7   16   17    8           1    1    3.28
 45-        8    8   17   18    9           1    1    3.28
 46-        9   10   19   20   11           1    1    3.28
 47-       10   11   20   21   12           1    1    3.28
 48-       11   12   21   22   13           1    1    3.28
 49-       12   13   22   23   14           1    1    3.28
 50-       13   14   23   24   15           1    1    3.28
```

Figure 4. USB Flap SAP IV Data Card Image

```
CARD                             D A T A   C A R D   I M A G E
 NO               1         2         3         4         5         6         7         8
         12345678901234567890123456789012345678901234567890123456789012345678901234567890
  51-      14   15   24   25   16        1    1    3.28
  52-      15   16   25   26   17        1    1    3.28
  53-      16   17   26   27   18        1    1    3.28
  54-
  55-
  56-       0    1         0.0      300.0
  57-        0.0       0.0      1.0       1
  58-           ACOUSTIC INPUT SPECTRUM (NED)
  59-       7    1.0
  60-      .000586  0.480
  61-      .001176  0.725
  62-      .002353  1.287
  63-      .004717  6.436
  64-      .009434  0.265
  65-      .018868  0.110
  66-      .033333  0.047
```


Figure 4. USB Flap SAP IV Data Card Image (Concluded)

PRINT OF FREQUENCIES

MODE NUMBER	CIRCULAR FREQUENCY (RAD/SEC)	FREQUENCY (CYCLES/SEC)	PERIOD (SEC)
1	1.9911E+02	3.1689E+01	3.1557E-02
2	2.3100E+02	3.6765E+01	2.7200E-02
3	2.5561E+02	4.0682E+01	2.4581E-02
4	4.9966E+02	7.9523E+01	1.2575E-02
5	7.7028E+02	1.2259E+02	8.1570E-03
6	8.0470E+02	1.2807E+02	7.8081E-03
7	1.0644E+03	1.6940E+02	5.9032E-03
8	1.4597E+03	2.3232E+02	4.3044E-03
9	1.6465E+03	2.6205E+02	3.8160E-03
10	1.7653E+03	2.8096E+02	3.5592E-03

Figure 5. USB Flap Mode Frequency Spectrum

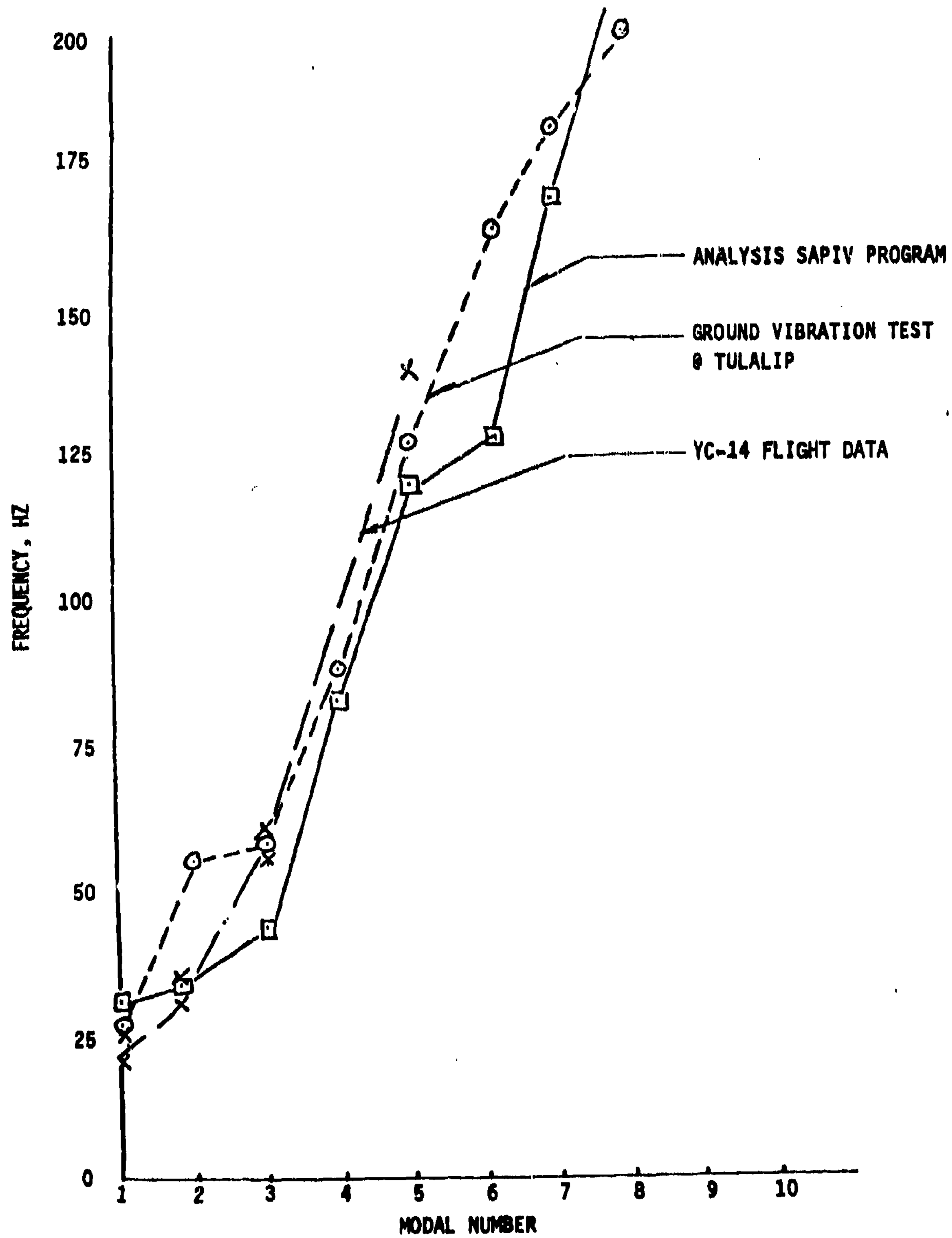

Figure 6. Comparison of Predicted and Measured YC-14 Flap Modal Properties

MODE DISPLACEMENTS/ROTATIONS

MODE NUMBER	EIGEN-VECTOR (MODE NUMBER)	X-TRANSLATION	Y-TRANSLATION	Z-TRANSLATION	X-ROTATION	Y-ROTATION	Z-ROTATION
1	1	.0	.0	-1.38687E+00	2.94576E-02	1.63608E-03	.0
	2	.0	.0	-4.41365E-01	8.08317E-03	-1.85087E-02	.0
	3	.0	.0	-9.63304E-01	2.37552E-02	1.34510E-02	.0
	4	.0	.0	1.97332E+00	-4.40696E-02	3.38639E-02	.0
	5	.0	.0	2.14197E+00	-5.34375E-02	4.65685E-02	.0
	6	.0	.0	-3.35280E-01	-1.22767E-02	-3.25751E-02	.0
	7	.0	.0	1.58329E+00	-2.45317E-02	6.34388E-02	.0
	8	.0	.0	7.36451E-01	6.46026E-03	5.10050E-02	.0
	9	.0	.0	6.39625E-02	5.75360E-02	6.12968E-02	.0
	10	.0	.0	-1.31332E+00	3.45600E-02	-9.42594E-02	.0
2	1	.0	.0	-5.45514E-01	2.79175E-02	1.74318E-03	.0
	2	.0	.0	-2.26241E-01	6.75630E-03	-1.54361E-02	.0
	3	.0	.0	-3.89752E-01	2.03746E-02	1.18999E-02	.0
	4	.0	.0	6.77165E-01	-4.11283E-02	2.27979E-02	.0
	5	.0	.0	8.45762E-01	-4.74621E-02	2.20970E-02	.0
	6	.0	.0	-5.18793E-01	2.44439E-03	-2.30872E-02	.0
	7	.0	.0	8.69752E-01	-3.51300E-02	2.46125E-02	.0
	8	.0	.0	6.51055E-01	-2.01869E-02	1.11487E-02	.0
	9	.0	.0	9.85694E-01	1.67308E-03	5.28031E-02	.0
	10	.0	.0	-4.20120E-01	2.86749E-02	-5.94484E-02	.0
3	1	.0	.0	.0	2.26143E-02	.0	.0
	2	.0	.0	.0	6.83815E-03	.0	.0
	3	.0	.0	.0	9.98599E-03	.0	.0
	4	.0	.0	.0 Fixed	-2.20752E-02	.0	.0
	5	.0	.0	.0 Hinge	-8.94123E-03	.0	.0
	6	.0	.0	.0 Point	4.19192E-02	.0	.0
	7	.0	.0	.0	-2.08565E-02	.0	.0
	8	.0	.0	.0	-7.61447E-03	.0	.0
	9	.0	.0	.0	-6.19774E-02	.0	.0
	10	.0	.0	.0	-5.95219E-03	.0	.0
4	1	.0	.0	4.64588E-02	1.27875E-02	3.64346E-03	.0
	2	.0	.0	6.94224E-02	1.92213E-03	-1.47400E-02	.0
	3	.0	.0	1.10091E-01	-1.51100E-03	5.14245E-03	.0
	4	.0	.0	-2.00229E-01	2.27908E-03	2.85754E-03	.0
	5	.0	.0	3.01261E-01	2.06239E-02	-6.77383E-03	.0
	6	.0	.0	1.36366E+00	5.04926E-02	3.57236E-02	.0
	7	.0	.0	-1.19199E-01	4.12278E-03	-1.83959E-02	.0
	8	.0	.0	4.39145E-01	2.50532E-02	1.03727E-02	.0
	9	.0	.0	-1.14426E+00	-1.14151E-03	-1.71487E-02	.0
	10	.0	.0	-6.07567E-01	-2.70348E-02	-6.55232E-02	.0

Figure 7. USB Flap Mode Shapes

MODE NUMBER	EIGEN-VECTOR	X-TRANSLATION	Y-TRANSLATION	Z-TRANSLATION	X-ROTATION	Y-ROTATION	Z-ROTATION
5	1	.0	.0	6.31858E-01	-1.78394E-14	4.32536E-03	.0
	2	.0	.0	9.20885E-02	-1.60336E-12	-1.69650E-02	.0
	3	.0	.0	-3.34540E-12	-6.13521E-03	4.68143E-13	.0
	4	.0	.0	1.70564E-11	1.02322E-02	1.51026E-13	.0
	5	.0	.0	6.21815E-01	-2.99291E-14	-3.79885E-03	.0
	6	.0	.0	2.08147E+00	1.63885E-15	5.44152E-02	.0
	7	.0	.0	3.41664E-11	4.67620E-03	1.43124E-12	.0
	8	.0	.0	8.22735E-01	-3.38684E-13	3.52324E-02	.0
	9	.0	.0	-1.76667E-10	6.97732E-02	-1.40797E-11	.0
	10	.0	.0	-1.06066E+00	-6.70268E-11	-8.46840E-02	.0
6	1	.0	.0	4.64568E-01	-1.27835E-02	3.64346E-03	.0
	2	.0	.0	6.94224E-02	-1.92213E-03	-1.47400E-02	.0
	3	.0	.0	-1.10091E-01	-1.51100E-03	-5.14245E-03	.0
	4	.0	.0	2.09229E-01	2.27998E-03	-2.85754E-03	.0
	5	.0	.0	3.01261E-01	-2.06239E-02	-6.77383E-03	.0
	6	.0	.0	1.36386E+00	-5.04928E-02	3.57236E-02	.0
	7	.0	.0	1.19199E-01	4.12278E-03	1.83959E-02	.0
	8	.0	.0	4.39145E-01	-2.50532E-02	1.03727E-02	.0
	9	.0	.0	1.14426E+00	-1.14151E-03	1.71487E-02	.0
	10	.0	.0	-6.07567E-01	2.78348E-02	-6.55232E-02	.0
7	1	.0	.0	.0	-2.26143E-02	.0	.0
	2	.0	.0	.0	-6.03815E-03	.0	.0
	3	.0	.0	.0	9.98599E-03	.0	.0
	4	.0	.0	.0 Fixed	-2.28752E-02	.0	.0
	5	.0	.0	.0 Hinge	8.94123E-03	.0	.0
	6	.0	.0	.0 Point	-4.19192E-02	.0	.0
	7	.0	.0	.0	-2.08565E-02	.0	.0
	8	.0	.0	.0	7.61447E-03	.0	.0
	9	.0	.0	.0	-6.19774E-02	.0	.0
	10	.0	.0	.0	5.95219E-03	.0	.0
8	1	.0	.0	-6.49514E-01	-2.79175E-02	1.79318E-03	.0
	2	.0	.0	-2.26241E-01	-6.75636E-03	-1.54361E-02	.0
	3	.0	.0	3.89752E-01	2.03746E-02	-1.18999E-02	.0
	4	.0	.0	-8.77165E-01	-4.11283E-02	-2.27979E-02	.0
	5	.0	.0	8.40762E-01	4.74621E-02	2.20970E-02	.0
	6	.0	.0	-5.18793E-01	-2.44439E-03	-2.30872E-02	.0
	7	.0	.0	-6.69752E-01	-3.51300E-02	-2.45125E-02	.0
	8	.0	.0	6.51855E-01	2.01869E-02	1.11487E-02	.0
	9	.0	.0	-9.85694E-01	1.67308E-03	-5.28831E-02	.0
	10	.0	.0	-4.20120E-01	-2.66749E-02	-5.94484E-02	.0
9	1	.0	.0	-1.33687E+00	-2.94976E-02	1.63806E-03	.0

Figure 7. USB Flap Mode Shapes (Continued)

MODE NUMBER	EIGEN-VECTOR	X-TRANSLATION	Y-TRANSLATION	Z-TRANSLATION	X-ROTATION	Y-ROTATION	Z-ROTATION
	2	.0	.0	-4.41365E-01	-8.08317E-03	-1.85887E-02	.0
	3	.0	.0	9.63384E-01	2.37552E-02	-1.34510E-02	.0
	4	.0	.0	-1.97332E+00	-4.48646E-02	-3.38839E-02	.0
	5	.0	.0	2.14197E+00	5.34375E-02	4.65685E-02	.0
	6	.0	.0	-3.35280E-01	1.22737E-02	-3.25751E-02	.0
	7	.0	.0	-1.58329E+00	-2.45317E-02	-6.34388E-02	.0
	8	.0	.0	7.36451E-01	-6.46026E-03	5.10050E-02	.0
	9	.0	.0	-6.39825E-02	5.75360E-02	-6.12958E-02	.0
	10	.0	.0	-1.31332E+00	-3.45600E-02	-9.42594E-02	.0
10	1	.0	.0	-1.43719E+00	2.94678E-02	1.61604E-03	.0
	2	.0	.0	1.66788E-01	6.13868E-03	-2.23277E-02	.0
	3	.0	.0	-1.32727E+00	2.51237E-02	1.48165E-02	.0
	4	.0	.0	8.95563E-01	-3.44450E-02	3.92333E-02	.0
	5	.0	.0	6.96088E-01	-2.89097E-02	5.20241E-02	.0
	6	.0	.0	5.75237E-01	-2.54354E-02	-2.72319E-02	.0
	7	.0	.0	-2.63876E-01	2.13177E-02	5.99120E-02	.0
	8	.0	.0	-6.96686E-01	5.84829E-02	4.11478E-02	.0
	9	.0	.0	-1.19975E+00	7.45496E-02	5.86144E-03	.0
	10	.0	.0	6.53853E-01	-4.67435E-03	-1.24866E-02	.0
11	1	.0	.0	-6.98601E-01	2.80235E-02	1.68330E-03	.0
	2	.0	.0	3.11385E-01	4.80873E-03	-2.23249E-02	.0
	3	.0	.0	-7.62667E-01	2.33724E-02	1.41412E-02	.0
	4	.0	.0	8.56502E-02	-2.69740E-02	3.15762E-02	.0
	5	.0	.0	6.61877E-02	-1.73608E-02	2.95936E-02	.0
	6	.0	.0	2.38727E-02	-1.50864E-02	-1.35461E-02	.0
	7	.0	.0	2.11204E-01	1.59805E-02	1.71433E-02	.0
	8	.0	.0	4.83920E-01	2.58651E-02	-2.76454E-03	.0
	9	.0	.0	1.28557E-01	2.08251E-02	5.66643E-04	.0
	10	.0	.0	7.35859E-01	2.85660E-03	-1.12611E-03	.0
12	1	.0	.0	-5.86916E-02	2.28753E-02	1.74392E-03	.0
	2	.0	.0	4.52121E-01	5.80661E-03	-2.19247E-02	.0
	3	.0	.0	-2.76622E-01	1.41842E-02	1.19551E-02	.0
	4	.0	.0	-4.08078E-01	-9.96044E-03	2.17729E-02	.0
	5	.0	.0	-3.06540E-02	1.05883E-02	7.27500E-03	.0
	6	.0	.0	-6.58456E-02	8.75479E-03	7.83213E-03	.0
	7	.0	.0	4.70571E-01	5.53665E-03	-1.81622E-02	.0
	8	.0	.0	6.02335E-01	-1.28128E-02	-1.91743E-02	.0
	9	.0	.0	-2.66343E-01	-3.64955E-02	-3.96139E-03	.0
	10	.0	.0	7.78794E-01	-2.06599E-03	6.93011E-04	.0
13	1	.0	.0	3.98801E-01	1.19169E-02	1.67322E-03	.0
	2	.0	.0	5.94821E-01	5.34138E-03	-2.18858E-02	.0

Figure 7. USB Flap Mode Shapes (Continued)

MODE NUMBER	EIGEN-VECTOR	X-TRANSLATION	Y-TRANSLATION	Z-TRANSLATION	X-ROTATION	Y-ROTATION	Z-ROTATION
	3	.0	.0	-4.93475E-02	3.82094E-03	6.72818E-03	.0
	4	.0	.0	-3.98264E-01	9.40839E-03	1.10835E-02	.0
	5	.0	.0	4.68186E-01	2.25672E-02	-4.50530E-03	.0
	6	.0	.0	3.50662E-01	1.87952E-02	3.43750E-02	.0
	7	.0	.0	4.39349E-01	-8.83276E-03	-2.19057E-02	.0
	8	.0	.0	1.18842E-01	-1.78086E-02	1.09347E-02	.0
	9	.0	.0	-9.18333E-01	3.25721E-03	-6.12075E-03	.0
	10	.0	.0	6.67460E-01	-3.09658E-03	-5.50892E-03	.0
14	1	.0	.0	5.45776E-01	-1.11026E-15	1.55968E-03	.0
	2	.0	.0	6.63071E-01	2.05160E-13	-2.16359E-02	.0
	3	.0	.0	-1.91667E-11	8.10231E-04	6.01799E-13	.0
	4	.0	.0	1.42106E-11	1.85093E-02	8.19367E-14	.0
	5	.0	.0	8.04644E-01	1.28100E-13	-6.65352E-03	.0
	6	.0	.0	6.31966E-01	-2.95941E-15	4.70686E-02	.0
	7	.0	.0	-5.76372E-12	-2.17868E-02	1.47142E-12	.0
	8	.0	.0	-1.55464E-01	-3.19318E-13	3.55870E-02	.0
	9	.0	.0	9.82329E-11	5.45688E-02	-1.46972E-12	.0
	10	.0	.0	5.91190E-01	-2.42413E-11	-8.91246E-03	.0
15	1	.0	.0	3.90881E-01	-1.19169E-02	1.67322E-03	.0
	2	.0	.0	5.94821E-01	-5.34138E-03	-2.18698E-02	.0
	3	.0	.0	4.93475E-02	3.82094E-03	-6.72818E-03	.0
	4	.0	.0	3.98264E-01	9.40839E-03	-1.10835E-02	.0
	5	.0	.0	4.69186E-01	-2.25672E-02	-4.50530E-03	.0
	6	.0	.0	3.50662E-01	-1.87952E-02	3.43750E-02	.0
	7	.0	.0	-4.39349E-01	-8.83276E-03	2.19057E-02	.0
	8	.0	.0	1.18842E-01	1.78086E-02	1.09347E-02	.0
	9	.0	.0	9.18333E-01	3.25721E-03	6.12075E-03	.0
	10	.0	.0	6.67460E-01	3.09658E-03	-5.50892E-03	.0
16	1	.0	.0	-5.06916E-02	-2.20753E-02	1.74392E-03	.0
	2	.0	.0	4.52121E-01	-5.00661E-03	-2.19247E-02	.0
	3	.0	.0	2.76022E-01	1.41842E-02	-1.19551E-02	.0
	4	.0	.0	4.08078E-01	-9.96044E-03	-2.17729E-02	.0
	5	.0	.0	-3.86540E-02	-1.05683E-02	7.17590E-03	.0
	6	.0	.0	-6.58456E-02	-8.76473E-03	7.83210E-03	.0
	7	.0	.0	-4.70971E-01	5.53665E-03	1.81622E-02	.0
	8	.0	.0	6.02335E-01	1.28138E-02	-1.91743E-02	.0
	9	.0	.0	2.66347E-01	-3.64955E-02	3.96139E-03	.0
	10	.0	.0	7.78794E-01	2.06509E-03	6.93011E-04	.0
17	1	.0	.0	-6.98601E-01	-2.80235E-02	1.68386E-03	.0
	2	.0	.0	3.11305E-01	-4.60873E-03	-2.28240E-02	.0
	3	.0	.0	7.62667E-01	2.33724E-02	-1.41412E-02	.0

Figure 7. USB Flap Mode Shapes (Continued)

MODE NUMBER	EIGEN-VECTOR	X-TRANSLATION	Y-TRANSLATION	Z-TRANSLATION	X-ROTATION	Y-ROTATION	Z-ROTATION
	4	.0	.0	-8.56502E-02	-2.69740E-02	-3.15762E-02	.0
	5	.0	.0	6.61477E-02	1.73608E-02	2.95534E-02	.0
	6	.0	.0	2.30727E-02	1.50564E-02	-1.35461E-02	.0
	7	.0	.0	-2.11204E-01	1.39385E-02	-1.71403E-02	.0
	8	.0	.0	4.83920E-01	-2.58651E-02	-2.76454E-03	.0
	9	.0	.0	-1.28557E-01	2.00251E-02	-5.86043E-04	.0
	10	.0	.0	7.35059E-01	-2.85668E-03	-1.12611E-03	.0
18	1	.0	.0	-1.43719E+00	-2.94870E-02	1.61684E-03	.0
	2	.0	.0	1.66706E-01	-6.13888E-03	-2.23277E-02	.0
	3	.0	.0	1.38727E+00	2.51237E-02	-1.46165E-02	.0
	4	.0	.0	-8.95563E-01	-3.44450E-02	-3.92333E-02	.0
	5	.0	.0	6.96080E-01	2.89097E-02	5.29241E-02	.0
	6	.0	.0	5.75237E-01	2.54354E-02	-2.72319E-02	.0
	7	.0	.0	2.63076E-01	2.13177E-02	-5.99120E-02	.0
	8	.0	.0	-6.96606E-01	-5.84829E-02	4.11478E-02	.0
	9	.0	.0	1.15979E+00	7.45496E-02	-5.86154E-03	.0
	10	.0	.0	6.53853E-01	4.67435E-03	-1.24866E-02	.0
19	1	.0	.0	-1.47948E+00	2.96839E-02	1.26015E-03	.0
	2	.0	.0	8.74988E-01	5.82572E-03	-2.43768E-02	.0
	3	.0	.0	-1.83415E+00	2.62246E-02	1.49171E-02	.0
	4	.0	.0	-3.57595E-01	-2.75939E-02	4.35500E-02	.0
	5	.0	.0	-9.71288E-01	-7.22556E-03	5.85079E-02	.0
	6	.0	.0	1.28206E+00	-4.10914E-02	-2.15126E-02	.0
	7	.0	.0	-2.02681E+00	6.80145E-02	5.84510E-02	.0
	8	.0	.0	-1.77796E+00	1.10772E-01	3.40608E-02	.0
	9	.0	.0	-2.57649E-01	7.48711E-02	-5.23800E-02	.0
	10	.0	.0	-6.32392E-01	-4.61772E-03	7.59425E-02	.0
20	1	.0	.0	-7.35463E-01	2.82177E-02	7.84699E-04	.0
	2	.0	.0	1.02123E+00	5.65045E-03	-2.46338E-02	.0
	3	.0	.0	-1.17885E+00	2.46919E-02	1.36056E-02	.0
	4	.0	.0	-9.83289E-01	-1.87054E-02	3.91147E-02	.0
	5	.0	.0	-1.02135E+00	8.38658E-03	4.17921E-02	.0
	6	.0	.0	2.79953E-01	-3.64824E-02	-5.24121E-03	.0
	7	.0	.0	-3.35913E-01	6.35408E-02	1.73840E-02	.0
	8	.0	.0	6.20698E-01	6.43738E-02	-1.31026E-02	.0
	9	.0	.0	1.09212E+00	1.62714E-02	-5.92981E-02	.0
	10	.0	.0	-6.58238E-01	1.48962E-03	7.59950E-02	.0
21	1	.0	.0	-7.67231E-02	2.26232E-02	-1.29185E-04	.0
	2	.0	.0	1.16957E+00	5.92178E-03	-2.51321E-02	.0
	3	.0	.0	-6.15776E-01	1.87158E-02	1.86345E-02	.0
	4	.0	.0	-1.20294E+00	2.76963E-03	3.09602E-02	.0

Figure 7. USB Flap Mode Shapes (Cont.)

MODE NUMBER	EIGEN-VECTOR	X-TRANSLATION	Y-TRANSLATION	Z-TRANSLATION	X-ROTATION	Y-ROTATION	Z-ROTATION
	5	.0	.0	-4.49612E-01	3.46310E-02	1.88453E-02	.0
	6	.0	.0	-4.78005E-01	-2.94530E-02	1.84501E-02	.0
	7	.0	.0	9.50261E-01	3.24191E-02	-2.15576E-02	.0
	8	.0	.0	1.66328E+00	-3.07766E-02	-2.11426E-02	.0
	9	.0	.0	4.41835E-01	-5.13757E-02	-3.69125E-02	.0
	10	.0	.0	-5.90398E-01	2.24424E-03	7.28895E-02	.0
22	1	.0	.0	3.79297E-01	1.25296E-02	-1.08924E-03	.0
	2	.0	.0	1.30856E+00	4.50180E-03	-2.51507E-02	.0
	3	.0	.0	-2.37121E-01	1.12728E-02	5.69589E-03	.0
	4	.0	.0	-8.24007E-01	2.56205E-02	1.72352E-02	.0
	5	.0	.0	5.25594E-01	3.46815E-02	-2.18935E-03	.0
	6	.0	.0	-7.70356E-01	-4.01206E-03	4.04190E-02	.0
	7	.0	.0	1.11103E+00	-2.38241E-02	-2.75327E-02	.0
	8	.0	.0	-4.61857E-01	-6.68835E-02	2.60574E-02	.0
	9	.0	.0	-6.15642E-01	-9.42237E-03	-5.80316E-03	.0
	10	.0	.0	-5.57261E-01	2.30034E-04	6.86796E-02	.0
23	1	.0	.0	5.41629E-01	1.68663E-14	-1.51161E-03	.0
	2	.0	.0	1.37028E+00	2.14642E-12	-2.50056E-02	.0
	3	.0	.0	-3.88736E-11	8.26709E-03	6.97143E-13	.0
	4	.0	.0	1.18629E-11	3.55168E-02	3.70837E-14	.0
	5	.0	.0	1.02377E+00	2.36905E-13	-1.04619E-02	.0
	6	.0	.0	-8.00546E-01	-2.03840E-15	4.93956E-02	.0
	7	.0	.0	-6.16194E-11	-5.36621E-02	2.45502E-12	.0
	8	.0	.0	-1.49166E+00	-2.71144E-13	5.87607E-02	.0
	9	.0	.0	-9.24986E-11	4.43158E-02	1.11350E-11	.0
	10	.0	.0	-5.57971E-01	-1.50550E-10	6.70465E-02	.0
24	1	.0	.0	3.79297E-01	-1.25298E-02	-1.08924E-03	.0
	2	.0	.0	1.30856E+00	-4.50180E-03	-2.51507E-02	.0
	3	.0	.0	2.37121E-01	1.12728E-02	-5.69589E-03	.0
	4	.0	.0	8.24007E-01	2.56205E-02	-1.72352E-02	.0
	5	.0	.0	5.25594E-01	-3.46815E-02	-2.18935E-03	.0
	6	.0	.0	-7.70356E-01	4.01206E-03	4.04190E-02	.0
	7	.0	.0	-1.11103E+00	-2.38241E-02	2.75327E-02	.0
	8	.0	.0	-4.61857E-01	6.68835E-02	2.60574E-02	.0
	9	.0	.0	6.15642E-01	-9.42237E-03	5.80316E-03	.0
	10	.0	.0	-5.57261E-01	-2.30034E-04	6.86796E-02	.0
25	1	.0	.0	-7.67231E-02	-2.26232E-02	-1.29185E-04	.0
	2	.0	.0	1.16957E+00	-5.92170E-03	-2.51321E-02	.0
	3	.0	.0	6.15776E-01	1.87150E-02	-1.06345E-02	.0
	4	.0	.0	1.20294E+00	2.78963E-03	-3.09602E-02	.0
	5	.0	.0	-4.49612E-01	-3.46310E-02	1.88453E-02	.0

Figure 7. USB Flap Mode Shapes (Cont.)

Node Displacements/Rotations

NODE NUMBER	EIGEN-VECTOR	X-TRANSLATION	Y-TRANSLATION	Z-TRANSLATION	X-ROTATION	Y-ROTATION	Z-ROTATION
	6	.0	.0	-4.76905E-01	2.04530E-02	1.84501E-02	.0
	7	.0	.0	-9.90261E-01	3.24191E-02	2.15976E-02	.0
	8	.0	.0	1.06328E+00	3.87766E-02	-2.11426E-02	.0
	9	.0	.0	-4.41835E-01	-5.13737E-02	3.69125E-02	.0
	10	.0	.0	-5.90398E-01	-2.24424E-03	7.28858E-02	.0
26	1	.0	.0	-7.35463E-01	-2.62177E-02	7.84699E-04	.0
	2	.0	.0	1.02123E+00	-5.65045E-03	-2.46330E-02	.0
	3	.0	.0	1.17885E+00	2.46915E-02	-1.36056E-02	.0
	4	.0	.0	9.85205E-01	-1.67054E-02	-3.91147E-02	.0
	5	.0	.0	-1.02135E+00	-8.30658E-03	4.17921E-02	.0
	6	.0	.0	2.79553E-01	3.64624E-02	-5.24121E-03	.0
	7	.0	.0	3.35913E-01	6.35406E-02	-1.73848E-02	.0
	8	.0	.0	6.20698E-01	-6.43738E-02	-1.31026E-02	.0
	9	.0	.0	-1.09212E+00	1.62714E-02	5.92901E-02	.0
	10	.0	.0	-6.56238E-01	-1.48962E-03	7.55950E-02	.0
27	1	.0	.0	-1.47940E+00	-2.90835E-02	1.25015E-03	.0
	2	.0	.0	8.74588E-01	-5.62572E-03	-2.43788E-02	.0
	3	.0	.0	1.83415E+00	2.62246E-02	-1.43171E-02	.0
	4	.0	.0	3.57595E-01	-2.75935E-02	-4.35900E-02	.0
	5	.0	.0	-9.71288E-01	7.22556E-03	5.65079E-02	.0
	6	.0	.0	1.28206E+00	4.10914E-02	-2.16126E-02	.0
	7	.0	.0	2.02001E+00	6.80145E-02	-5.85510E-02	.0
	8	.0	.0	-1.77756E+00	-1.10772E-01	3.40608E-02	.0
	9	.0	.0	2.57649E-01	7.48711E-02	5.23600E-02	.0
	10	.0	.0	-6.32392E-01	4.61772E-03	7.59425E-02	.0

E I G E N S O L U T I O N   T I M E   L O G

EIGENSOLUTION = 5.13
PRINTING = .26

Figure 7. USB Flap Mode Shapes (Concluded)

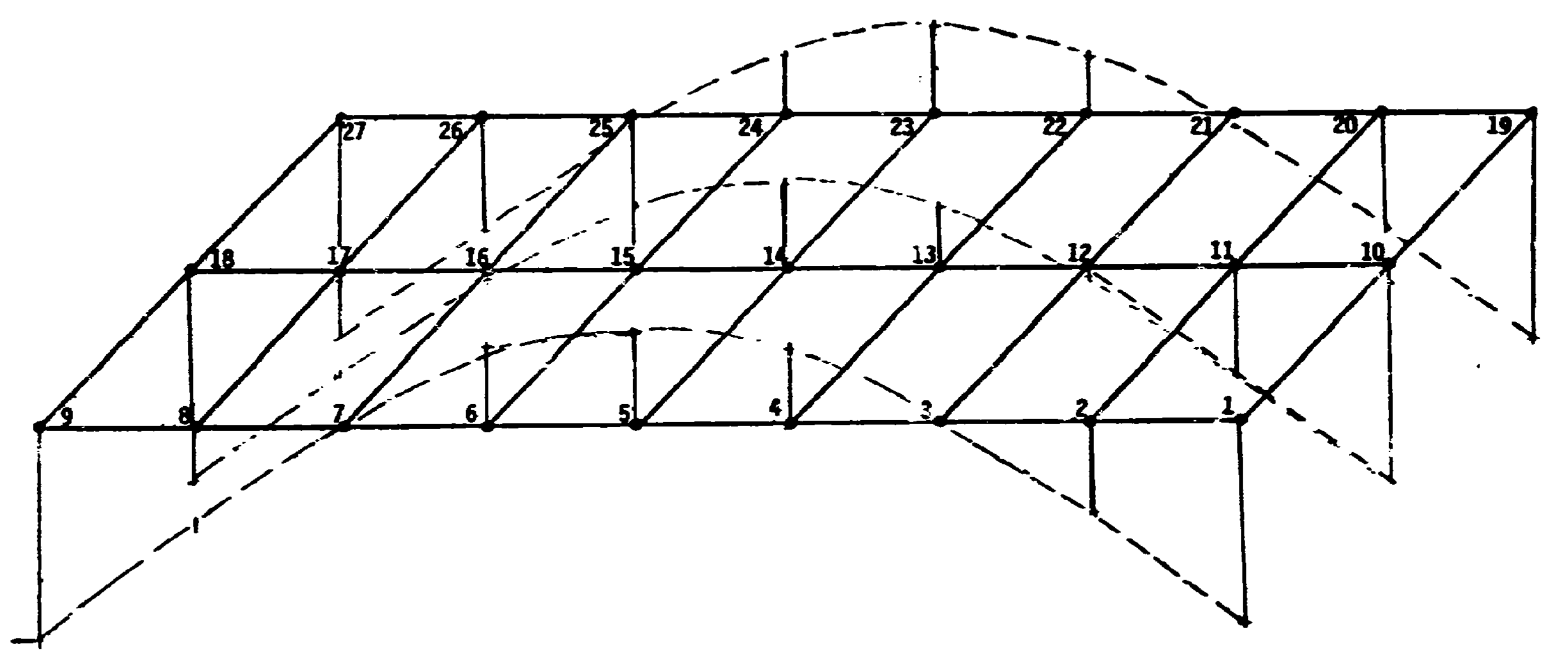

Figure 8. USB Flap Mode 1, 31.689 Hz

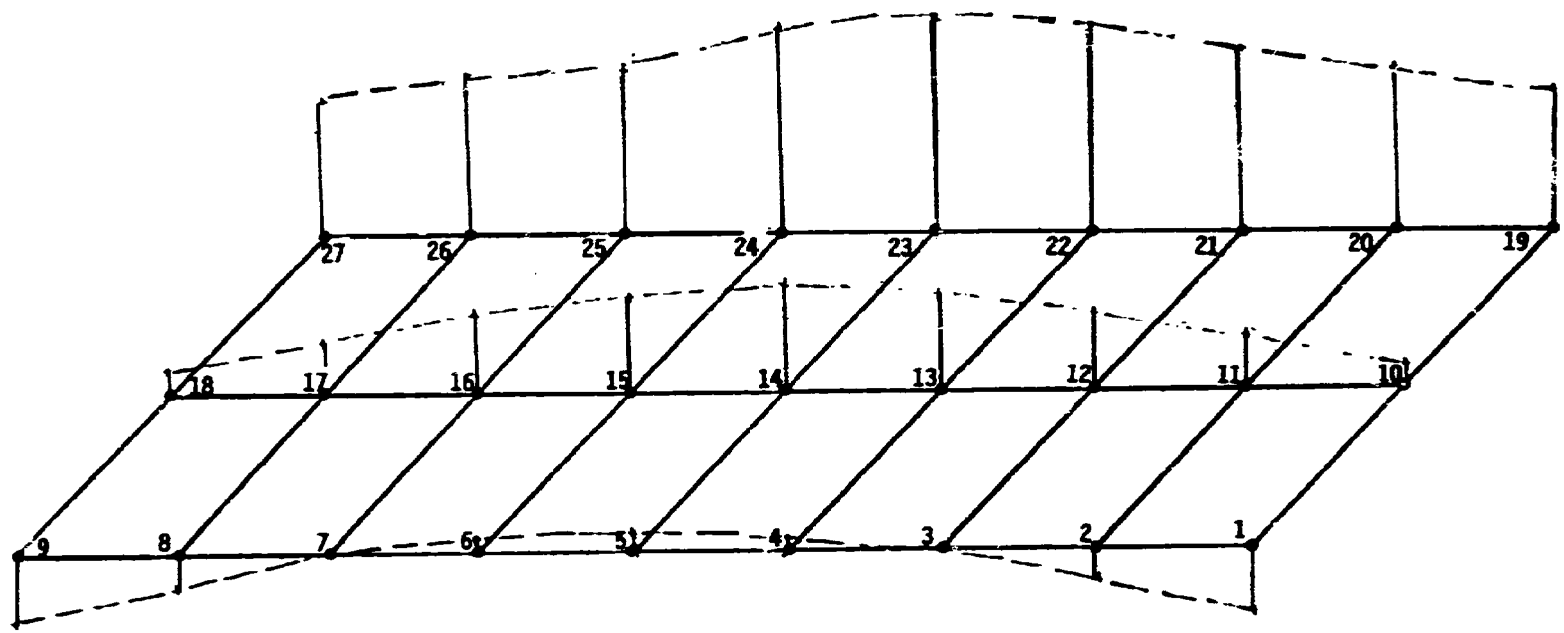

Figure 9. USB Flap Mode 2, 36.765 Hz

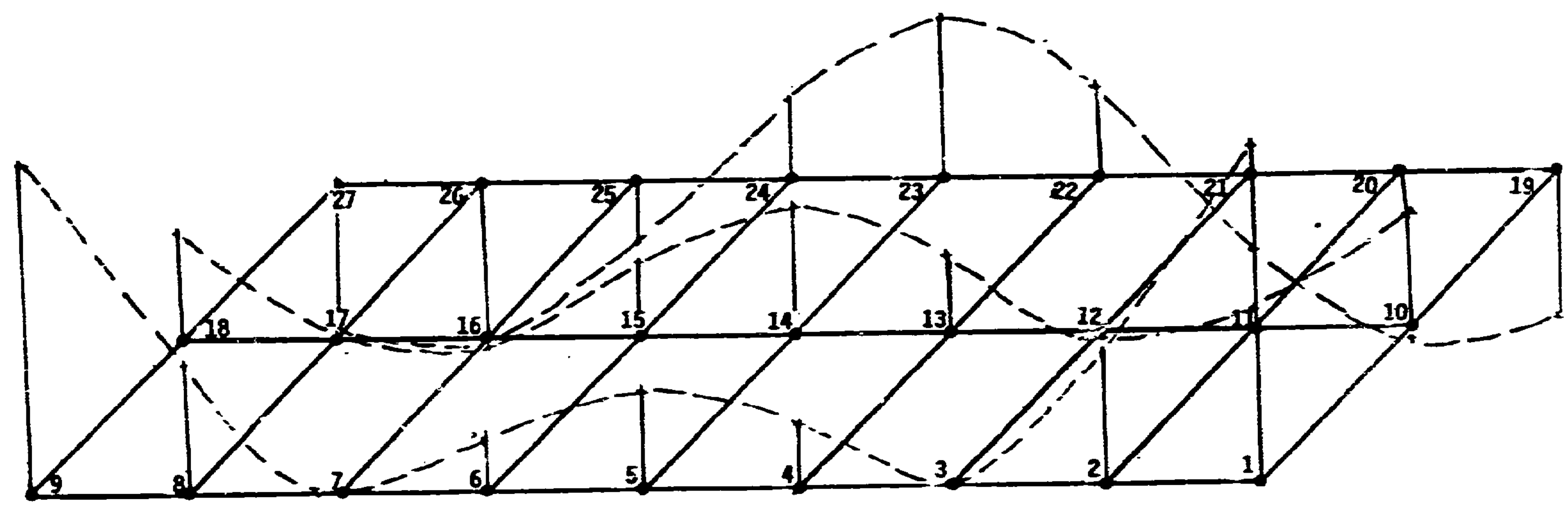

Figure 10. USB Flap Mode 5, 122.59 Hz

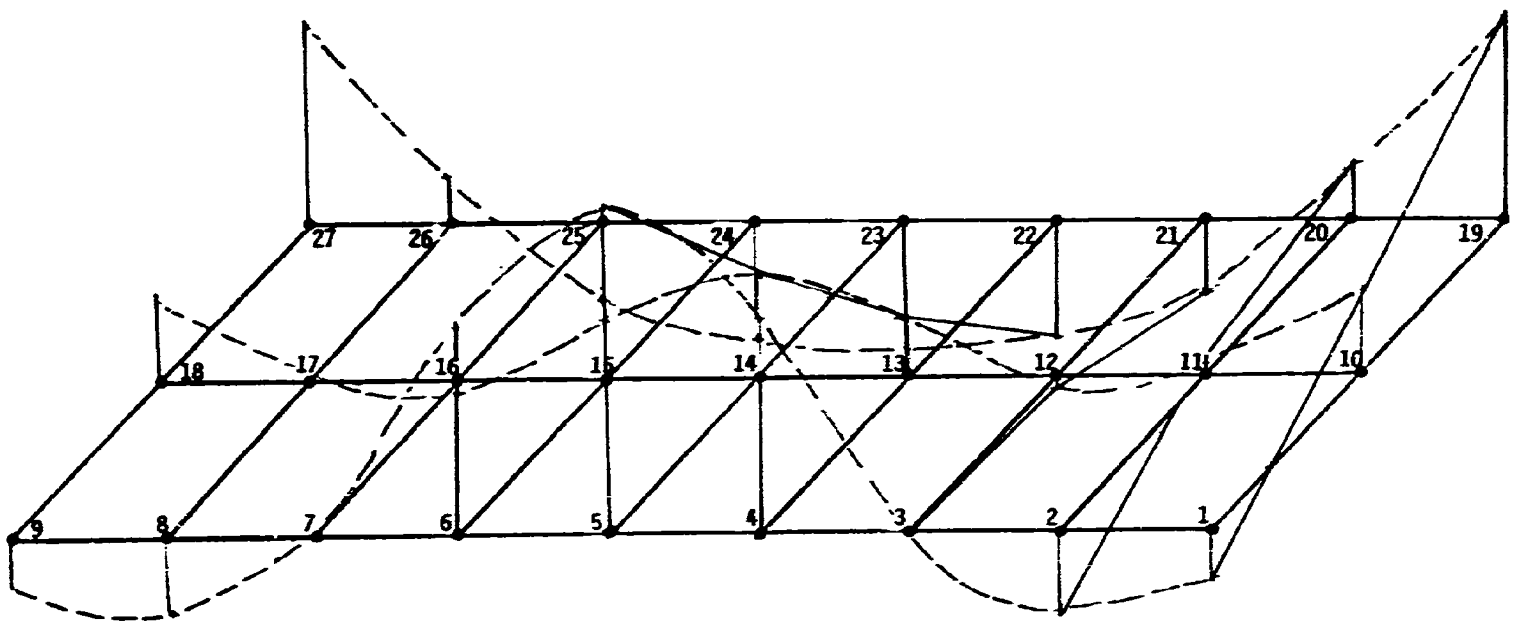

Figure 11. USB Flap Mode 6, 128.07 Hz

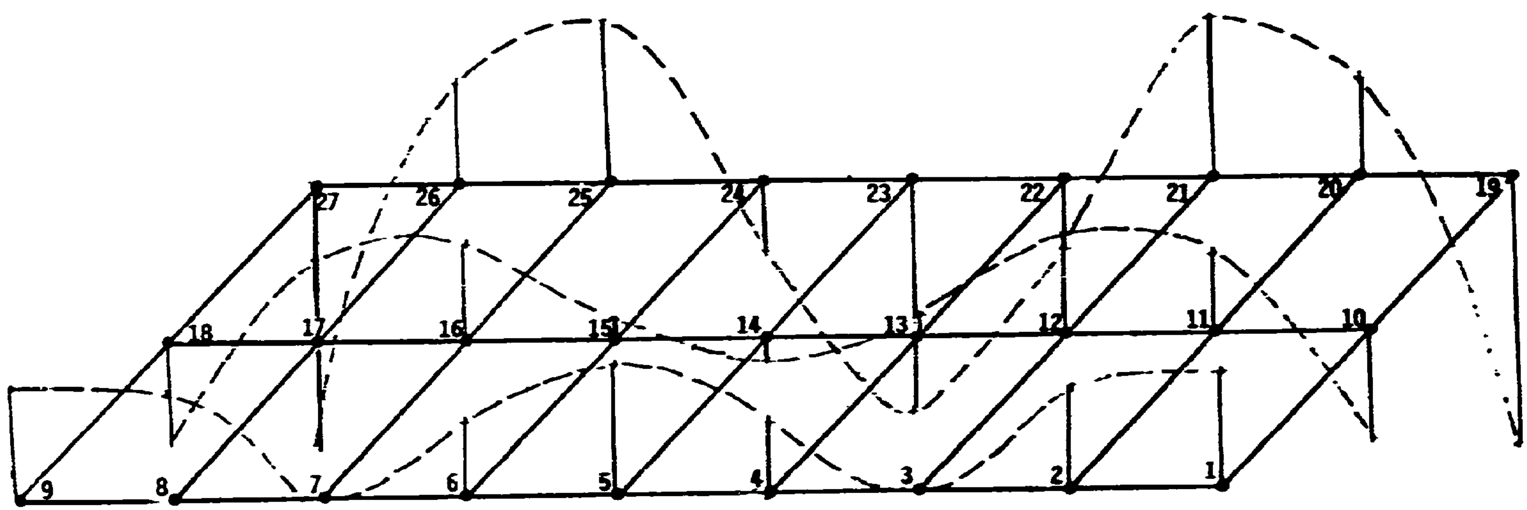

Figure 12. USB Flap Mode 8, 232.32 Hz

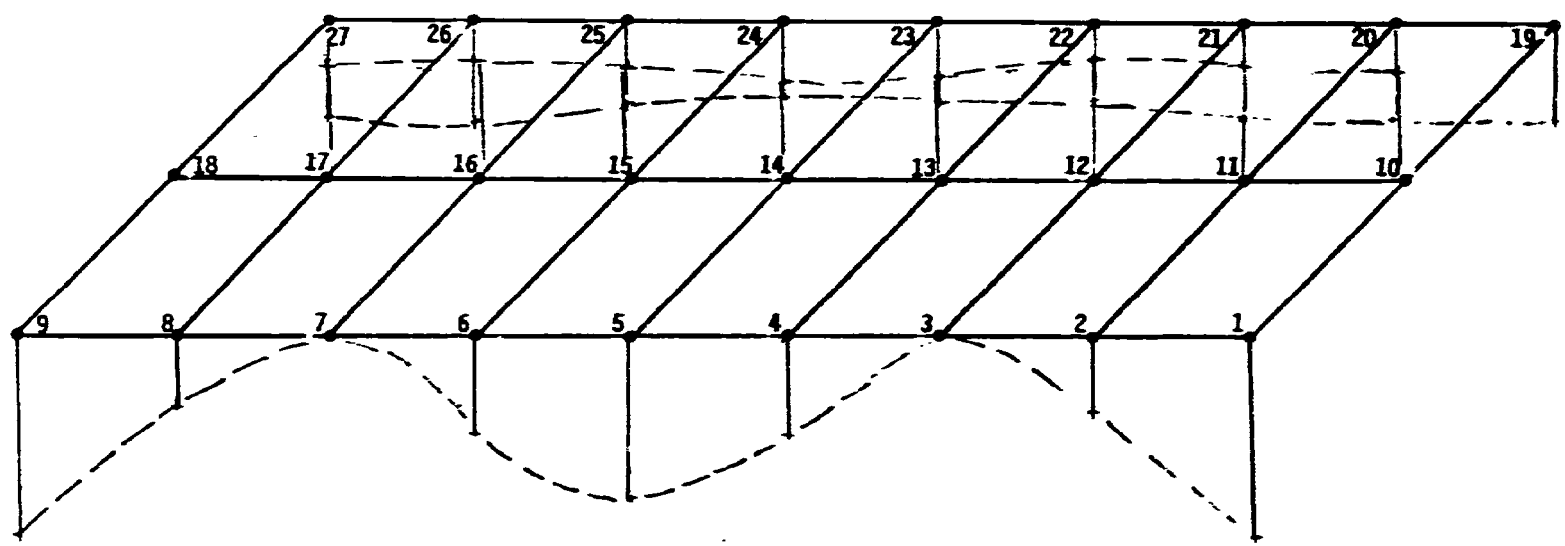

Figure 13. USB Flap Mode 10, 280.96 Hz

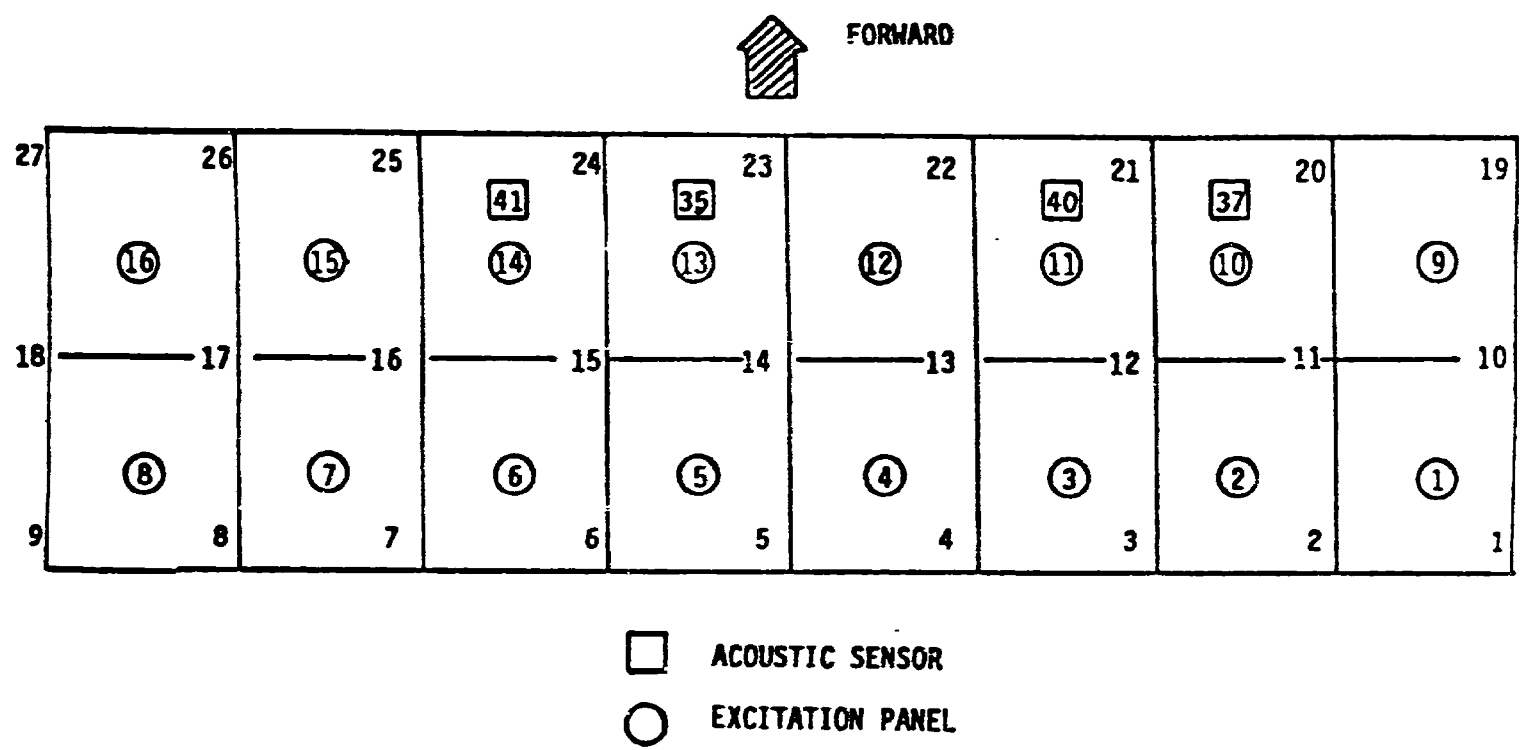

Figure 14. USB Flap with Pressure Transducer

O MEASURED DATA

X EXTRAPOLATED DATA

1	2	3	4	5	6	7	8	9	10	11	12	13	14	15	16	
X	X	X	X	X				X	X							1
	X	X	X	X	X			X	X	X						2
		X	X	X	X	X			X	X	X					3
			X	X	X	X	X			X	X	X				4
				X	X	X	X				X	X	X			5
					X	X	X					X	X	X		6
						X	X						X	X	X	7
							X							X	X	8
								X	X	X	X	X				9
									O	X	X	X	O			10
										O	X	X	O	X		11
											X	X	X	X	X	12
												O	O	X	X	13
													O	X	X	14
														X	X	15
															X	16

Figure 15. Map of Upper Triangle of the CPSD Matrix for Model I

```
-----------------------------------------------------------------
CASE WITH DENSE CPSD MATRIX

RESULTS FOR LOAD SET NO.   1
-----------------------------------------------------------------
FREQ(  1) = 26.0000 CYCLES/SEC.  (163.3629 RAD./SEC.)

             LOADS                MAGNITUDE    PHASE ANGLE  OUTPUT SPECTRUM

1  4.20446E-01 -3.10586E-02   4.21591E-01   6.20945E+00   4.45530E-05  RAD/HZ
2  8.68226E-01 -6.58905E-02   8.70723E-01   6.20744E+00   1.44707E-04
3  6.27072E-01 -7.73540E-02   6.31825E-01   6.16045E+00   8.78214E-05
-----------------------------------------------------------------
FREQ(  2) = 27.0000 CYCLES/SEC.  (169.6461 RAD./SEC.)

             LOADS                MAGNITUDE    PHASE ANGLE  OUTPUT SPECTRUM

1  5.12306E-01 -4.35952E-02   5.14183E-01   6.19771E+00   5.95748E-05
2  1.06409E+00 -9.41555E-02   1.06825E+00   6.19493E+00   1.94427E-04
3  8.72508E-01 -1.26749E-01   8.81666E-01   6.13892E+00   1.29991E-04
-----------------------------------------------------------------
FREQ(  3) = 28.0000 CYCLES/SEC.  (175.9293 RAD./SEC.)

             LOADS                MAGNITUDE    PHASE ANGLE  OUTPUT SPECTRUM

1  6.41327E-01 -6.70450E-02   6.44822E-01   6.17902E+00   8.11786E-05
2  1.34253E+00 -1.45753E-01   1.35041E+00   6.17504E+00   2.66944E-04
3  1.27335E+00 -2.26209E-01   1.29329E+00   6.10737E+00   2.05109E-04
-----------------------------------------------------------------
FREQ(  4) = 29.0000 CYCLES/SEC.  (182.2125 RAD./SEC.)
```

Figure 16. Example of Print-Out for Three Accelerometer Locations for Model I

FREQUENCY (HZ)	DIAGONAL CPSD MATRIX					
	1 1421 (10-3)		2 1417 (10-3)		3 1428 (10-3)	
	G^2/RAD	G^2/HZ	G^2/RAD	G^2/HZ	G^2/RAD	G^2/HZ
26	.044	.28	.145	.91	.088	.055
27	.059	.37	.194	1.22	.130	.82
28	.081	.51	.267	1.68	.205	1.29
29	.114	.72	.380	2.39	.363	2.28
30	.170	1.07	.588	3.69	.821	5.16
31	.322	2.02	1.247	7.84	3.410	21.43
32	.636	4.00	2.604	16.36	8.171	51.34
33	.660	4.15	2.234	14.04	2.172	13.65
34	1.177	7.40	3.836	24.10	1.966	12.35
35	2.821	17.72	9.104	57.20	3.725	23.40
36	11.265	70.78	36.255	227.80	13.920	87.46
37	29.75	186.92	95.70	601.30	37.15	233.42
38	6.53	41.03	21.06	132.32	8.98	56.42
39	3.27	20.55	10.61	66.66	5.74	36.07
40	5.51	34.62	18.11	113.79	12.68	79.67
42	2.74	17.22	9.02	56.67	5.82	36.57
43	1.34	8.42	4.41	27.71	2.56	16.08
45	.648	4.07	2.13	13.38	1.07	6.72
50	.307	1.93	1.009	6.34	.417	2.62
60	.192	1.21	.620	3.90	.236	1.48
70	.433	2.72	1.260	7.92	.323	2.03
75	1.960	12.32	5.38	33.80	.898	5.64
76	3.217	20.21	8.783	55.19	1.356	8.52
77	5.97	37.51	16.21	101.85	2.345	14.23
78	13.048	81.98	35.230	221.36	4.867	30.58
79	30.497	191.62	82.315	517.20	11.002	69.13
80	33.669	211.55	90.780	570.	11.978	75.26
81	16.47	103.48	44.44	279.	5.88	36.95

Figure 17. YC-14 Flap Accelerometer Response Predictions, G=.03

FREQUENCY (HZ)	DIAGONAL CPSD MATRIX 1 1421 (10^{-3}) G^2/RAD	G^2/HZ	2 1417 (10^{-3}) G^2/RAD	G^2/HZ	3 1428 (10^{-3}) G^2/RAD	G^2/HZ
85	2.455	15.43	6.686	42.	.994	6.25
90	.939	5.90	2.610	16.4	.346	2.17
100	.454	2.85	1.310	8.23	.281	1.77
110	.329	2.07	.984	6.18	19.35	121.58
120	.350	2.20	1.676	10.53	.143	0.90
122	.500	3.14	3.42	21.49	.141	0.89
123	.591	3.71	3.98	25.01	.144	0.90
124	.604	3.80	3.48	21.87	.149	0.94
125	.622	3.91	3.101	19.48	.160	1.01
126	.697	4.38	3.223	20.25	.182	1.14
127	.823	5.17	3.774	23.7	.220	1.38
128	.859	5.40	4.020	25.26	.246	1.55
129	.660	4.15	3.080	19.35	.210	1.32
130	.459	2.88	2.034	12.78	.159	1.00
135	.270	1.70	.833	5.23	.085	.53
140	.279	1.75	.718	4.51	.076	.48
150	.424	2.66	.805	5.06	.068	.43
160	1.387	8.71	1.974	12.40	.068	.43
165	4.967	31.21	6.554	41.18	.087	.55
167	10.53	66.16	13.73	86.27	.122	.77
168	15.52	97.52	20.206	126.96	.154	.97
170	20.05	125.98	26.18	165.	.188	1.18
171	15.50	97.39	20.32	128.	.161	1.01
175	3.995	25.10	5.401	34.	.087	.55
185	0.758	4.76	1.148	7.2	.066	.41
195	0.358	2.25	.598	3.8	.065	.41

Figure 17. YC-14 Flap Accelerometer Response Predictions, G=.03 (Concluded)

ACCEL. NO.	STRUCTURAL DAMPING					FLIGHT TEST YC-14
	.03	.06	.09	.12	.15	
1	1.67	1.180	.968	.845	.763	0.716
7	2.55	1.821	1.511	1.334	1.217	1.20
8	1.18	0.8547	0.717	.639	.588	0.404

Figure 18. RMS Acceleration Values for YC-14 USB Flap for Frequency Range 20 - 200 Hz

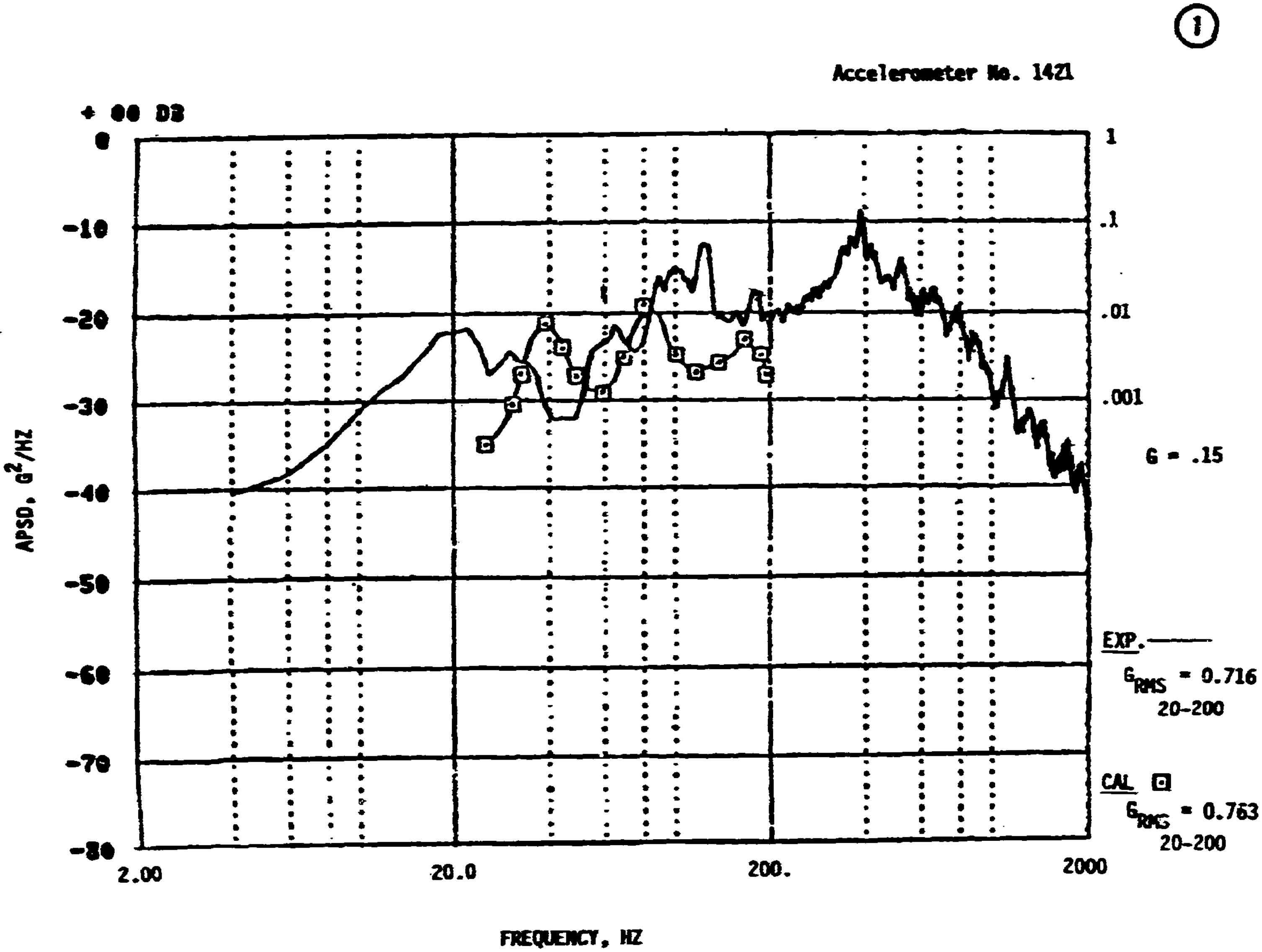

Figure 19. USB Flap Response Comparison of Model I with Prediction, Accelerometer 1421

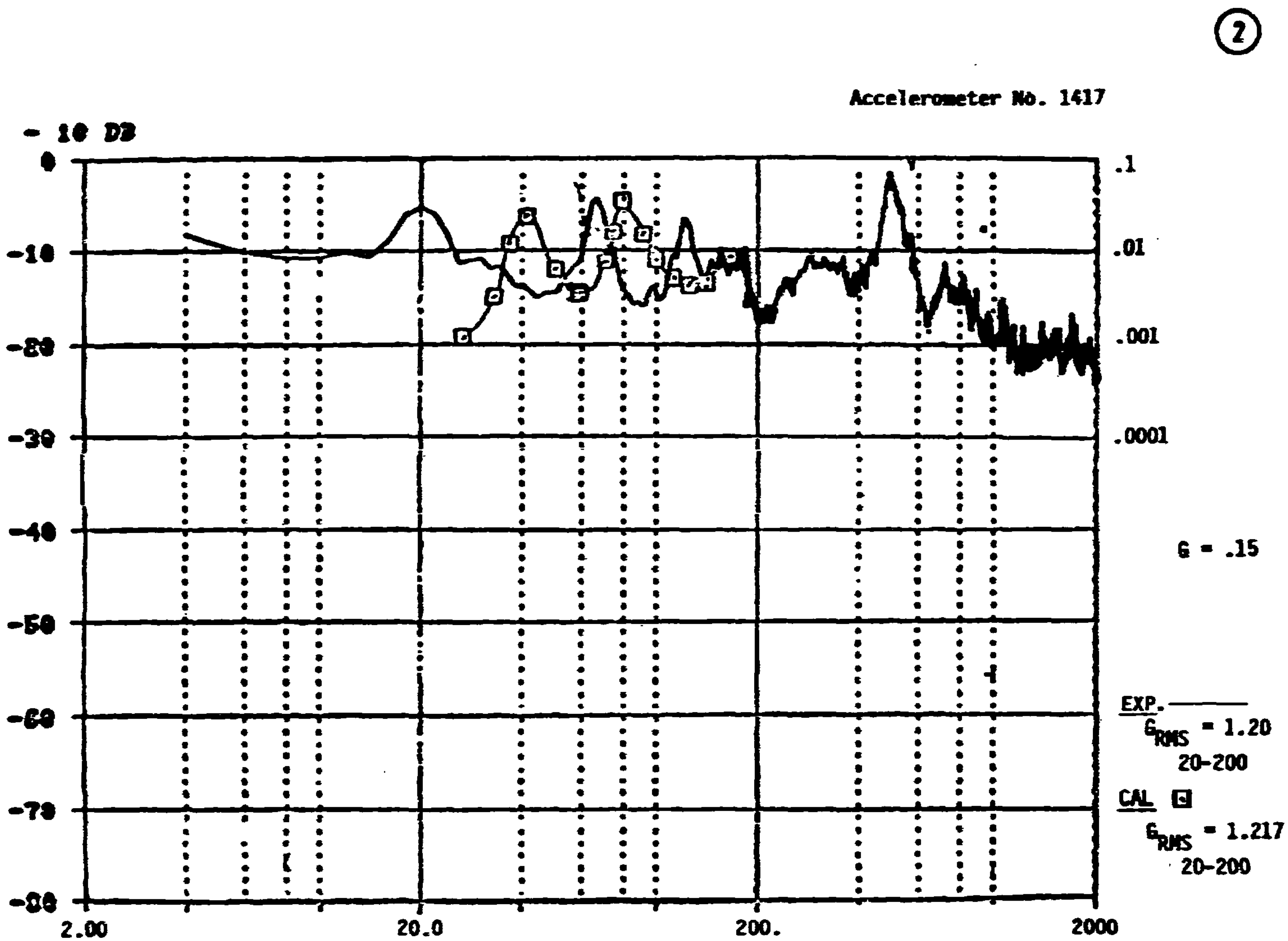

Figure 20. USB Flap Response Comparison of Model I with Prediction, Accelerometer 1417

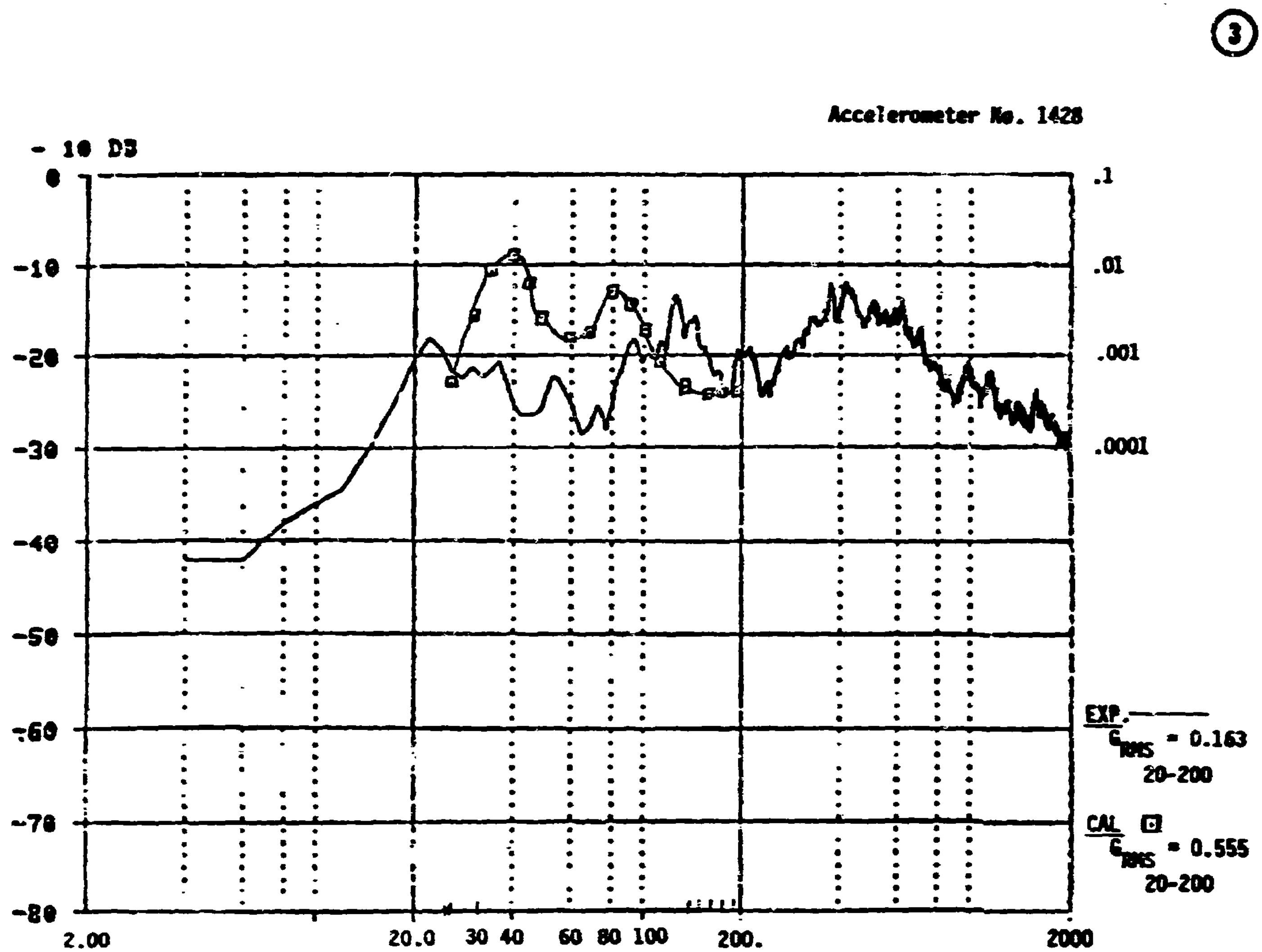

Figure 21. USB Flap Response Comparison of Model I with Prediction, Accelerometer 1428

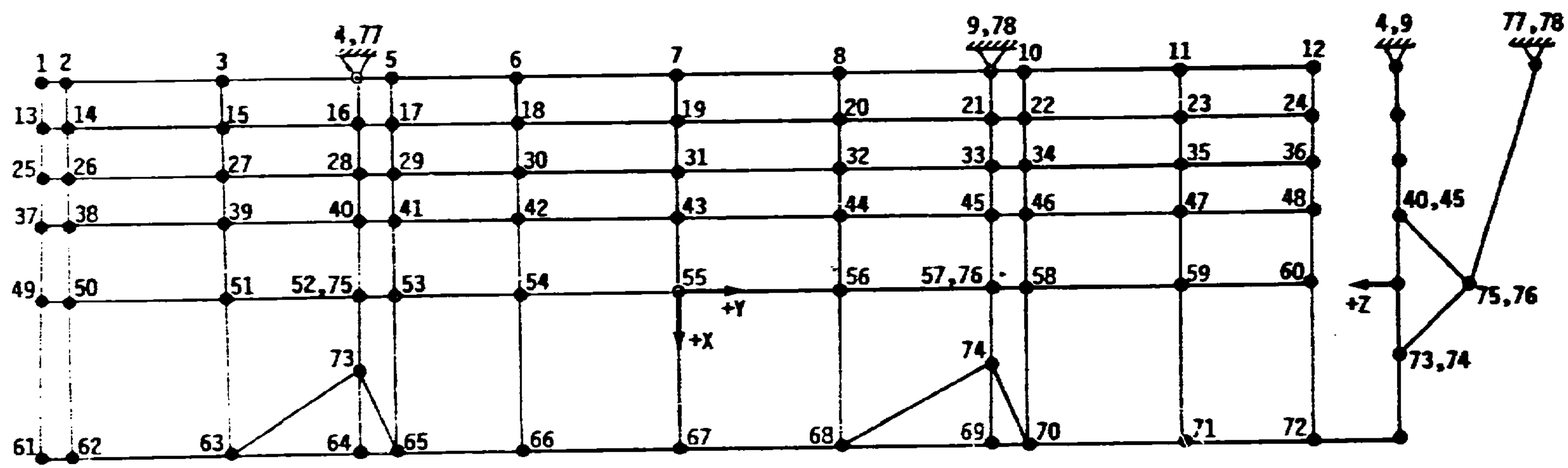

Figure 22. YC-14 USB Flap Model II Finite Element Model Node Points

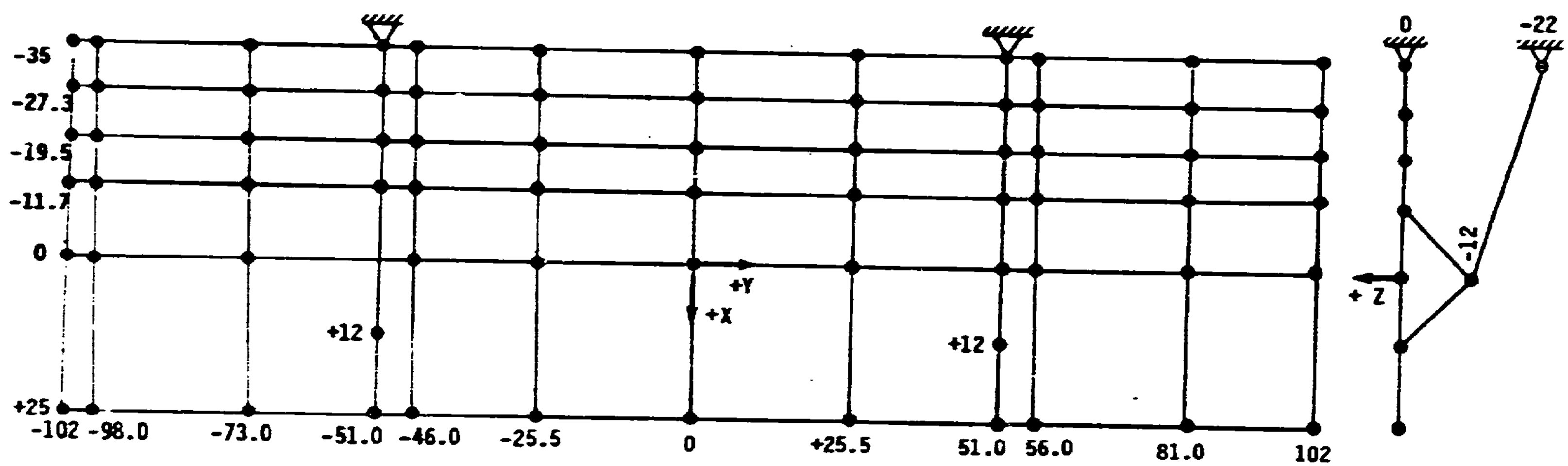

Figure 23 YC-14 USB Flap Finite Element Model Coordinates

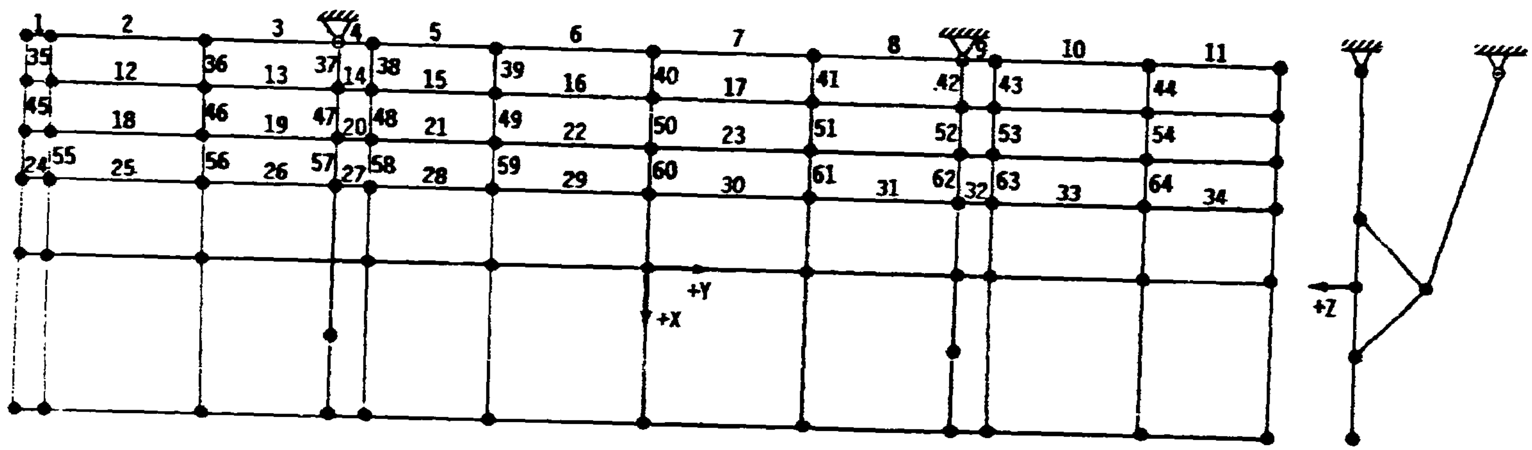

GEOM	CONSISTS OF	MAT'L	A_{AX}	AS_2	AS_3	J	I_2	I_3
1	LEADING EDGE	Ti	.65	.18	.47	.0005	2.1	.02
2	HAT SECTION	Ti	.25	.15	.10	.0002	.675	.613
3	REAR SPAR	Ti	1.195	.45	.745	.001	19.8	.235
4	REAR SPAR & HAT	Ti	1.45	.6	.845	.0012	20.5	.85
5	RIB '	Ti	1.20	.5	.7	.0008	9.0	.19
5	RIB	Al	1.20	.5	.7	.0008	9.0	.19
6	ACTUATOR BRACKET	Al	1.50	.75	.75	.008	2.25	.14

Figure 24. YC-14 USB Flap Finite Element Model Beam Elements (Revised)

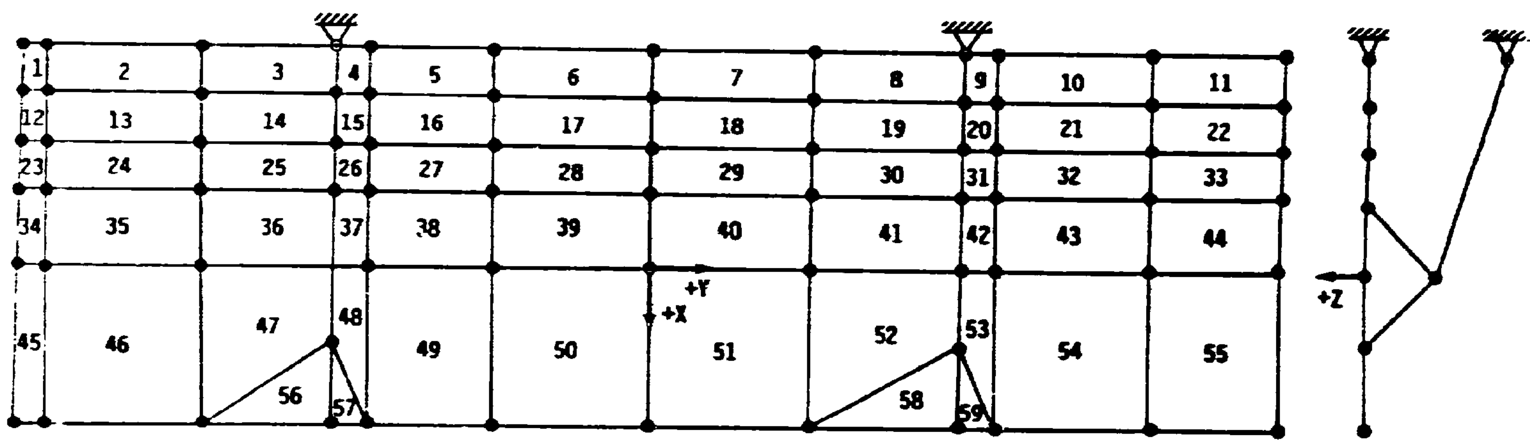

GEOM	CONSISTS OF	MATERIAL	THICKNESS	LB SEC/IN^4
1	UPPER AND LOWER SKINS, MAIN USB FLAP	AL	3.0	.0000505
2	SAME AS 1	Al		
3	AFT PORTION OF MAIN USB FLAP	AL		
4	SAME AS 3	Al		
5	AFT USB FLAP	AL		
6	SAME AS 5	Al		

Figure 25. USB Flap Finite Element Model Plate Elements

PRINT OF FREQUENCIES

MODE NUMBER	CIRCULAR FREQUENCY (RAD/SEC)	FREQUENCY (CYCLES/SEC)	PERIOD (SEC)	TOLERANCE
1	2.0025E+02	3.1877E+01	3.1371E-02	4.6433E-14
2	2.1295E+02	3.3893E+01	2.9505E-02	1.0268E-14
3	2.1880E+02	3.4823E+01	2.8717E-02	.0
4	2.7242E+02	4.3356E+01	2.3065E-02	1.6625E-14
5	4.0046E+02	6.3735E+01	1.5690E-02	5.8074E-15
6	6.7244E+02	1.0702E+02	9.3438E-03	3.2954E-14
7	7.9420E+02	1.2640E+02	7.9113E-03	1.1812E-13
8	8.6483E+02	1.3764E+02	7.2652E-03	.0
9	1.0030E+03	1.5963E+02	6.2645E-03	1.4642E-11
10	1.3226E+03	2.1049E+02	4.7509E-03	8.4452E-11
11	1.7284E+03	2.7509E+02	3.6352E-03	1.7796E-09
12	1.8649E+03	2.9680E+02	3.3693E-03	8.0798E-08
13	1.9682E+03	3.1325E+02	3.1923E-03	3.3342E-07

Figure 26. Natural Modes of Medium STOL Flaps, Model II

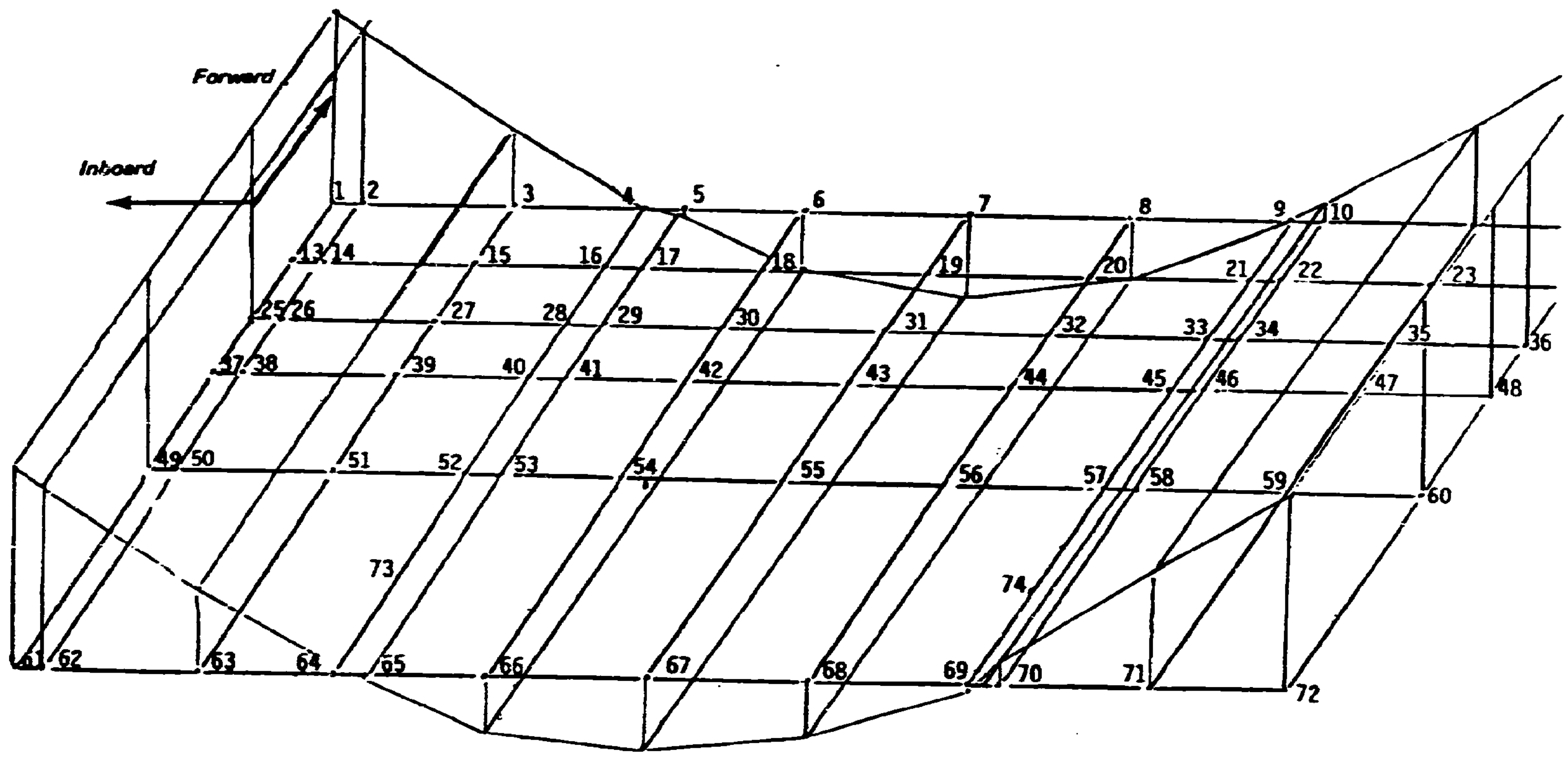

Figure 27. YC-14 USB Flap Finite Element Model II Mode 1 Frequency = 31.88 Hz

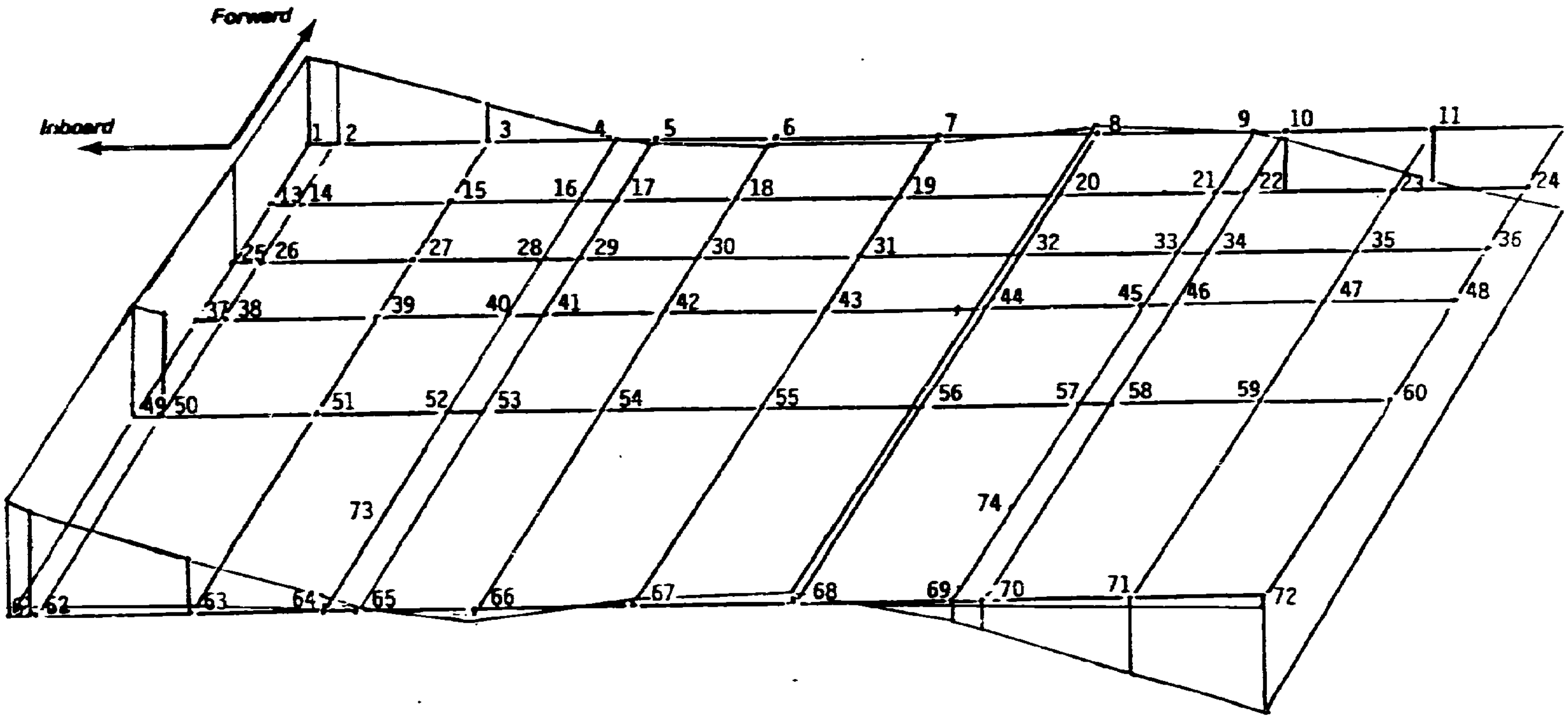

Figure 28. Mode 2 Frequency = 33.90 Hz

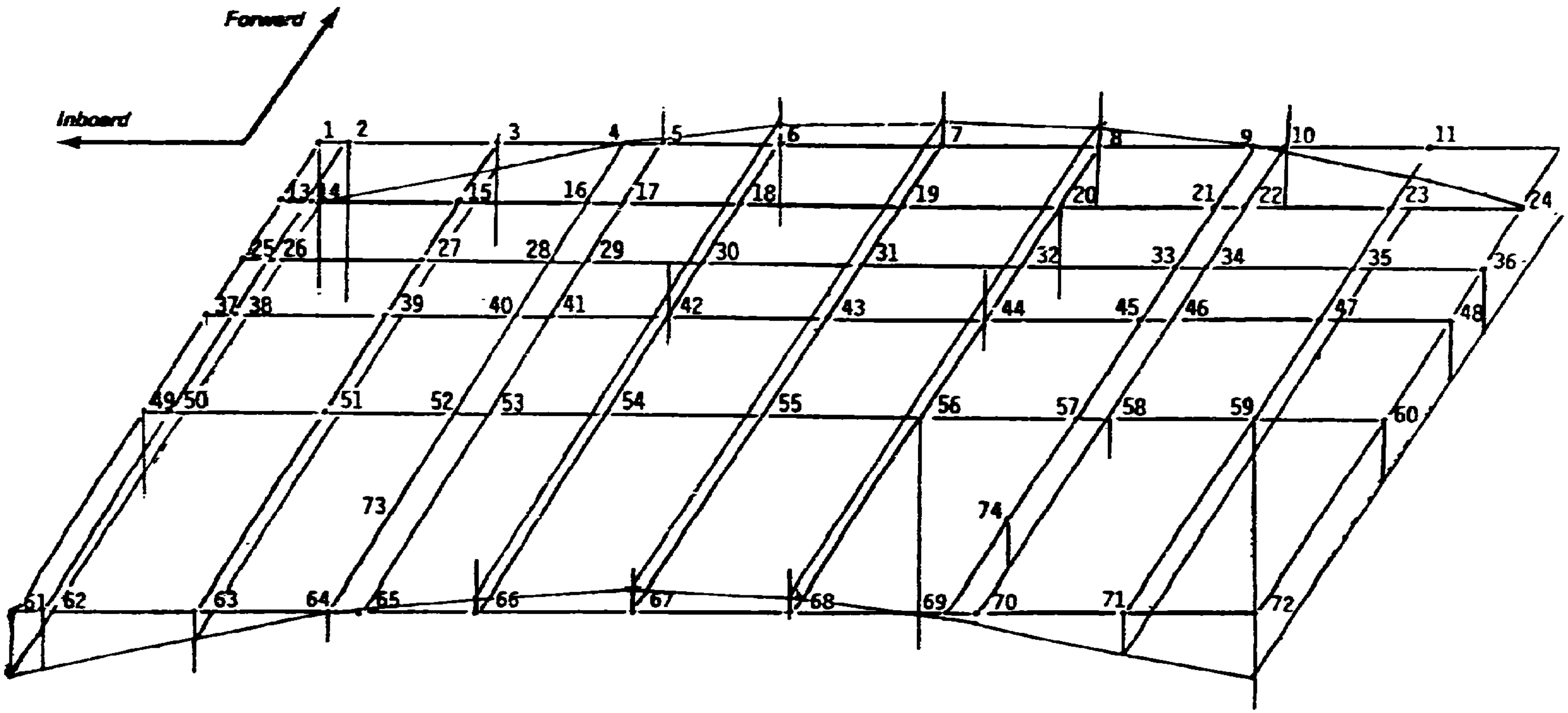

Figure 29. Mode 3 Frequency = 34.8 Hz

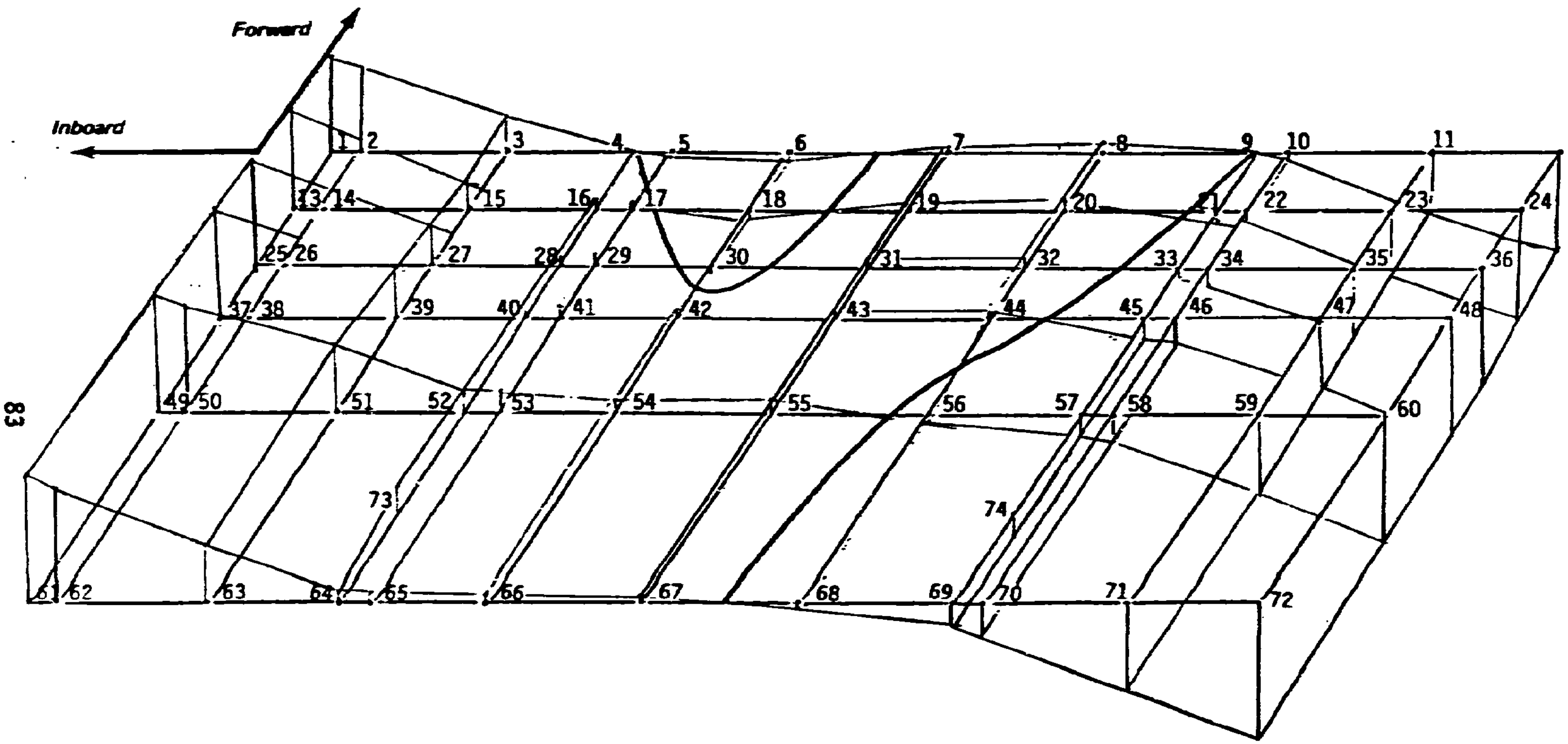

Figure 30. Mode 4 Frequency = 43.35 Hz

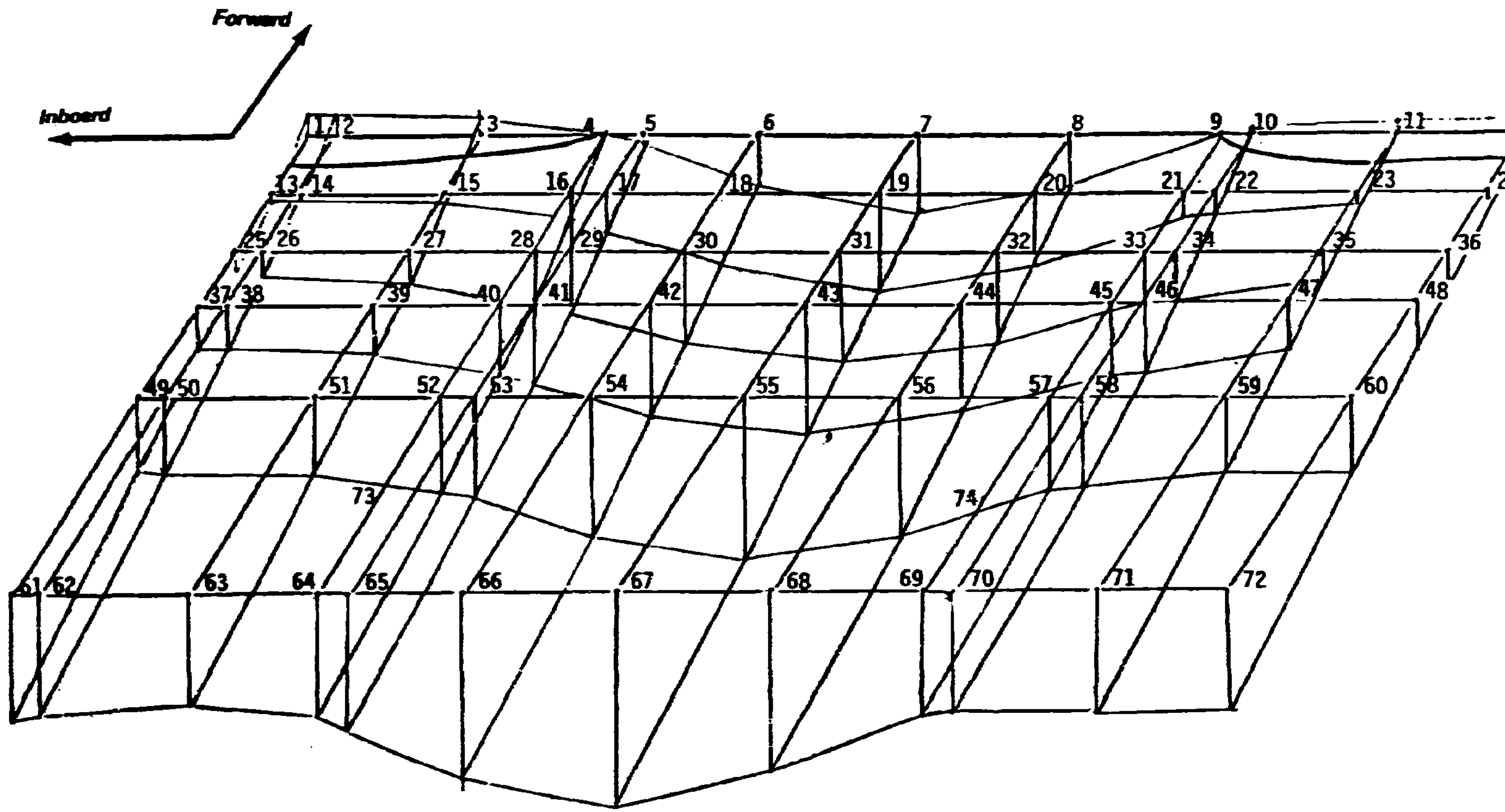

Figure 31. Mode 5 Frequency = 63.73 Hz

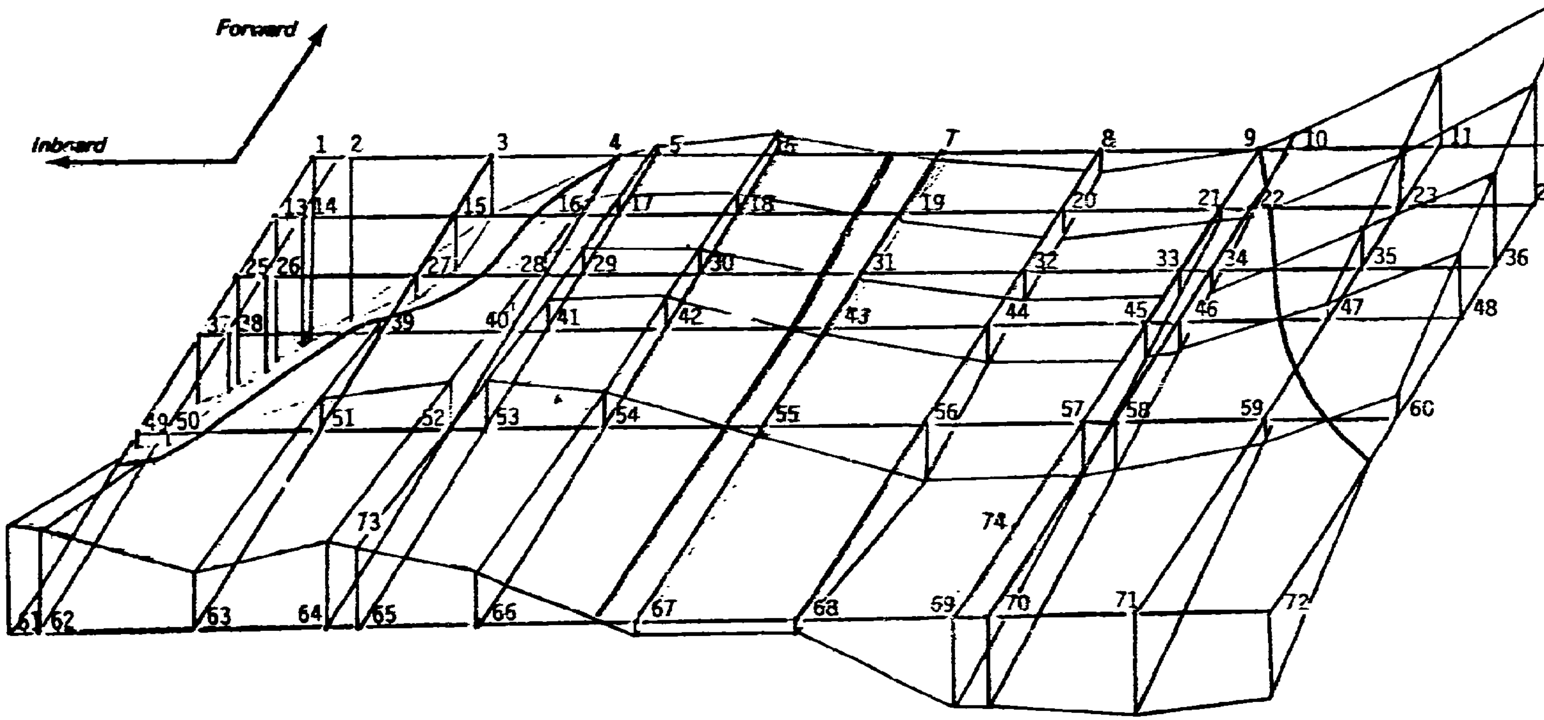

Figure 32. Mode 6 Frequency = 107.02 Hz

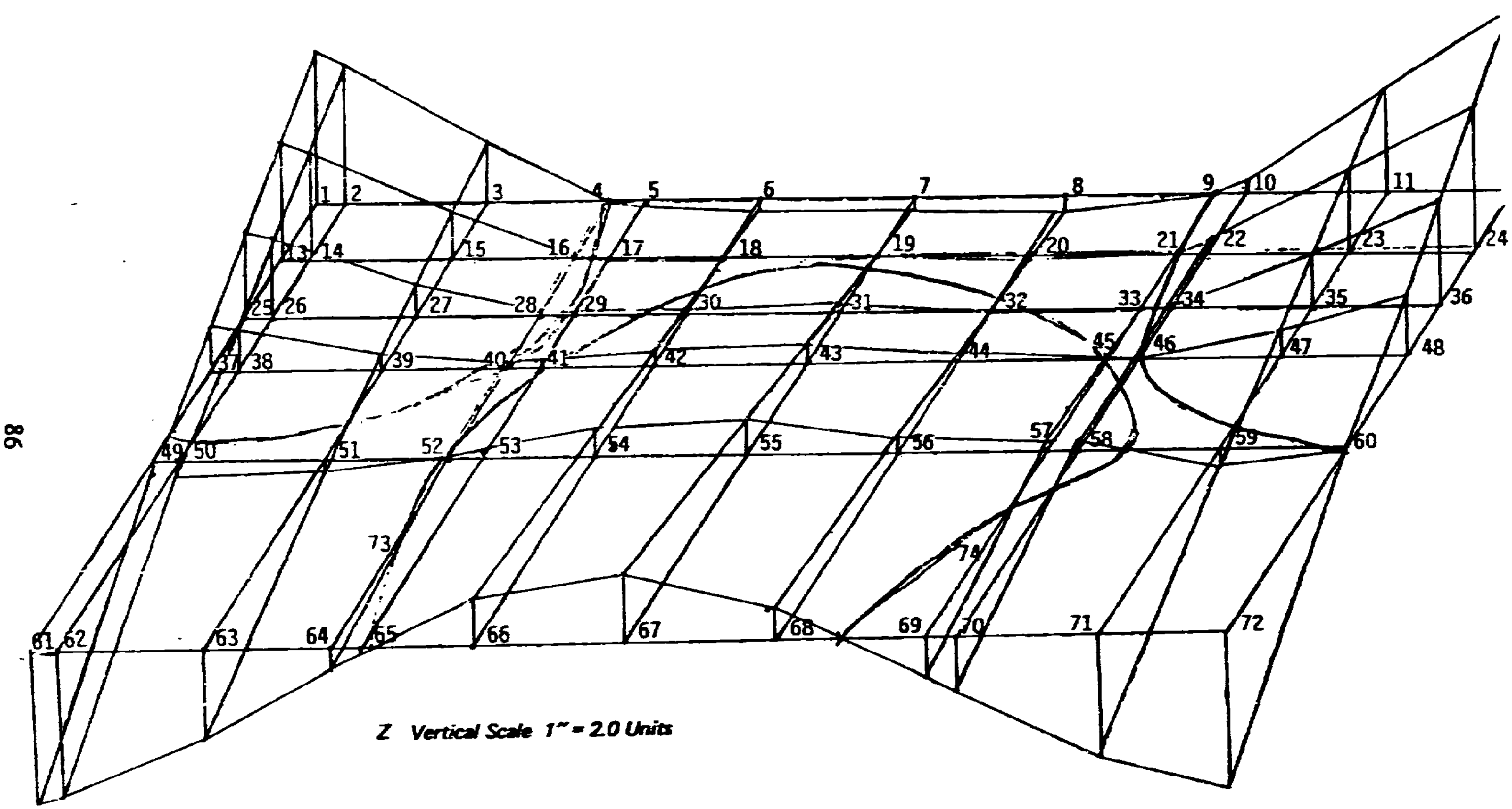

Figure 33. Mode 7 Frequency = 126.40 Hz

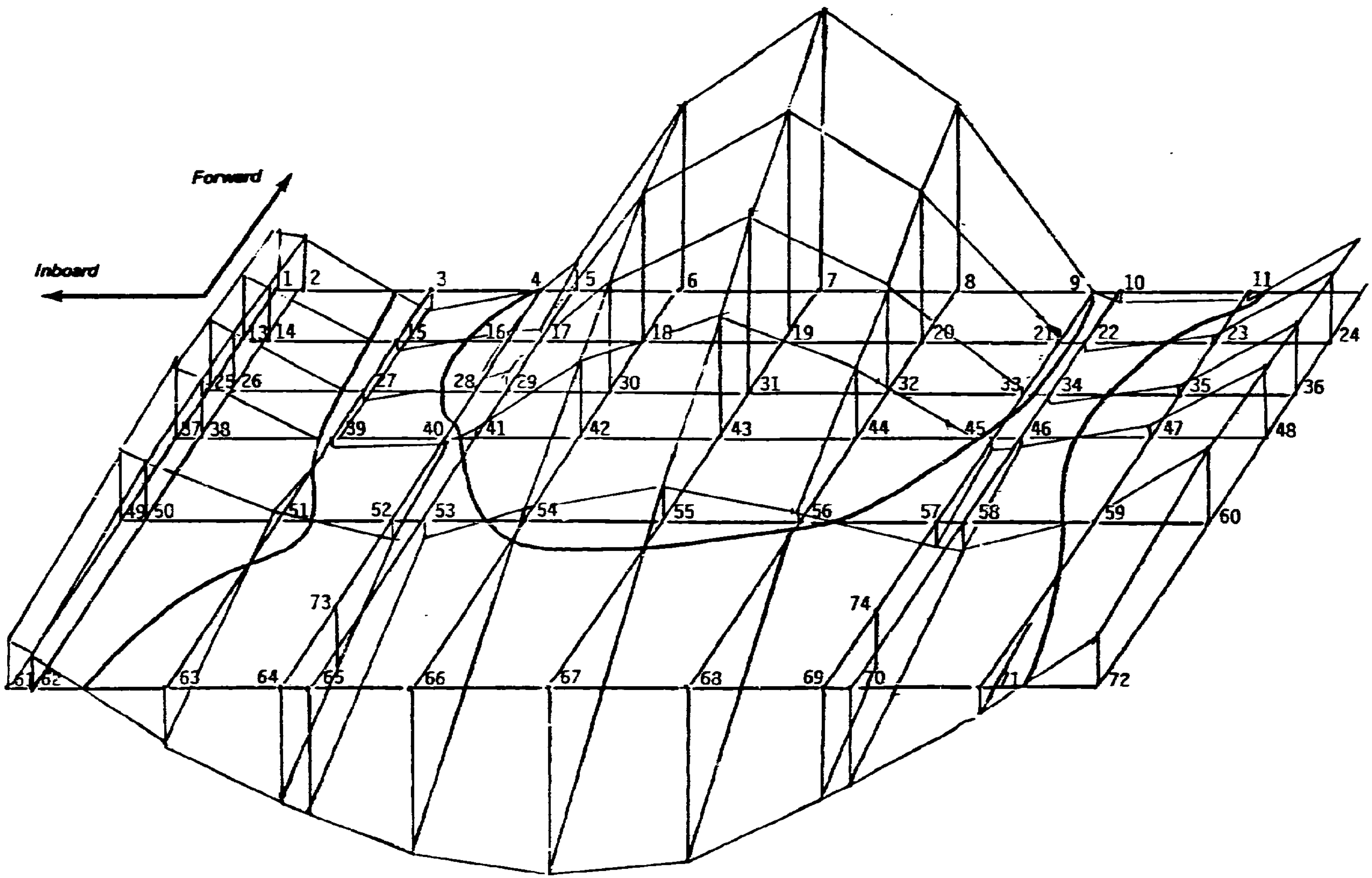

Figure 34. Mode 8 Frequency = 137.64 Hz

THIS REPORT HAS BEEN DELIMITED
AND CLEARED FOR PUBLIC RELEASE
UNDER DOD DIRECTIVE 5200.20 AND
NO RESTRICTIONS ARE IMPOSED UPON
ITS USE AND DISCLOSURE.

DISTRIBUTION STATEMENT A

APPROVED FOR PUBLIC RELEASE;
DISTRIBUTION UNLIMITED.

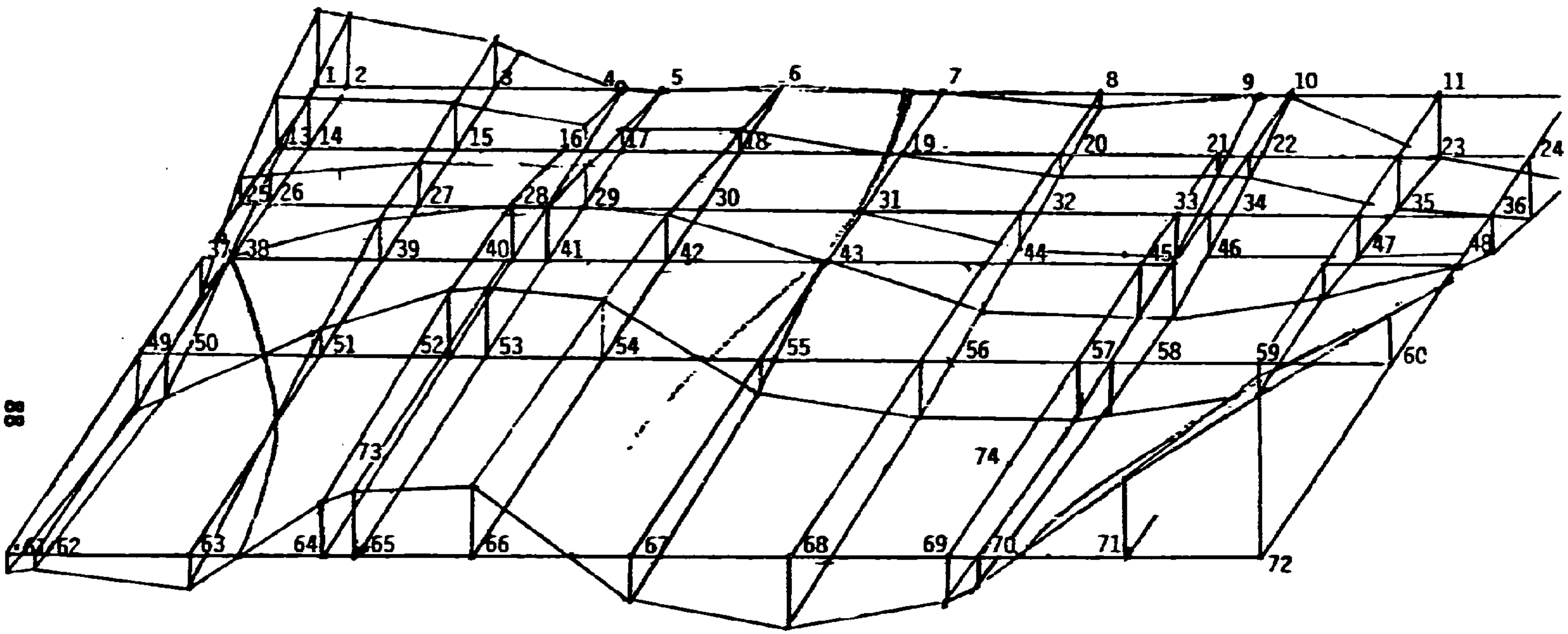

Figure 35. Mode 9 Frequency = 159.63 Hz

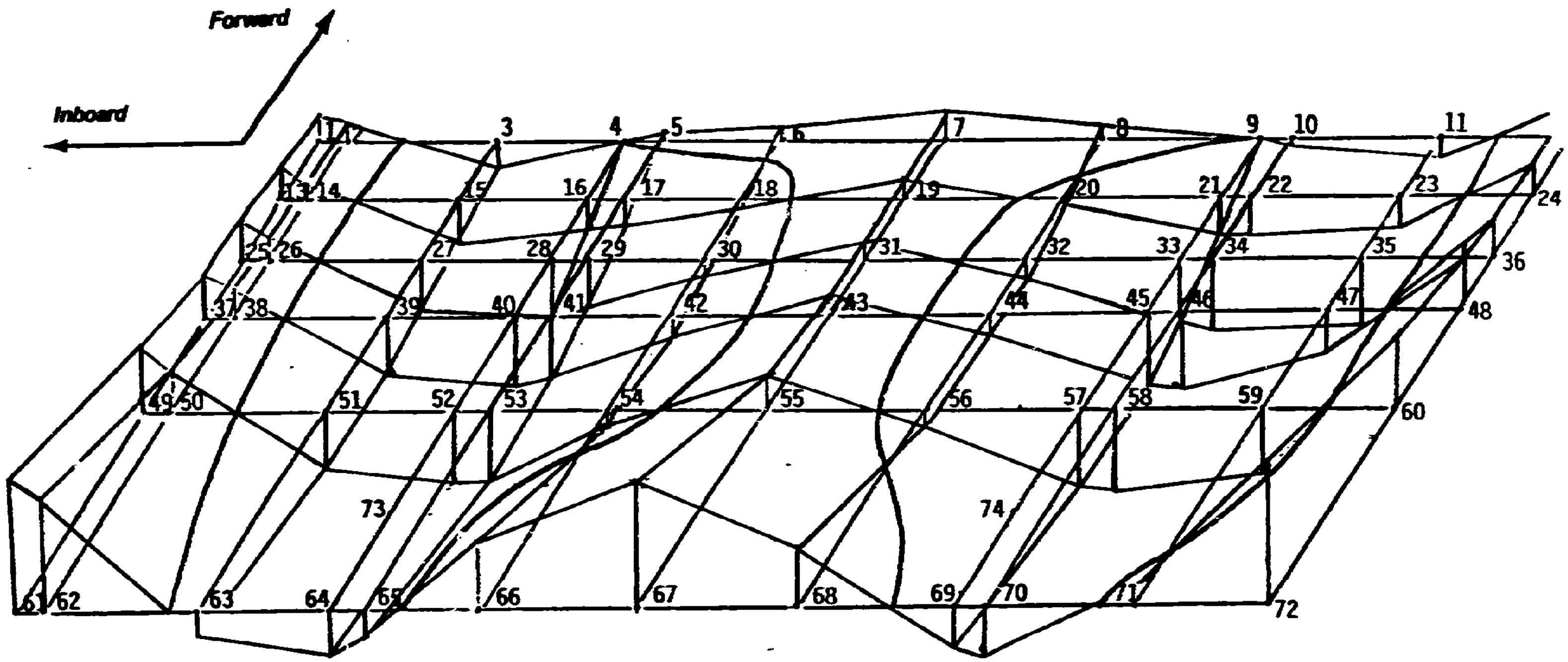

Figure 36. YC-14 USB Flap Finite Element Model II, Mode 10, Frequency = 210.49 Hz

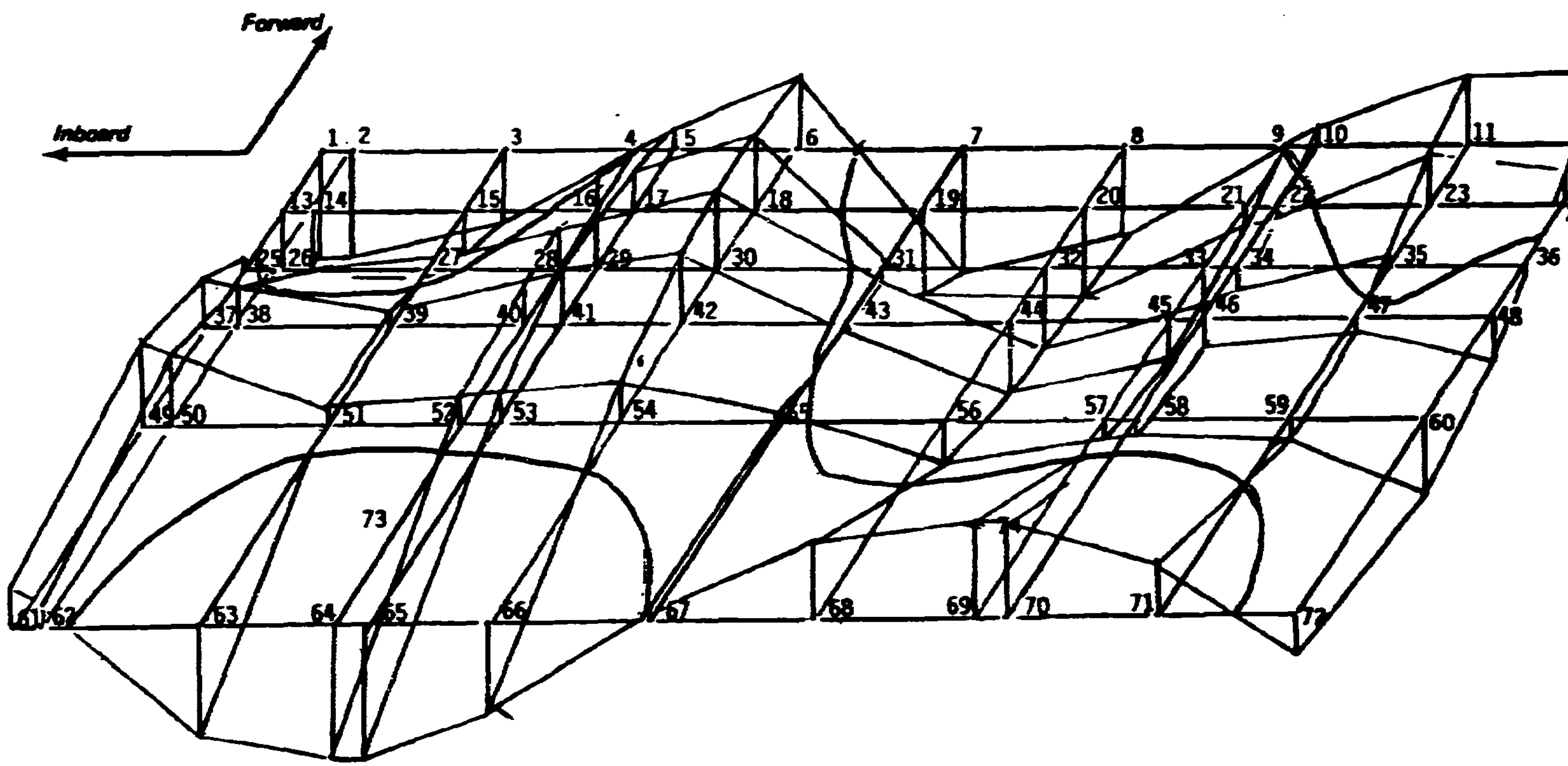

Figure 37. Mode 11, Frequency = 275.09 Hz

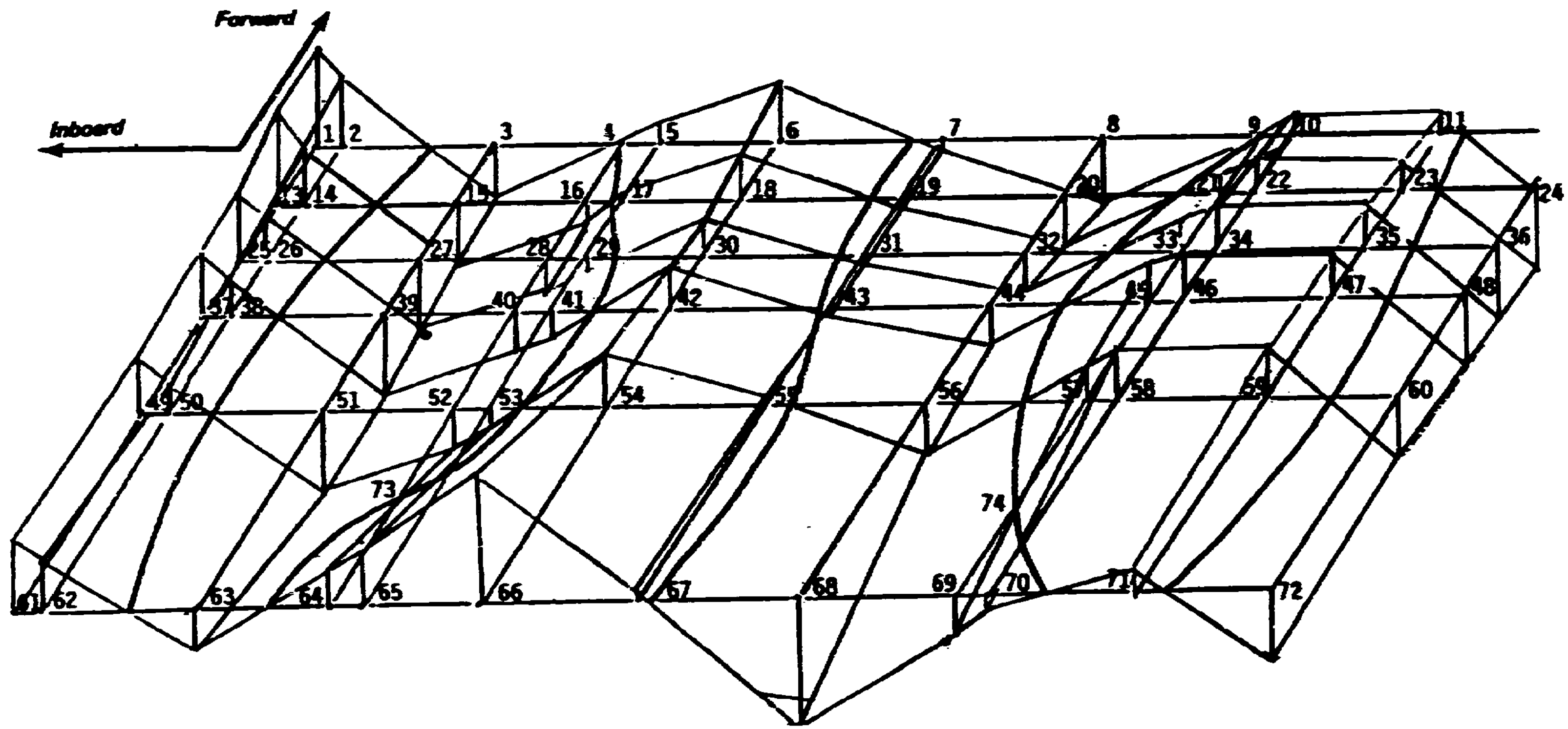

Figure 38. Mode 12 , Frequency = 296.80 Hz

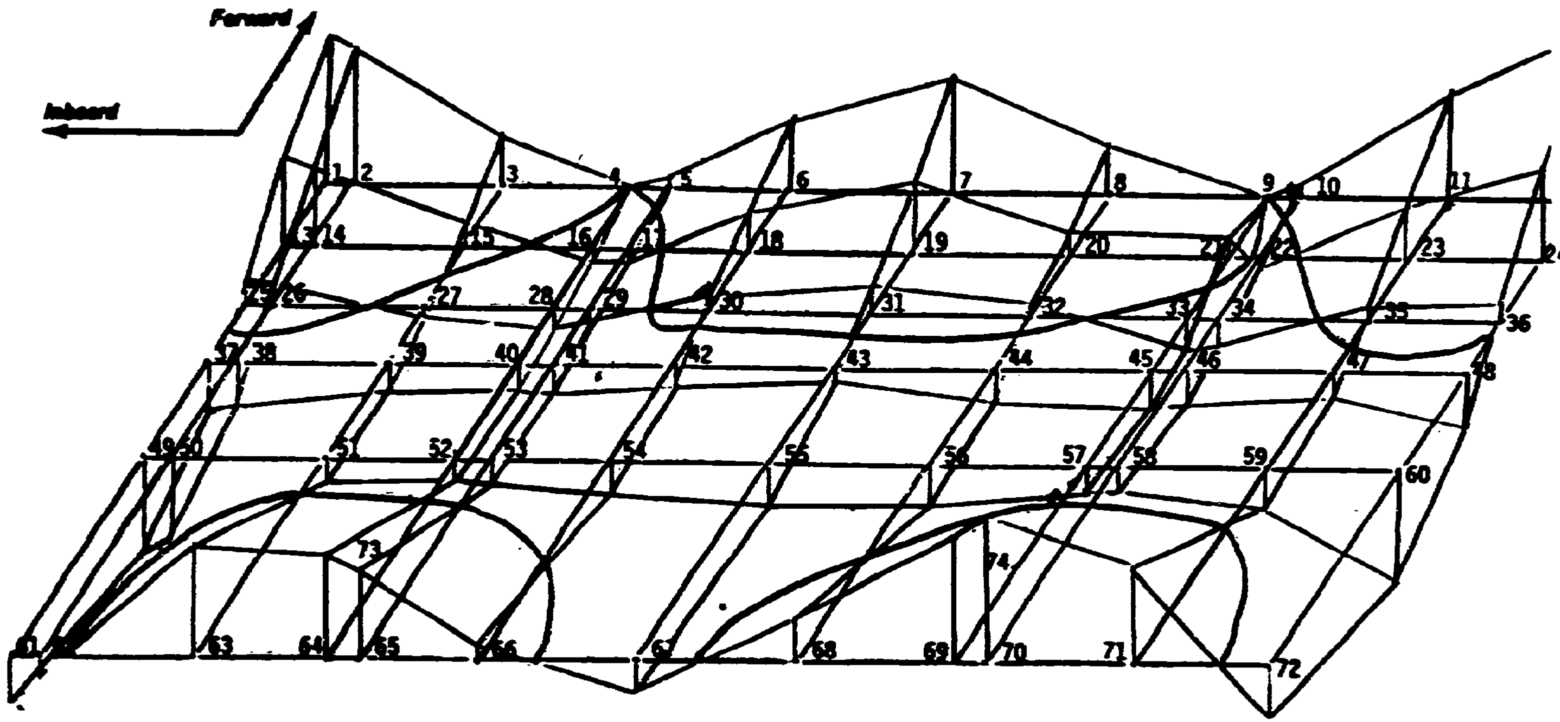

Figure 39. Mode 13 , Frequency = 313.25 Hz

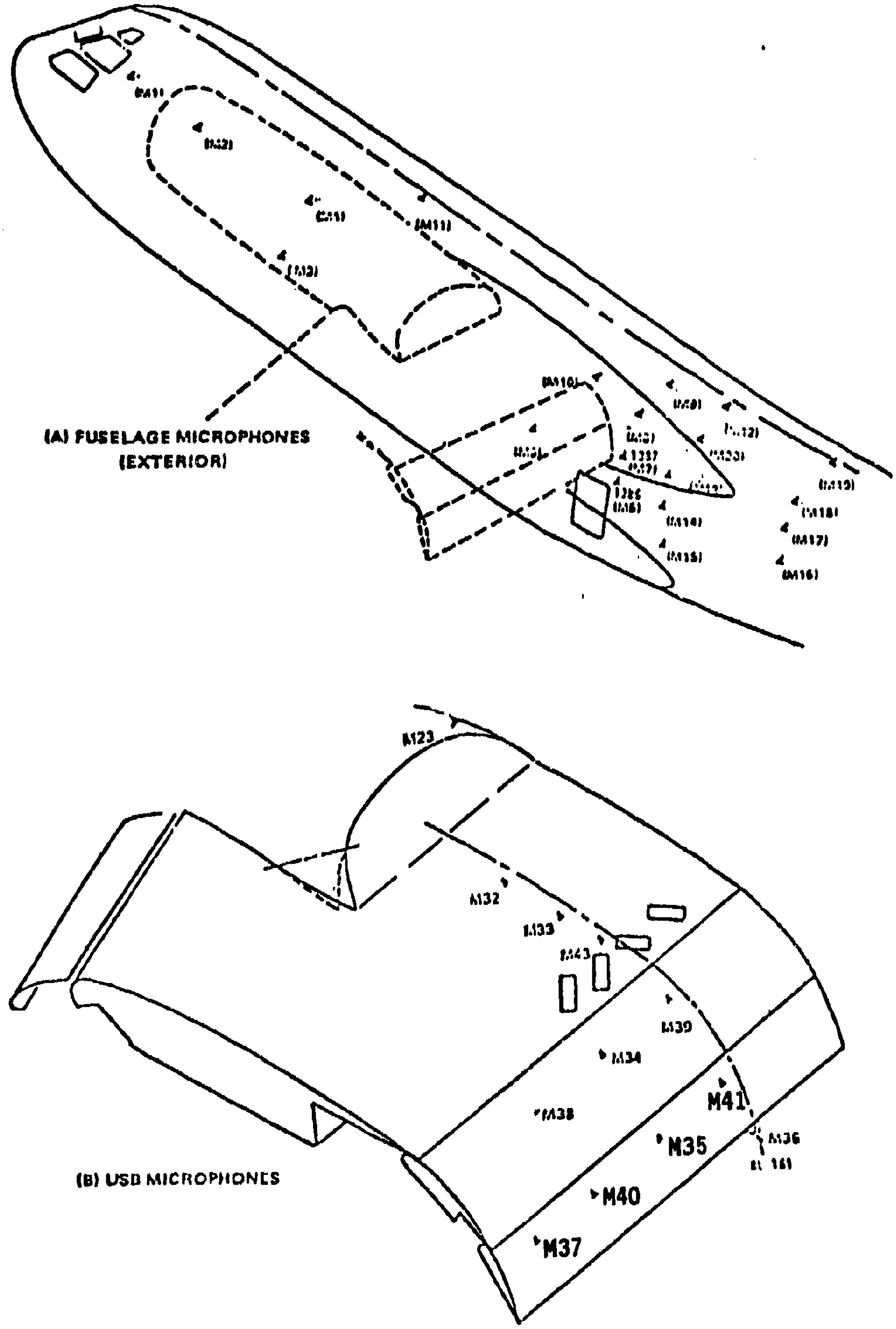

Figure 40. Instrumentation for Concurrent NASA Flap Loads Measurements Program

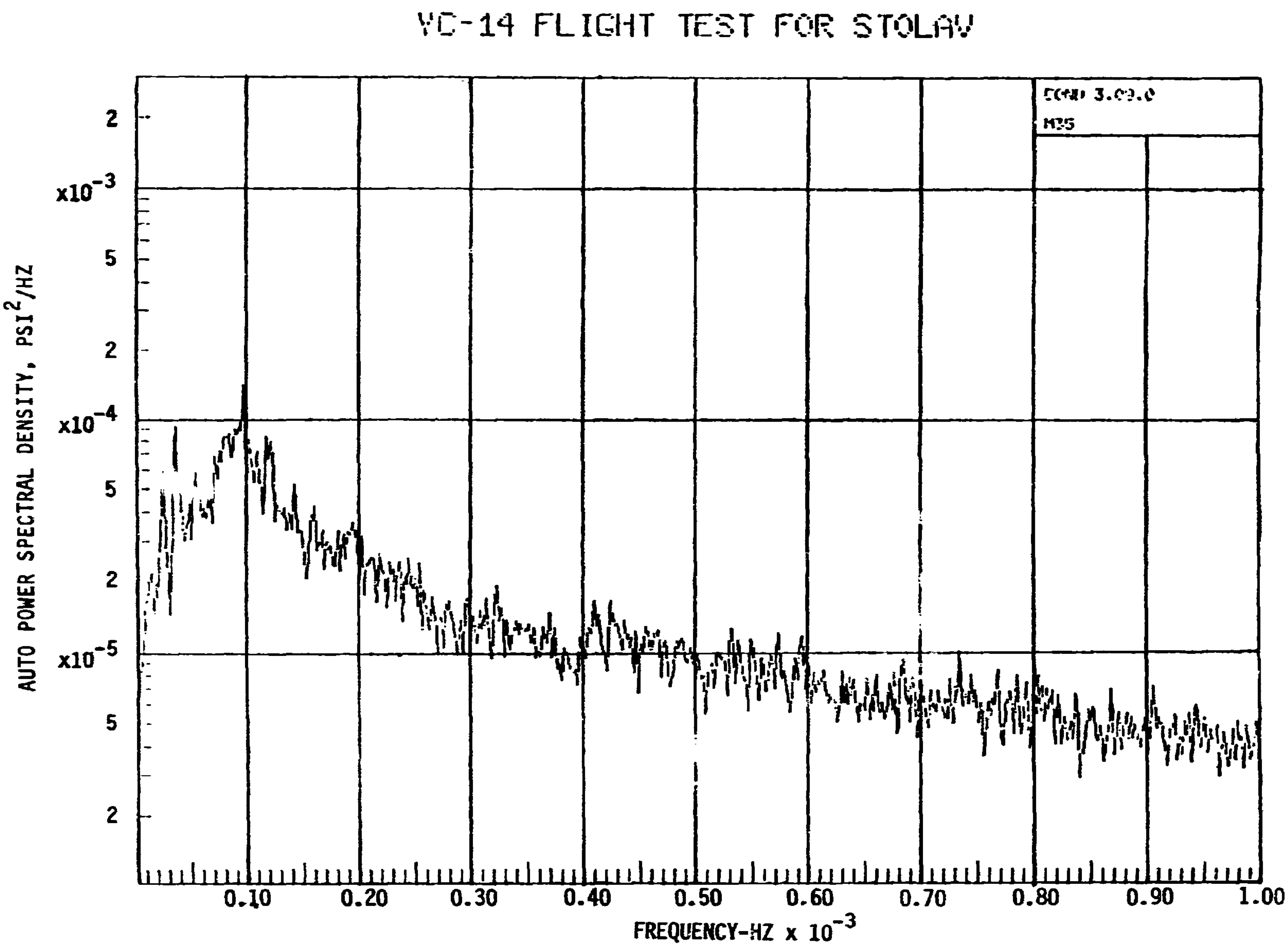

Figure 41. USB Flap Acoustic Excitation Spectrum, Microphone M35

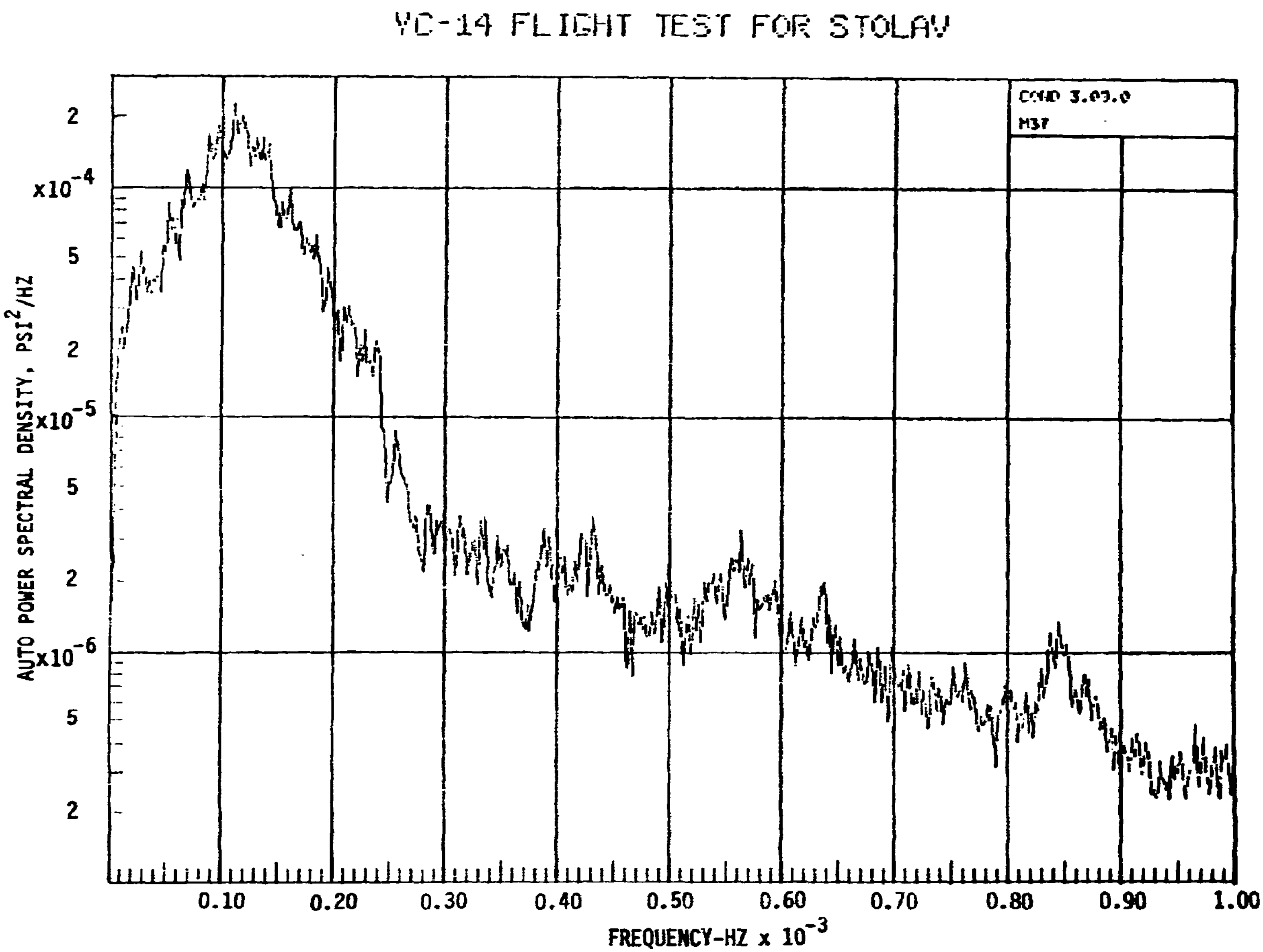

Figure 42. USB Flap Acoustic Excitation Spectrum, Microphone M37

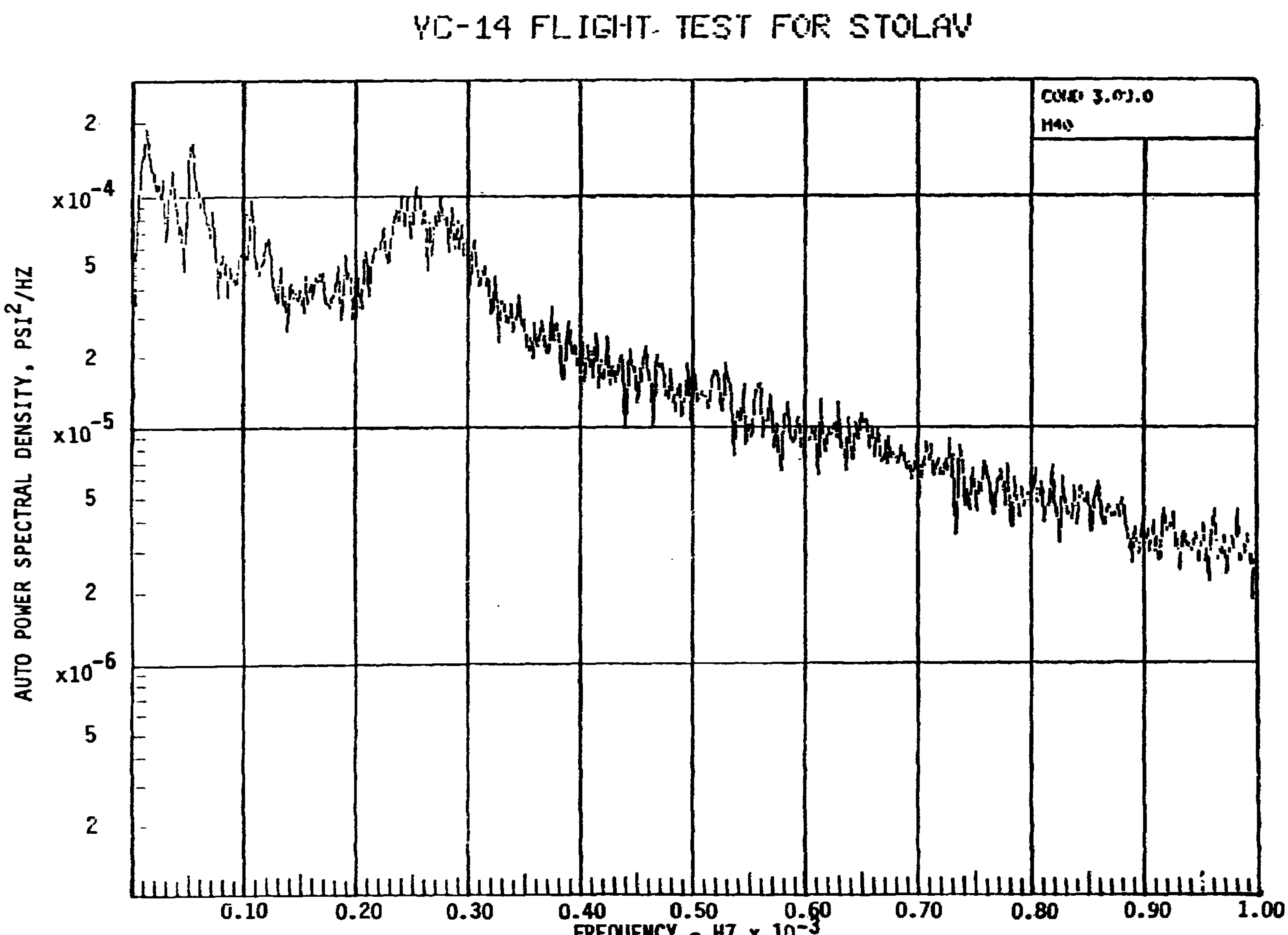

Figure 43. USB Flap Acoustic Excitation Spectrum, Microphone M40

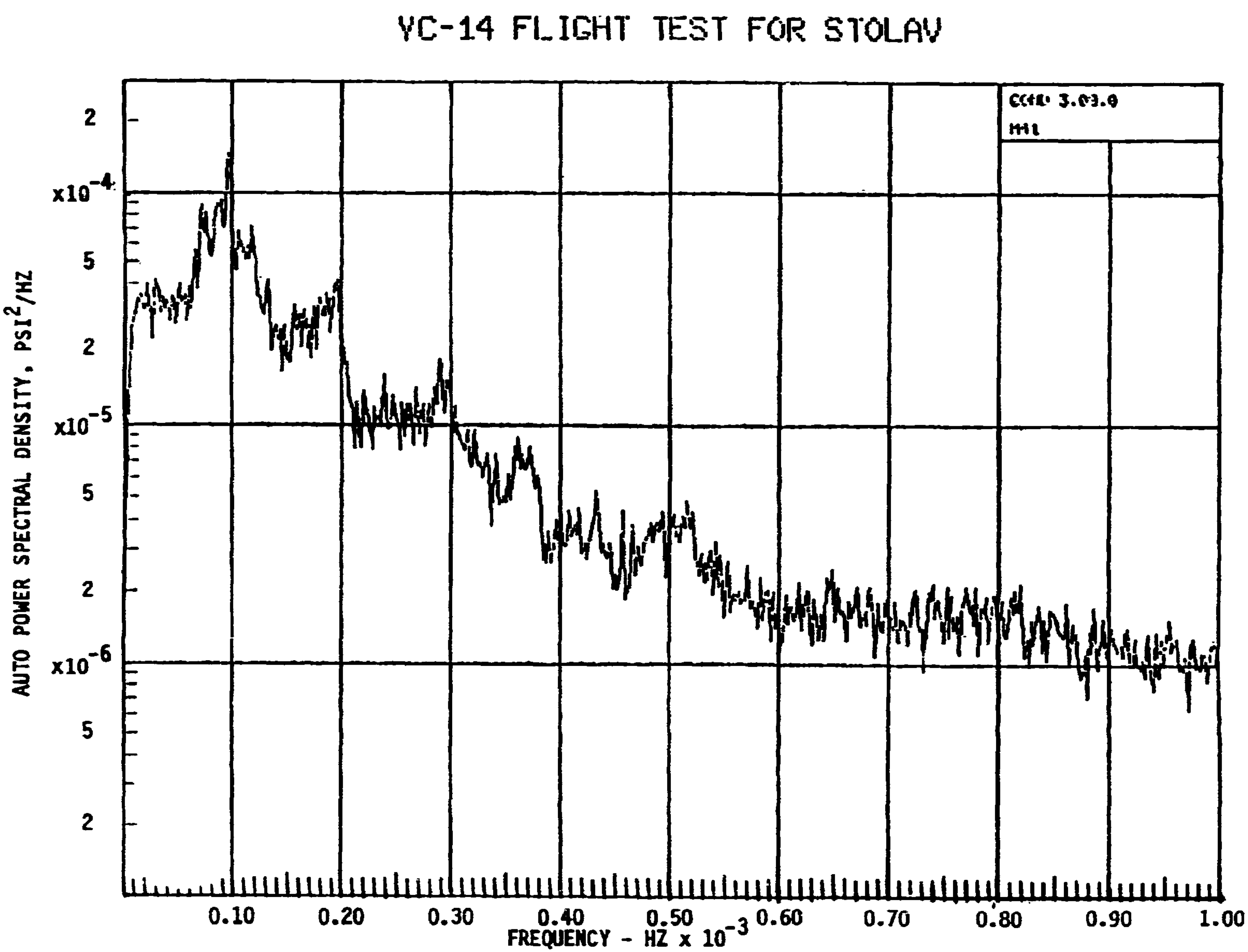

Figure 44. USB Flap Acoustic Excitation Spectrum, Microphone M41

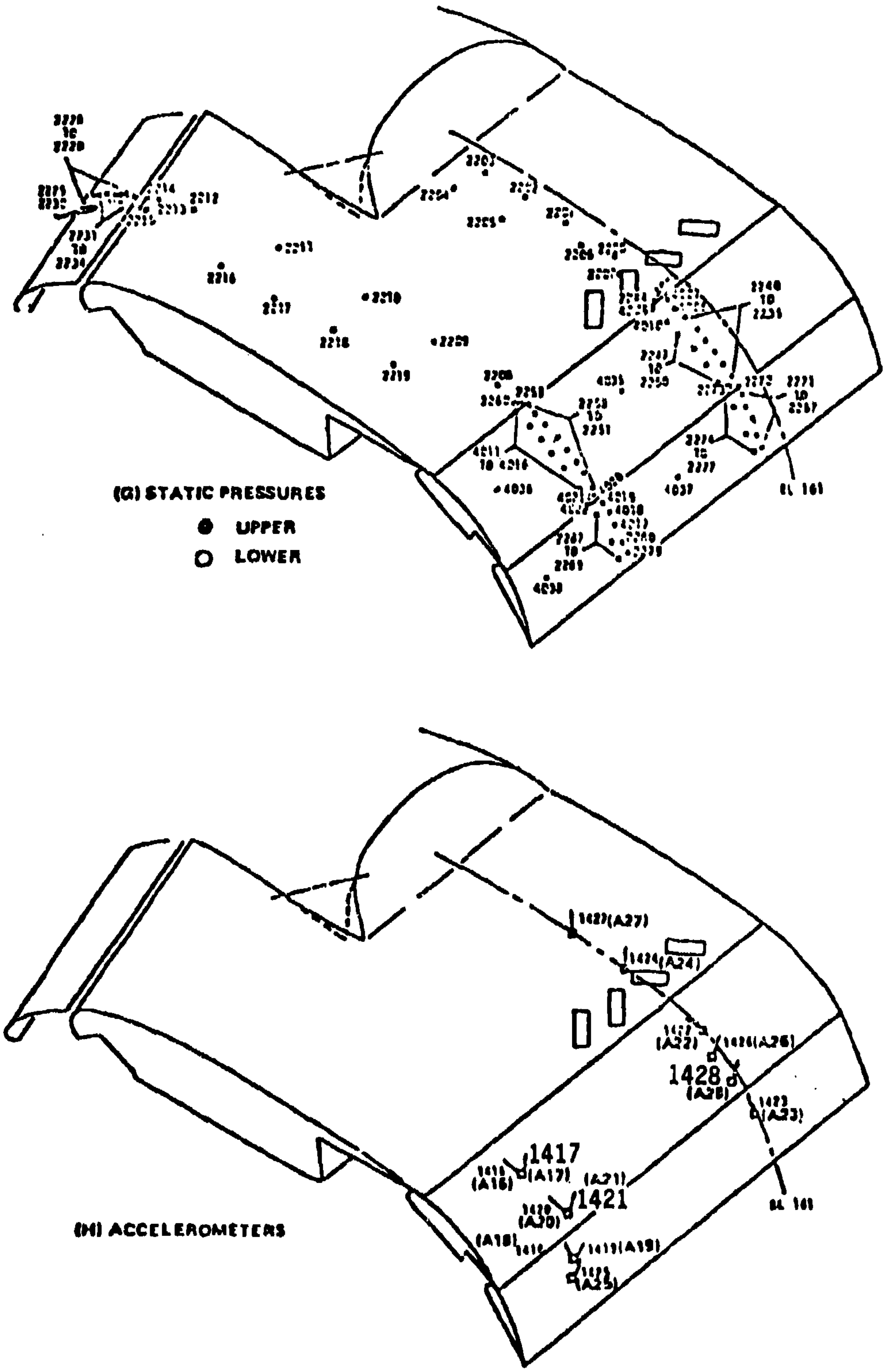

Figure 45. Accelerometer Locations on USB Flap

DIAGONAL CPSD
RESPONSE CALCULATIONS

USB FLAP
78 MODE MODEL
(MODEL II)

(HZ) FREQUENCY	1417 $(x10^{-3})$ G^2/HZ	1421 $(x10^{-3})$ G^2/HZ	1428 $(x10^{-3})$ G^2/HZ	TOTAL DAMPING VALUE USED
26	.036	.0139	.0259	G=.06
32	.341	.155	.349	
43.4	9.56	4.03	9.19	
50.0	8.30	.514	1.44	
63.8	92.08	34.034	92.55	
88.0	2.98	1.08	3.025	
107.5	75.912	22.304	73.89	
124	5.7936	2.0127	3.8501	
128	7.0678	1.5011	3.7327	
195	.74264	.37913	1.0940	
26	.035	.0137	.0254	G=.10
43.7	3.6667	1.5378	3.4905	
50.3	1.2609	.49857	1.364	
50.3	33.663	12.451	33.567	
89.0	2.9726	1.0658	3.0150	
108.5	28.254	8.4583	26.635	
	.7428	.3781	1.0887	
26	.034074	.013313	.024537	G=.15
44.1	1.8287	.76069	1.7040	
51	1.1757	.47078	1.1990	
64.5	15.403	5.7060	15.140	
88.0	2.8845	1.0515	2.8217	
109.0	13.945	4.2501	12.743	
195.0	0.74311	0.37615	2.0787	

Figure 46. YC-14 USB Flap Response Predictions

FREQ(53) = .5100E+02 CYCLES/SEC. (.3204E+03 RAD./SEC.)

	LOADS		MAGNITUDE	PHASE ANGLE (RAD.)	OUTPUT SPECTRUM LOAD/(RAD./LEN.)
1	.97749E-01	.14098E-01	.98760E-01	.14324E+00	.13731E-02
2	.62205E-01	.92159E-02	.62983E-01	.14685E+00	.53411E-03
	-.13300E+00	-.13382E-01	.13367E+00	.32419E+01	.15186E-02

FREQ(54) = .5200E+02 CYCLES/SEC. (.3267E+03 RAD./SEC.)

	LOADS		MAGNITUDE	PHASE ANGLE (RAD.)	OUTPUT SPECTRUM LOAD/(RAD./LEN.)
1	.90173E-01	.11149E-01	.90860E-01	.12301E+00	.15350E-02
2	.57346E-01	.72995E-02	.57809E-01	.12661E+00	.58815E-03
3	-.12596E+00	-.10066E-01	.12636E+00	.32214E+01	.16608E-02

Figure 47. Sample Page of USB Flap Accelerometer Response Predictions

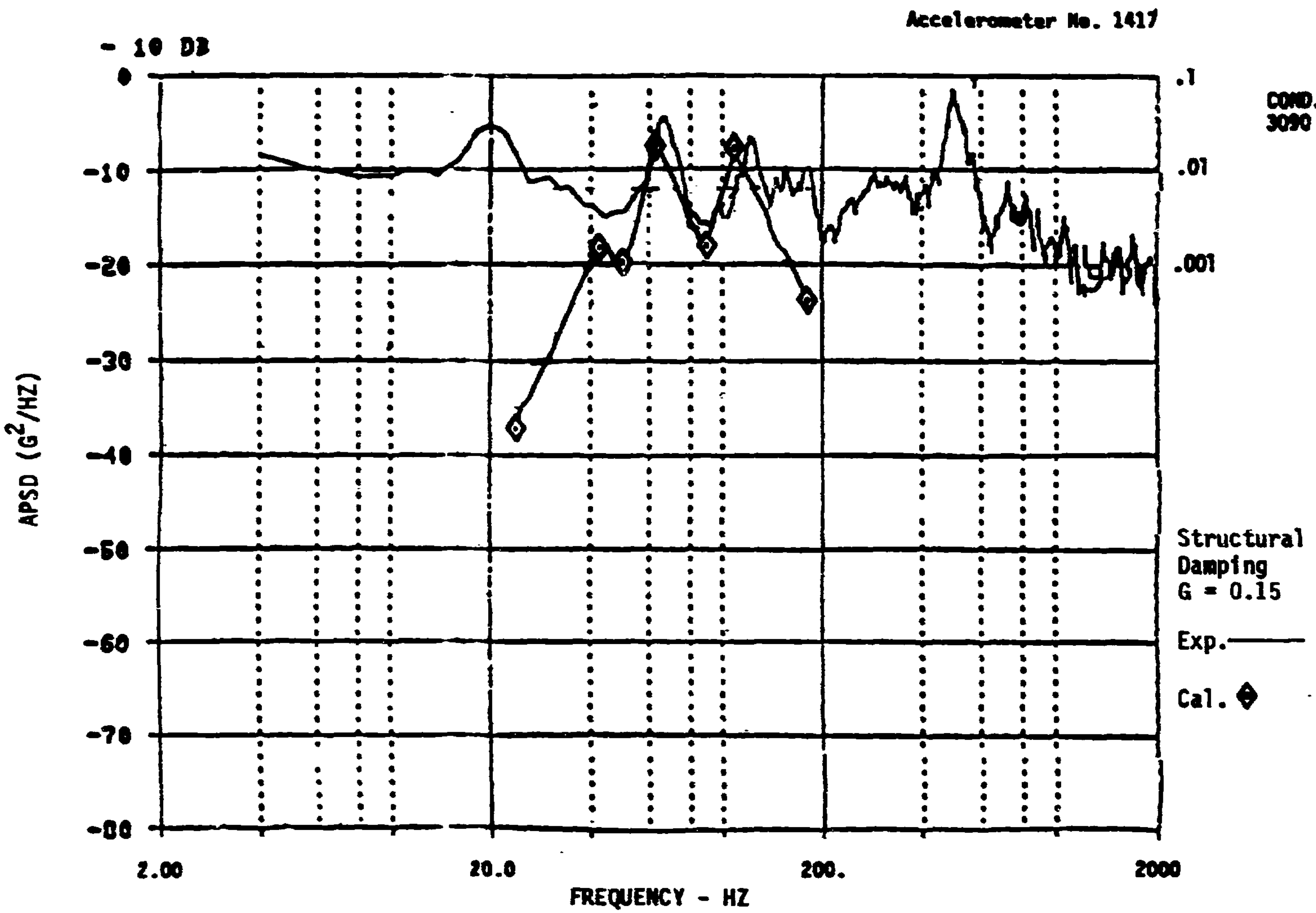

Figure 48 USB Flap Model II Response Prediction Comparison with Flight Data Accelerometer 1417

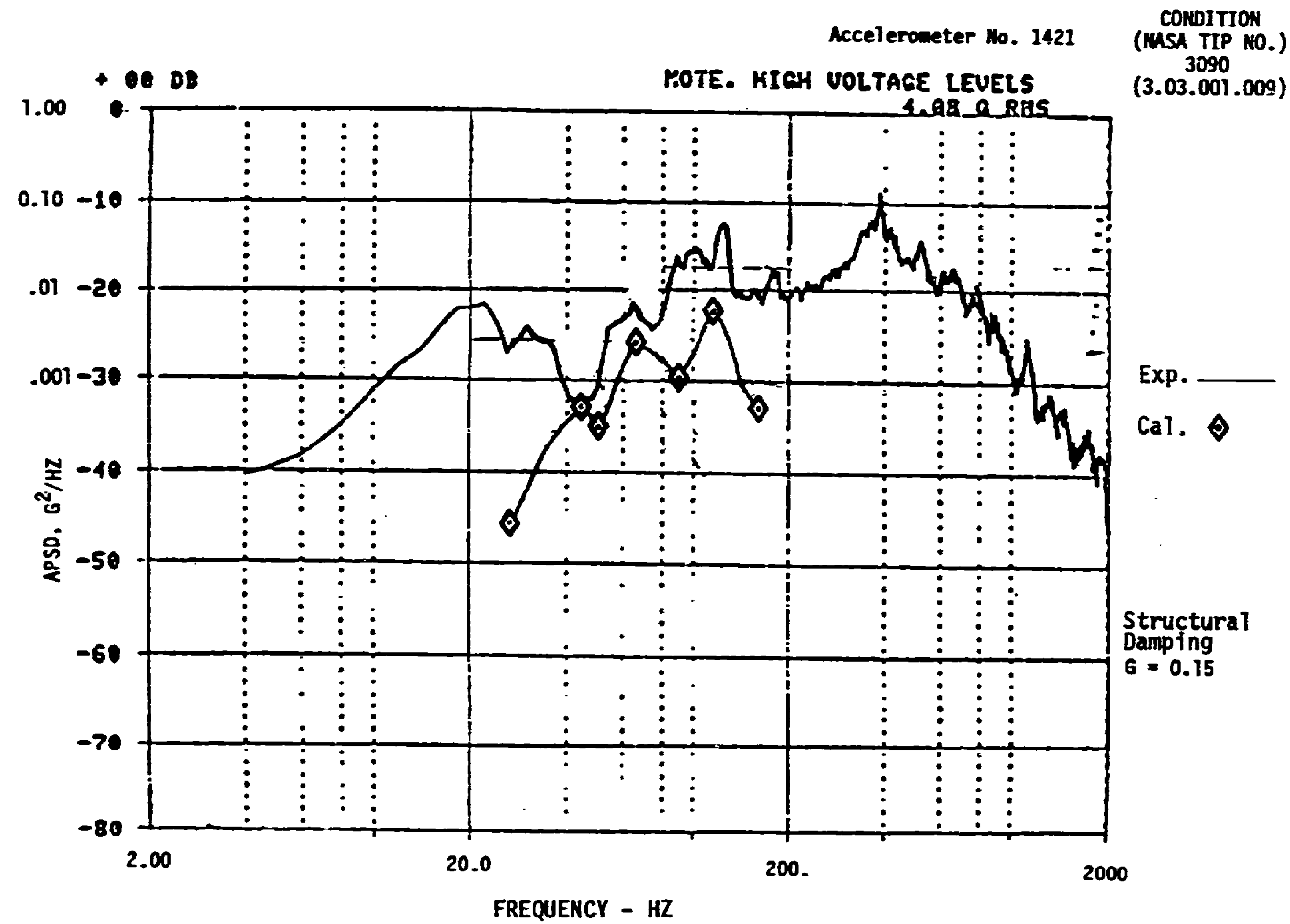

Figure 49. USB Flap Model II Response Comparison
Accelerometer 1421

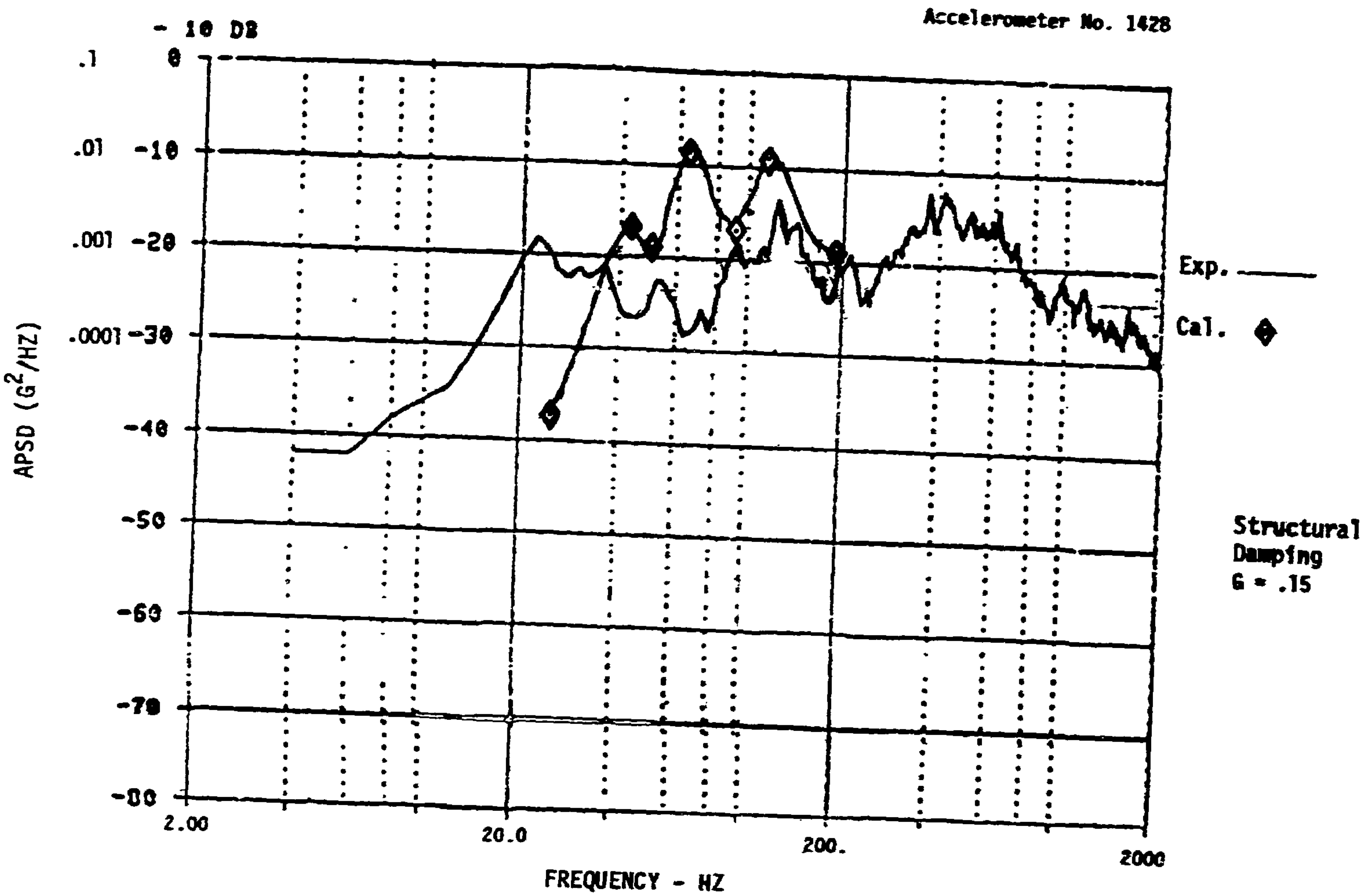

Figure 50. USB Flap Model II Response Comparison
Aceelerometer 1428

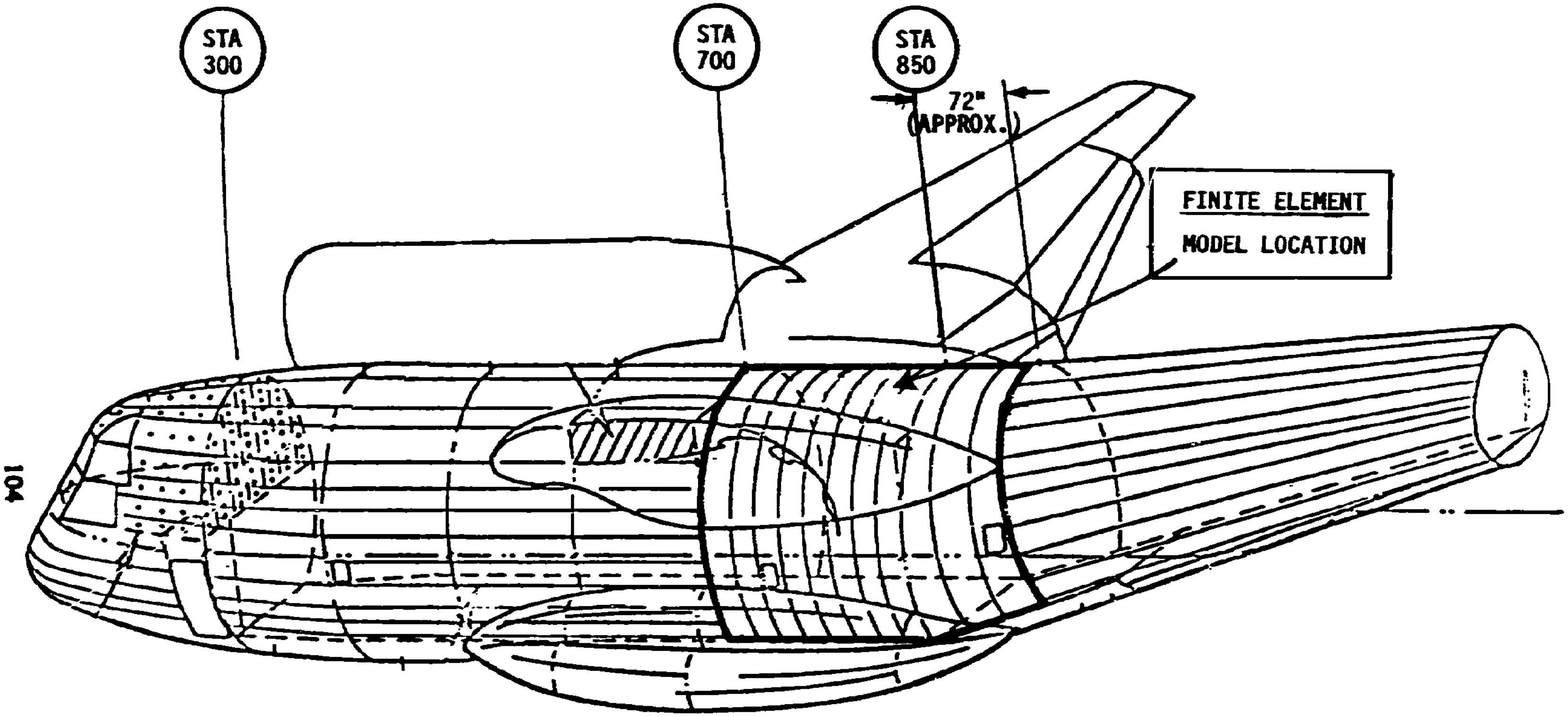

Figure 51. Location of Fuselage Finite Element Model

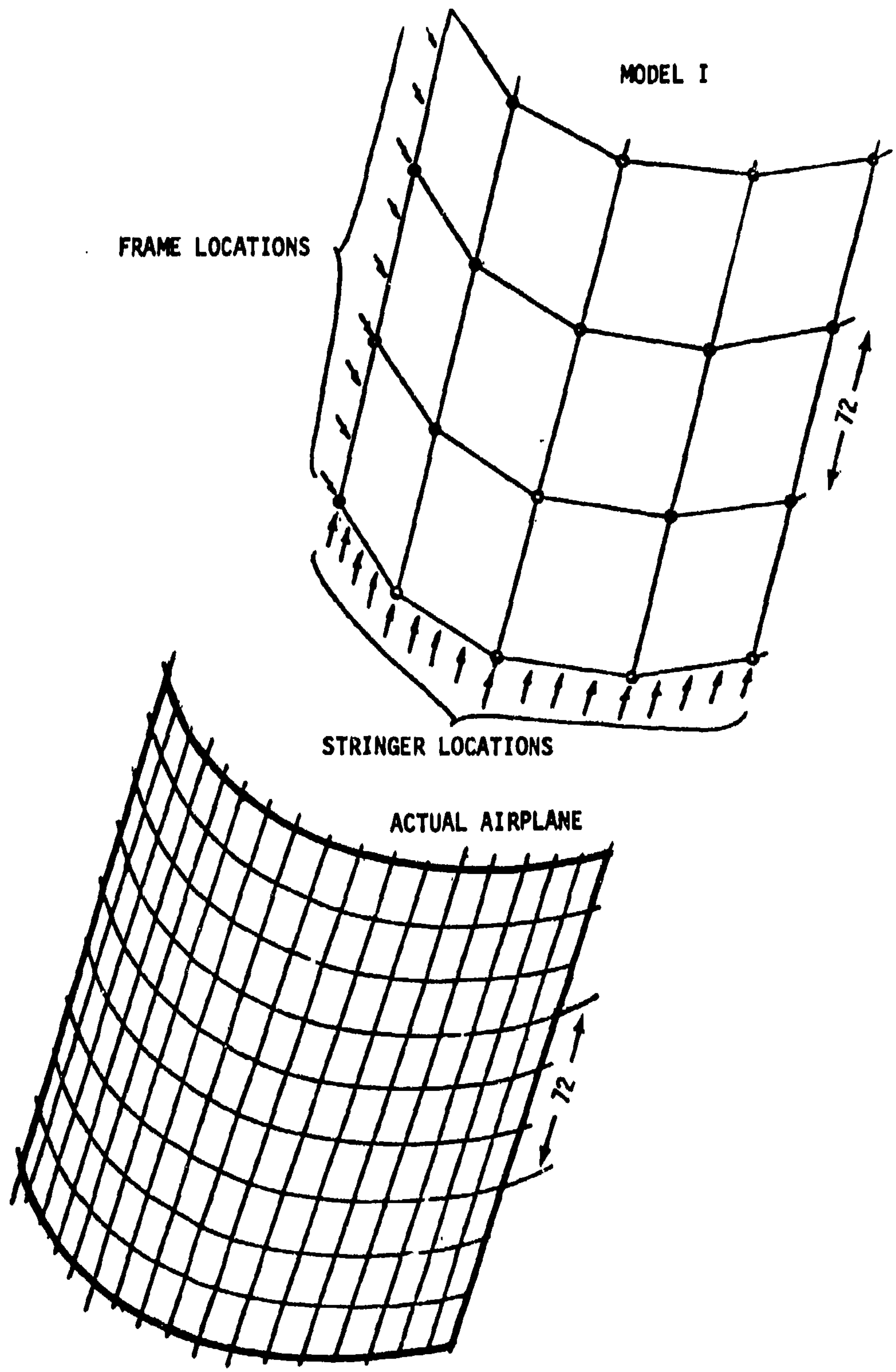

Figure 52. Low Frequency Fuselage Model I

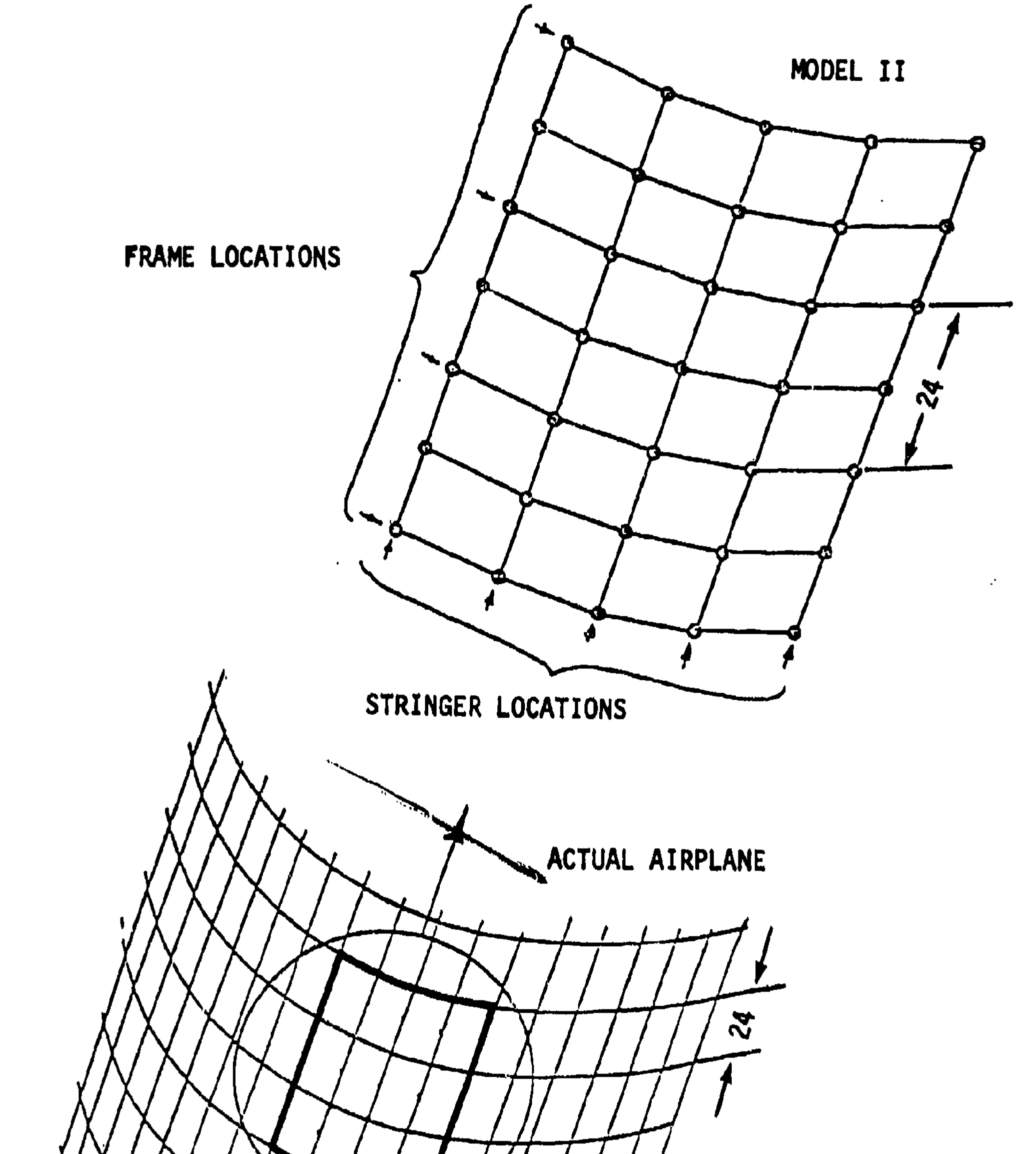

Figure 53. Mid-Frequency Fuselage Model II

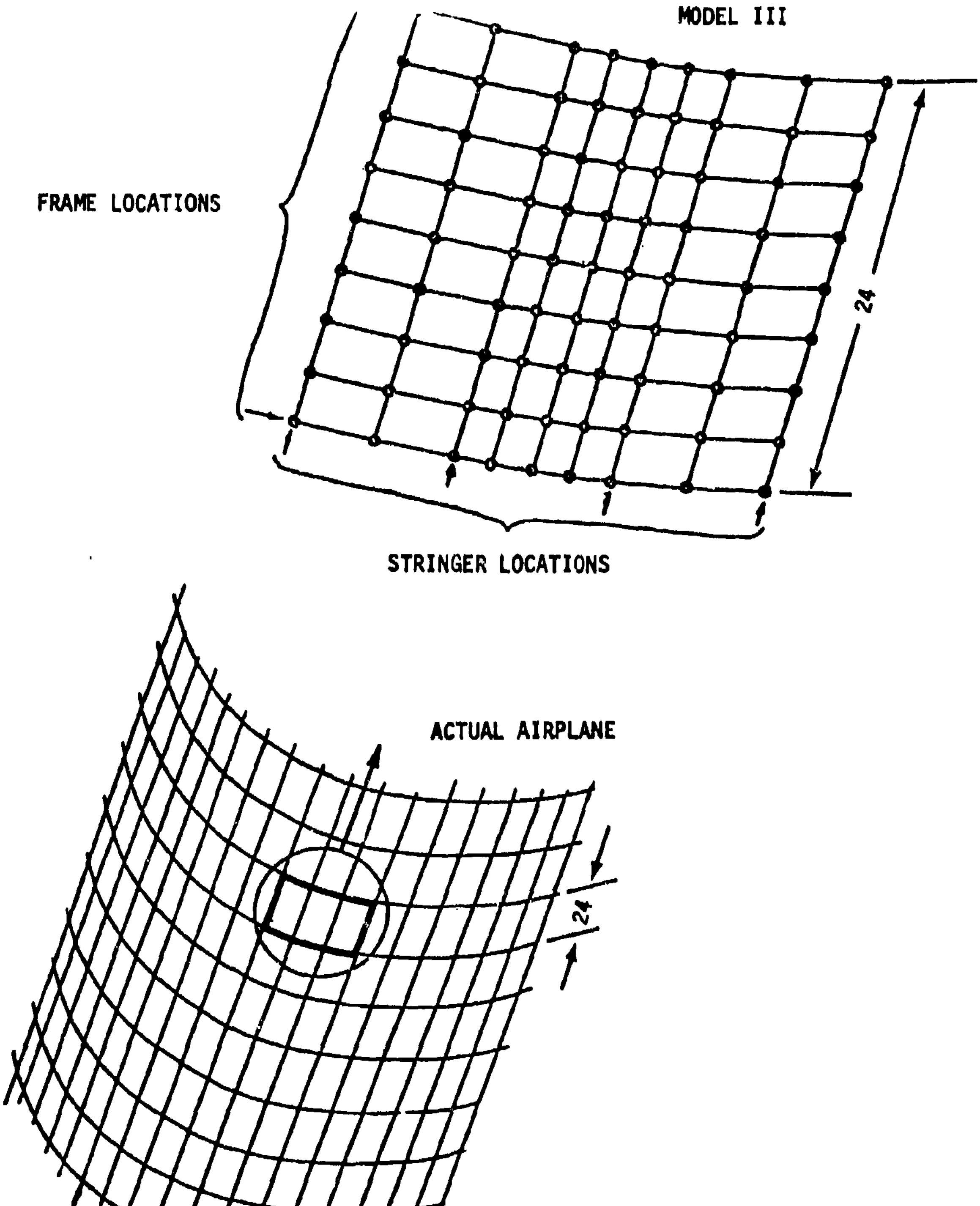

Figure 54. High Frequency Fuselage Model III

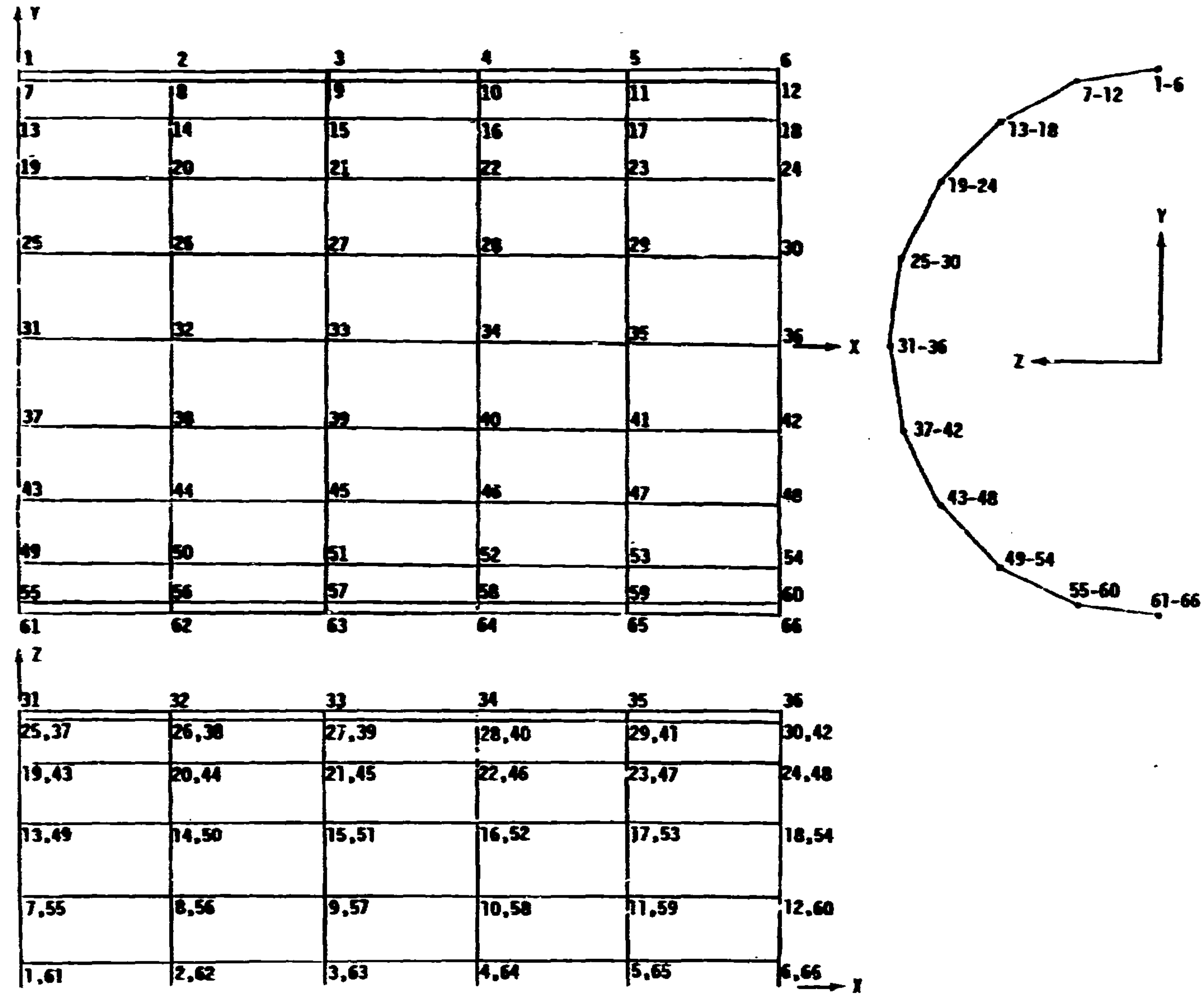

Figure 55. Low Frequency Fuselage Model I Node Points

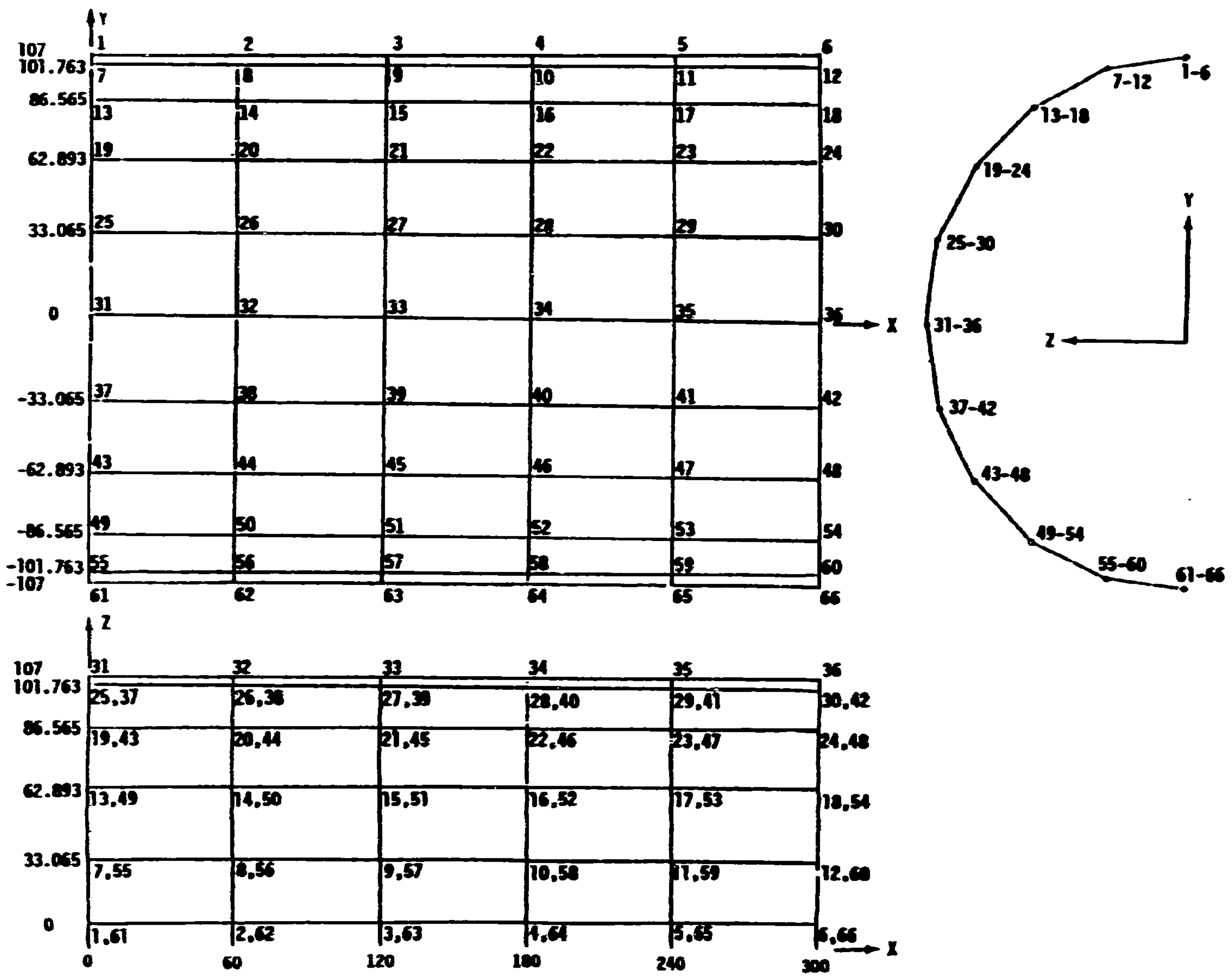

Figure 56. Low Frequency Fuselage Model I Coordinates

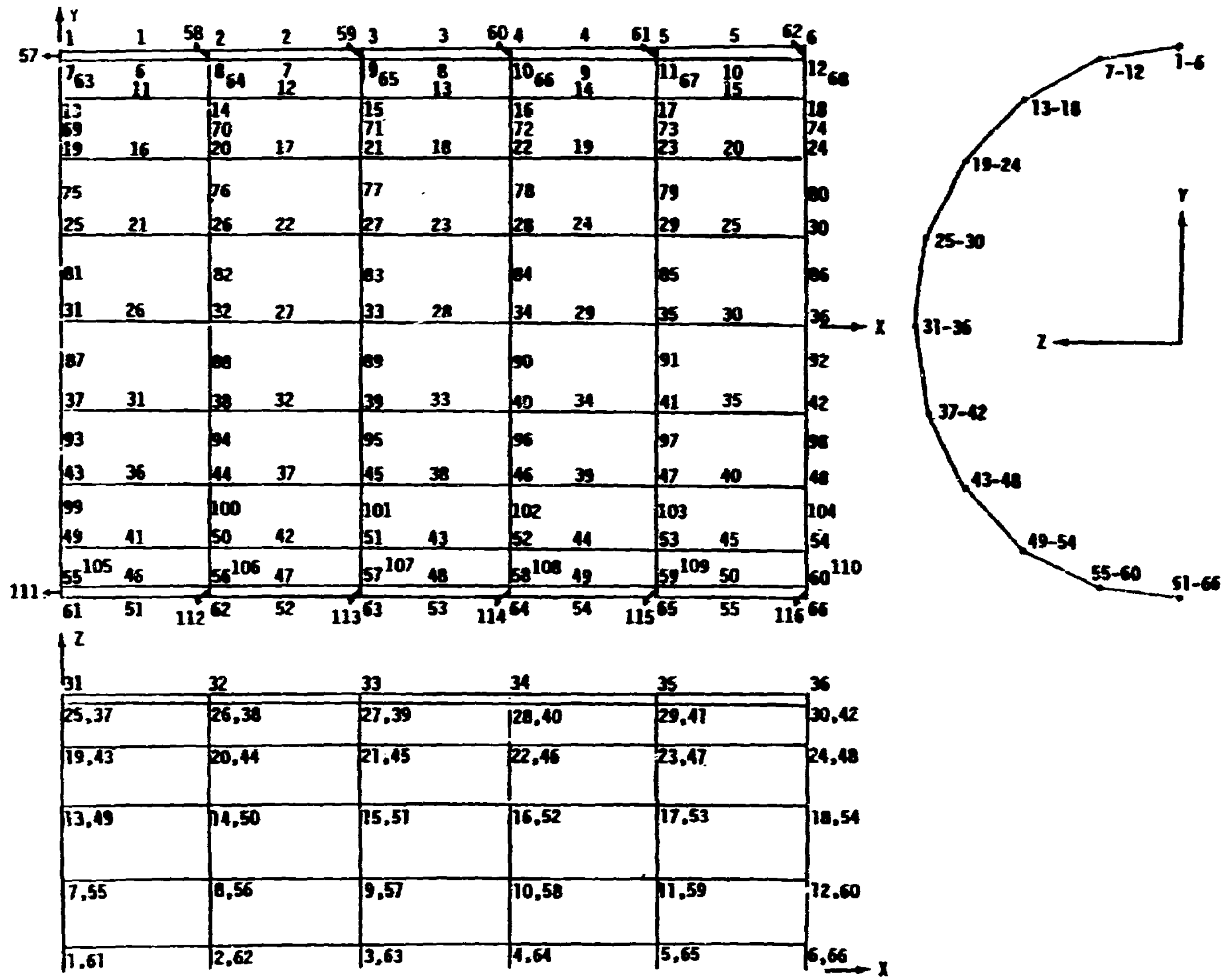

Figure 57. Low Frequency Fuselage Model I Beam Elements

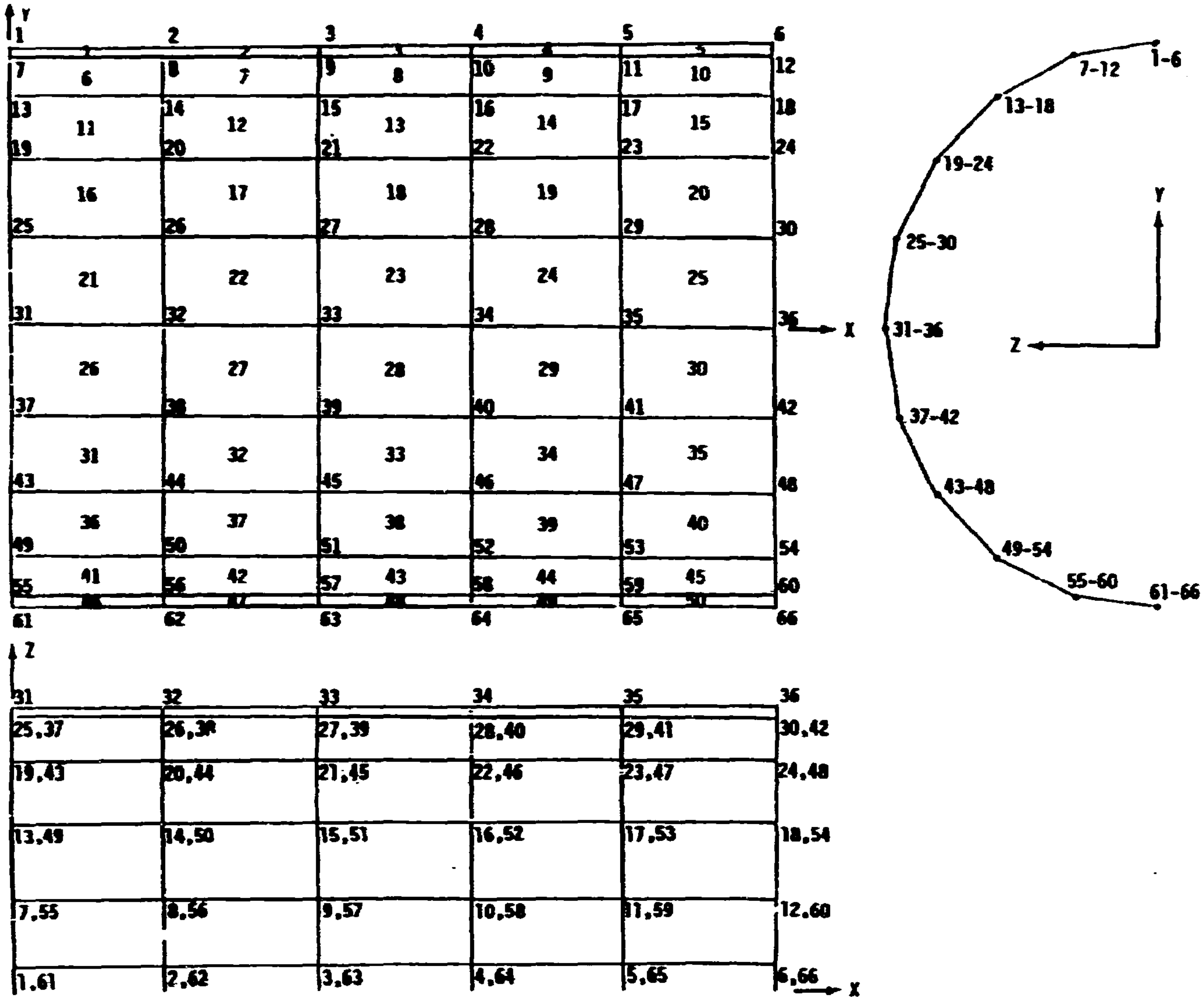

Figure 58. Low Frequency Fuselage Model I Plate Elements

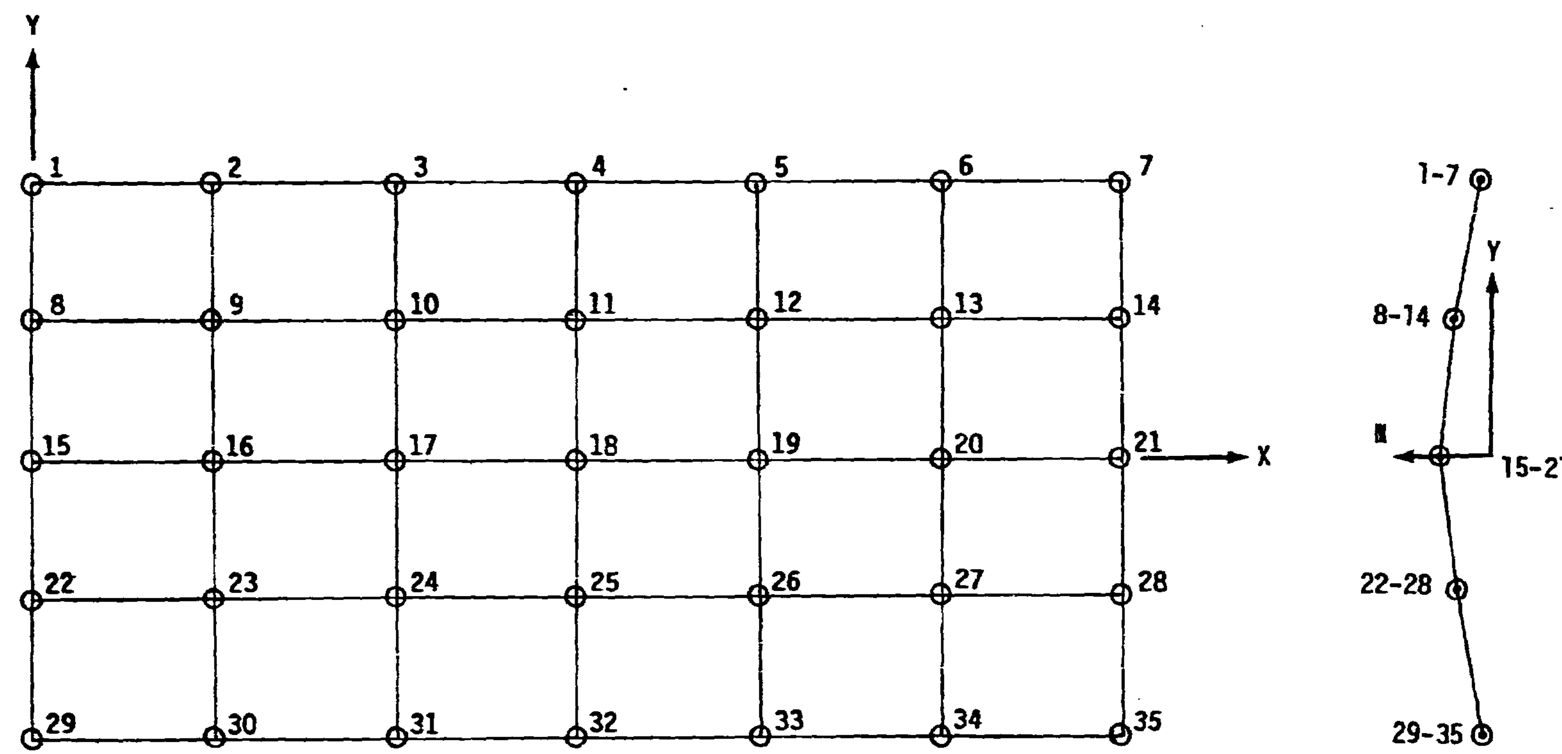

Figure 59. Fuselage Model II (Nodes) Local

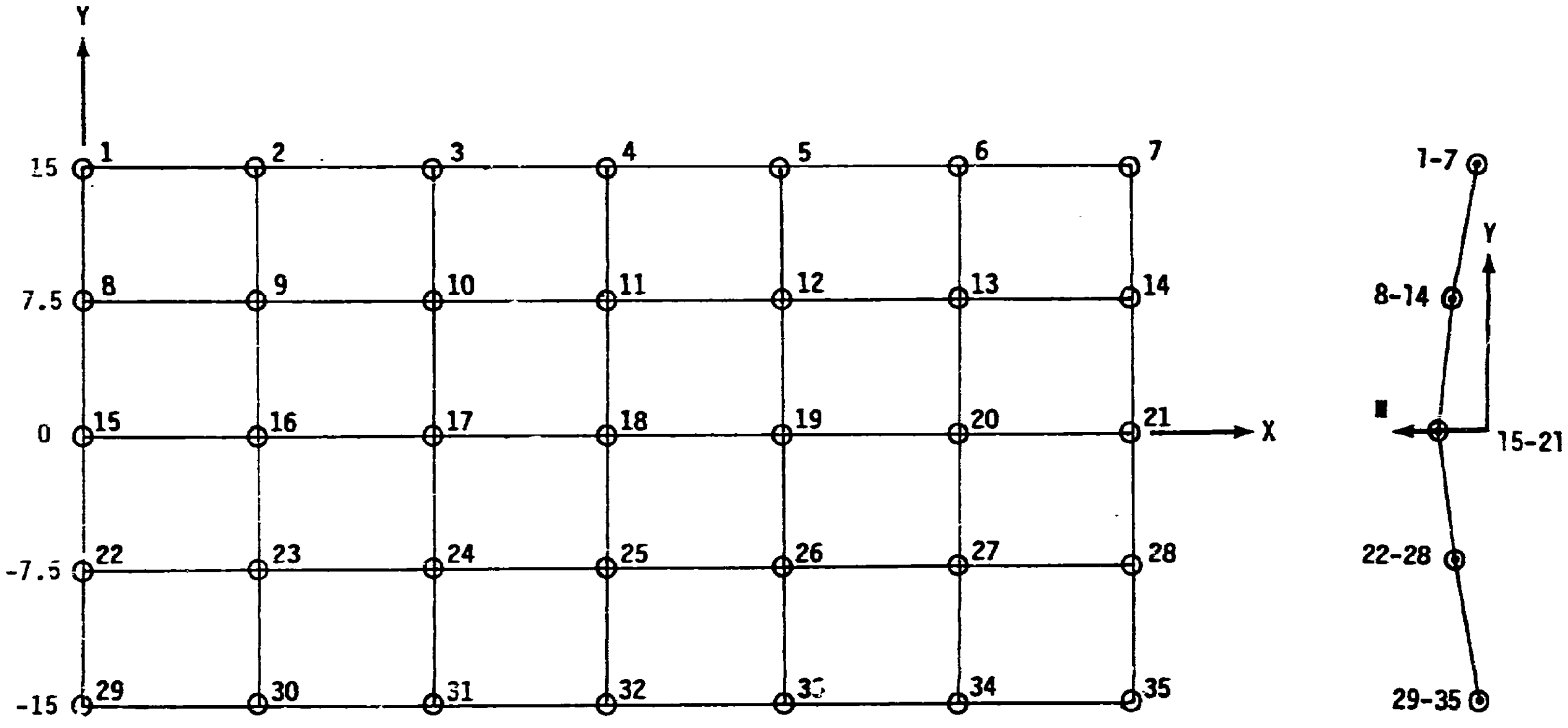

Figure 60. Fuselage Model II (Nodes) Coordinates

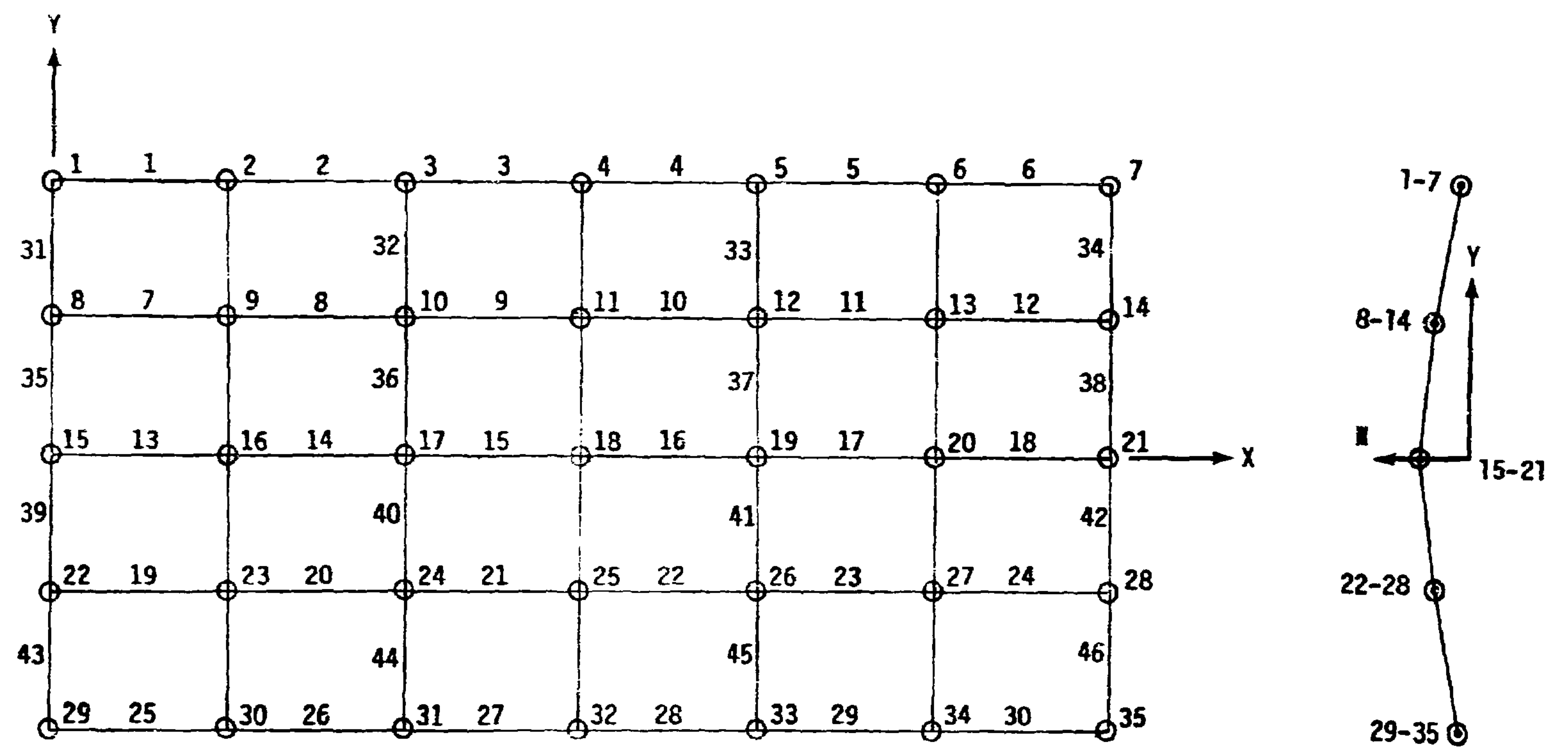

Figure 61. Fuselage Model II (Nodes) Beam Elements

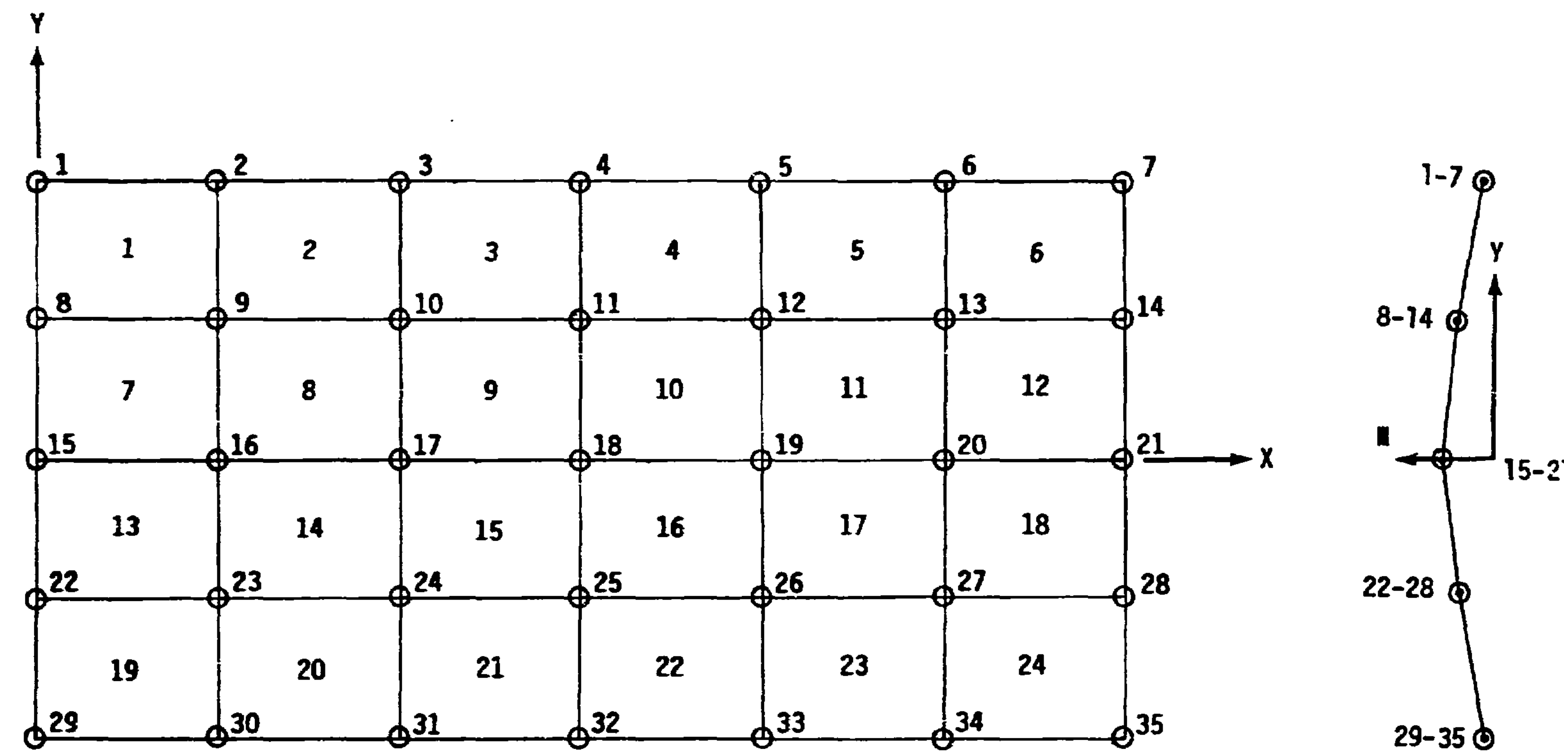

Figure 62. Fuselage Model II (Nodes) Plate Elements

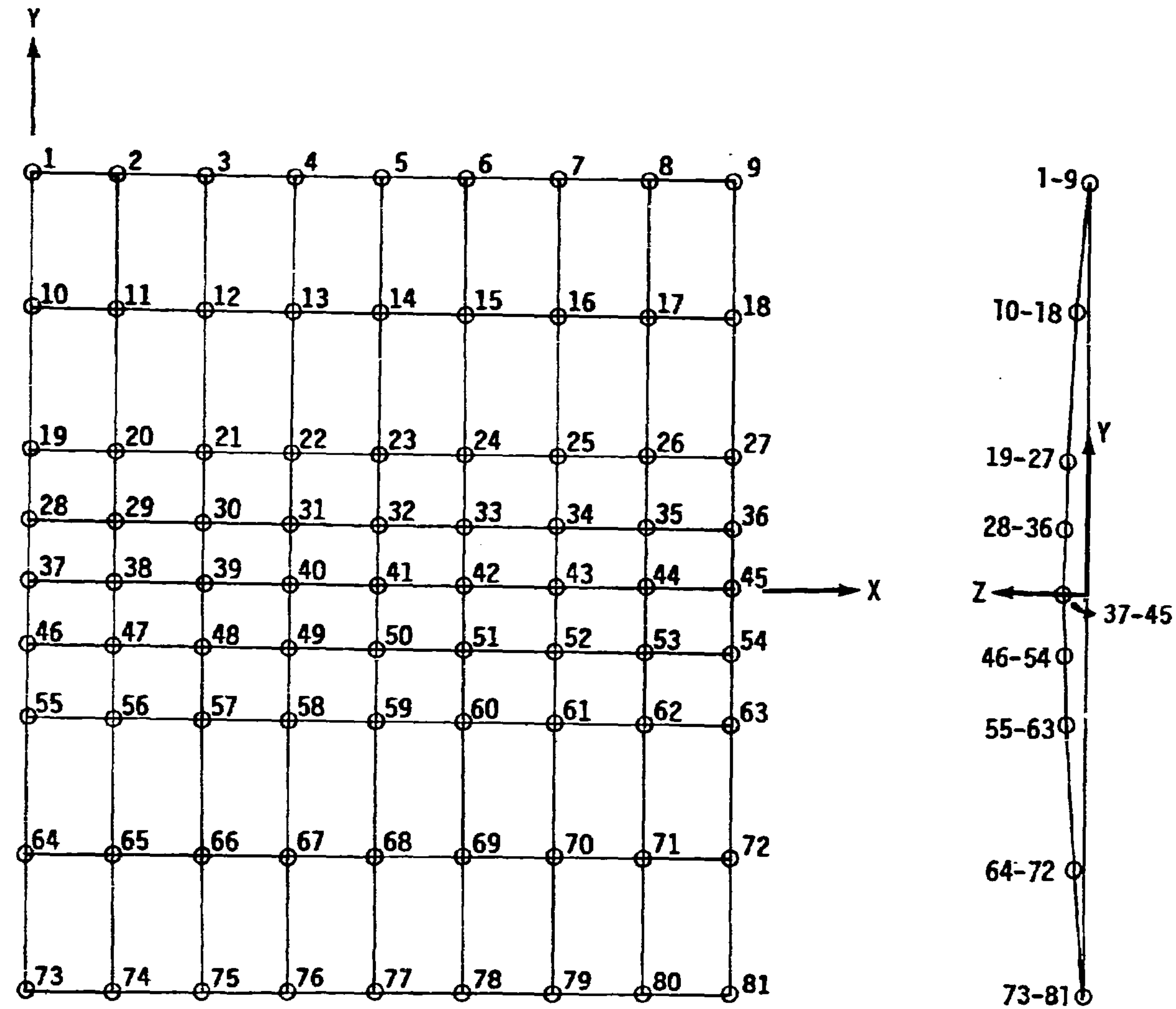

Figure 63. Fuselage Skin Model III (Nodes)

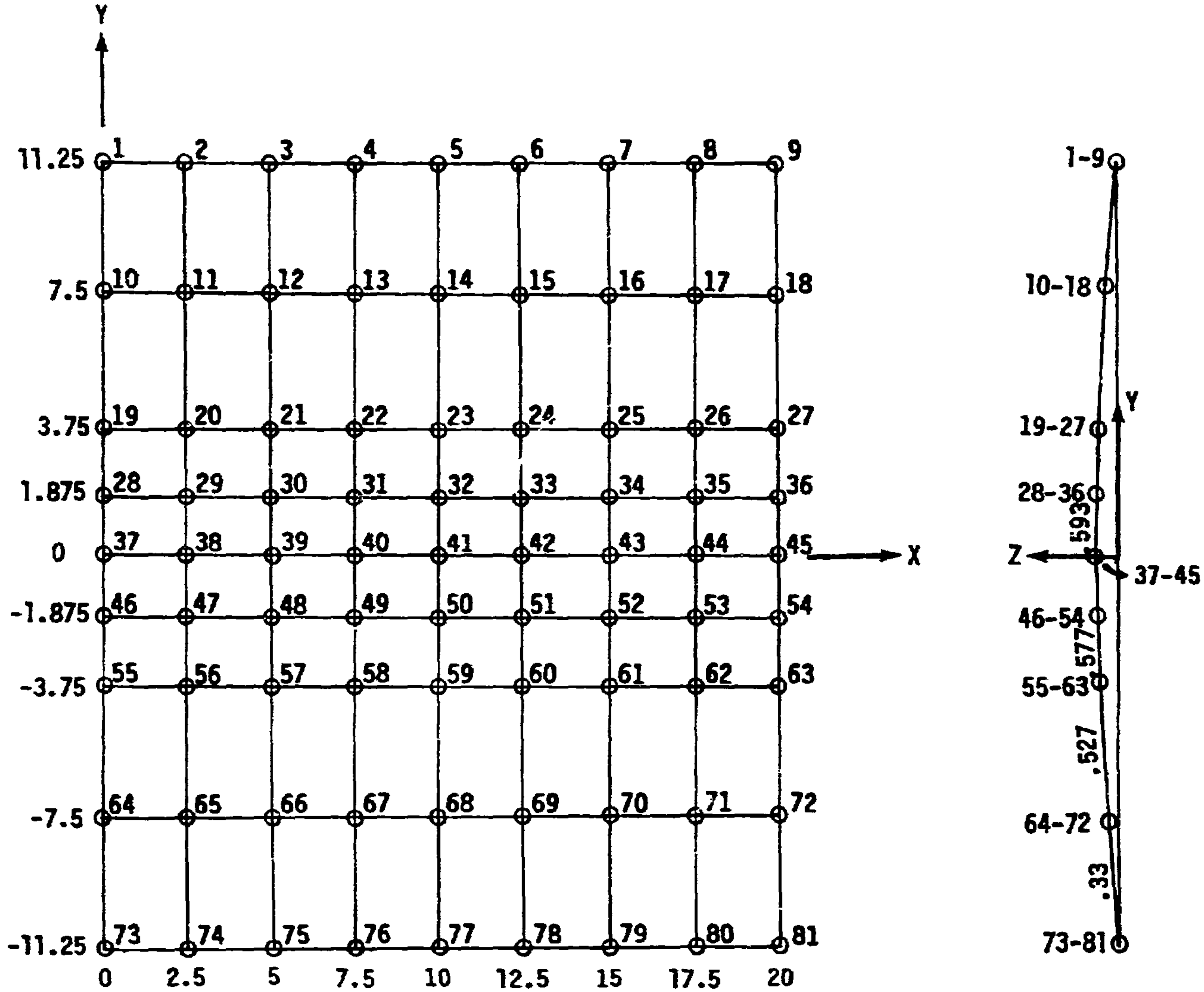

Figure 64. Fuselage Skin Model III (Coordinates)

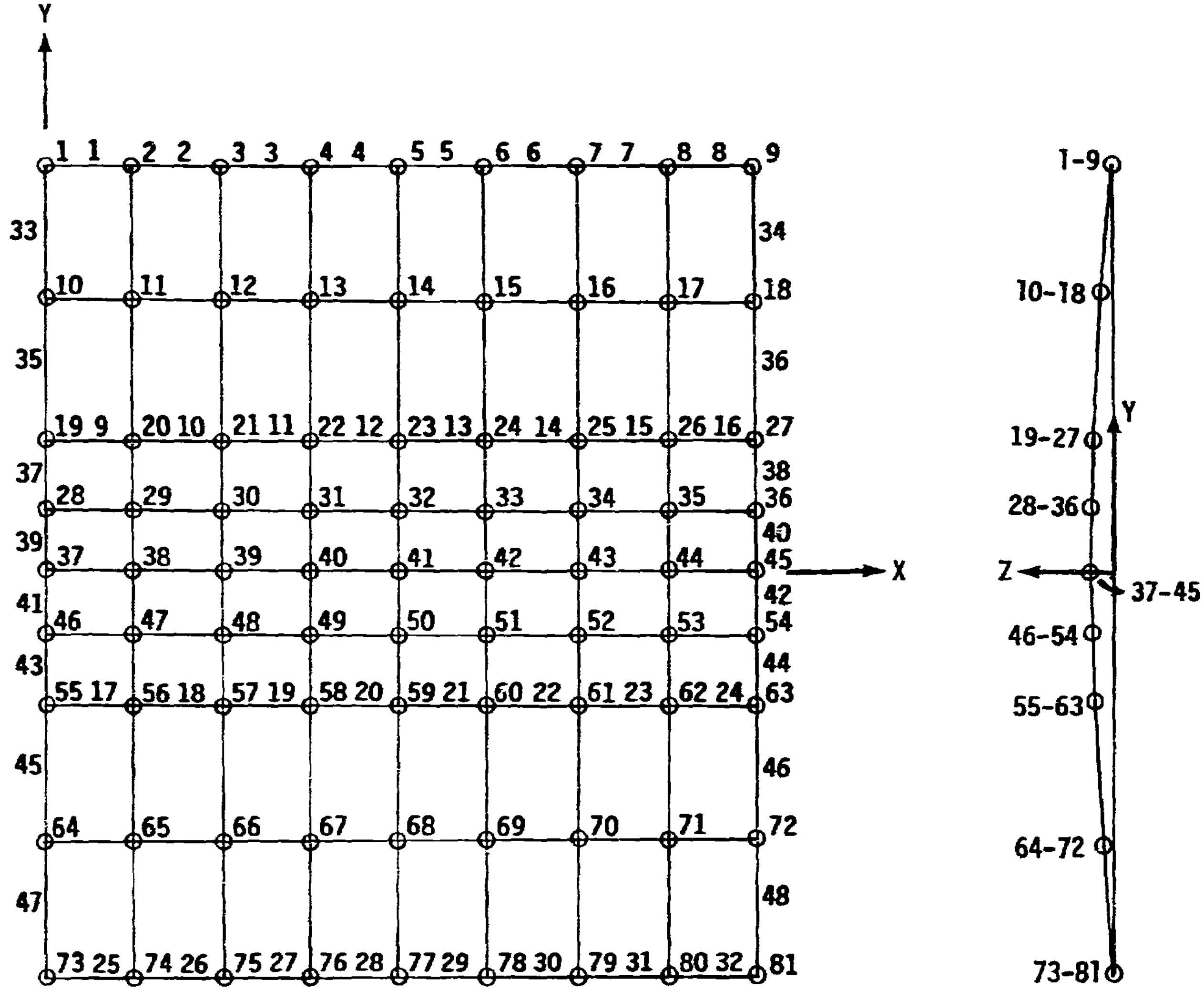

Figure 65. Fuselage Skin Model III (Beam Elements)

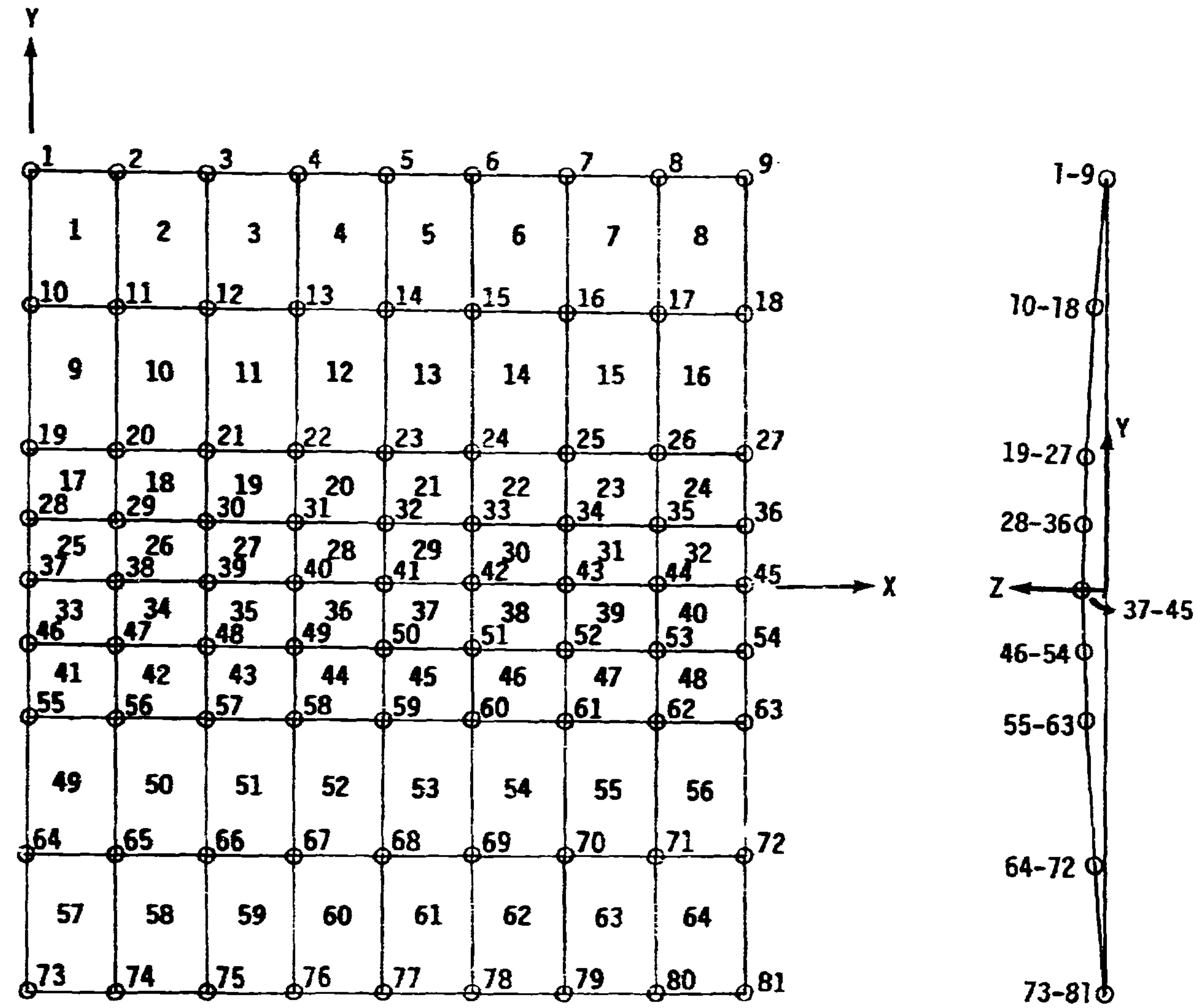

Figure 66. Fuselage Skin Model III (Plate Elements)

GEOM	ELEMENT	MAT'L	A_{AX}	AS_2	AS_3	J	I_2	I_3	t	P
1a	STRINGER	A_L	1.20	.64	.56	.00152	.32228	.43832	--	.000259
1b	FRAME	A_L	2.07	.81	1.26	.00375	9.549	.2517	--	.000259
2	SKIN PANEL	A_L	--	--	--	--	--	--	.064	.00259
LOW FREQUENCY, FUSELAGE MODEL I AND MID FREQUENCY, FUSELAGE MODEL II										
1a	STRINGER	A_L	.30	.16	.14	.00038	.08057	.10958	--	.000259
1b	FRAME	A_L	.69	.27	.42	.00125	3.183	.0839	--	.000259
2	SKIN	A_L	--	--	--	--	--	--	.064	.000259
HIGH FREQUENCY, FUSELAGE MODEL III										

Figure 67. Fuselage Element Properties of Models

PRINT OF FREQUENCIES

MODE NUMBER	CIRCULAR FREQUENCY (RAD/SEC)	FREQUENCY (CYCLE/SEC)	PERIOD (SEC)	TOLERANCE
1	8.1962E+01	1.3045E+01	7.6660E-02	1.7330E-14
2	1.5684E+02	2.4962E+01	4.0061E-02	4.7325E-15
3	2.4543E+02	3.9062E+01	2.5600E-02	3.8652E-15
4	3.2668E+02	5.1993E+01	1.9233E-02	1.3090E-14
5	3.8055E+02	6.0566E+01	1.6511E-02	1.2862E-14
6	3.8588E+02	6.1414E+01	1.6283E-02	1.2509E-14
7	4.5579E+02	7.2541E+01	1.3785E-02	8.9662E-15
8	4.8097E+02	7.6548E+01	1.3064E-02	.0
9	5.2873E+02	8.4151E+01	1.1883E-02	3.1782E-12
10	5.6127E+02	8.9328E+01	1.1195E-02	3.5477E-14
11	5.6681E+02	9.0211E+01	1.1085E-02	1.0923E-09
12	5.8724E+02	9.3462E+01	1.0700E-02	1.0985E-09
13	6.3042E+02	1.0033E+02	9.9667E-03	2.4357E-10
14	6.3438E+02	1.0096E+02	9.9045E-03	5.8566E-10
15	6.6225E+02	1.0540E+02	9.4877E-03	1.0992E-08
16	6.7555E+02	1.0752E+02	9.3009E-03	5.1638E-09
17	6.8793E+02	1.0949E+02	9.1335E-03	2.4776E-05
18	6.9020E+02	1.0985E+02	9.1035E-03	2.0665E-08
19	7.1097E+02	1.1315E+02	8.8375E-03	6.4099E-05
20	7.3308E+02	1.1667E+02	8.5710E-03	2.6744E-06

Figure 68. Natural Modes of Low Frequency YC-14 Fuselage Model I

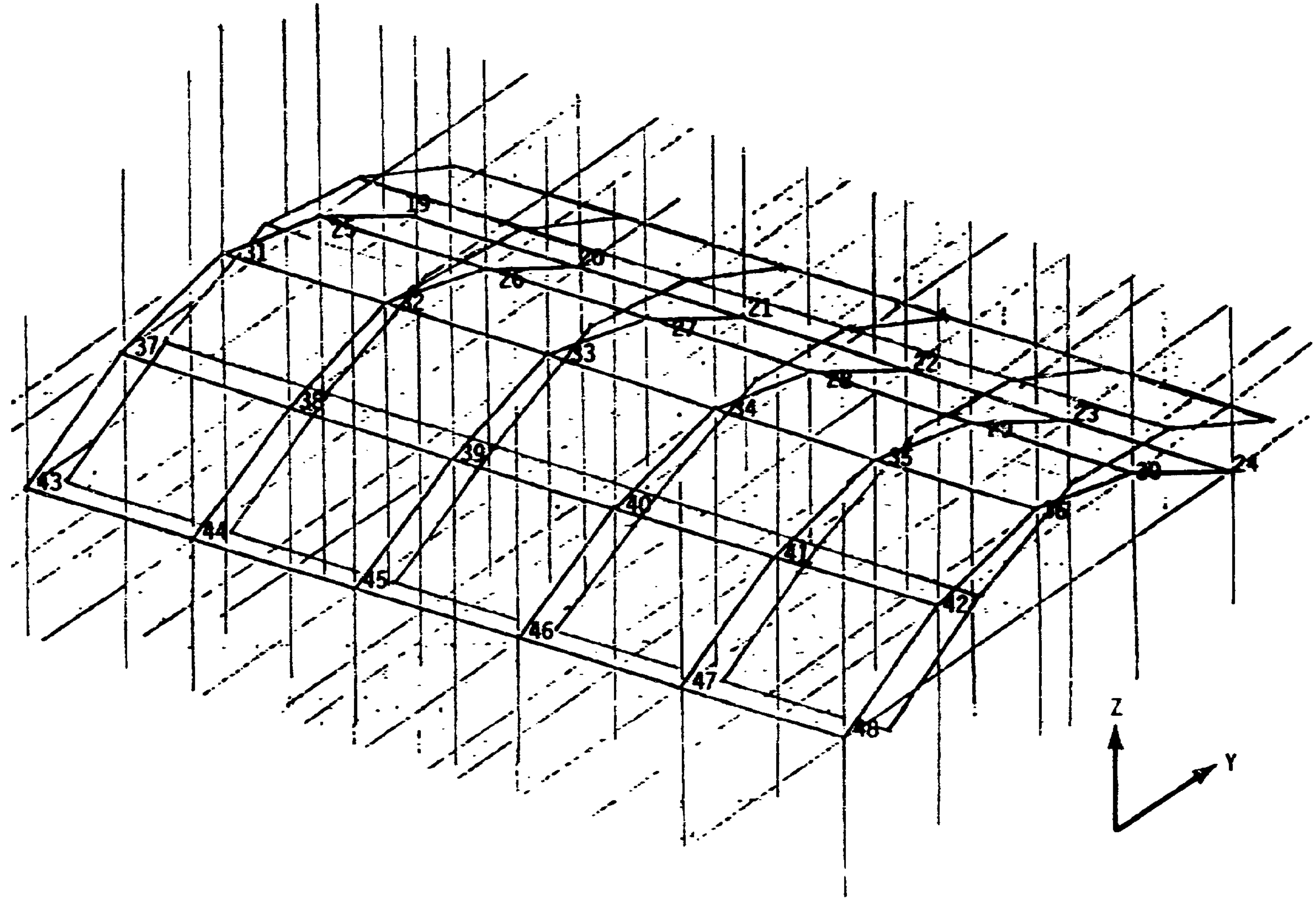

Figure 69. Fuselage Model I, Frequency = 13.045 Hz

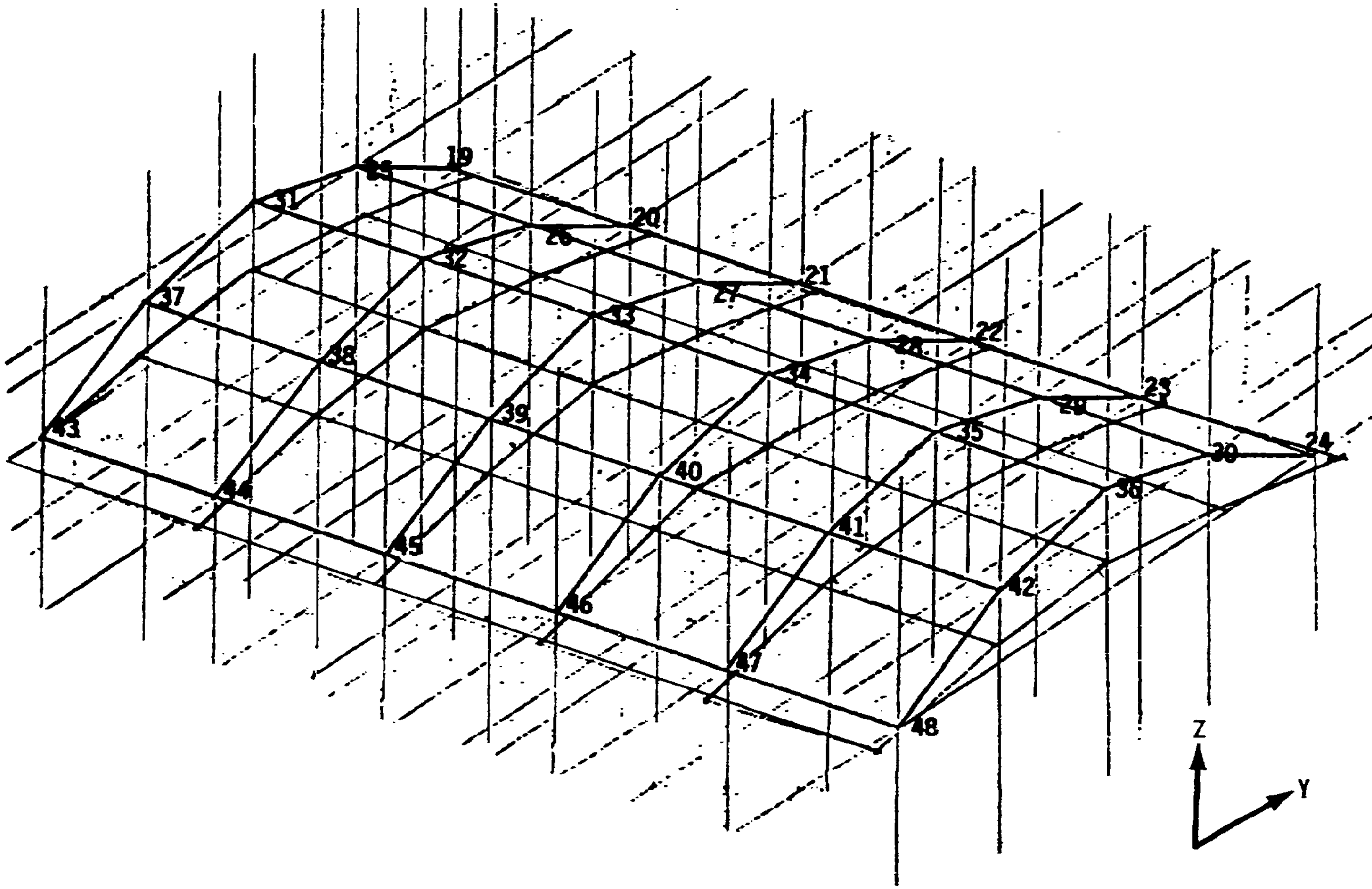

Figure 70. Fuselage Model I, Frequency = 24.962 Hz

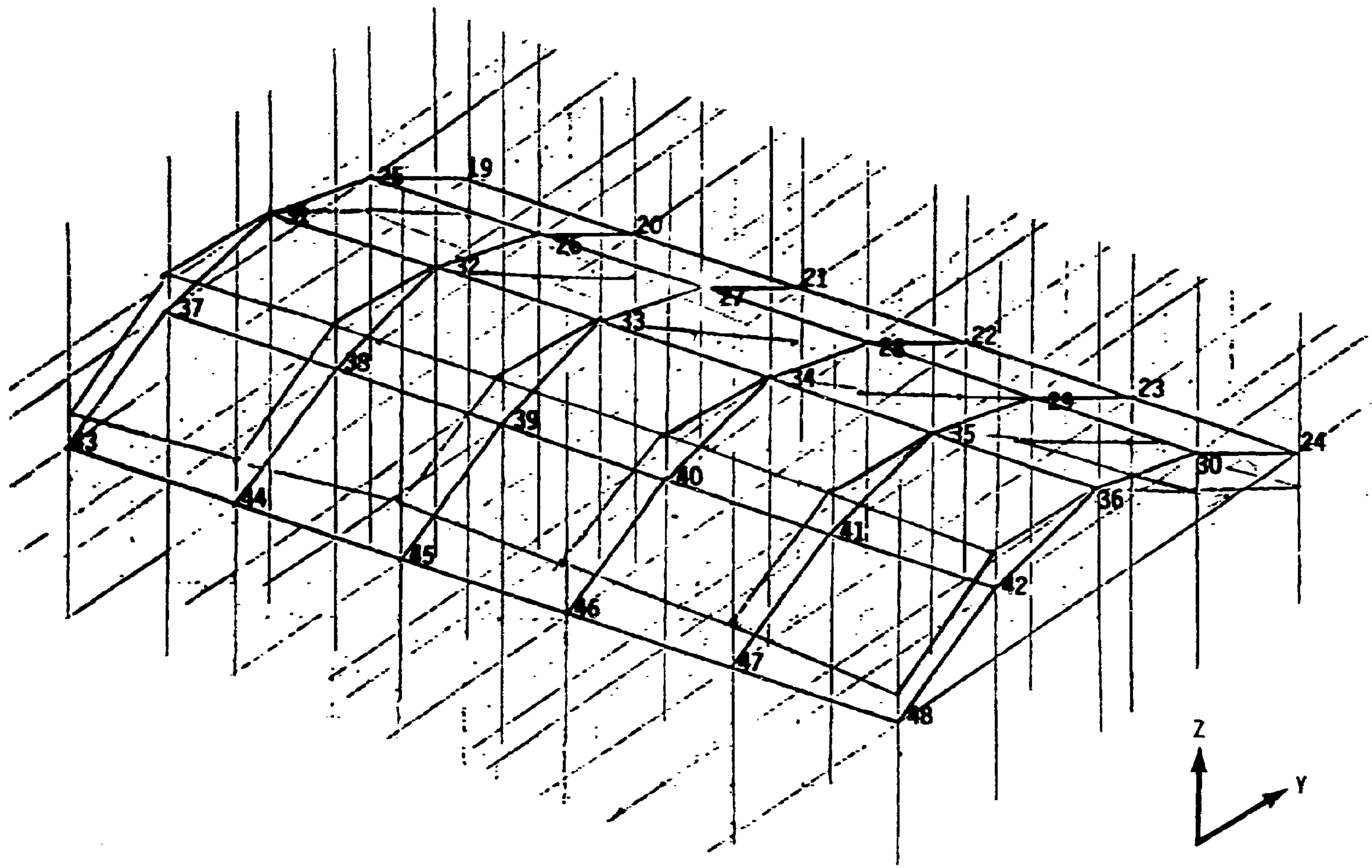

Figure 71. Fuselage Model I, Frequency = 39.062 Hz

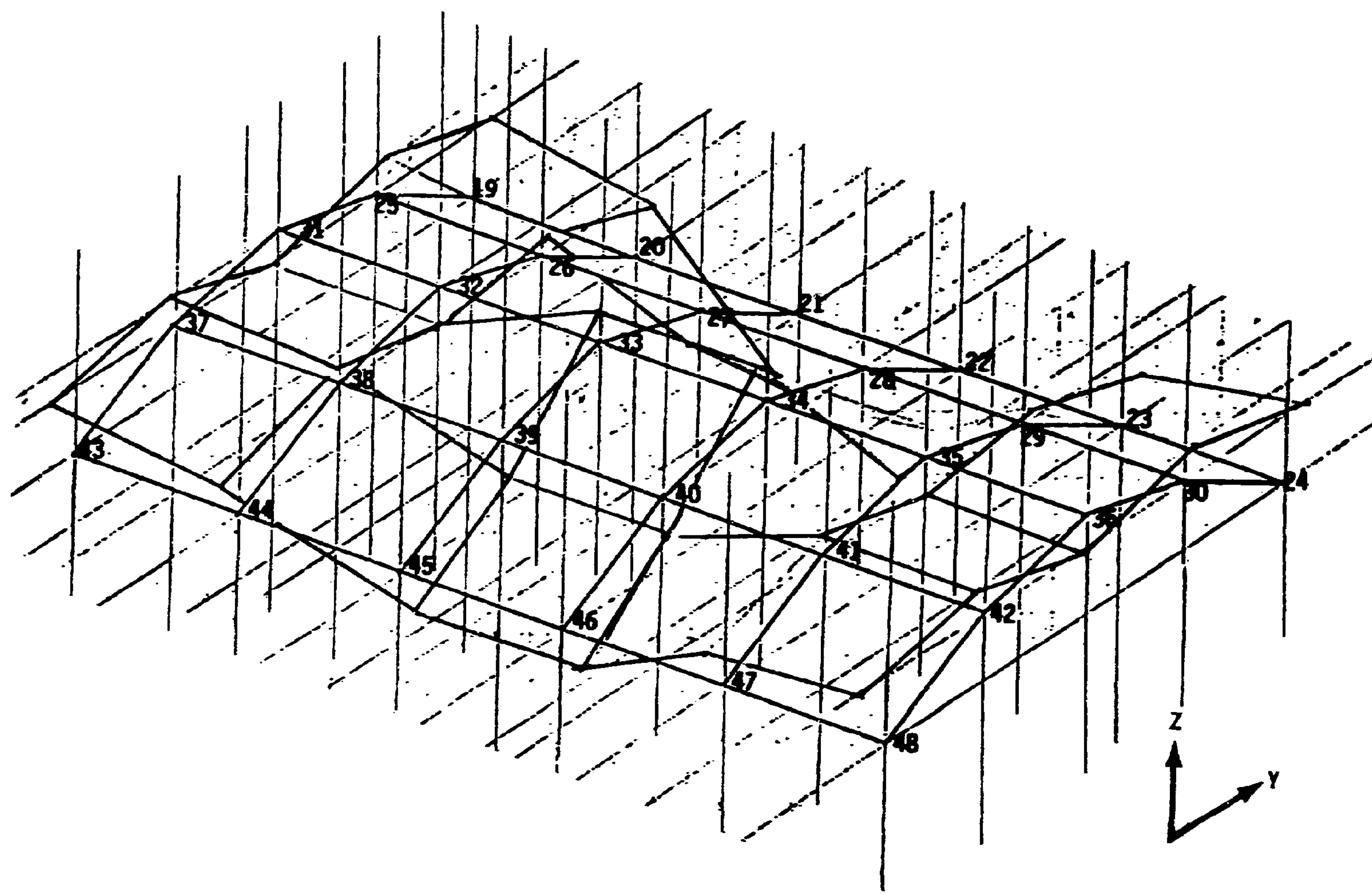

Figure 72. Fuselage Model I, Frequency = 51.993 Hz

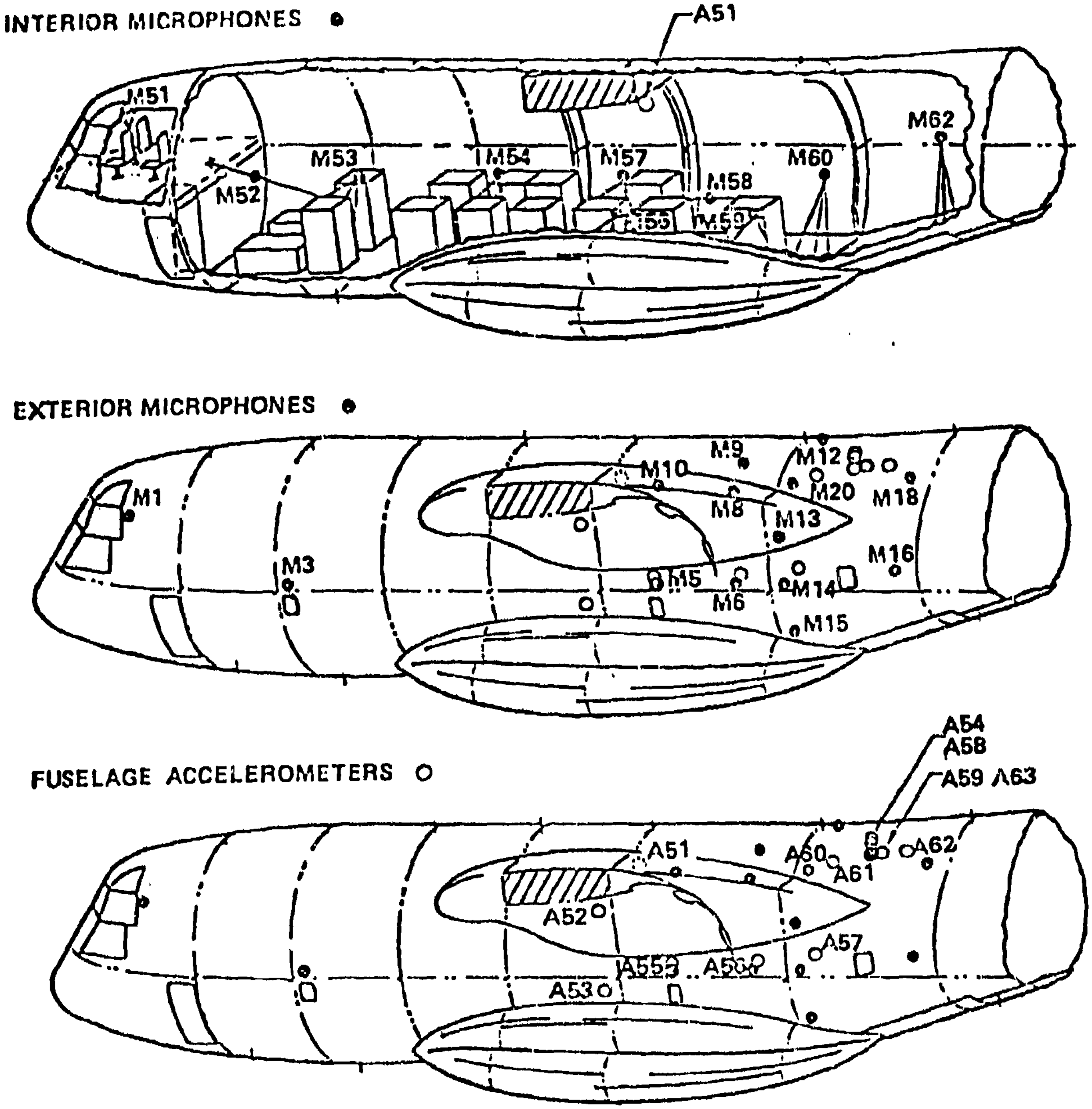

Figure 73. YC-14 Instrumentation Locations for Fuselage

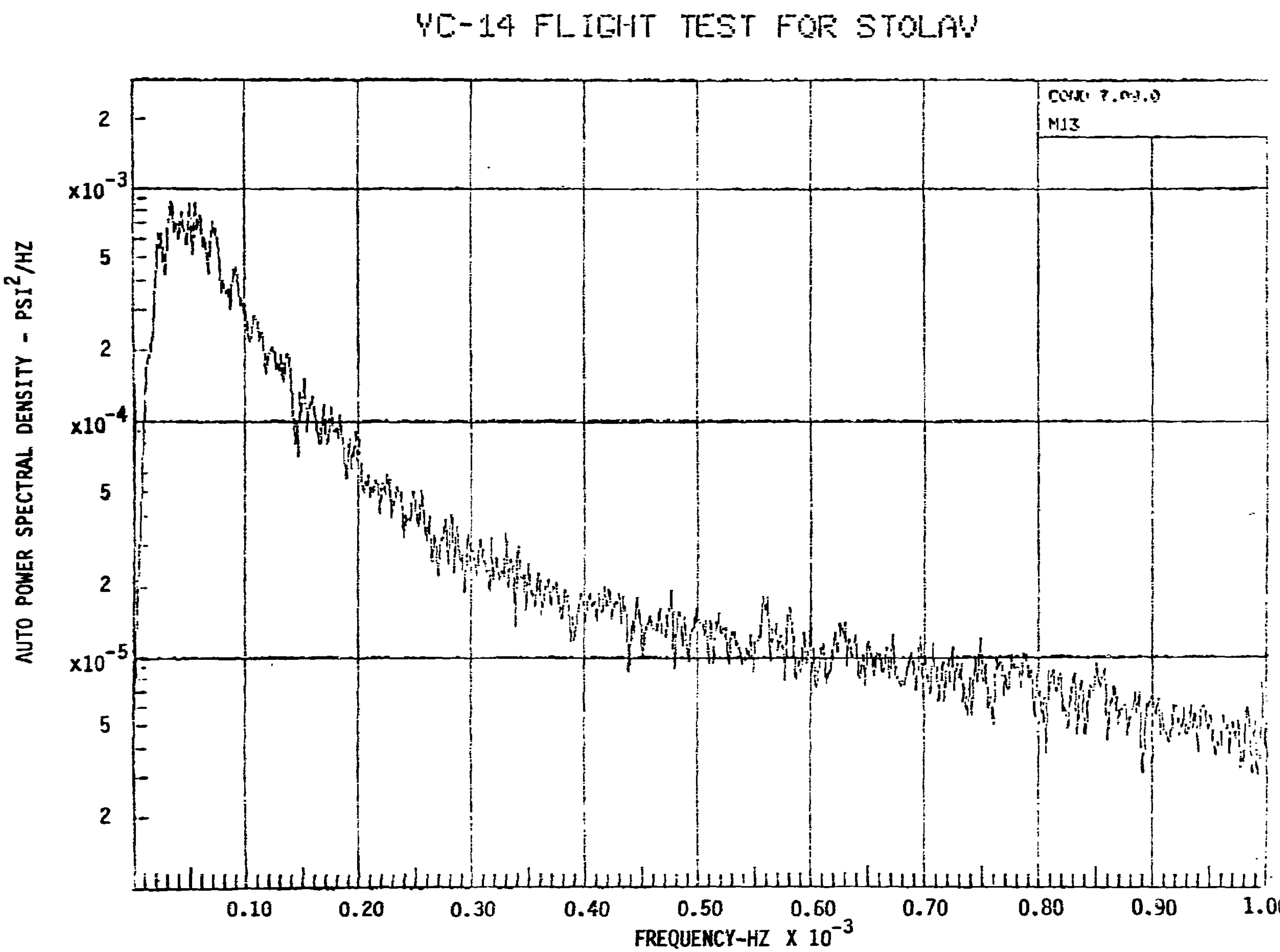

Figure 74. Microphone M13 Data Used for Fuselage Model Excitation

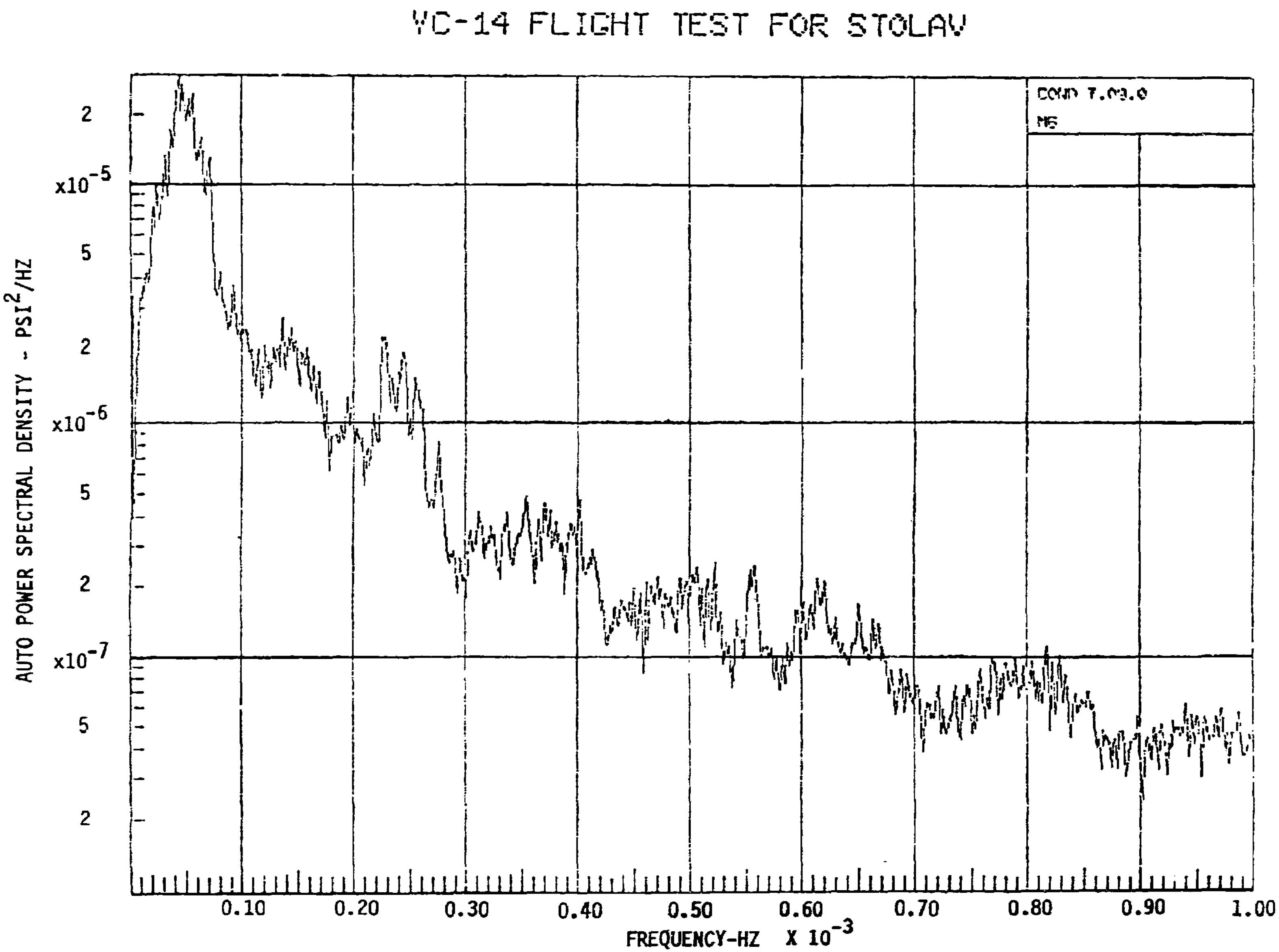

Figure 75. Microphone M6 Data Used for Fuselage Model Excitation

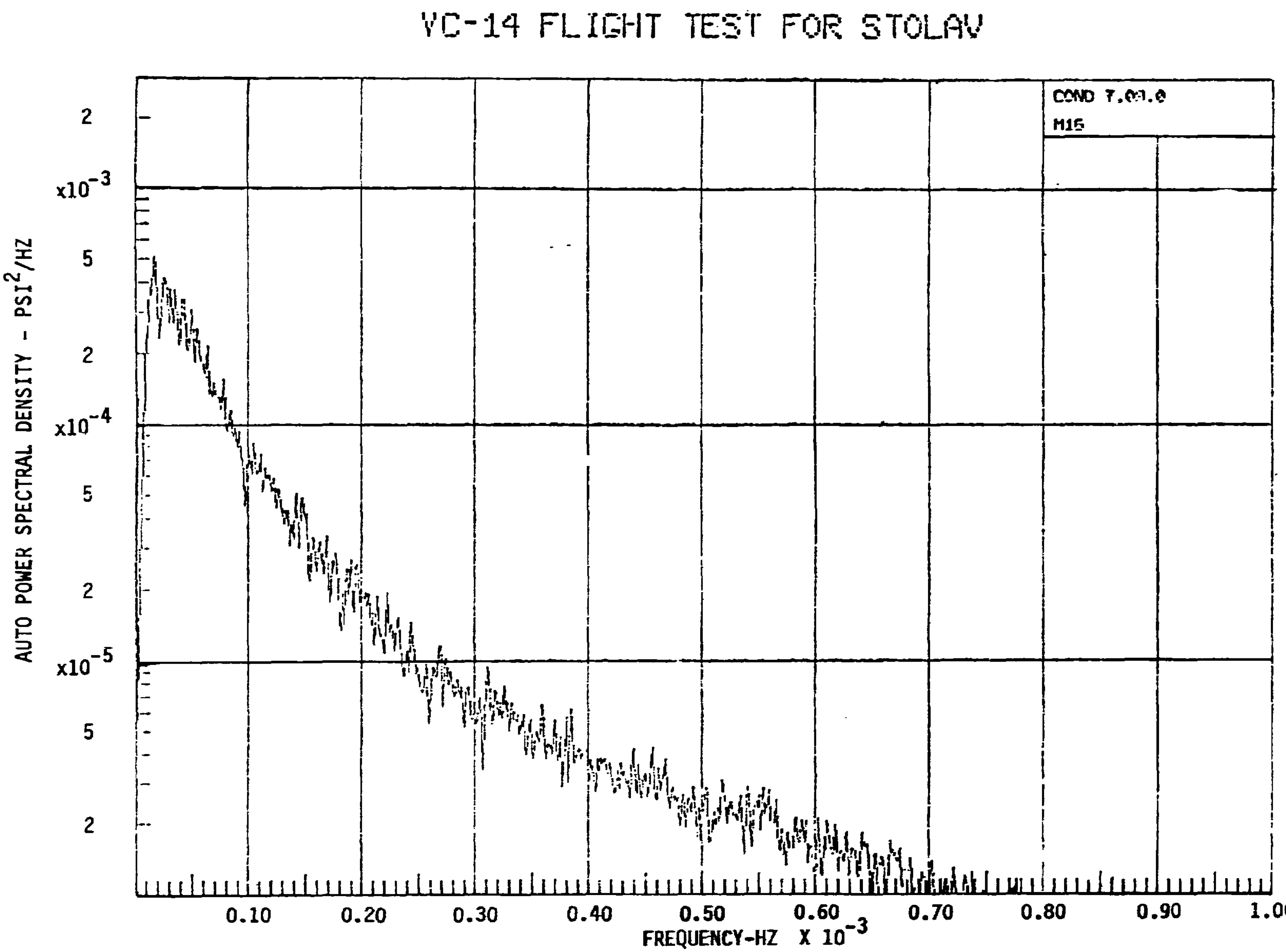

Figure 76. Microphone M16 Data Used for Fuselage Model Excitation

FREQUENCY (CPS)	M16 $x10^{-4}$	M6 $x10^{-6}$	M13 $x10^{-4}$	M20 $x10^{-5}$ (1400)			M18 $x10^{-5}$ (1398)
PSI²/Hz				DB	M13	MULT	M16
25	4.0	7.0	3.0	-8	7	4.29	5.58
32	3.0	4.0	6.0	-11	13.5	4.44	2.22
41	2.8	12.0	7.0	-11		5.19	2.08
50	2.5	23.0	7.0	-11		5.19	1.85
66	1.7	10.0	5.5	-14	27	2.04	0.67
84	1.1	3.0	4.0	-14		1.48	0.41
100	0.7	2.2	3.0	-14		1.11	0.26
133	0.45	1.8	1.8	-13	21	0.86	0.22
167	0.25	1.4	1.0	-13		0.48	0.12
200	0.19	1.0	0.9	-12	14.5	0.62	0.13

Figure 77. Microphone Data for Medium STOL

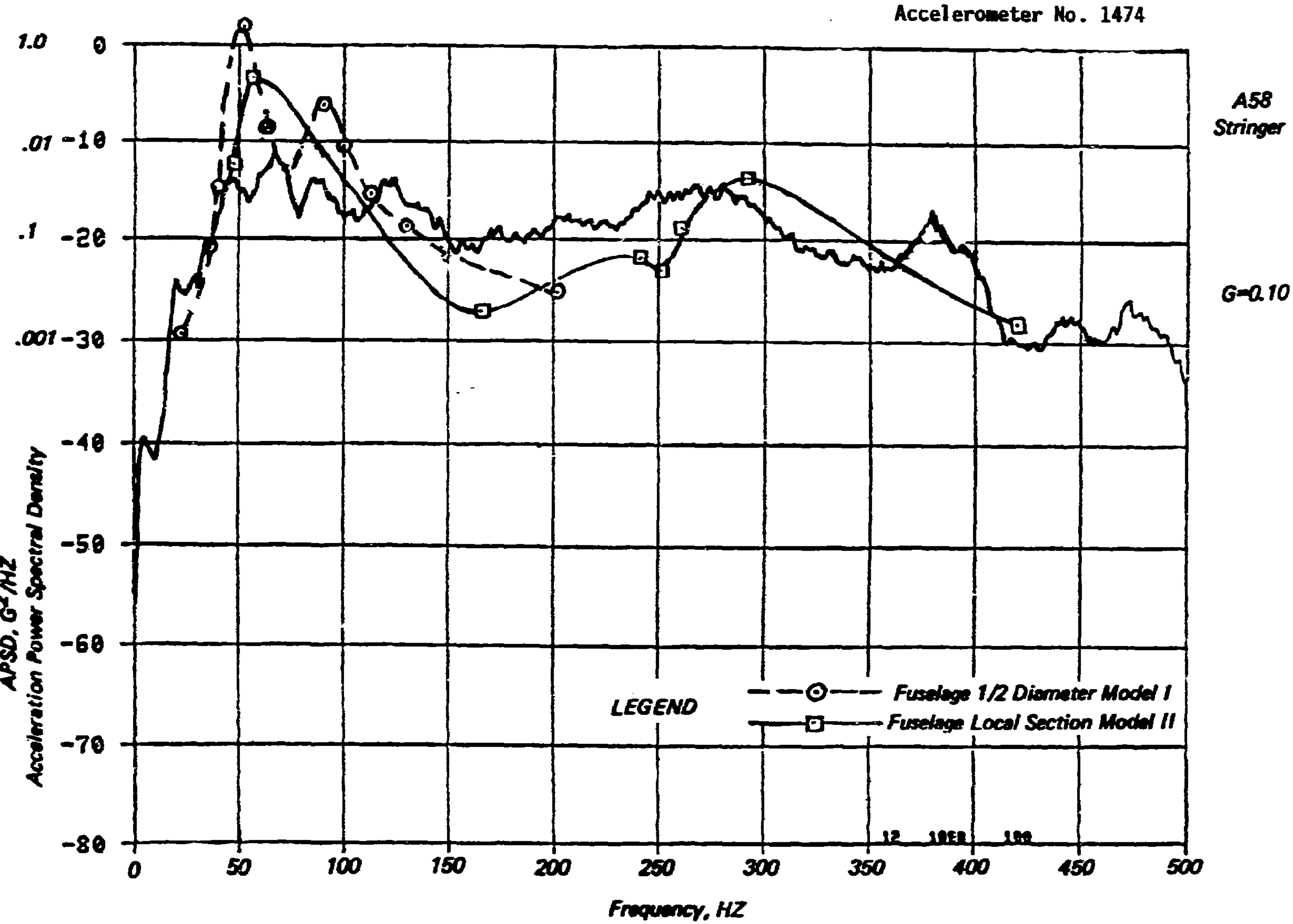

Figure 78. Calculated Response of Models I and II for Stringer Accelerometer A58 Compared to Flight Test Data

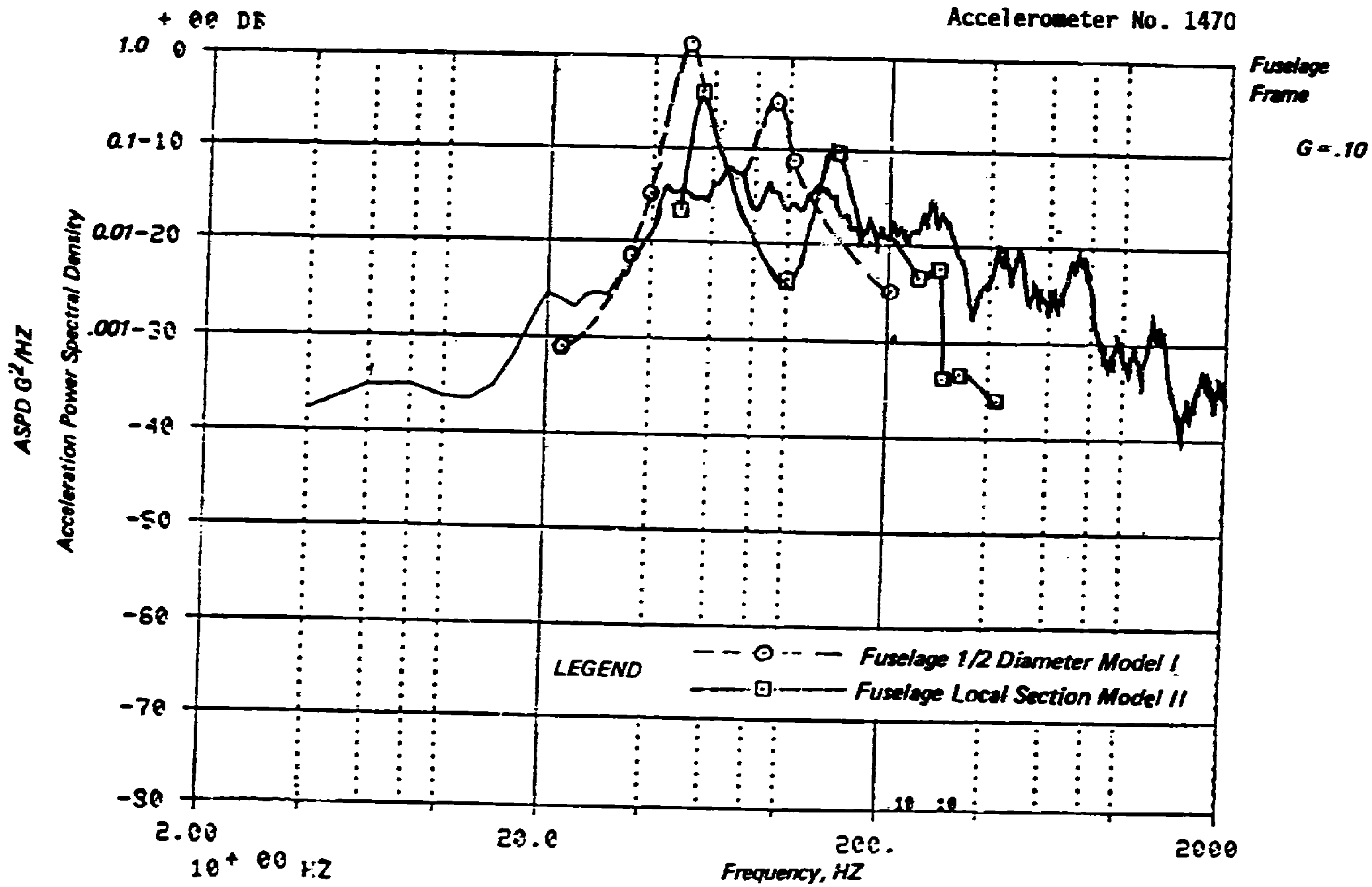

Figure 79. Calculated Response of Models I and II for Fuselage Frame Accelerometer A59 Compared to Flight Test Data

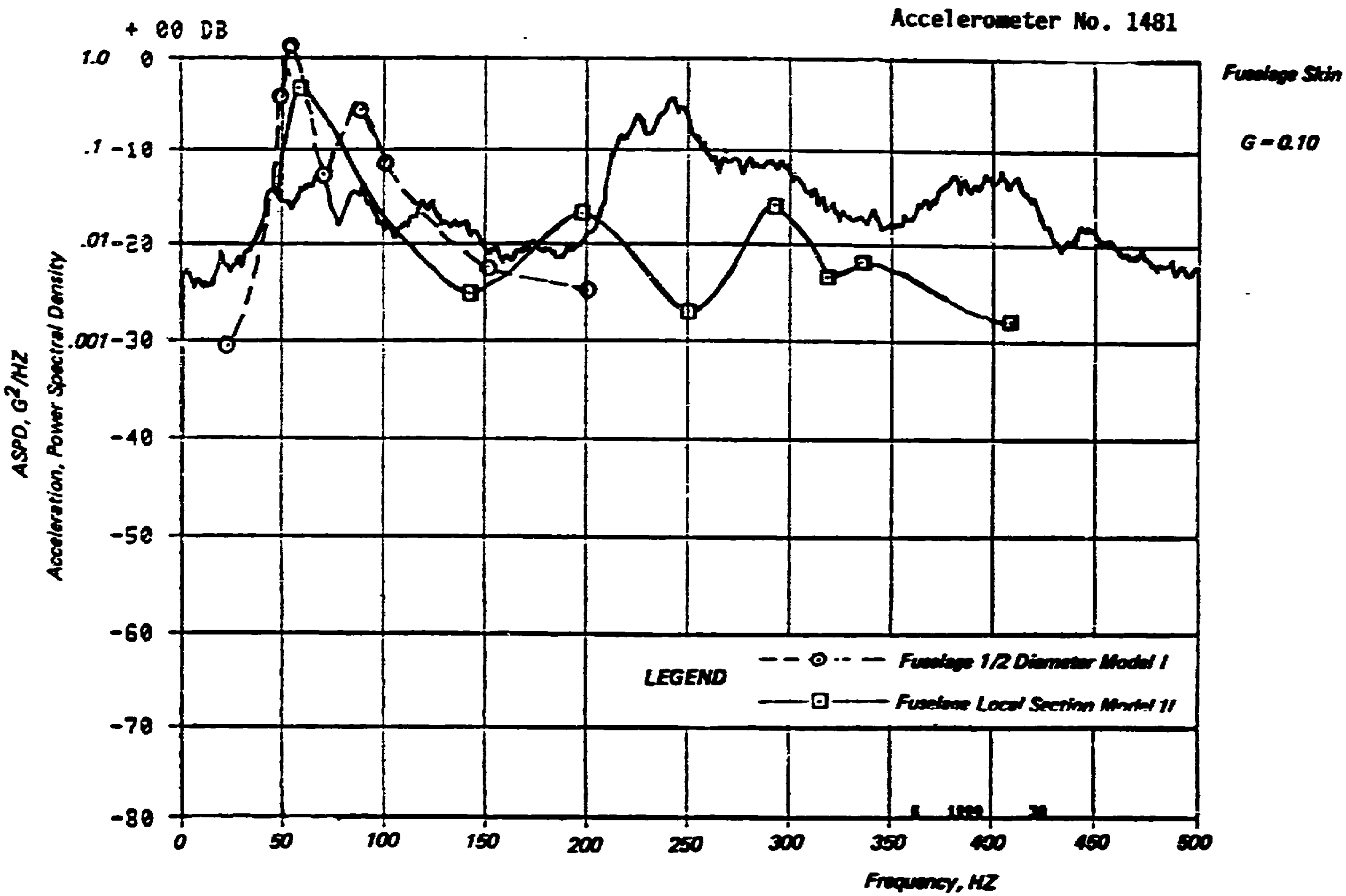

Figure 80. Calculated Response of Models I and II for Fuselage Skin Accelerometer A61 Compared to Flight Test Data

PRINT OF FREQUENCIES

MODE NUMBER	CIRCULAR FREQUENCY (RAD/SEC)	FREQUENCY (CYCLES/SEC)	PERIOD (SEC)
1	3.7583E+02	5.9816E+01	1.6718E-02
2	9.1463E+02	1.4557E+02	6.8697E-03
3	1.1921E+03	1.8973E+02	5.2705E-03
4	1.4743E+03	2.3464E+02	4.2619E-03
5	1.7848E+03	2.8406E+02	3.5204E-03
6	2.1097E+03	3.3577E+02	2.9782E-03
7	2.1473E+03	3.4175E+02	2.9261E-03
8	2.2246E+03	3.5405E+02	2.8245E-03

Figure 81. USB Flap Model II Frequency Spectrum

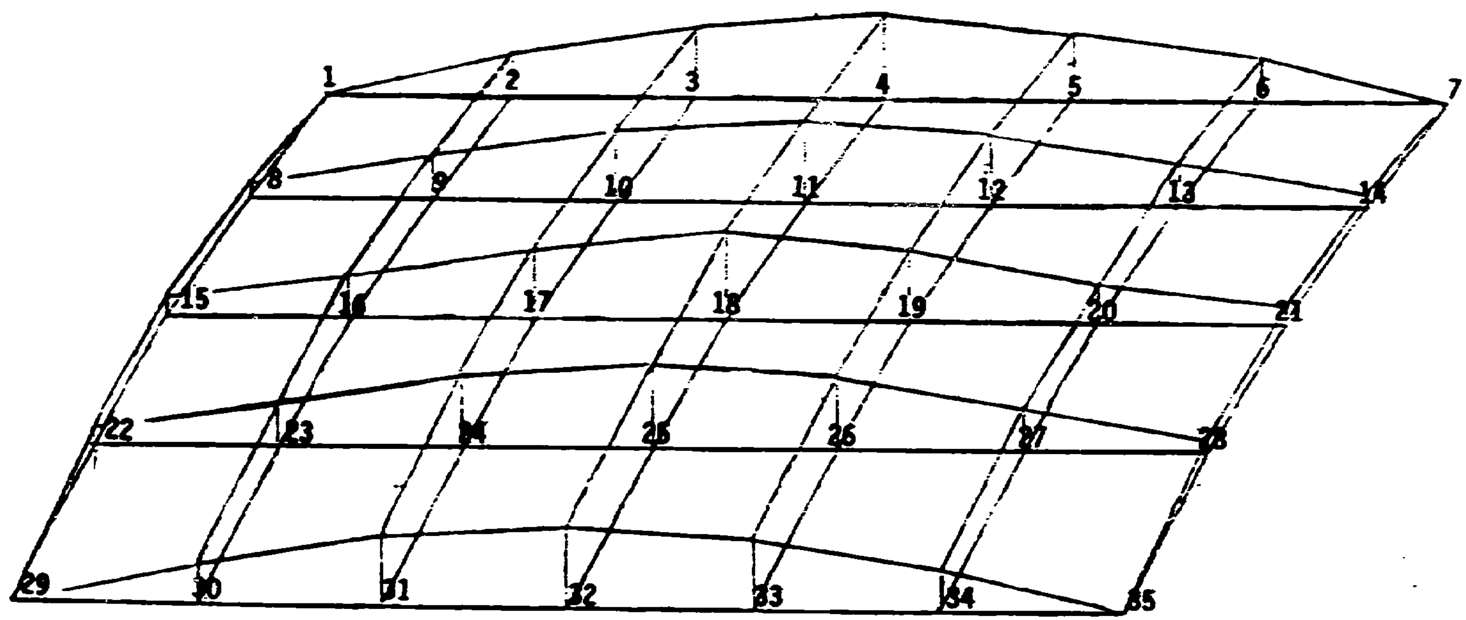

Figure 82. Fuselage Model II Modal Plots, Frequency = 59.8 Hz

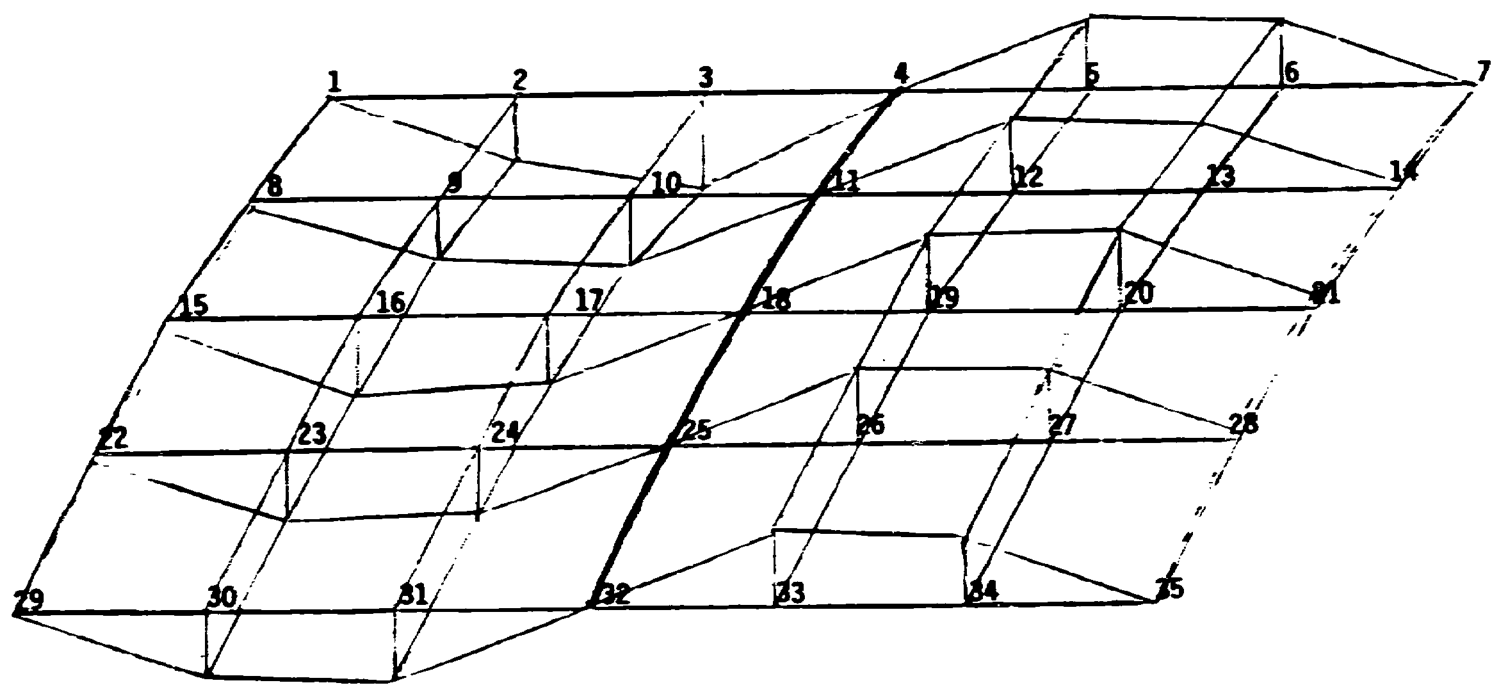

Figure 83. Fuselage Model II Modal Plots, Frequency = 145.57 Hz

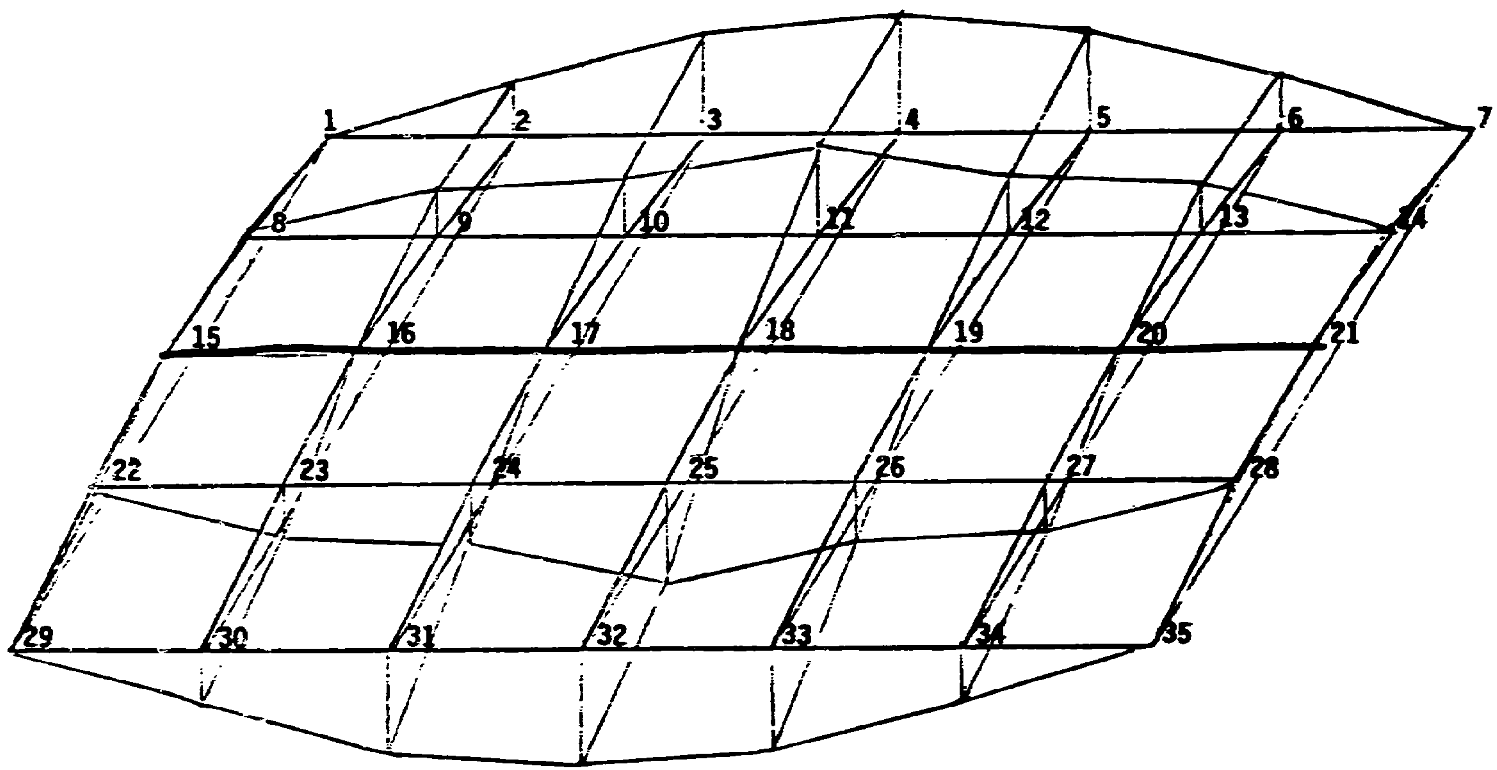

Figure 84. Fuselage Model II Modal Plots. Frequency = 189.73 Hz

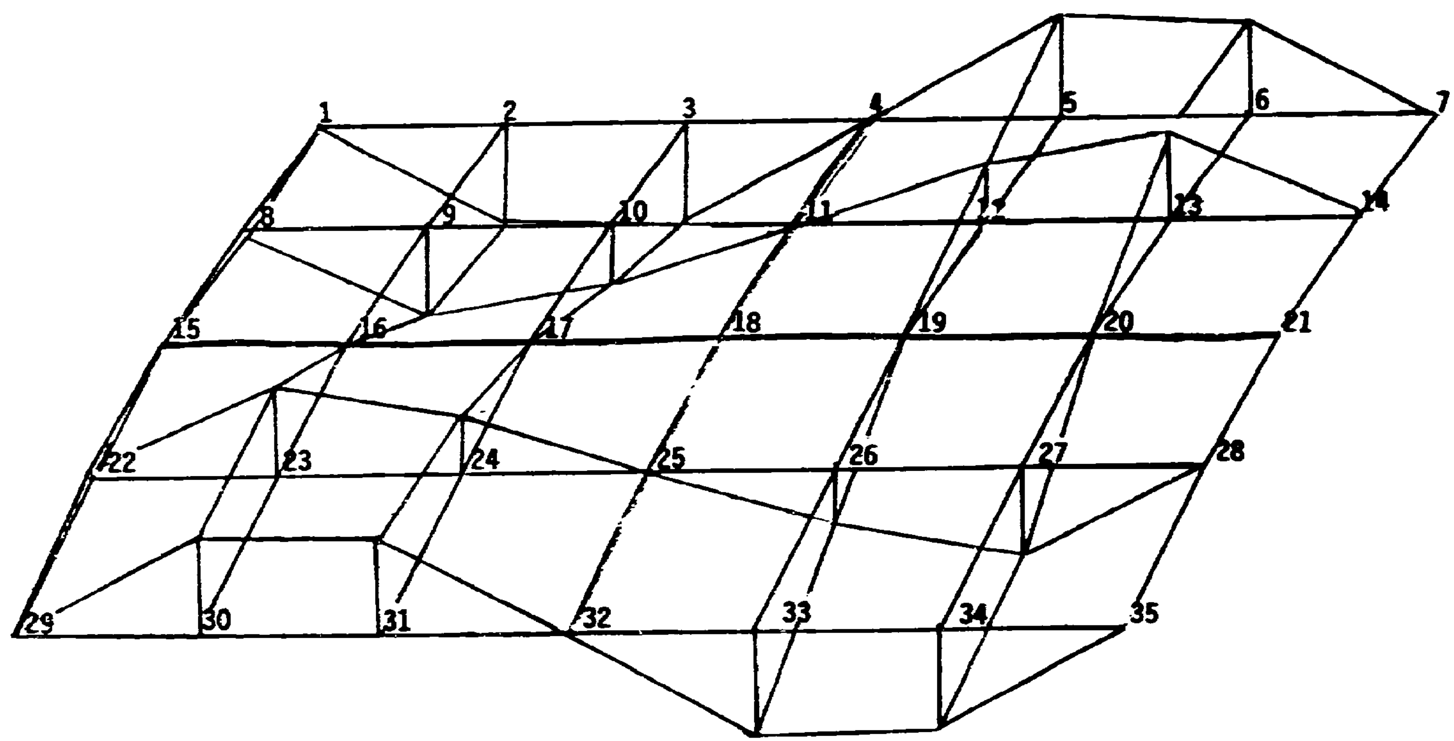

Figure 85. Fuselage Model II Modal Plots, Frequency = 234.64 Hz

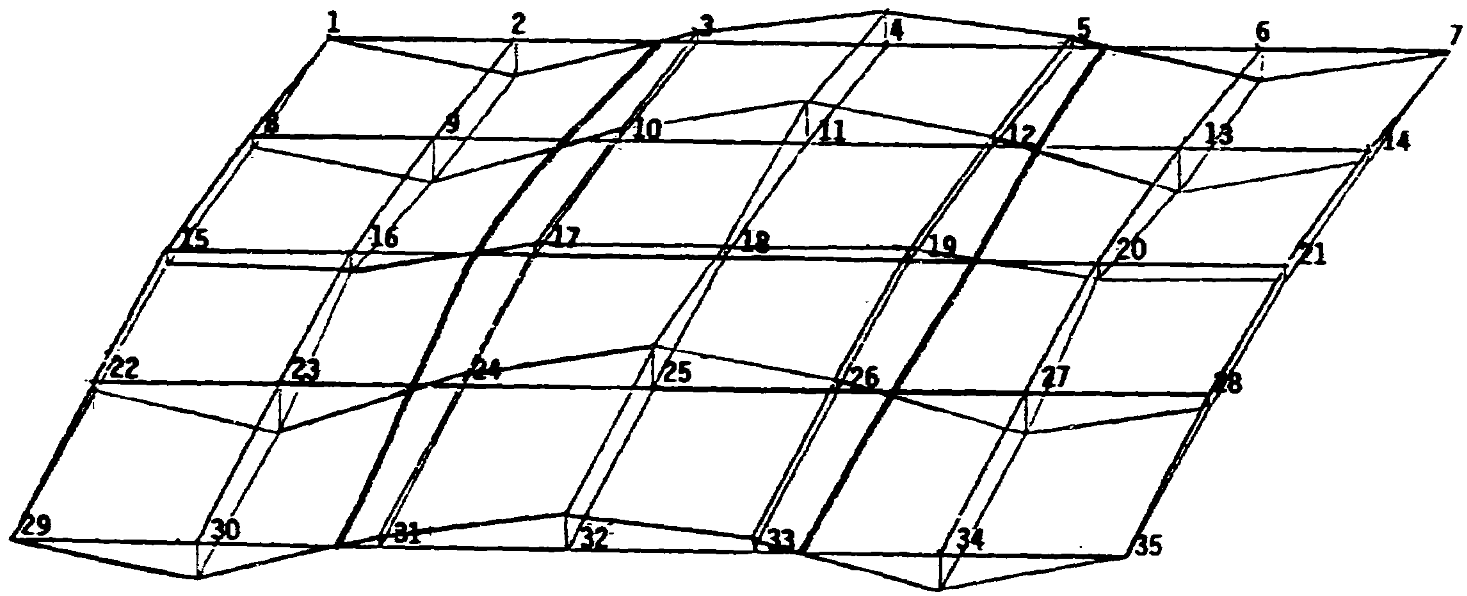

Figure 86. Fuselage Model II Modal Plots, Frequency = 284.06 Hz

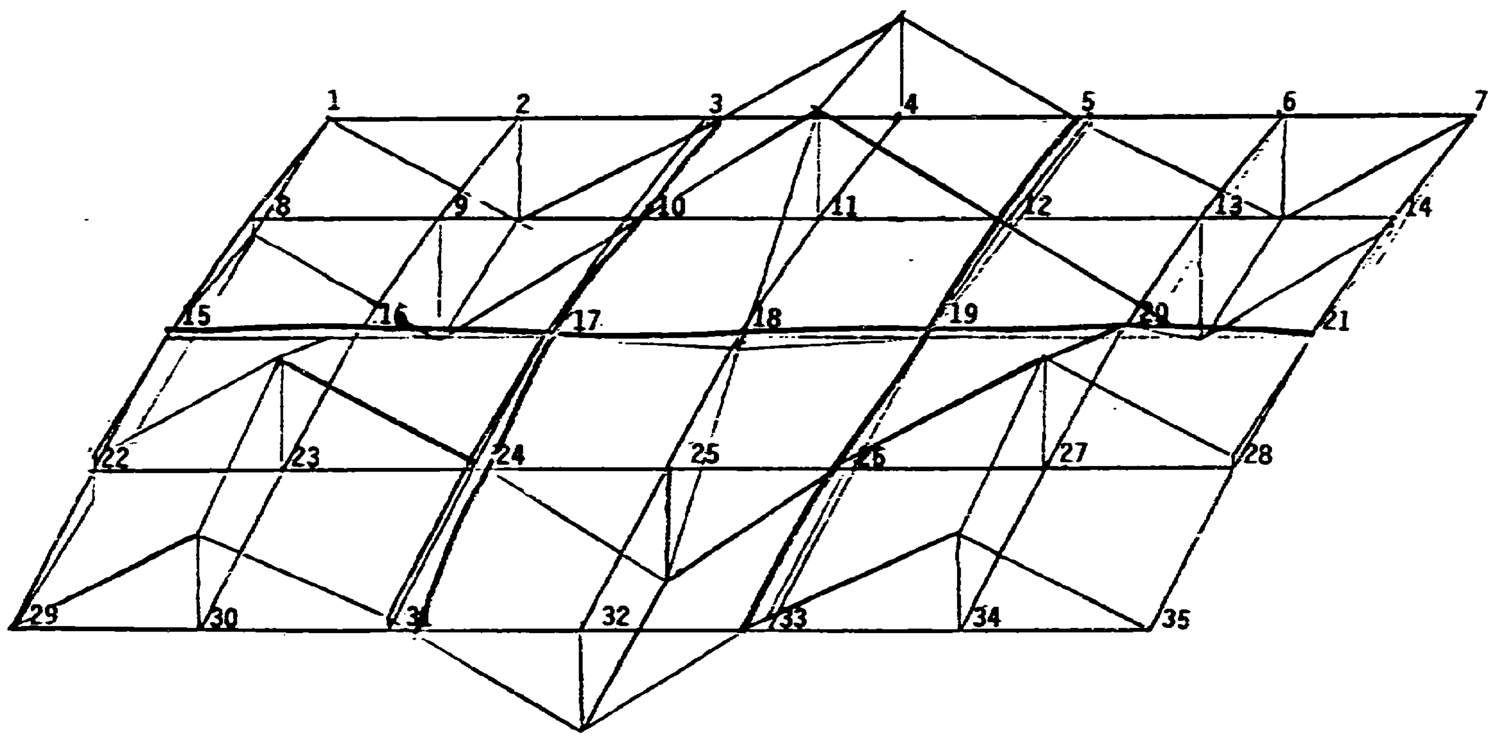

Figure 87. Fuselage Model II Modal Plots, Frequency = 335.77 Hz

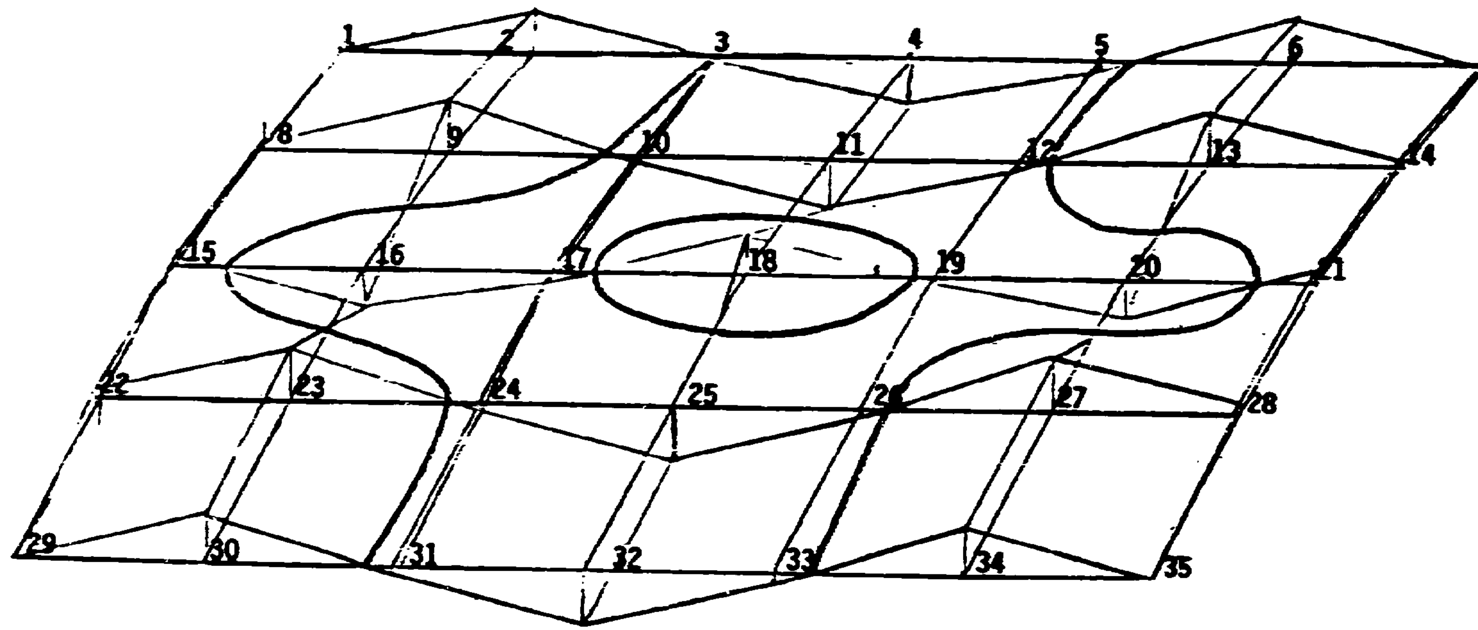

Figure 88. Fuselage Model II Modal Plots, Frequency = 341.17 Hz

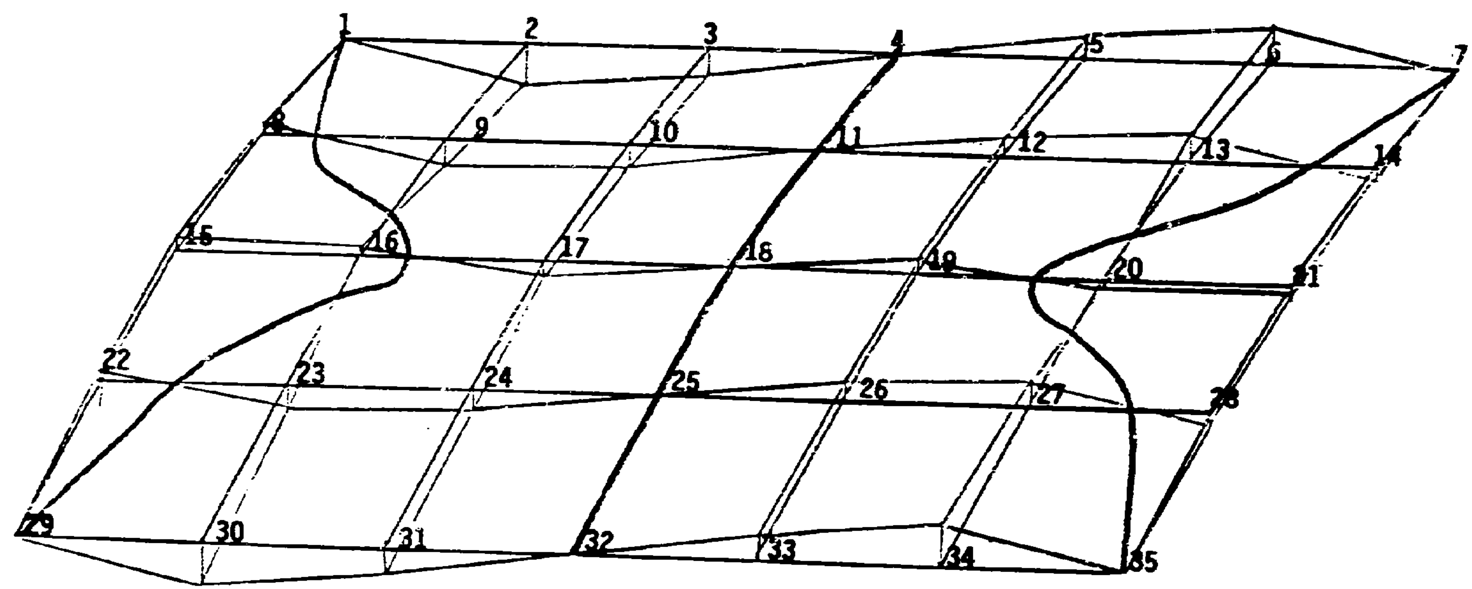

Figure 89. Fuselage Model II Modal Plots, Frequency = 354.05 Hz

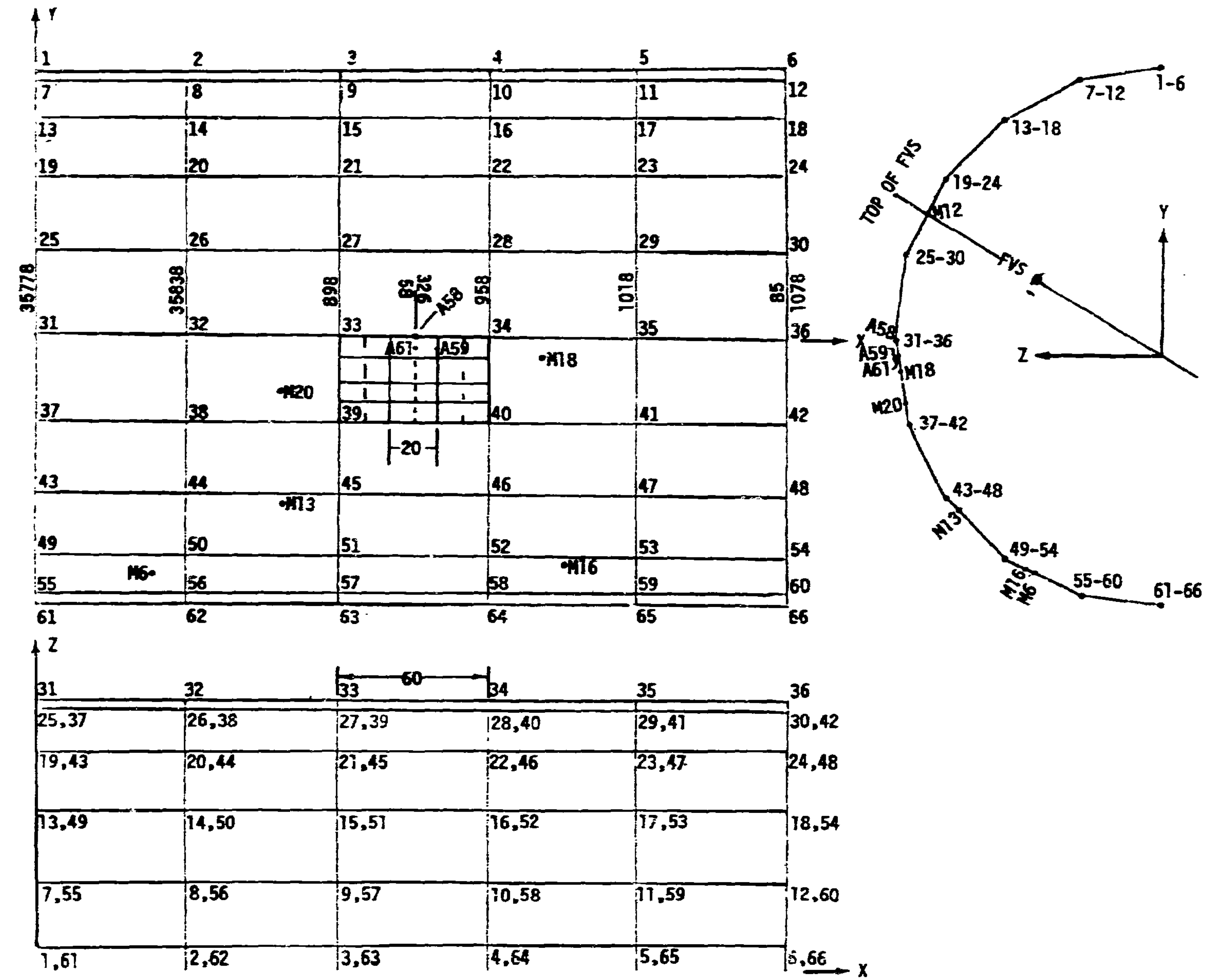

Figure 90. Orientation of Fuselage Model II.

MODE NUMBER	CIRCULAR FREQUENCY (RAD/SEC)	FREQUENCY (CYCLES/SEC)	PERIOD (SEC)	TOLERANCE
1	1.6934E+03	2.6951E+02	3.7105E-03	1.5590E-14
2	2.0484E+03	3.26[illegible]1E+02	3.[illegible]674E-02	.0
3	2.3650E+03	3.7641E+02	2.6567E-03	.0
4	2.4407E+03	3.6844E+02	2.5744E-03	1.0006E-14
5	2.7456E+03	4.3697E+02	2.2825E-03	1.5814E-14
6	3.[illegible]64[illegible]E+03	4.8777E+02	2.[illegible]501E-03	1.2692E-14
7	3.2850E+03	5.2283E+02	1.9127E-03	5.5234E-15
8	3.4715E+03	5.5250E+02	1.8100E-03	4.9460E-15
9	3.9858E+03	6.34[illegible]4E+02	1.5772E-03	3.7557E-15
10	4.6623E+03	7.42[illegible]3E+02	1.3477E-03	3.1995E-11
11	4.7021E+03	7.4836E+02	1.3363E-03	5.0682E-13
12	5.0263E+03	7.9996E+02	1.2501E-03	2.4297E-04
13	5.2176E+03	8.304[illegible]E+02	1.2042E-03	1.9677E-05
14	5.2777E+03	8.3998E+02	1.19[illegible]5E-03	1.9436E-10
15	5.3253E+03	8.4754E+02	1.1799E-03	1.1812E-07
16	5.4527E+03	8.6782E+02	1.1523E-03	6.81[illegible]4E-05
17	5.7079E+03	9.0844E+02	1.1[illegible]6E-03	1.0707E-06
18	6.0547E+03	9.6364E+02	1.0377E-03	1.3[illegible]E-05
19	6.1749E+03	9.8277E+02	1.0175E-03	4.2977E-05
20	6.2018E+03	9.8705E+02	1.0131E-03	1.4598E-03

Figure 91. High Frequency Model III Frequency Spectrum

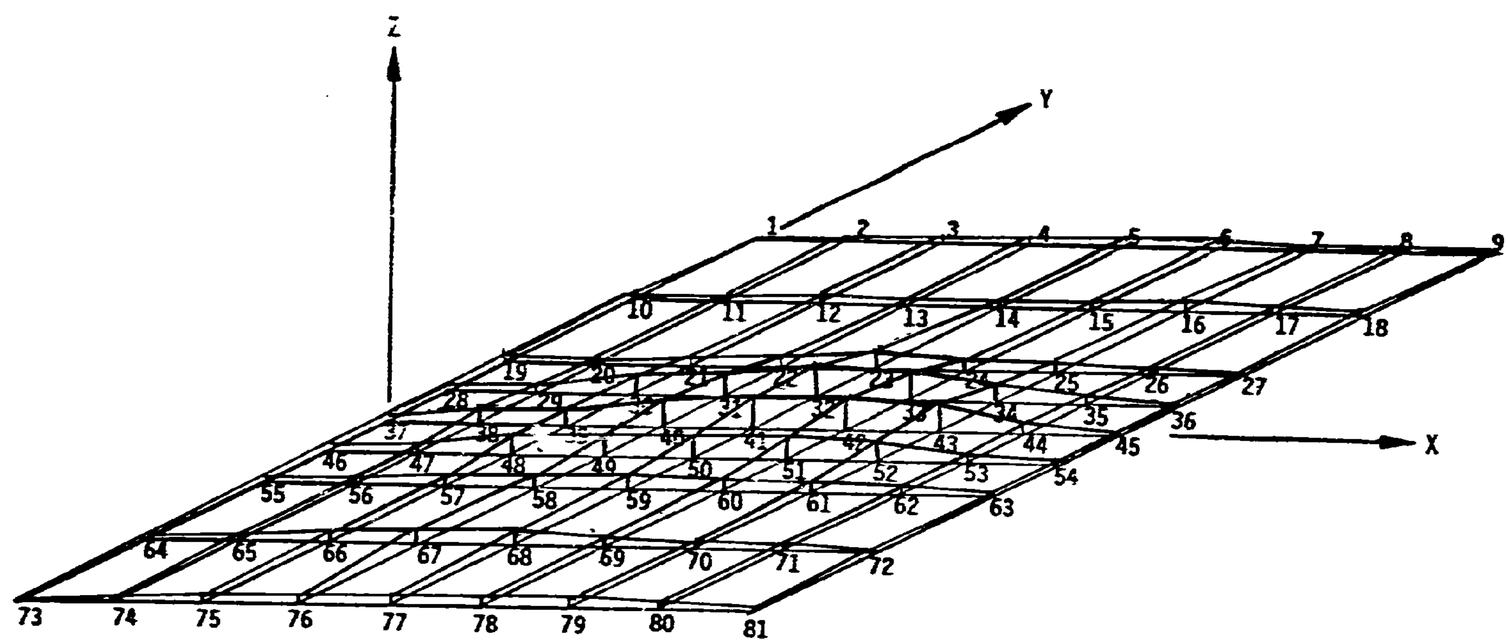

Figure 92. Fuselage Model III Modal Plot, Frequency = 269.51 Hz

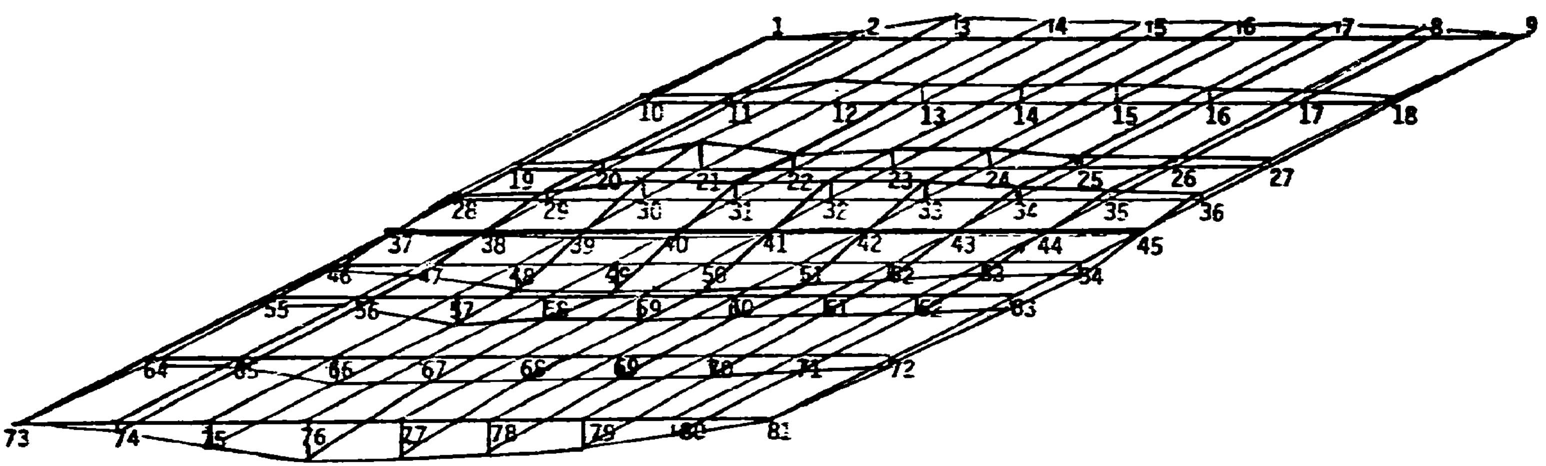

Figure 93. Fuselage Model III Modal Plot, Frequency = 326.01 Hz

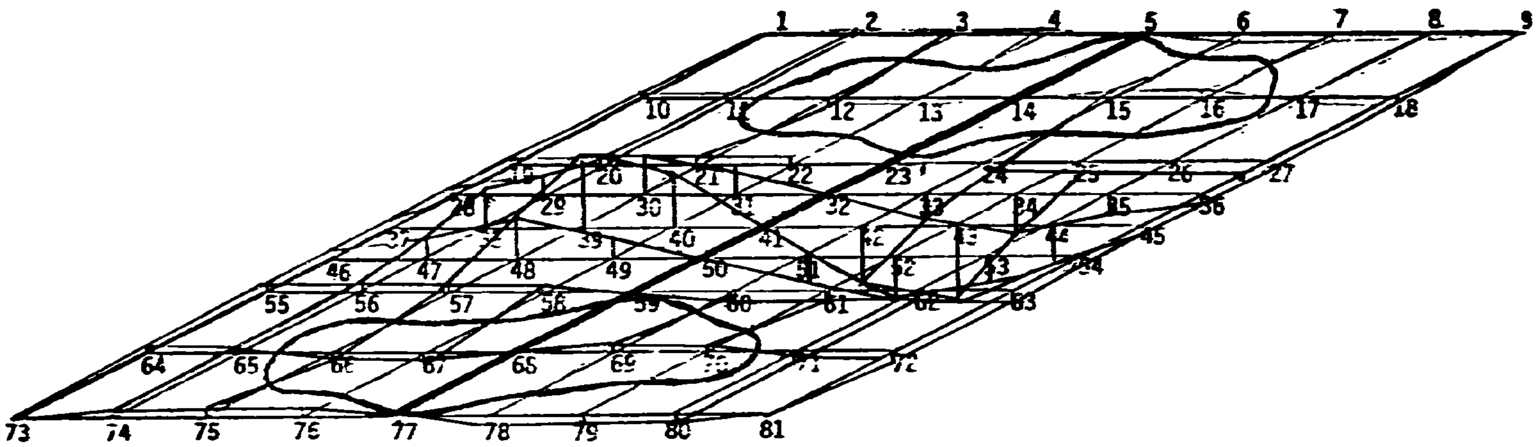

Figure 94. Fuselage Model III Modal Plot, Frequency - 376.41 Hz

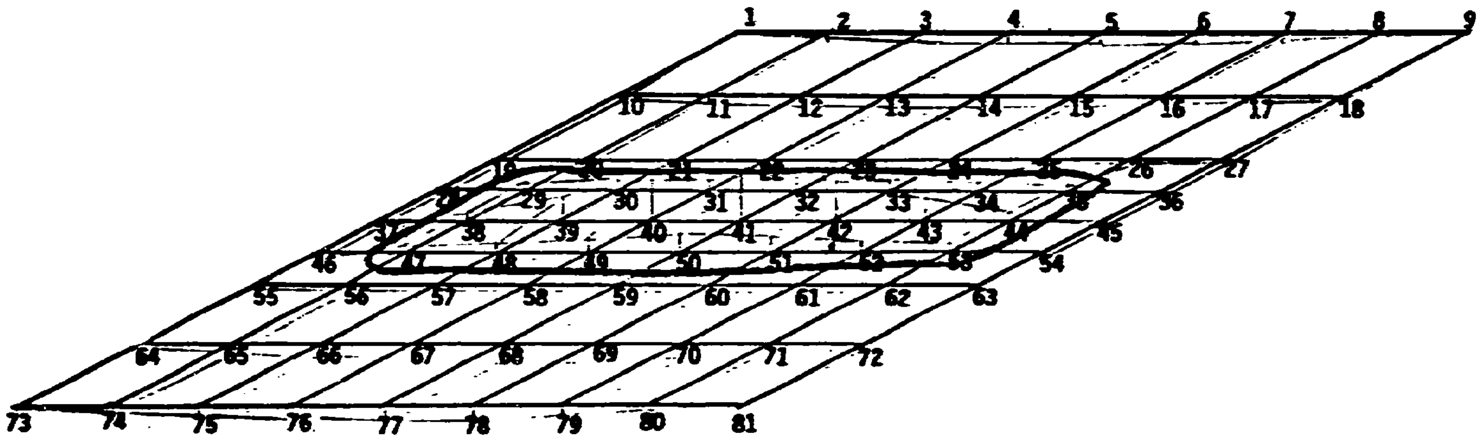

Figure 95. Fuselage Model III Modal Plot, Frequency = 388.44 Hz

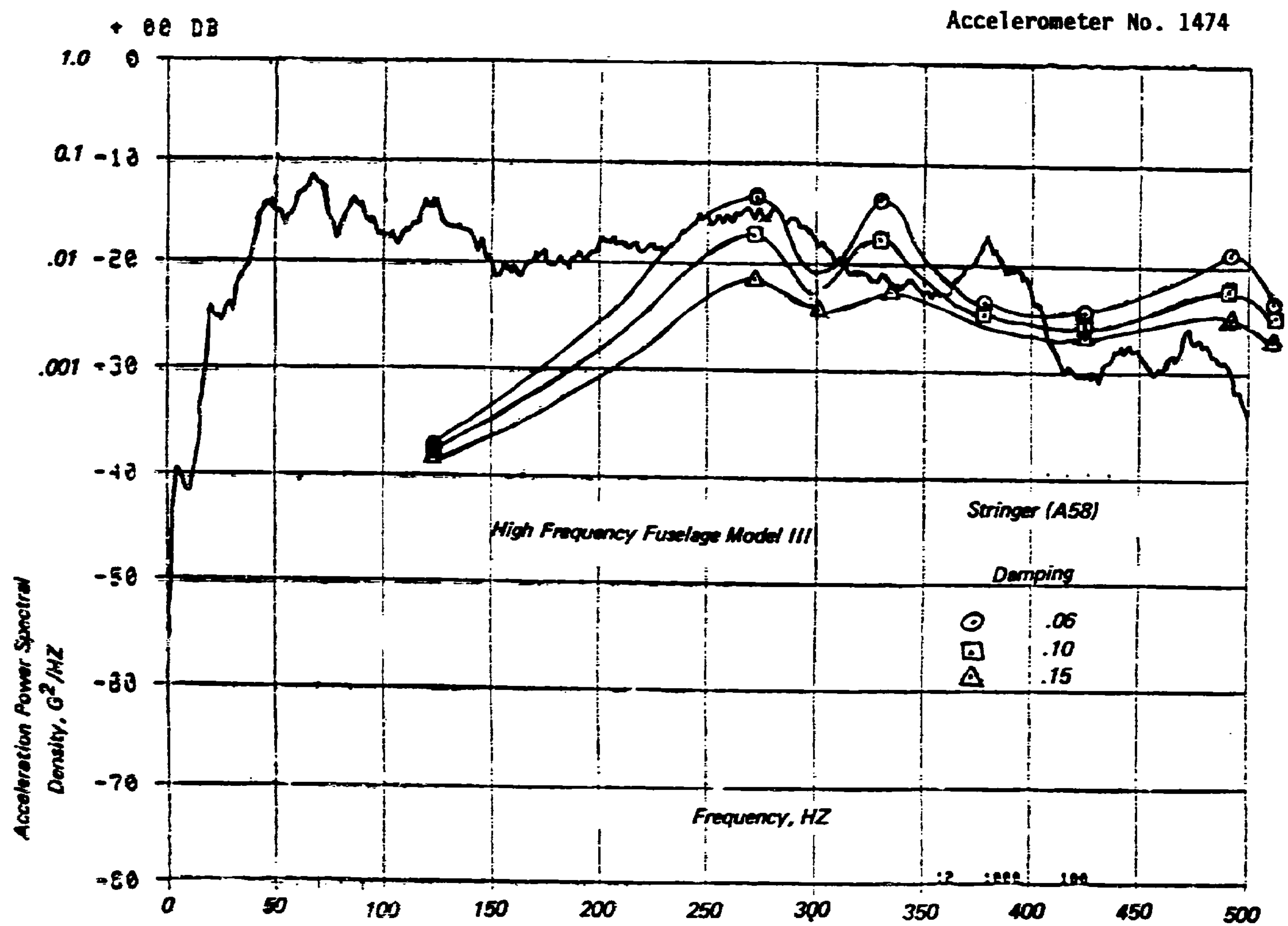

Figure 96. USB Flap Model III Response Comparison With Stringer Accelerometer (A58) for Three Sets of Assumed Damping

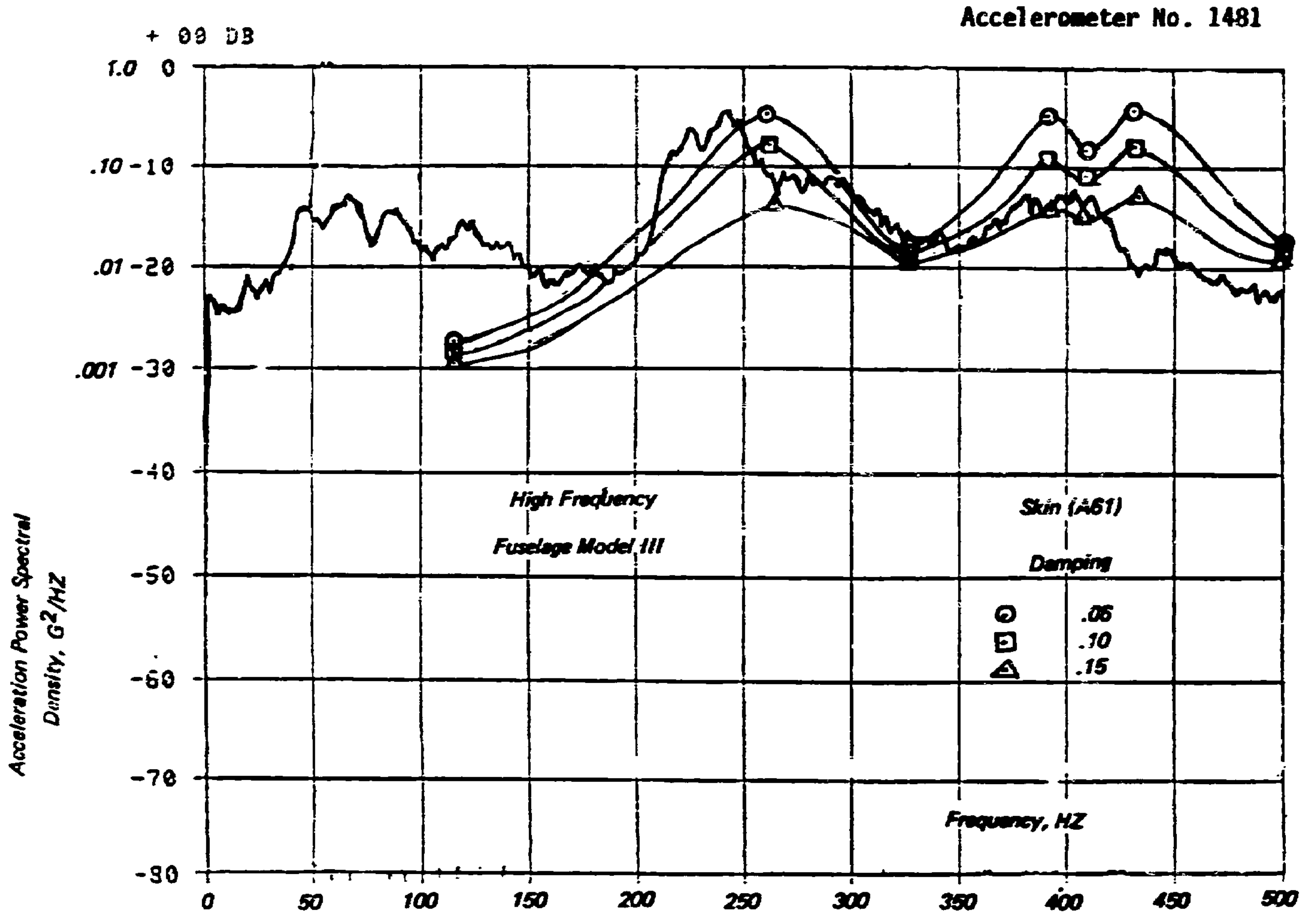

Figure 97. USB Flap Model III Response Comparison with Skin Mounted Accelerometer (A61) for Three Sets of Assumed Damping

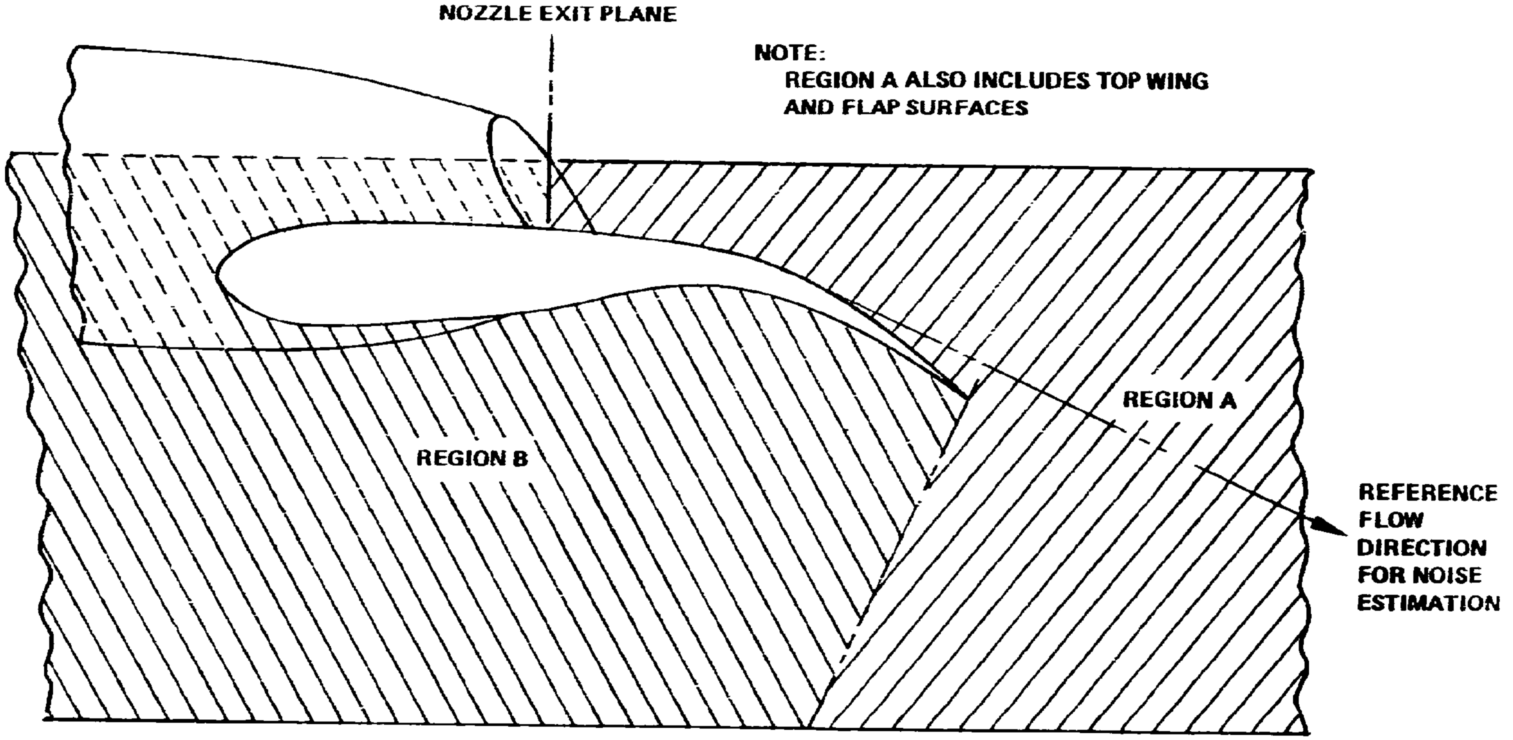

Figure 98. General Regions for Application of USB STOL Airplane Estimation Procedure

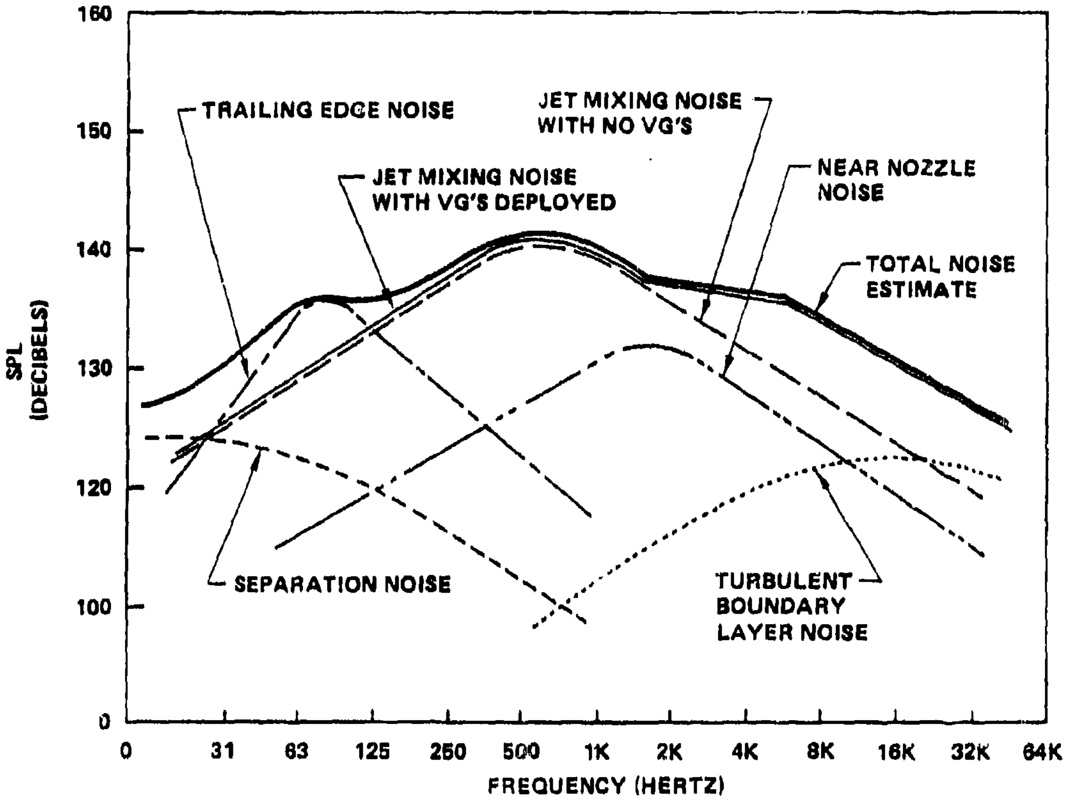

Figure 99. General Arrangement of Component Noise Source Estimates Making Up Total Noise Estimates (For Typical Climbout Condition)

- APPLIES TO ANY USB/STOL AIRPLANE CONFIGURATION WITH
  - NOZZLE FLUSH TO WING SURFACE
  - LOW-SPEED OPERATION FROM TAKEOFF THROUGH CRUISE ($V_A/V_J < 1$)
  - NOZZLE ASPECT RATIO UP TO ~6
  - BYPASS RATIO FROM ~2 TO ~6
- ACCOUNTS FOR
  - ENGINE MIXED JET VELOCITY (V_j)
  - ENGINE MIXED JET DENSITY (ρ_j)
  - AIRPLANE FORWARD SPEED (V_A)
  - SIZE AND POSITION OF NOZZLE WITH RESPECT TO FUSELAGE
  - NOZZLE CONFIGURATION
  - USB FLAP ANGLE
  - WING/FLAP CONFIGURATION
  - VORTEX GENERATORS (IF PRESENT)
  - NOZZLE SIDE DOOR (IF OPEN)
  - FLOW TURNING CAPABILITY OF NOZZLE/FLAP SYSTEM

Figure 100. Scope of USB/STOL Aircraft Noise Estimation Procedure

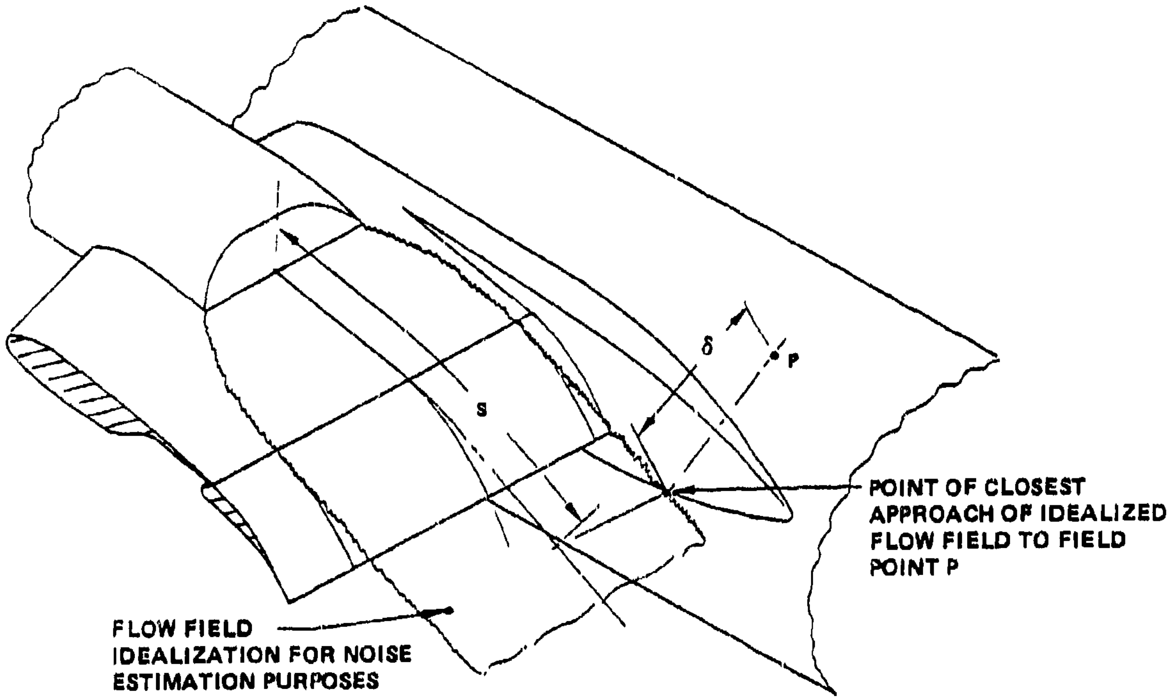

Figure 101. Conceptual Relation of Typical Field Point P to Flow Field

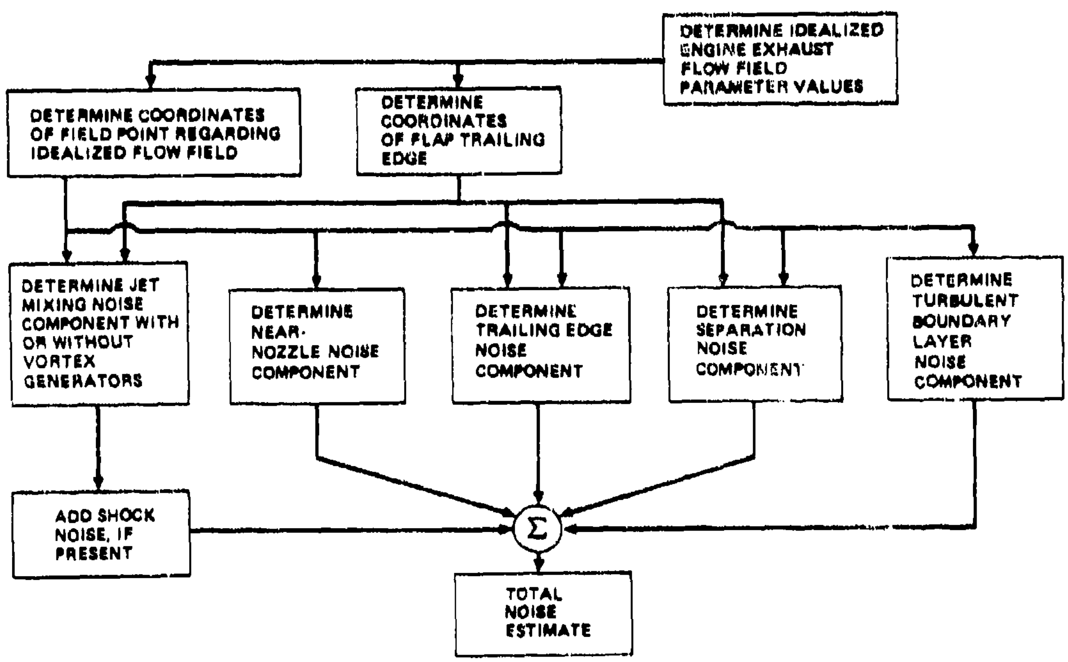

Figure 102. Summary Flow Diagram for USB/STOL Aircraft Fluctuating Pressure Estimation Procedure

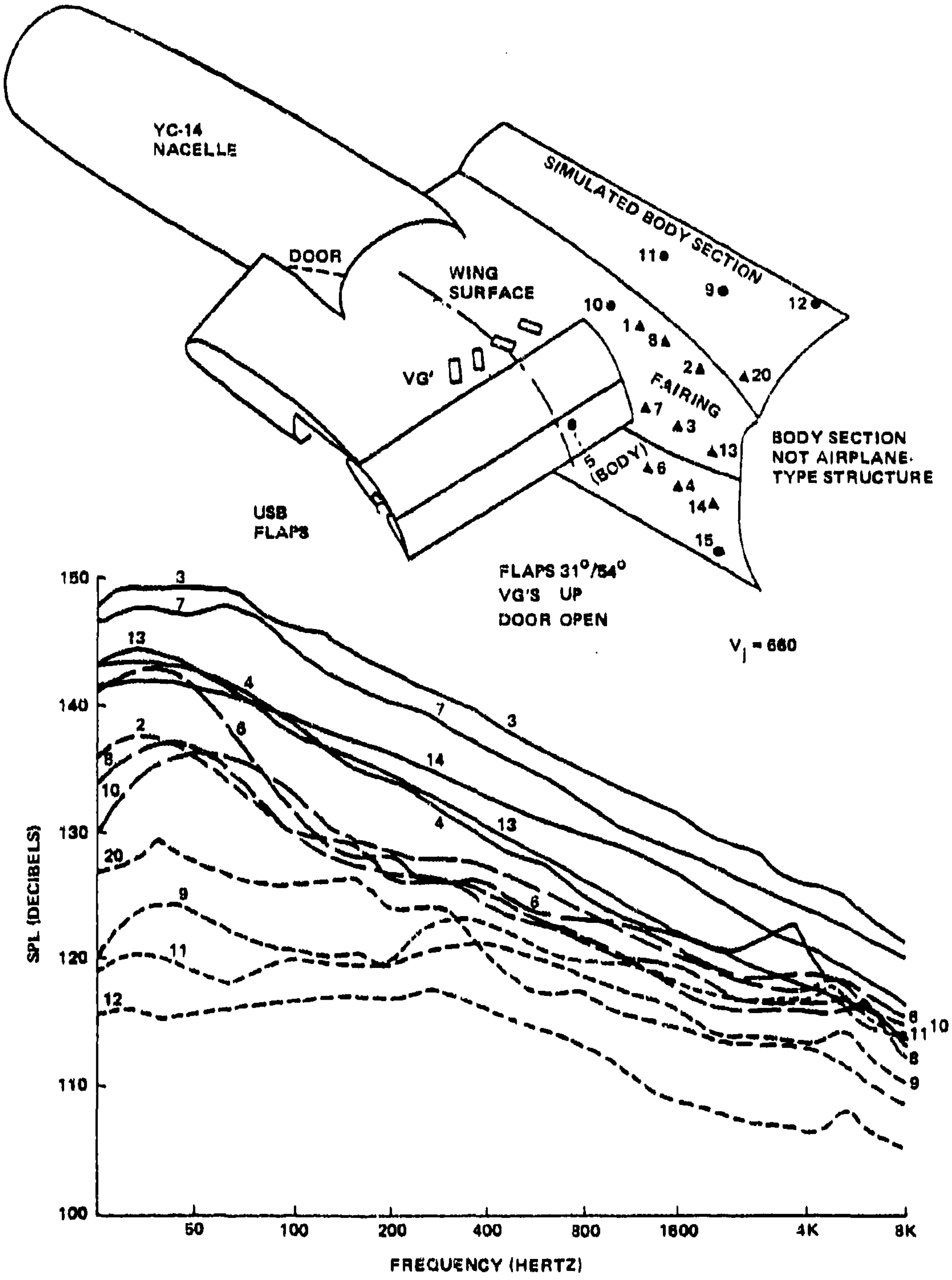

Figure 103. YC-14 Propulsion Verification Test Body-Microphone Spectra

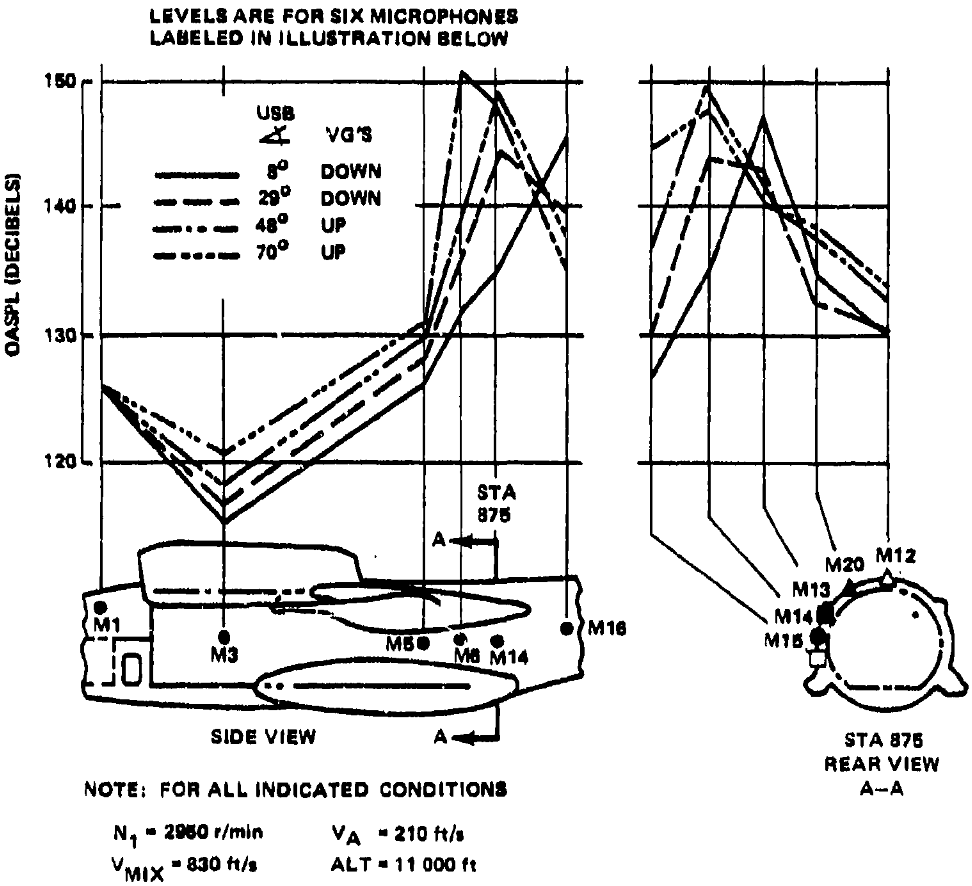

Figure 104. Effect of USB Flap Position on Exterior Fuselage Overall Levels

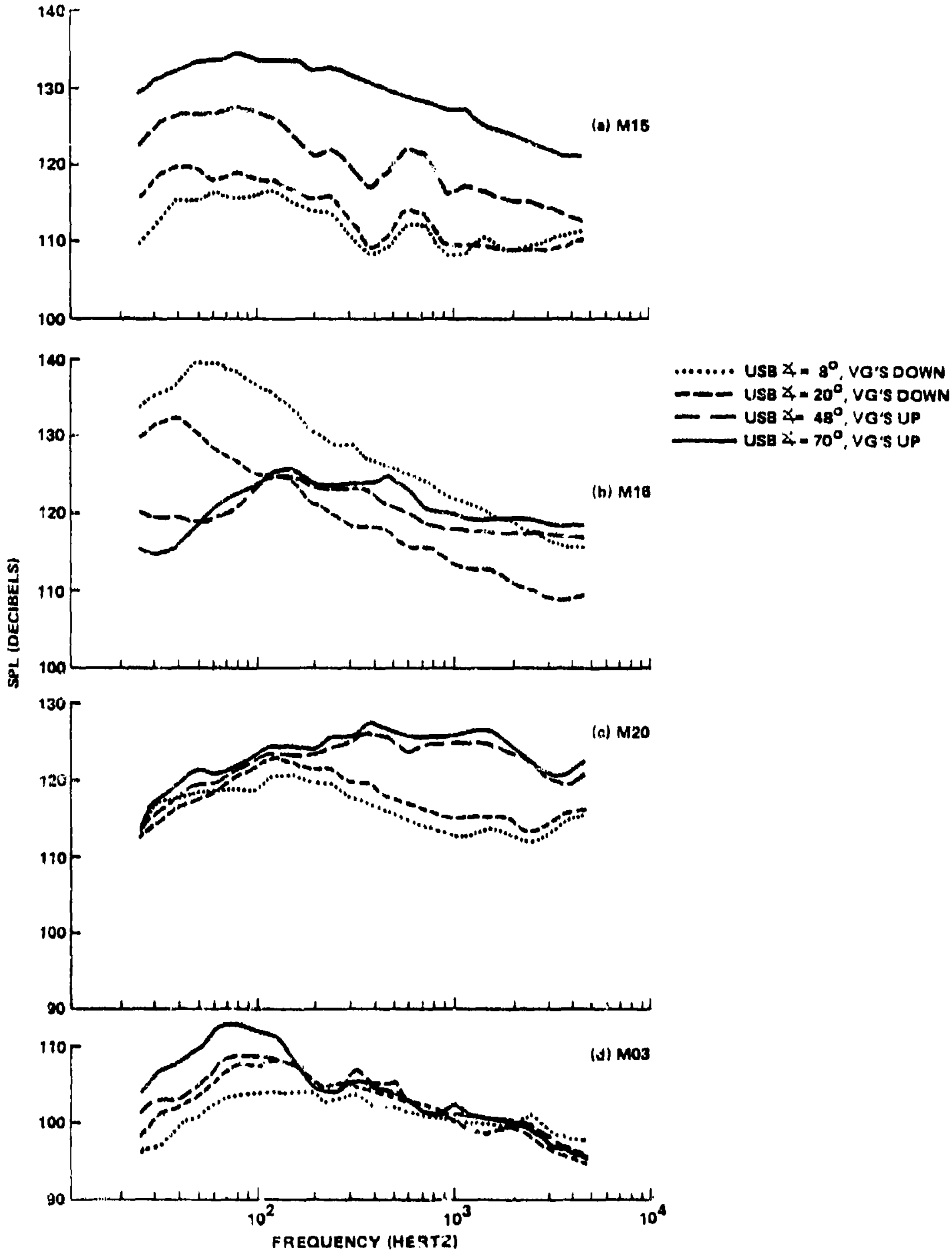

Figure 105. Effect of USB Flap Position on Exterior Fuselage Spectra

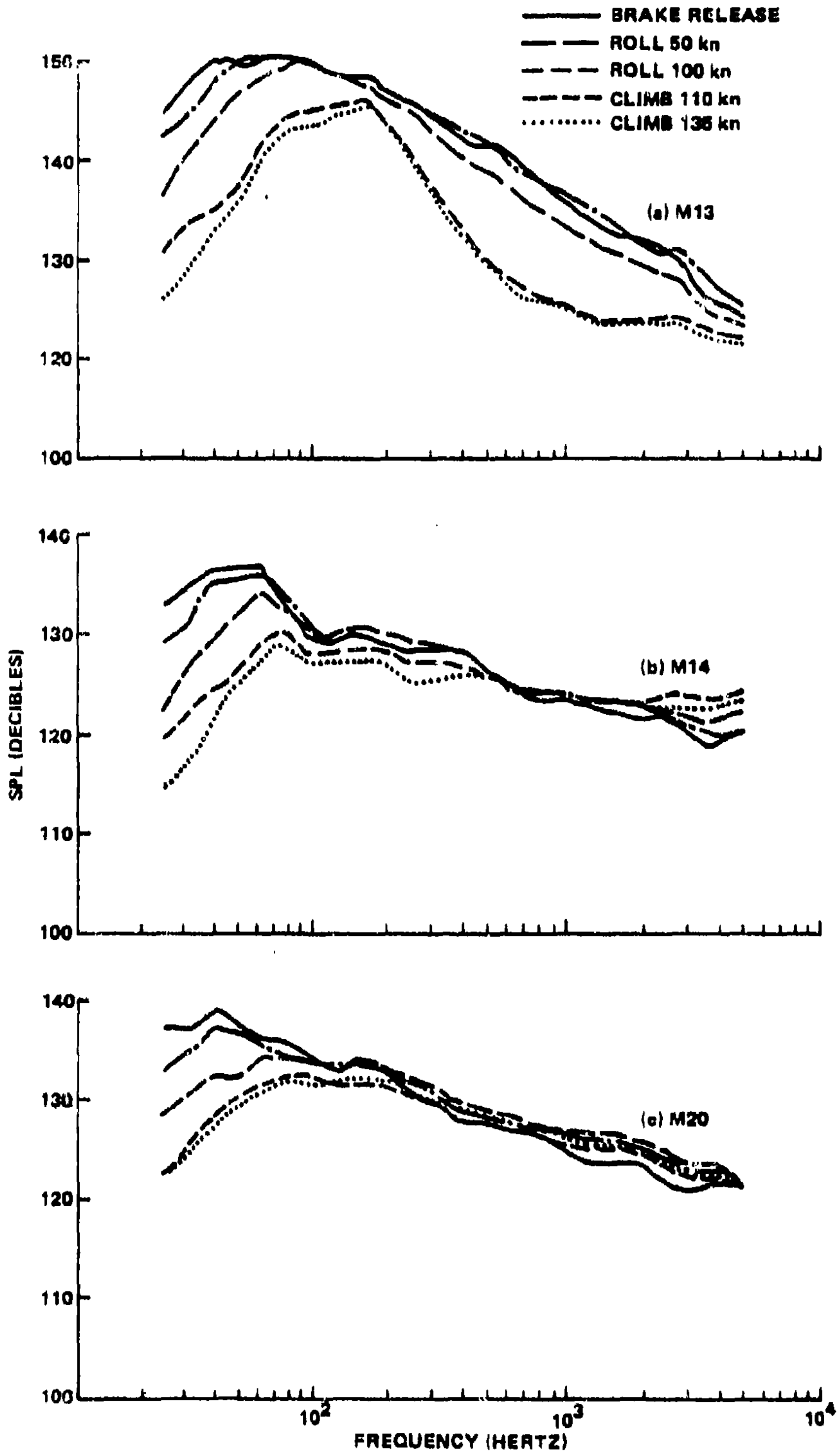

Figure 106. Variation in Exterior Fuselage Noise Spectra During Takeoff

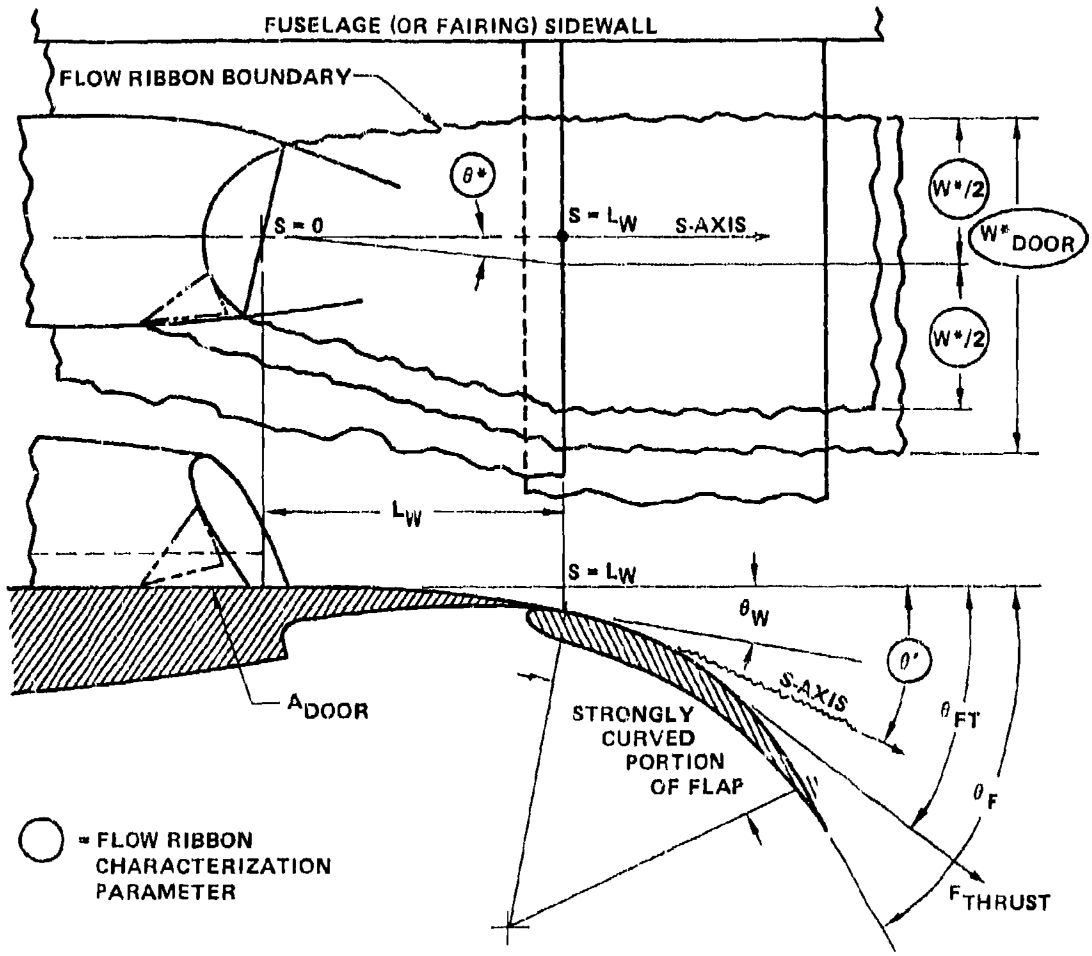

Figure 107. Flow Ribbon Characterization Parameters

V_A = airplane forward velocity

V_J = engine mixed exhaust jet velocity

θ_{FT} = static flow turning capability of propulsion/flap system (when trailing edge flap system is at θ_F degrees)

ρ_J = engine mixed exhaust jet density

C_J = engine mixed exhaust sound speed

Figure 108. Airplane Operating Parameters Used in Estimation Procedure

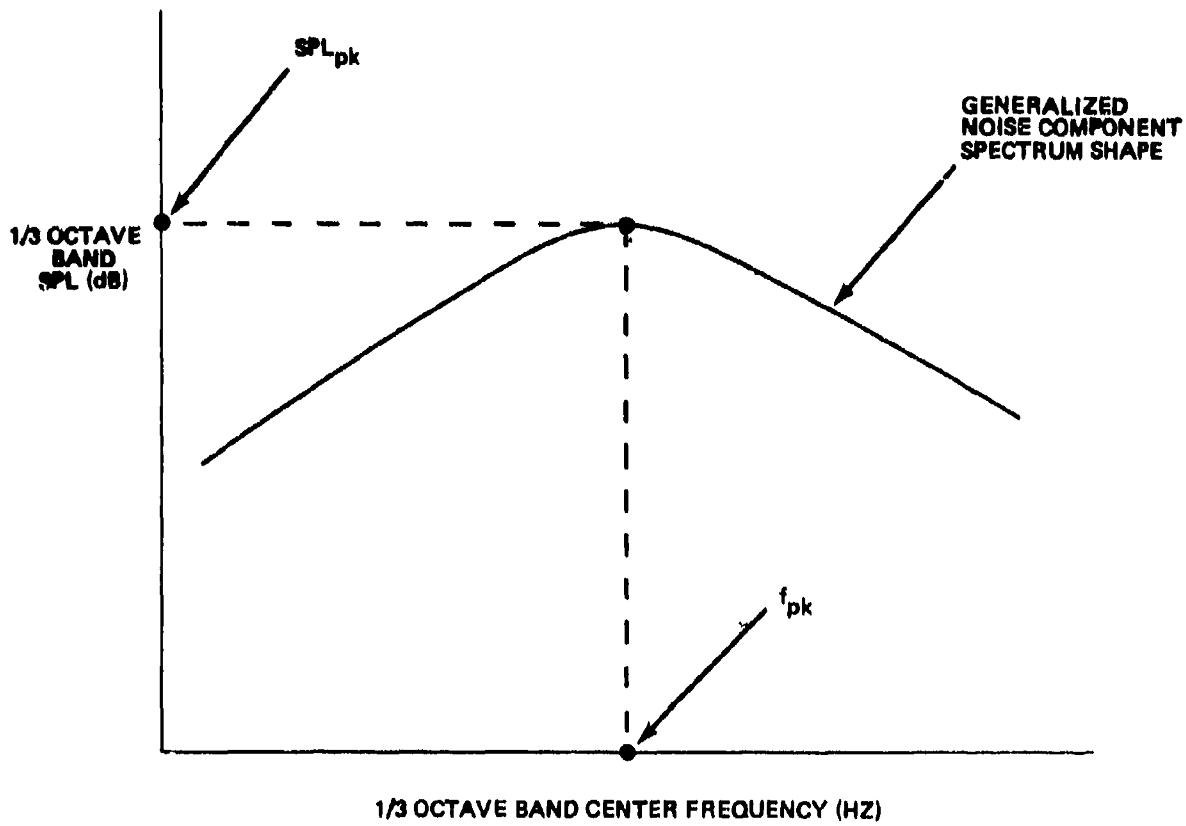

Figure 109. Component Noise Characterization Parameters

θ_{KD}^{U}	= 22°	r_f	= 68 in
θ_{KU}^{D}	= 0°	x_o	= 161 in
θ_{KI}^{O}	= 0°	y_o	= 640 in
θ_{KO}^{I}	= 22°	z_o	= 265 in
θ_{TB}	= 20°	z_1	= 257 in
θ_{SK}	= 0°	ℓ_T	= 26 in
θ_W	= 15°	y_f	= 114 in
A_{EFF}	= 3168 in^2	ℓ_{FAN}	= 220 in
A_{DOOR}	= 288 in^2		
A_{VG}	= 81 in^2		
N_{NG}	= 4		
W	= 112 in		
ℓ_W	= 117 in		

Note: See appendix A of Volume II for symbol definitions

Figure 110. YC-14 Geometry Parameter Values Used in Noise Prediction Procedure Exercise

	MEASUREMENT POINT DESIGNATION	BUTTOCK LINE (X) COORD	BODY STATION (y) COORD	WATER LINE (Z) COORD	COMMENT
	MO5	107 (in)	750 (in)	180 (in)	FUSELAGE
	M06	107	825	180	FUSELAGE
	M08	82	820	255	WING/BODY FAIRING
	M12	0	875	280	FUSELAGE
	M13	102	875	220	WING/BODY FAIRING
	M14	107	875	180	FUSELAGE
	M15	99	875	137	FUSELAGE
	M16	99	988	193	FUSELAGE
	M20	71	875	254	FUSELAGE
	M33	166	690	262	WING, 4ft AFT OF NOZZLE
	M37	285	802	218	AFT USB FLAP
NOTE	M38	248	769	254	MAIN USE FLAP
	M39	171	769	254	MAIN USB FLAP
	M41	171	802	218	AFT USB FLAP

Note: Coordinates correspond to USB flaps at 60°

Figure 111. YC-14 Measurement Locations Used for Prediction Procedure Exercise

CONDITION NO.	ALTITUDE (FT)	NOTE ① ρ_J ($LB\text{-}SEC^2/FT^4$)	V_J (FT/SEC)	V_A (FT/SEC)	$\measuredangle$ USB (DEGREES)	NOTE ② θ_{FT} (DEGREES)	COMMENT
3160	7650	.00195	204	674	60	53	STOL APPROACH
7132	0	.00238	42	1100	0	15	BRAKE RELEASE
7133	0	.00238	84	1100	0	15	ROLL, 50 KNCTS
7134	0	.00238	168	1070	0	15	ROLL, 100 KNOTS
7135	50	.00238	186	1050	0	15	CLIMB, 110 KNOTS
7136	100	.00238	220	1050	0	15	CLIMB, 135 KNOTS
7196	10,000	.00176	225	830	9	23	STOL APPROACH (VG'S DOWN)
7193	11,000	.00170	210	830	29	36	STOL APPROACH (VG'S DOWN)
7195	10,000	.00176	215	830	41	46	STOL APPROACH (VG'S UP)
7192	10,700	.00172	213	830	70	55	STOL APPROACH (VG'S UP)

Note: ① Assume mixed jet density = ambient air density

② From figure 7.2-7, NASA CR-159053, July 1979

Figure 112. YC-14 Operating Condition Parameter Values Used for Prediction Method Exercise

MEASUREMENT POINT LOCATION	CONDITION NUMBER									
	3160	7132	7133	7134	7135	7136	7196	7193	7195	7192
M05		●								
M06		●								
M08		●								
M12		●								
M13		●					●	●	●	●
M14		●					●	●	●	●
M15		●								
M16		●								
M20		●	●	●	●	●				
M33	●									
M37	●									
M38	●									
M39	●									
M41	●									

Figure 113. Measurement Point/Operating Condition Cross Reference List for Prediction Procedure Exercise

PREDICTION PROCEDURE DEMONSTRATION

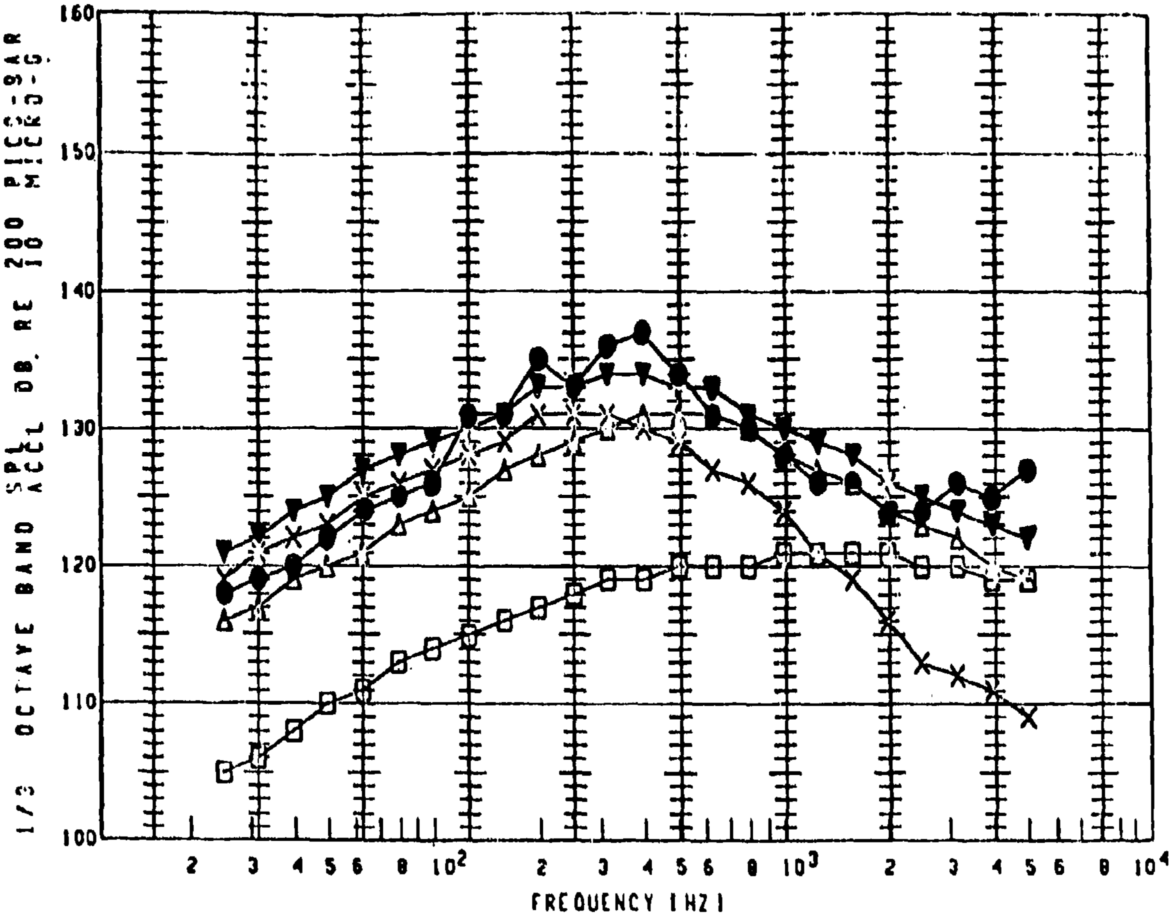

PLOT SYMBOL	X-DUCER NO.	COND. NO.	ALT. (FT)	SPEED (FPS)	N1 (RPM)	VMIX (FPS)	USBFA (DEG)	OVERALL (DB)
●	M33	3160	7650	204	2463	674	60	144
▼	M33	3160						144
⊡	M33	3160						132
◊	M33	3160						99
⊙	M33	3160						0
Δ	M33	3160						140
X	M33	3160						140

NOTES

●	WING 4FT AFT NOZ CL BL166	FLAPS 45 USB 60
▼	PREDICTED TOTAL NOISE.CREATED	79/03/16.
⊡	PREDICTED TOL NOISE	79/03/16.
◊	PREDICTED SEP NOISE	79/03/16.
⊙	PREDICTED EDGE NOISE	79/03/16.
Δ	PREDICTED NN NOISE	79/03/16.
X	PREDICTED MIXING NOISE	79/03/16.

Figure 114. Results for M33 at Condition 3160

PREDICTION PROCEDURE DEMONSTRATION

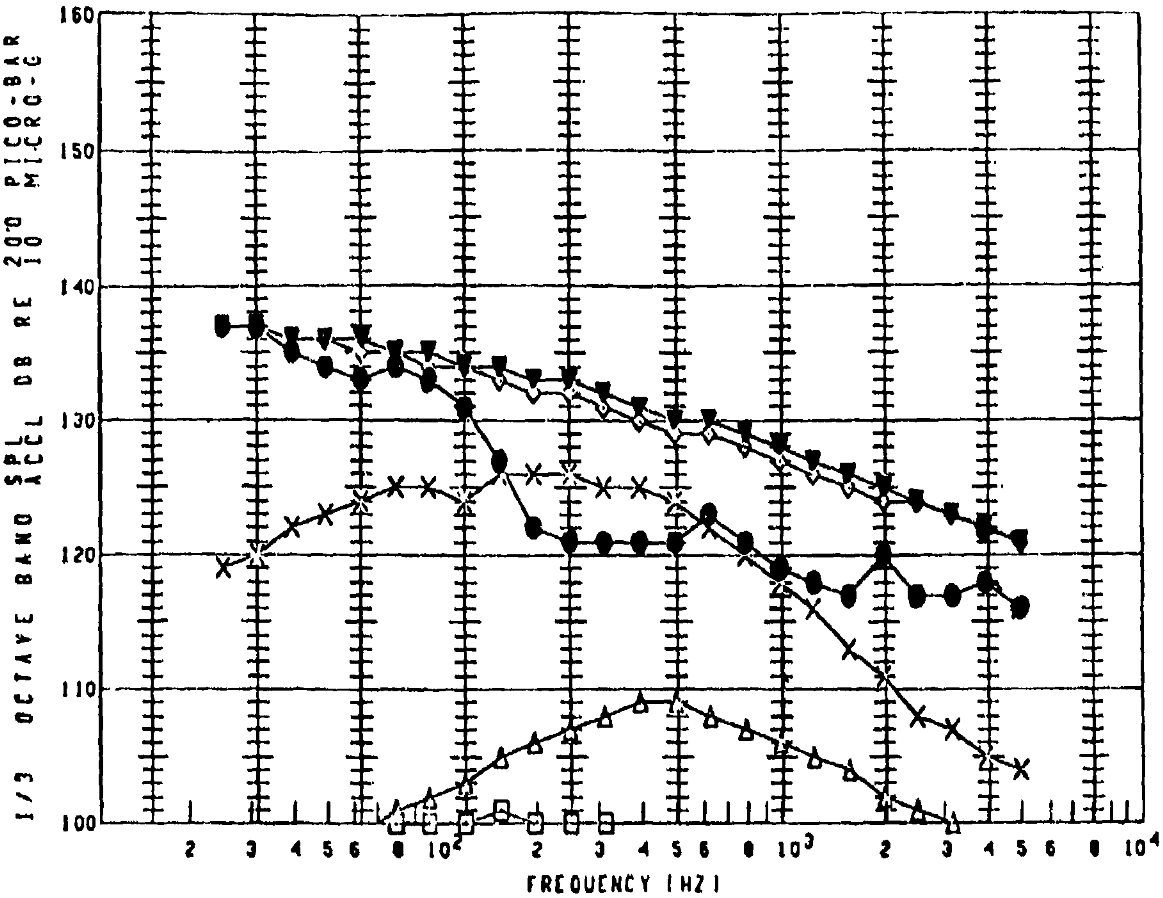

PLOT SYMBOL	X-DUCER NO.	COND. NO.	ALT. (FT)	SPEED (FPS)	N1 (RPM)	VMIX (FPS)	USBFA (DEG)	OVERALL (DB)
●	M37	3160	7650	204	2463	674	60	144
▼	M37	3160						147
⊡	M37	3160						112
◊	M37	3160						146
◊	M37	3160						90
△	M37	3160						118
X	M37	3160						136

NOTES

●	AFT USB FLAP BL285	FLAPS 45 USB 60
▼	PREDICTED TOTAL NOISE,CREATED	79/03/16.
⊡	PREDICTED TBL NOISE	79/03/16.
◊	PREDICTED SEP NOISE	79/03/16.
◊	PREDICTED EDGE NOISE	79/03/16.
△	PREDICTED NN NOISE	79/03/16.
X	PREDICTED MIXING NOISE	79/03/16.

Figure 115. Results for M37 at Condition 3160

PREDICTION PROCEDURE DEMONSTRATION

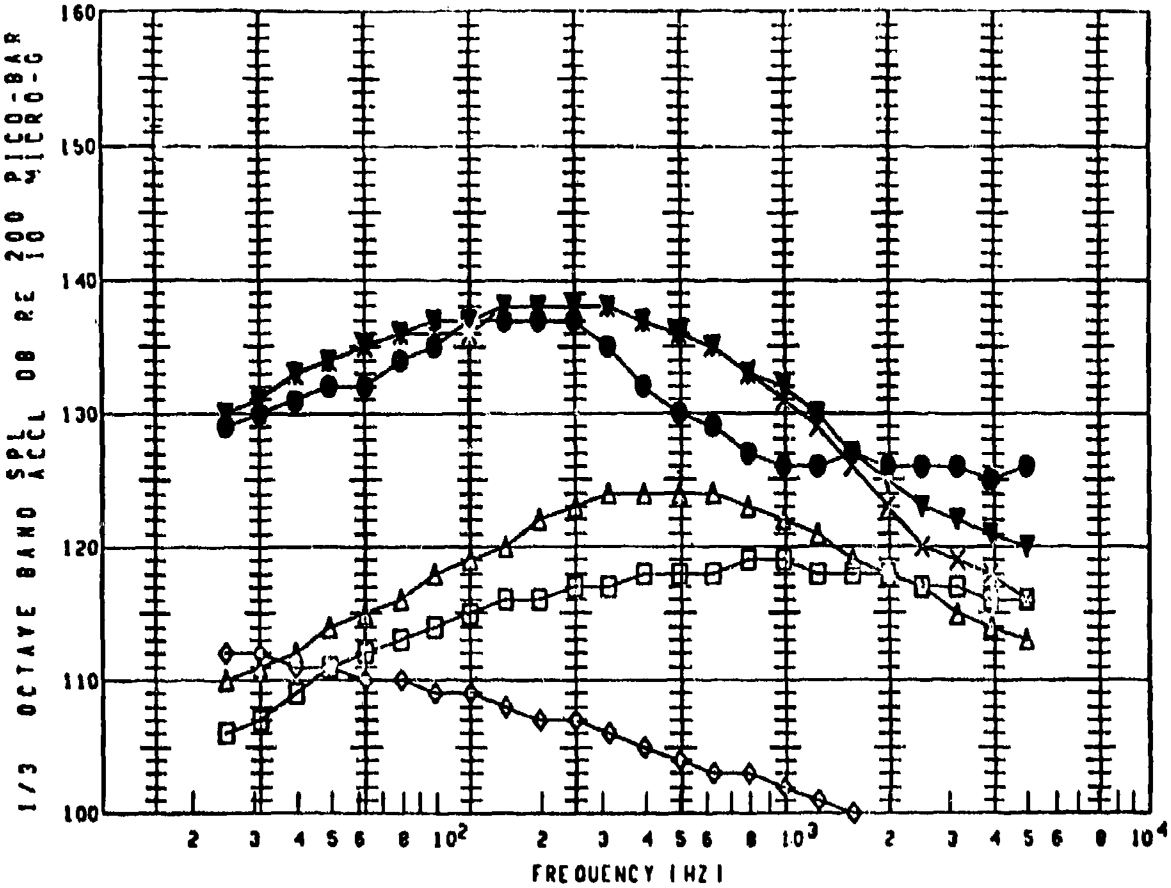

PLOT SYMBOL	X-DUCER NO.	COND. NO.	ALT. (FT)	SPEED (FPS)	N1 (RPM)	VMIX (FPS)	USBFA (DEG)	OVERALL (DB)
●	M38	3160	7650	204	2463	674	60	146
▼	M38	3160						148
⊡	M38	3160						130
◇	M38	3160						121
◇	M38	3160						100
△	M38	3160						134
X	M38	3160						148

NOTES

●	MAIN USB FLAP	BL248	FLAPS 45 USB 60
▼	PREDICTED TOTAL NOISE.CREATED		79/03/16.
⊡	PREDICTED TBL NOISE		79/03/16.
◇	PREDICTED SEP NOISE		79/03/16.
◇	PREDICTED EDGE NOISE		79/03/16.
△	PREDICTED NN NOISE		79/03/16.
X	PREDICTED MIXING NOISE		79/03/16.

Figure 116. Results for M38 at Condition 3160

PREDICTION PROCEDURE DEMONSTRATION

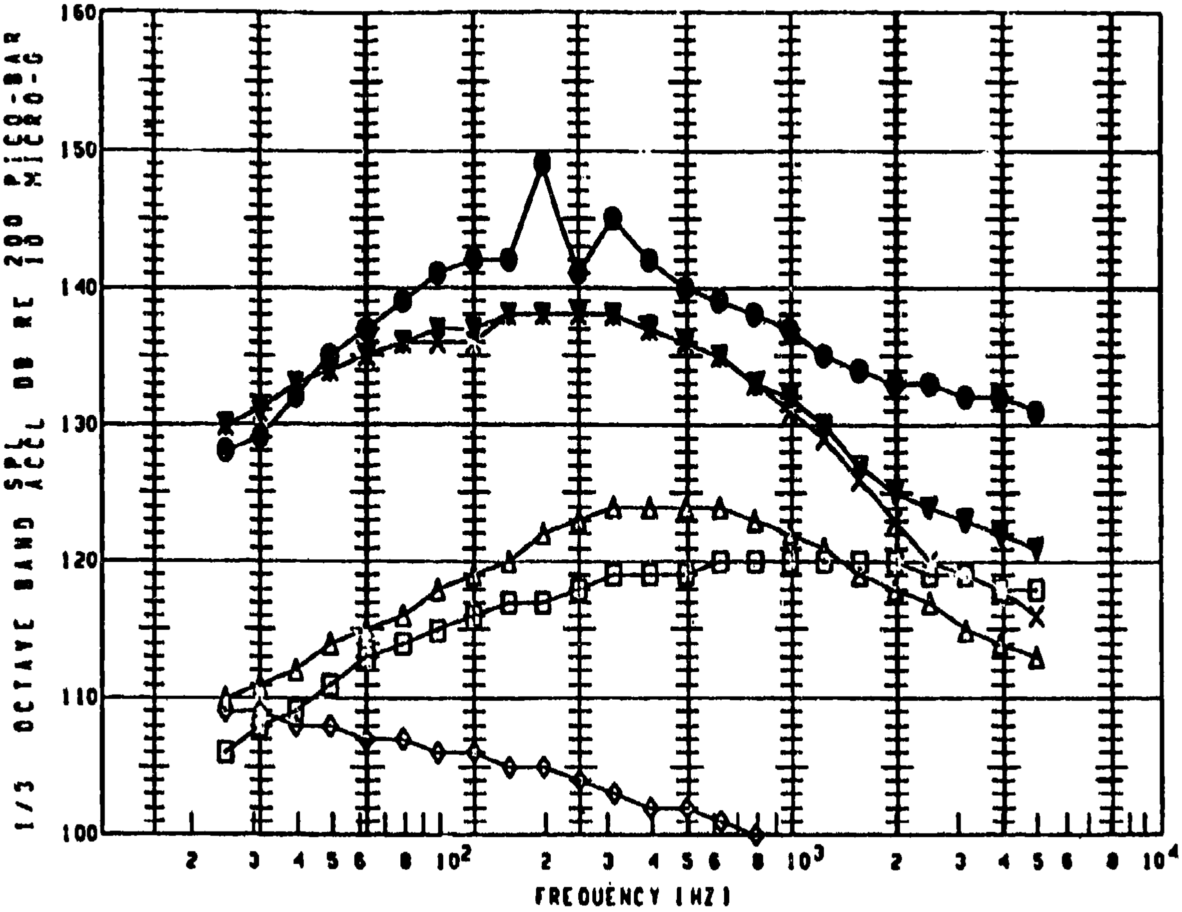

PLOT SYMBOL	X-DUCER NO.	COND. NO.	ALT. (FT)	SPEED (FPS)	N1 (RPM)	VMIX (FPS)	USBFA (DEG)	OVERALL (DB)
●	M39	3160	7650	204	2463	674	60	154
▼	M39	3160						148
⊡	M39	3160						132
◊	M39	3160						118
◊	M39	3160						105
Δ	M39	3160						134
X	M39	3160						148

NOTES		
●	MAIN USB FLAP BL171	FLAPS 45 USB 60
▼	PREDICTED TOTAL NOISE, CREATED	79/03/16.
⊡	PREDICTED TBL NOISE	79/03/16.
◊	PREDICTED SEP NOISE	79/03/16.
◊	PREDICTED EDGE NOISE	79/03/16.
Δ	PREDICTED NN NOISE	79/03/16.
X	PREDICTED MIXING NOISE	79/03/16.

Figure 117. Results for M39 at Condition 3160

PREDICTION PROCEDURE DEMONSTRATION

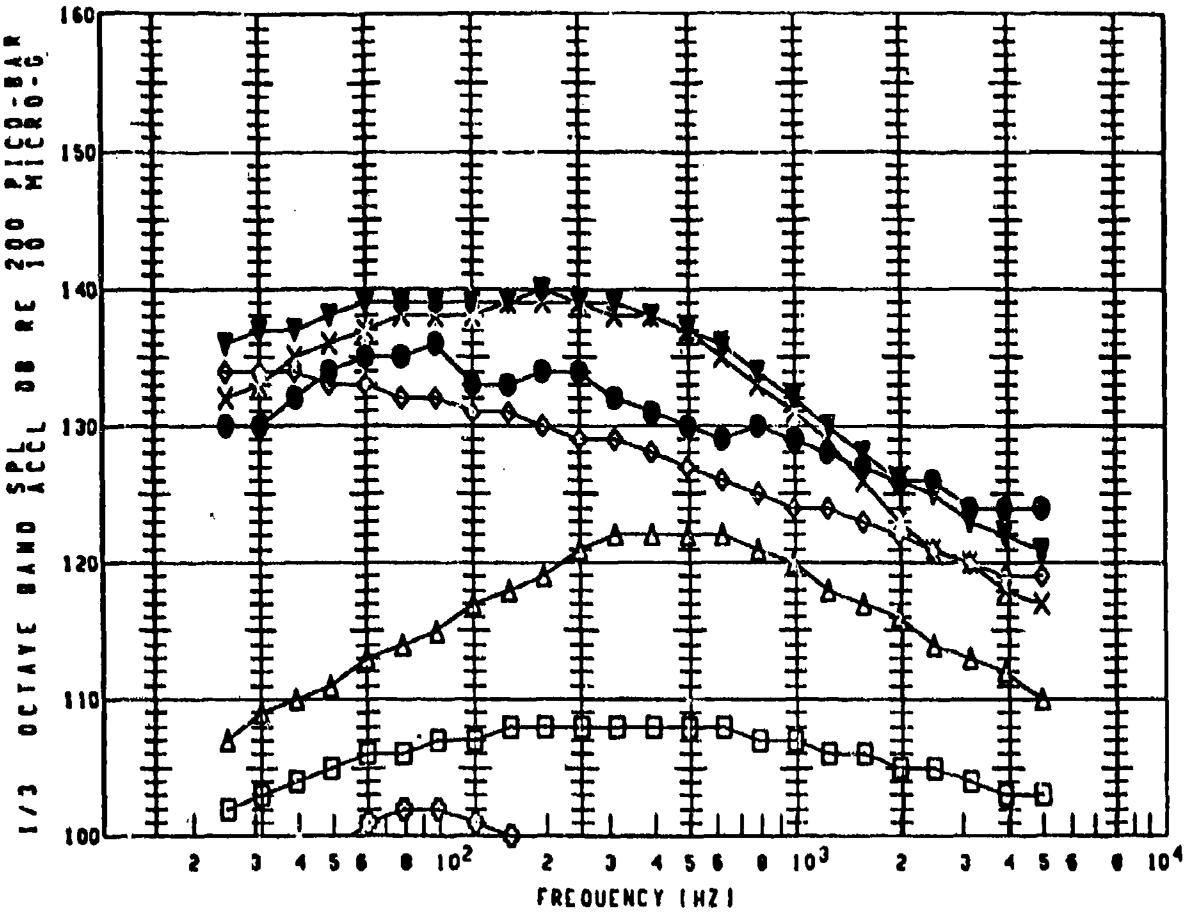

PLOT SYMBOL	X-DUCER NO.	COND. NO.	ALT. (FT)	SPEED (FPS)	N1 (RPM)	VMIX (FPS)	USBFA (DEG)	OVERALL (DB)
●	M41	3160	7650	204	2463	674	60	145
▼	M41	3160						150
⊡	M41	3160						120
◊	M41	3160						144
◈	M41	3160						110
Δ	M41	3160						132
X	M41	3160						149

NOTES

●	AFT USB FLAP	BL171	FLAPS 45 USB 60
▼	PREDICTED TOTAL NOISE.CREATED		79/03/16.
⊡	PREDICTED TBL NOISE		79/03/16.
◊	PREDICTED SEP NOISE		79/03/16.
◈	PREDICTED EDGE NOISE		79/03/16.
Δ	PREDICTED NN NOISE		79/03/16.
X	PREDICTED MIXING NOISE		79/03/16.

Figure 118. Results for M41 at Condition 3160

PREDICTION PROCEDURE DEMONSTRATION

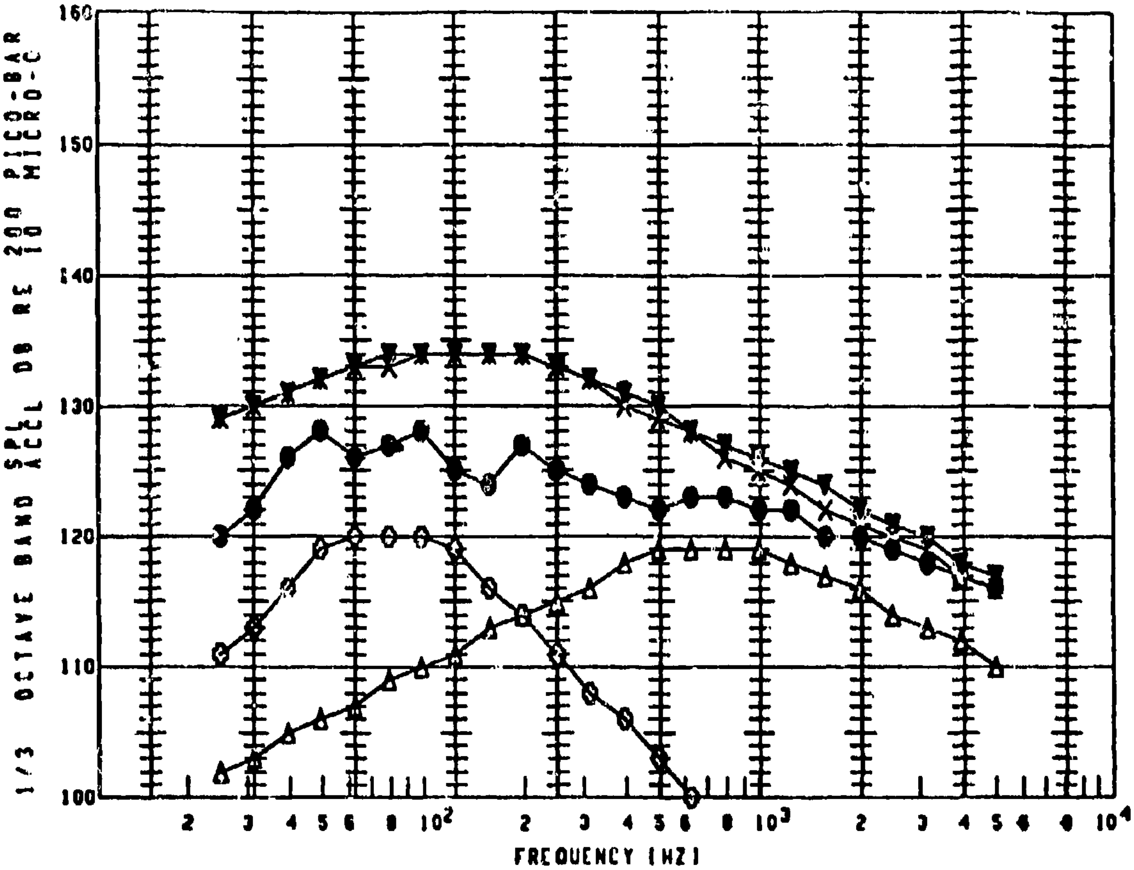

PLOT SYMBOL	X-DUCER NO.	COND. NO.	ALT. (FT)	SPEED (FPS)	N1 (RPM)	VMIX (FPS)	USBFA (DEG)	OVERALL (DB)
●	M05	7132	0	42	3540	1100	0	138
▼	M05	7132						144
⊡	M05	7132						0
⧫	M05	7132						0
⊙	M05	7132						128
Δ	M05	7132						129
X	M05	7132						144

NOTES

●	EXT BODY BS750 VL180 BL107	BRAKE RELEASE
▼	PREDICTED TOTAL NOISE CREATED	79/03/16.
⊡	PREDICTED TBL NOISE	79/03/16.
⧫	PREDICTED SEP NOISE	79/03/16.
⊙	PREDICTED EDGE NOISE	79/03/16.
Δ	PREDICTED NN NOISE	79/03/16.
X	PREDICTED MIXING NOISE	79/03/16.

Figure 119. Results for M05 at Condition 7132

PREDICTION PROCEDURE DEMONSTRATION

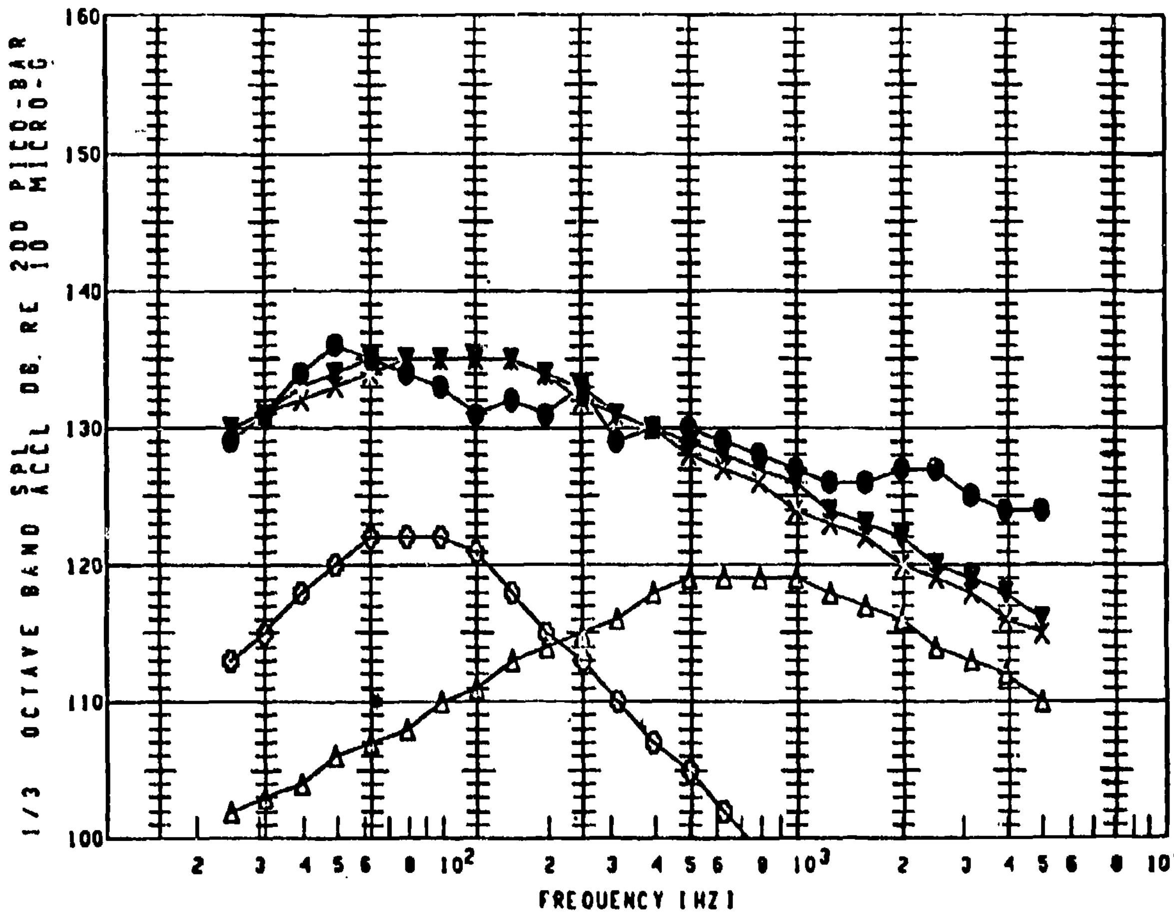

PLOT SYMBOL	X-DUCER NO.	COND. NO.	ALT. (FT)	SPEED (FPS)	N1 (RPM)	VMIX (FPS)	USBFA (DEG)	OVERALL (DB)
●	M06	7132	0	42	3540	1100	0	145
▼	M06	7132						145
⊡	M06	7132						0
◈	M06	7132						0
⊙	M06	7132						130
Δ	M06	7132						129
X	M06	7132						145

NOTES

●	EXT BODY BS825 VL180 BL107	BRAKE RELEASE
▼	PREDICTED TOTAL NOISE.CREATED	79/03/16.
⊡	PREDICTED TBL NOISE	79/03/16.
◈	PREDICTED SEP NOISE	79/03/16.
⊙	PREDICTED EDGE NOISE	79/03/16.
Δ	PREDICTED NN NOISE	79/03/16.
X	PREDICTED MIXING NOISE	79/03/16.

Figure 120. Results for M06 at Condition 7132

PREDICTION PROCEDURE DEMONSTRATION

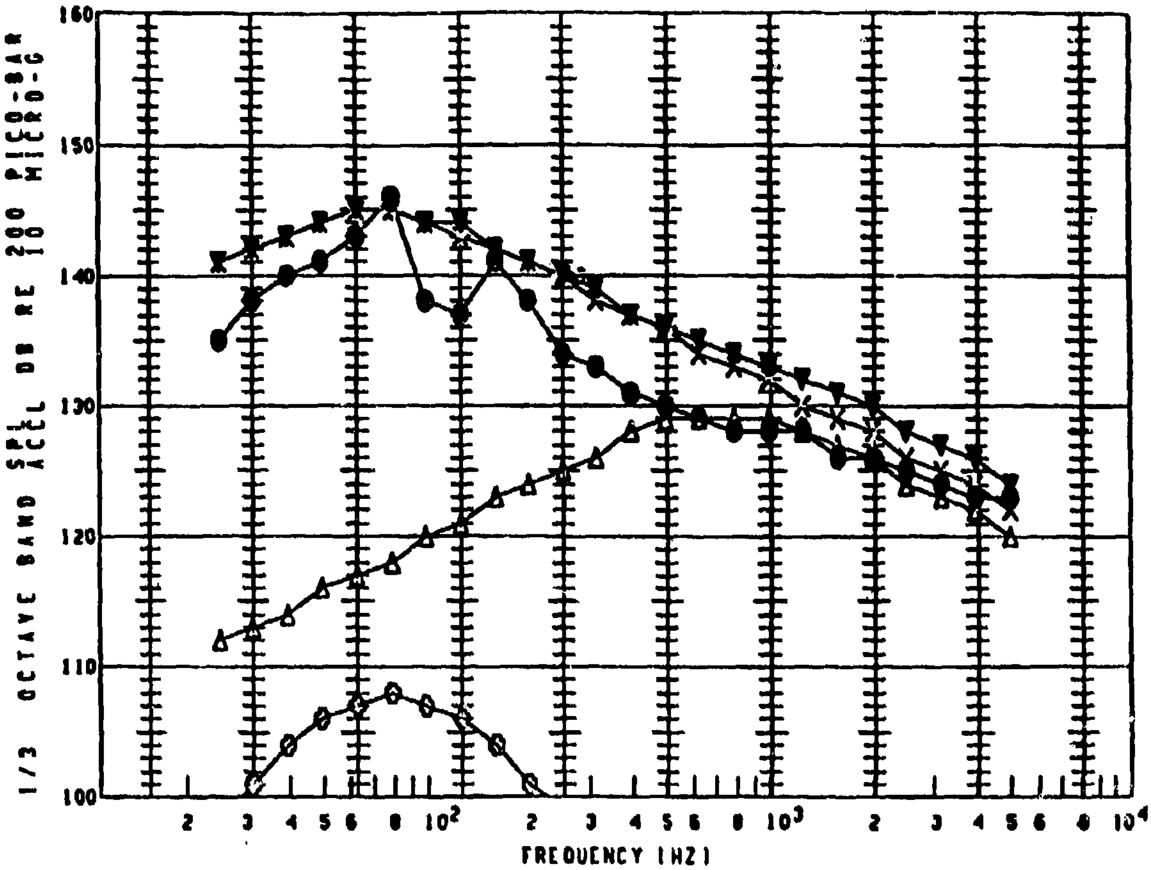

PLOT SYMBOL	X-DUCER NO.	COND. NO.	ALT. (FT)	SPEED (FPS)	N1 (RPM)	VMIX (FPS)	USBFA (DEG)	OVERALL (DB)
●	M08	7132	0	42	3540	1100	0	151
▼	M08	7132						154
⊡	M08	7132						0
◊	M08	7132						0
◊	M08	7132						115
Δ	M08	7132						139
X	M08	7132						154

NOTES

●	EXT FAIR 8S820 VL255 BL082	BRAKE RELEASE
▼	PREDICTED TOTAL NOISE,CREATED	79/03/16.
⊡	PREDICTED TBL NOISE	79/03/16.
◊	PREDICTED SEP NOISE	79/03/16.
◊	PREDICTED EDGE NOISE	79/03/16.
Δ	PREDICTED NN NOISE	79/03/16.
X	PREDICTED MIXING NOISE	79/03/16.

Figure 121. Results for M08 at Condition 7132

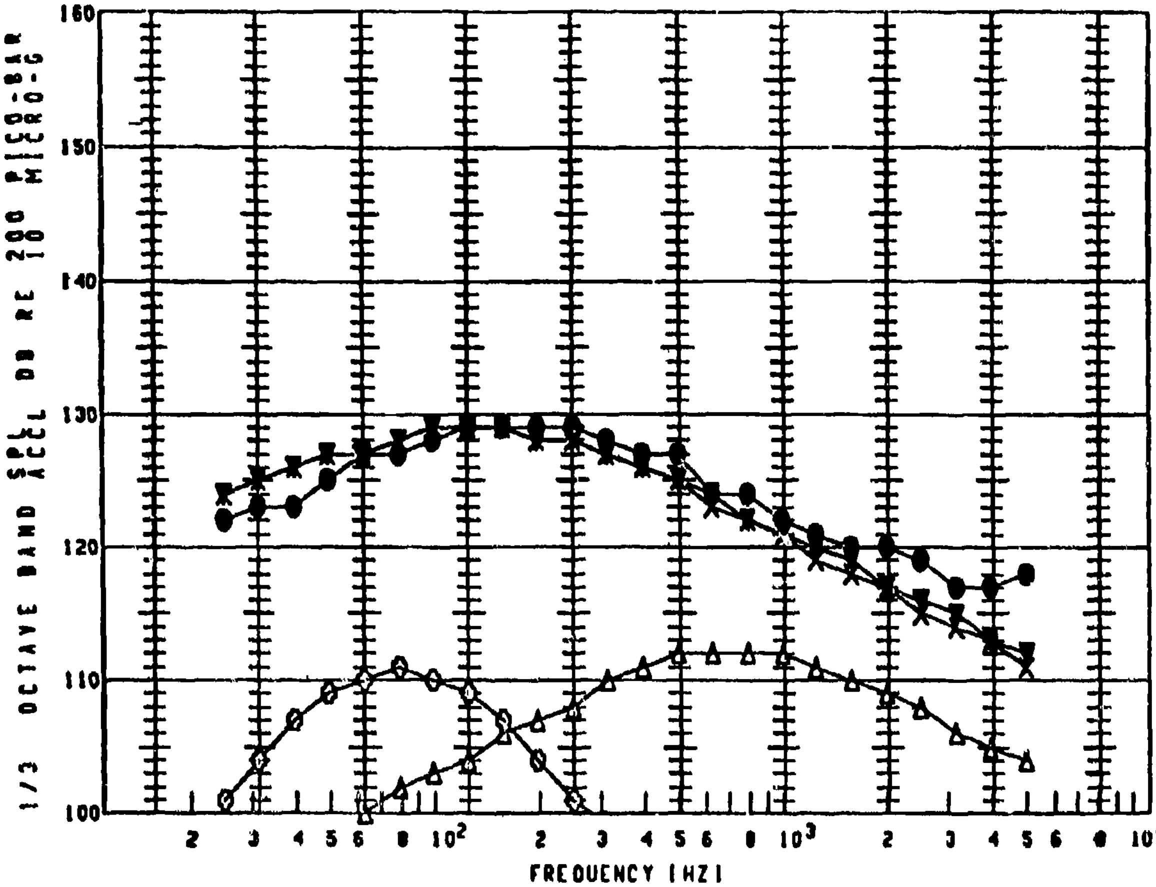

PLOT SYMBOL	X-DUCER NO.	COND. NO.	ALT. (FT)	SPEED (FPS)	N1 (RPM)	VMIX (FPS)	USBFA (DEG)	OVERALL (DB)
●	M12	7132	0	42	3540	1100	0	139
▼	M12	7132						139
⊡	M12	7132						0
◊	M12	7132						0
⊙	M12	7132						118
Δ	M12	7132						122
X	M12	7132						139

NOTES

●	EXT BODY BS875 VL280 BL 0	BRAKE RELEASE
▼	PREDICTED TOTAL NOISE.CREATED	79/03/16.
⊡	PREDICTED TBL NOISE	79/03/16.
◊	PREDICTED SEP NOISE	79/03/16.
⊙	PREDICTED EDGE NOISE	79/03/16.
Δ	PREDICTED NN NOISE	79/03/16.
X	PREDICTED MIXING NOISE	79/03/16.

Figure 122. Results for M12 at Condition 7132

PREDICTION PROCEDURE DEMONSTRATION

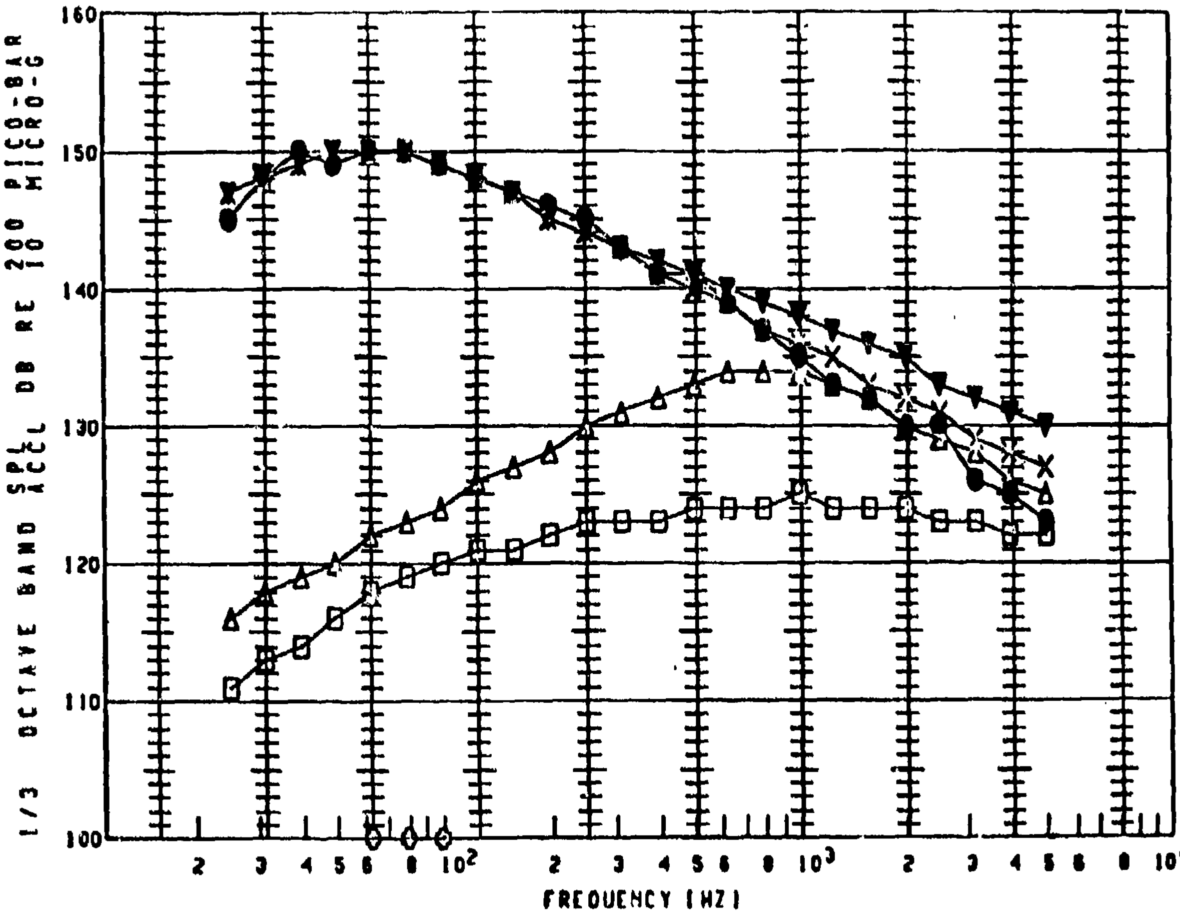

PLOT SYMBOL	X-DUCER NO.	COND. NO.	ALT. (FT)	SPEED (FPS)	N1 (RPM)	VMIX (FPS)	USBFA (DEG)	OVERALL (DB)
●	M13	7132	0	42	3540	1100	0	159
▼	M13	7132						159
⊡	M13	7132						136
◊	M13	7132						0
⊙	M13	7132						108
Δ	M13	7132						144
X	M13	7132						159

NOTES

●	EXT FAIR BS875 WL220 BL102	BRAKE RELEASE
▼	PREDICTED TOTAL NOISE CREATED	79/03/16.
⊡	PREDICTED TBL NOISE	79/03/16.
◊	PREDICTED SEP NOISE	79/03/16.
⊙	PREDICTED EDGE NOISE	79/03/16.
Δ	PREDICTED NN NOISE	79/03/16.
X	PREDICTED MIXING NOISE	79/03/16.

Figure 123. Results for M13 at Condition 7132

PREDICTION PROCEDURE DEMONSTRATION

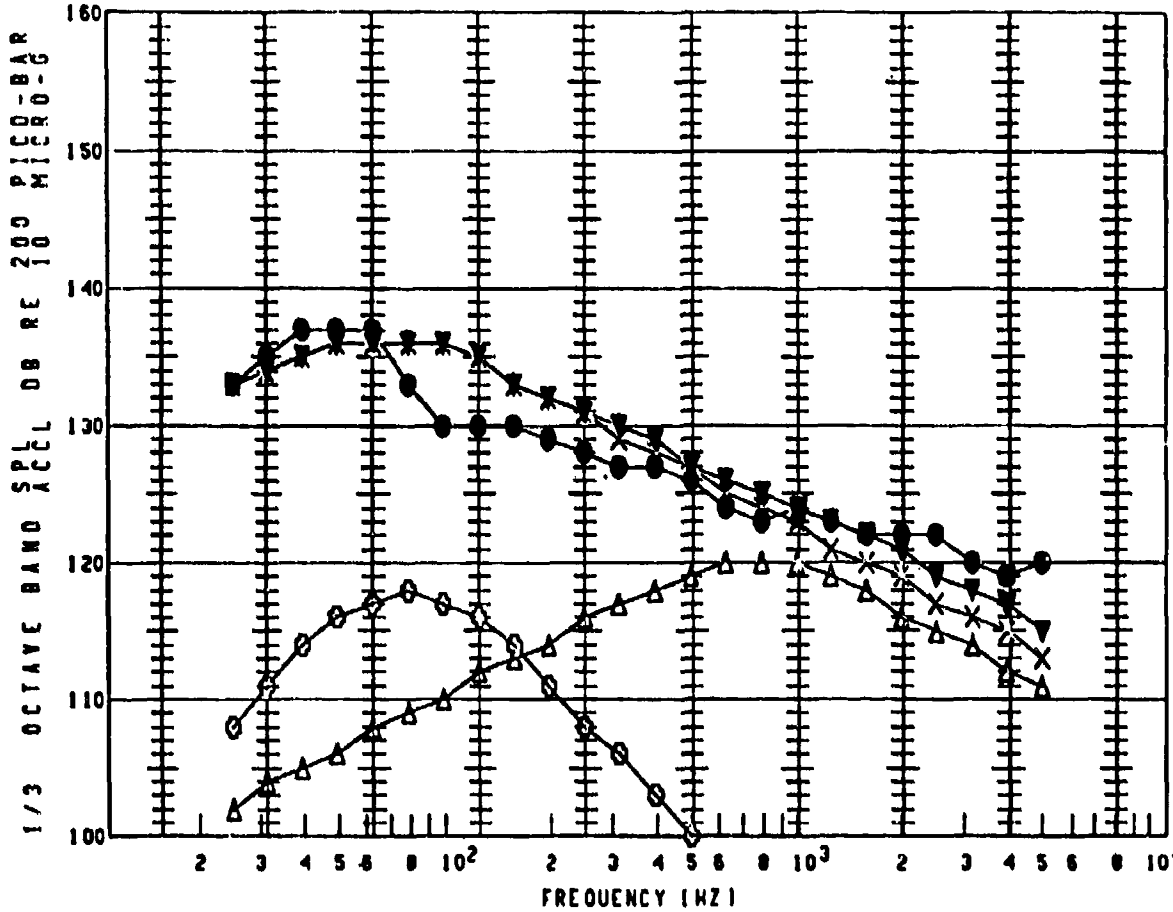

PLOT SYMBOL	X-DUCER NO.	COND. NO.	ALT. (FT)	SPEED (FPS)	N1 (RPM)	VMIX (FPS)	USBFA (DEG)	OVERALL (DB)
●	M14	7132	0	42	3540	1100	0	145
▼	M14	7132						146
⊡	M14	7132						0
◊	M14	7132						0
⊘	M14	7132						125
Δ	M14	7132						130
X	M14	7132						145

NOTES

●	EXT BODY BS875 VL180 BL107	BRAKE RELEASE
▼	PREDICTED TOTAL NOISE.CREATED	79/03/16.
⊡	PREDICTED TBL NOISE	79/03/16.
◊	PREDICTED SEP NOISE	79/03/16.
⊘	PREDICTED EDGE NOISE	79/03/16.
Δ	PREDICTED NN NOISE	79/03/16.
X	PREDICTED MIXING NOISE	79/03/16.

Figure 124. Results for M14 at Condition 7132

PREDICTION PROCEDURE DEMONSTRATION

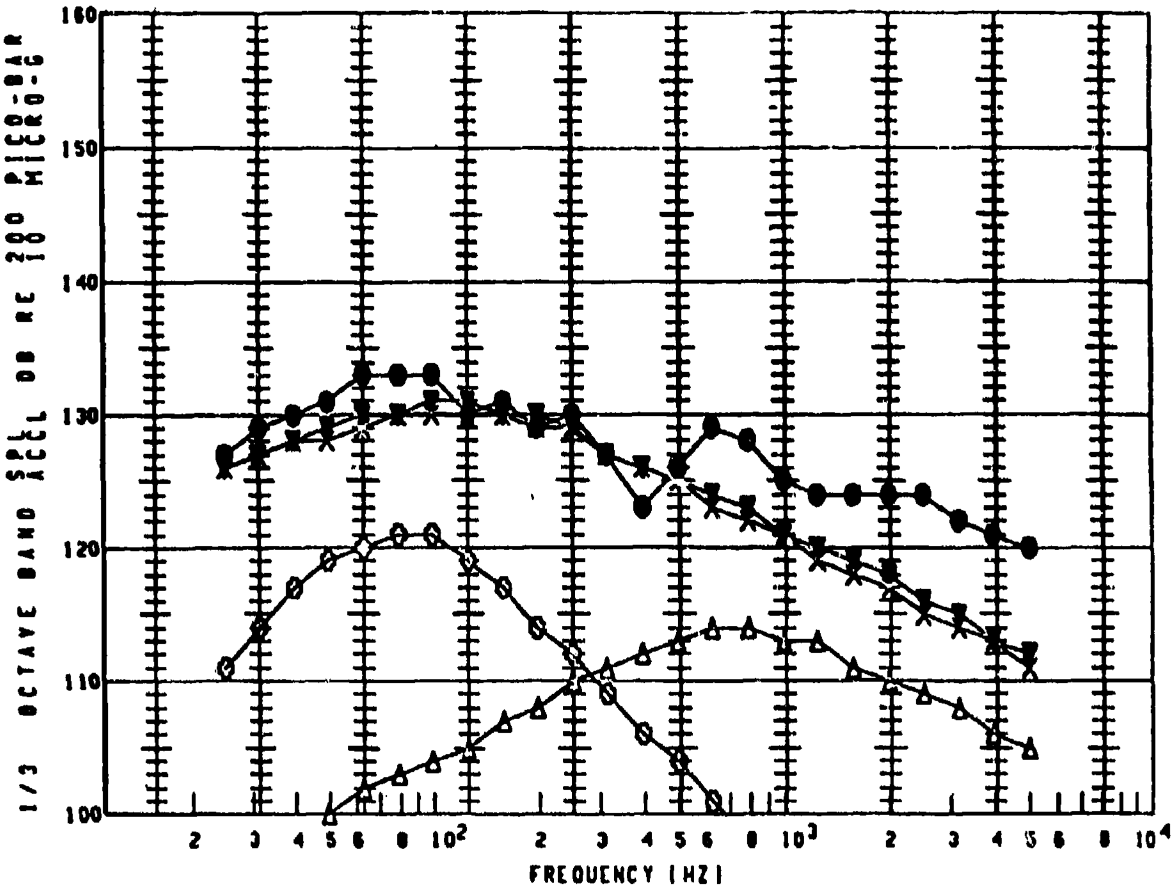

PLOT SYMBOL	X-DUCER NO.	COND. NO.	ALT. (FT)	SPEED (FPS)	NI (RPM)	VMIX (FPS)	USBFA (DEG)	OVERALL (DB)
●	M15	7132	0	42	3540	1100	0	143
▼	M15	7132						141
⊡	M15	7132						0
◈	M15	7132						0
◊	M15	7132						128
Δ	M15	7132						123
X	M15	7132						140

NOTES

●	EXT BODY BS875 VL137 BL099	BRAKE RELEASE
▼	PREDICTED TOTAL NOISE,CREATED	79/03/16.
⊡	PREDICTED TBL NOISE	79/03/16.
◈	PREDICTED SEP NOISE	79/03/16.
◊	PREDICTED EDGE NOISE	79/03/16.
Δ	PREDICTED NN NOISE	79/03/16.
X	PREDICTED MIXING NOISE	79/03/16.

Figure 125. Results for M15 at Condition 7132

PREDICTION PROCEDURE DEMONSTRATION

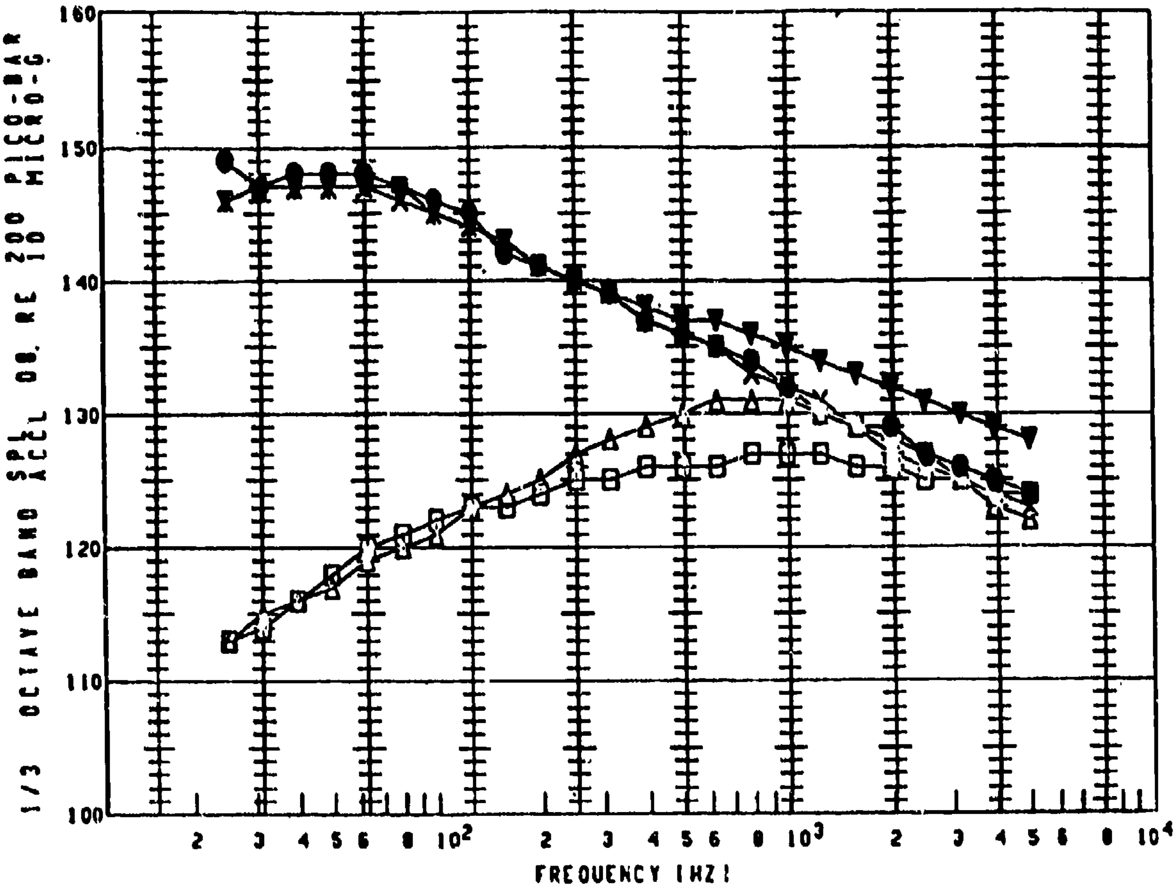

PLOT SYMBOL	X-DUCER NO.	COND. NO.	ALT. (FT)	SPEED (FPS)	N1 (RPM)	VMIX (FPS)	USBFA (DEG)	OVERALL (DB)
●	M16	7132	0	42	3540	1100	0	157
▼	M16	7132						156
⊡	M16	7132						138
◇	M16	7132						0
⊙	M16	7132						93
Δ	M16	7132						141
X	M16	7132						156

NOTES

●	EXT BODY BS988 VL193 BL099	BRAKE RELEASE
▼	PREDICTED TOTAL NOISE,CREATED	79/03/16.
⊡	PREDICTED TBL NOISE	79/03/16.
◇	PREDICTED SEP NOISE	79/03/16.
⊙	PREDICTED EDGE NOISE	79/03/16.
Δ	PREDICTED NN NOISE	79/03/16.
X	PREDICTED MIXING NOISE	79/03/16.

Figure 126. Results for M16 at Condition 7132

PREDICTION PROCEDURE DEMONSTRATION

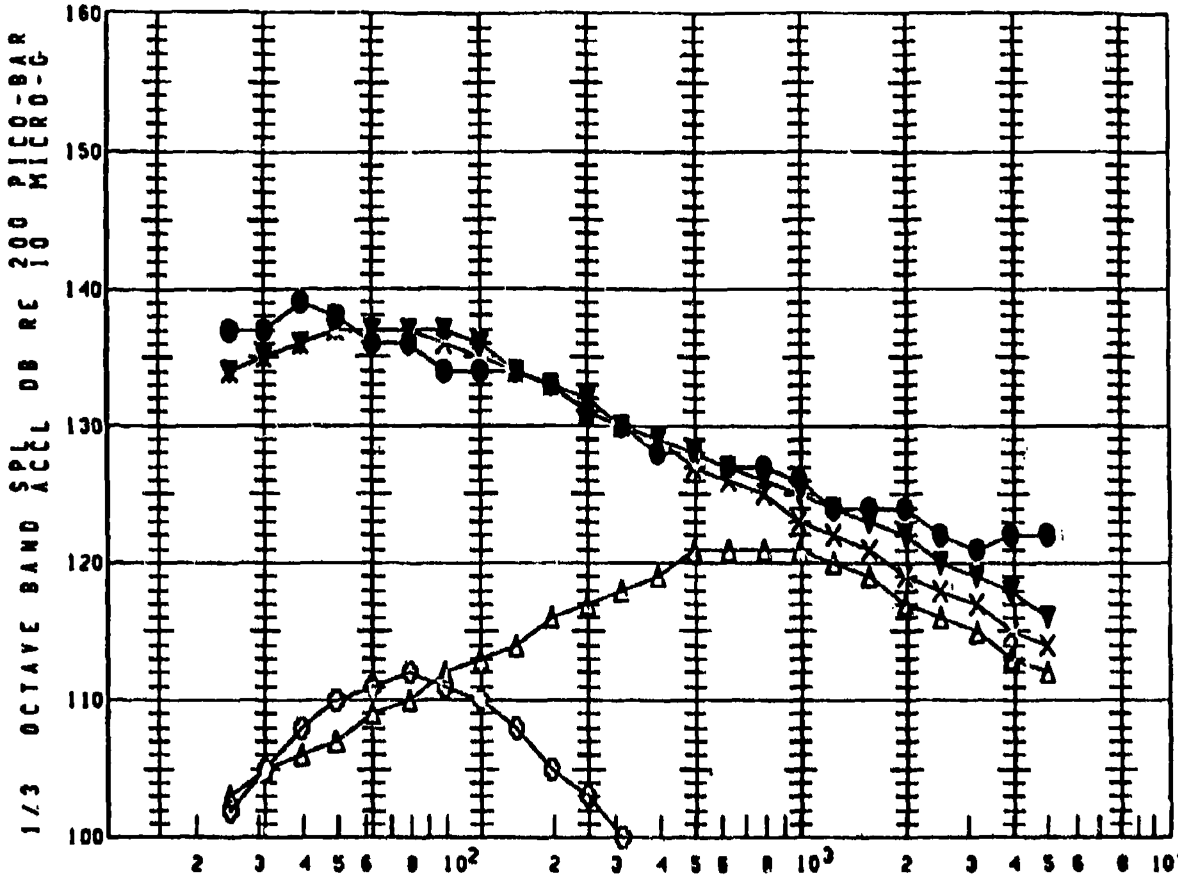

PLOT SYMBOL	X-DUCER NO.	COND. NO.	ALT. (FT)	SPEED (FPS)	N1 (RPM)	VMIX (FPS)	USBFA (DEG)	OVERALL (DB)
●	M20	7132	0	42	3540	1100	0	147
▼	M20	7132						146
⊡	M20	7132						0
◈	M20	7132						0
◇	M20	7132						119
Δ	M20	7132						131
X	M20	7132						146

NOTES

●	EXT BODY BS875 VL254 BL071	BRAKE RELEASE
▼	PREDICTED TOTAL NOISE CREATED	79/03/16.
⊡	PREDICTED TBL NOISE	79/03/16.
◈	PREDICTED SEP NOISE	79/03/16.
◇	PREDICTED EDGE NOISE	79/03/16.
Δ	PREDICTED NN NOISE	79/03/16.
X	PREDICTED MIXING NOISE	79/03/16.

Figure 127. Results for M20 at Condition 7132

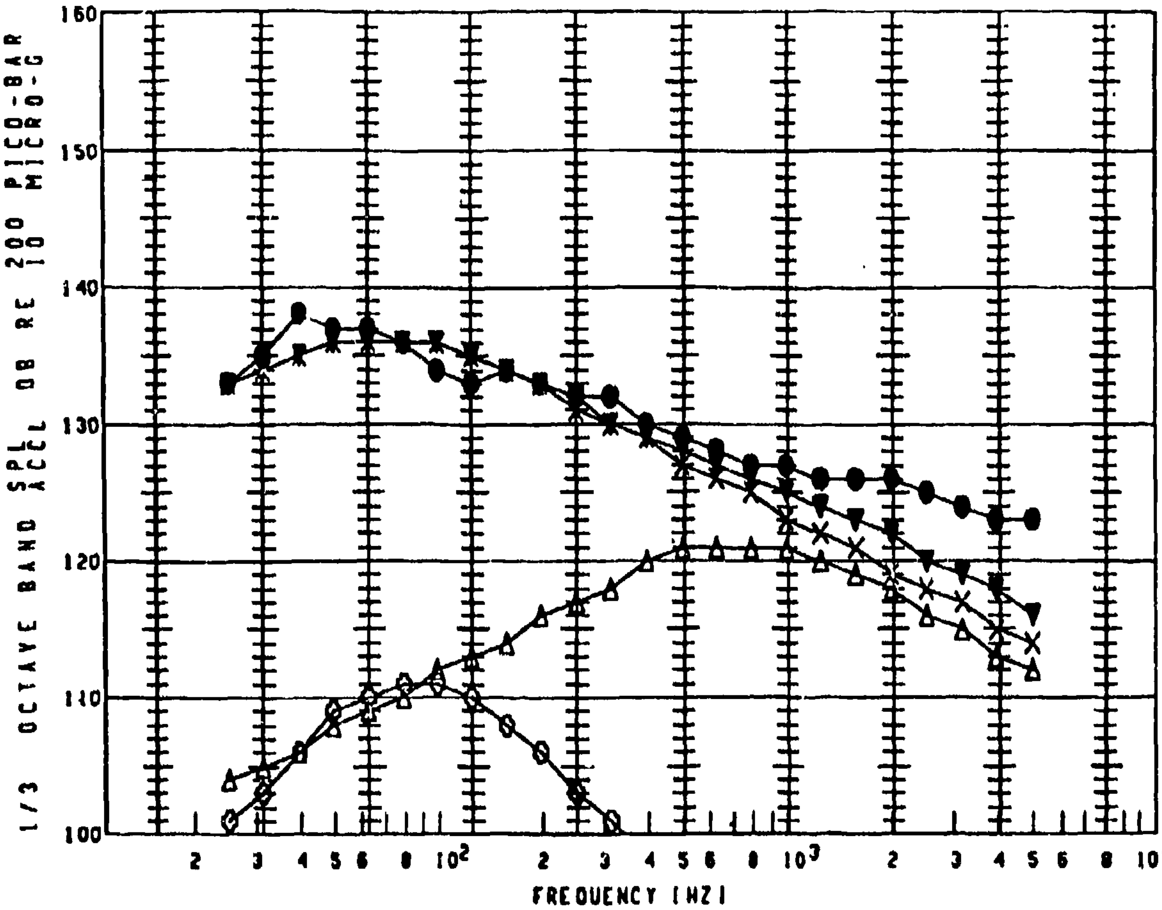

PLOT SYMBOL	X-DUCER NO.	COND. NO.	ALT. (FT)	SPEED (FPS)	N1 (RPM)	VMIX (FPS)	USBFA (DEG)	OVERALL (DB)
●	M20	7133	0	84	3690	1100	0	146
▼	M20	7133						146
⊡	M20	7133						97
◊	M20	7133						0
⬨	M20	7133						119
Δ	M20	7133						131
X	M20	7133						146

NOTES

●	EXT BODY BS875 VL254 BL071	ROLL.50 KNTS
▼	PREDICTED TOTAL NOISE.CREATED	79/07/10.
⊡	PREDICTED TBL NOISE	79/07/10.
◊	PREDICTED SEP NOISE	79/07/10.
⬨	PREDICTED EDGE NOISE	79/07/10.
Δ	PREDICTED NN NOISE	79/07/10.
X	PREDICTED MIXING NOISE	79/07/10.

Figure 128. Results for M20 at Condition 7133

PREDICTION PROCEDURE DEMONSTRATION

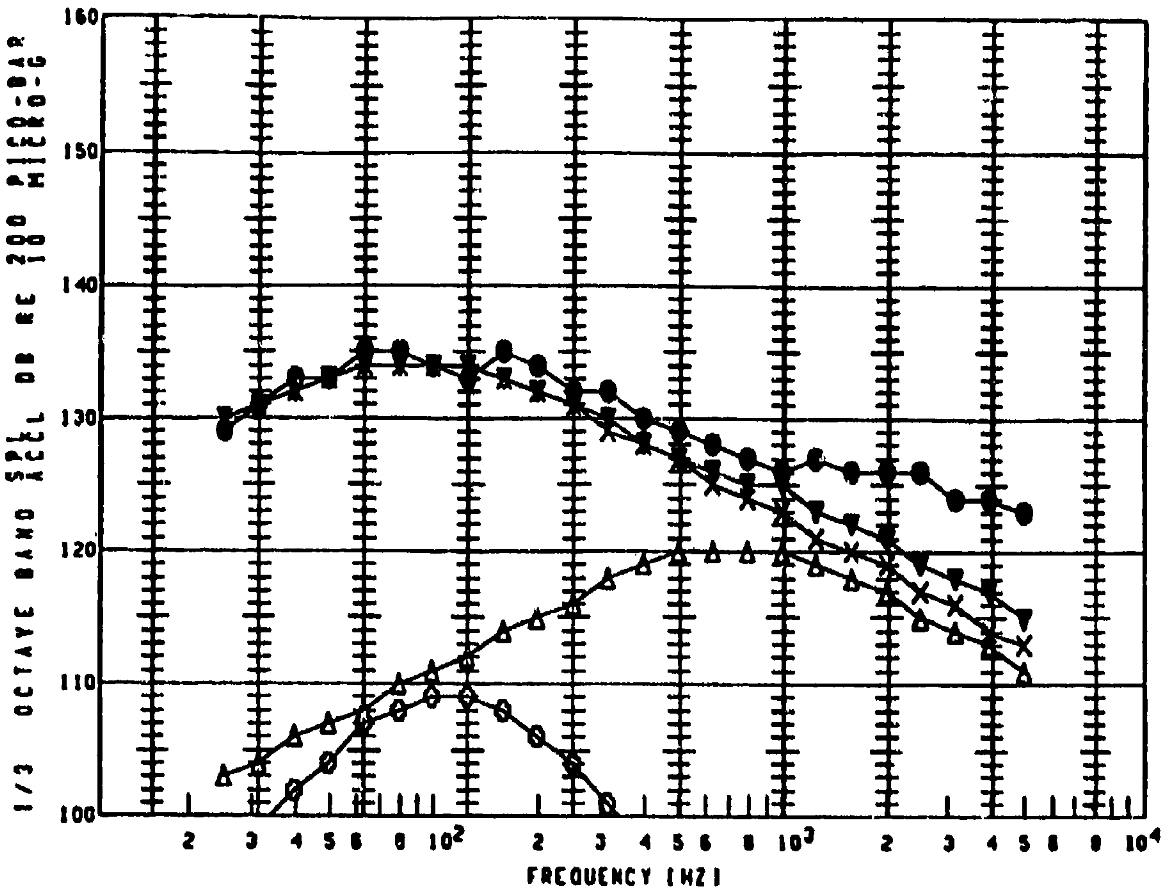

PLOT SYMBOL	X-DUCER NO.	COND. NO.	ALT. (FT)	SPEED (FPS)	NI (RPM)	VMIX (FPS)	USBFA (DEG)	OVERALL (DB)
●	M20	7134	0	168	3720	1070.	0	145
▼	M20	7134						144
⊡	M20	7134						110
◊	M20	7134						0
⊙	M20	7134						117
Δ	M20	7134						130
X	M20	7134						144

NOTES

●	EXT BODY BS875 VL254 BL071	ROLL.100 KNTS
▼	PREDICTED TOTAL NOISE.CREATED	79/07/10.
⊡	PREDICTED TBL NOISE	79/07/10.
◊	PREDICTED SEP NOISE	79/07/10.
⊙	PREDICTED EDGE NOISE	79/07/10.
Δ	PREDICTED NN NOISE	79/07/10.
X	PREDICTED MIXING NOISE	79/07/10.

Figure 129. Results for M20 at Condition 7134

PREDICTION PROCEDURE DEMONSTRATION

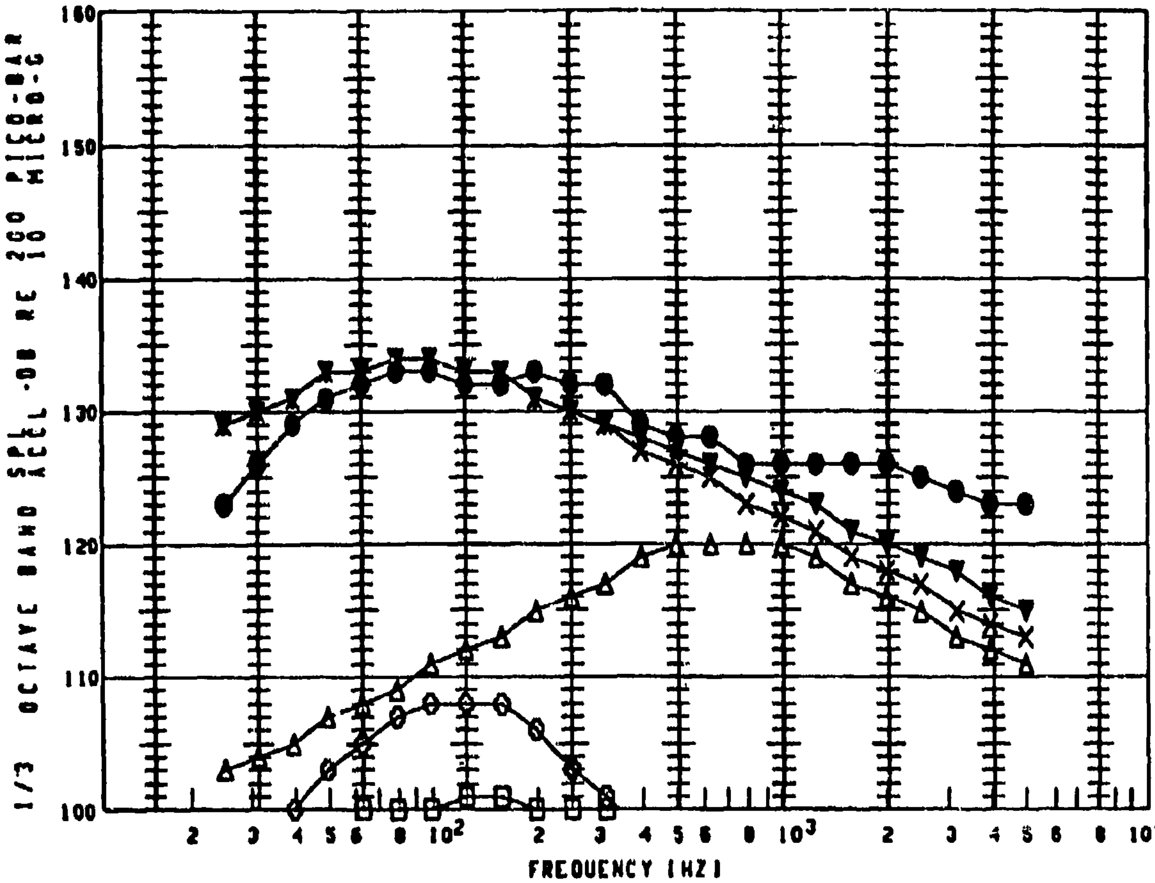

PLOT SYMBOL	X-DUCER NO.	COND. NO.	ALT. (FT)	SPEED (FPS)	N1 (RPM)	VMIX (FPS)	USBFA (DEG)	OVERALL (DB)
●	M20	7135	50	186	3700	1050	0	143
▼	M20	7135						143
⊡	M20	7135						112
◊	M20	7135						0
⊙	M20	7135						116
Δ	M20	7135						130
X	M20	7135						143

NOTES

●	EXT BODY BS875 VL254 BL071	CLIMB,110 KNTS
▼	PREDICTED TOTAL NOISE CREATED	79/07/10.
⊡	PREDICTED TBL NOISE	79/07/10.
◊	PREDICTED SEP NOISE	79/07/10.
⊙	PREDICTED EDGE NOISE	79/07/10.
Δ	PREDICTED NN NOISE	79/07/10.
X	PREDICTED MIXING NOISE	79/07/10.

Figure 130. Results for M20 at Condition 7135

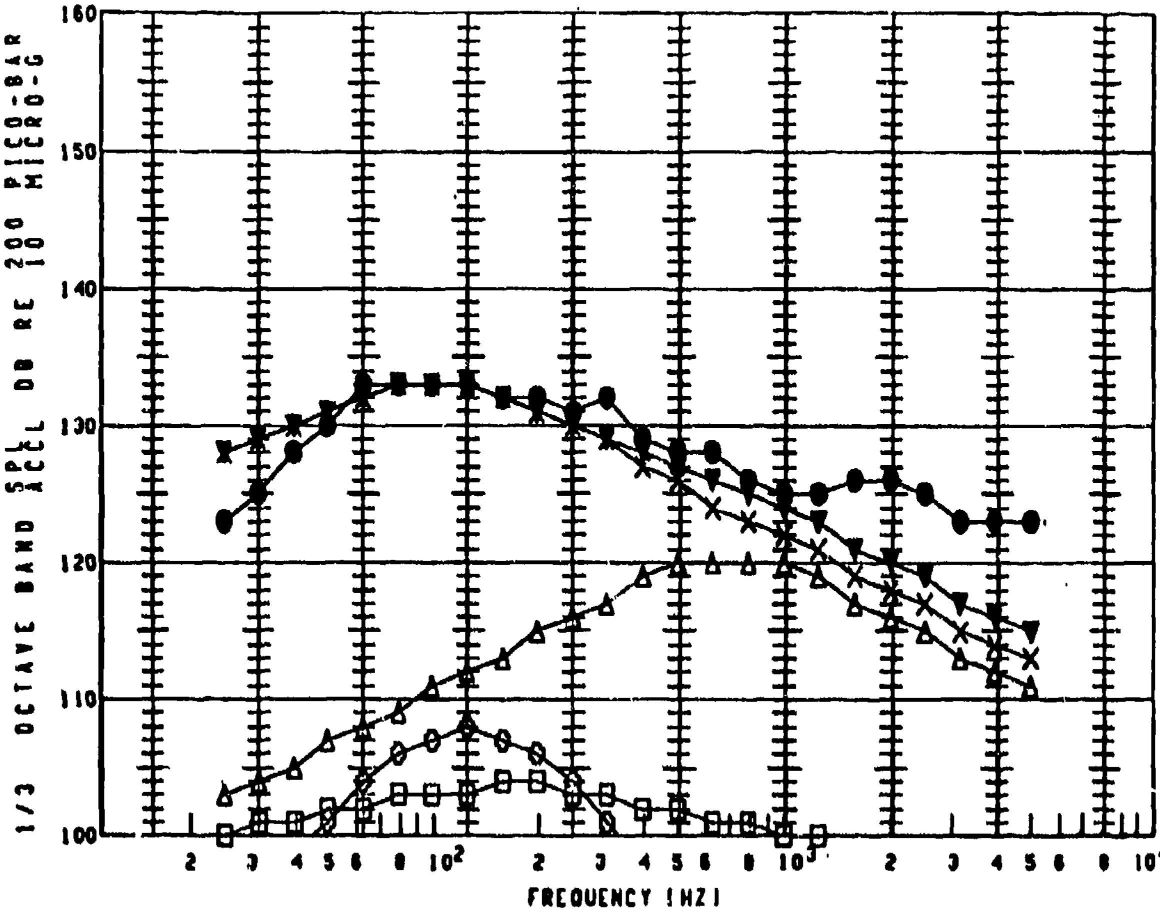

PLOT SYMBOL	X-DUCER NO.	COND. NO.	ALT. (FT)	SPEED (FPS)	N1 (RPM)	VMIX (FPS)	USBFA (DEG)	OVERALL (DB)
●	M20	7136	100	220	3710	1050	0	143
▼	M20	7136						143
⊡	M20	7136						115
◊	M20	7136						0
◊	M20	7136						115
Δ	M20	7136						130
X	M20	7136						143

NOTES

●	EXT BODY BS075 VL254 BL071	CLIMB,135 KNTS
▼	PREDICTED TOTAL NOISE,CREATED	79/07/10.
⊡	PREDICTED TBL NOISE	79/07/10.
◊	PREDICTED SEP NOISE	79/07/10.
◊	PREDICTED EDGE NOISE	79/07/10.
Δ	PREDICTED NN NOISE	79/07/10.
X	PREDICTED MIXING NOISE	79/07/10.

Figure 131. Results for M20 at Condition 7136

PREDICTION PROCEDURE DEMONSTRATION

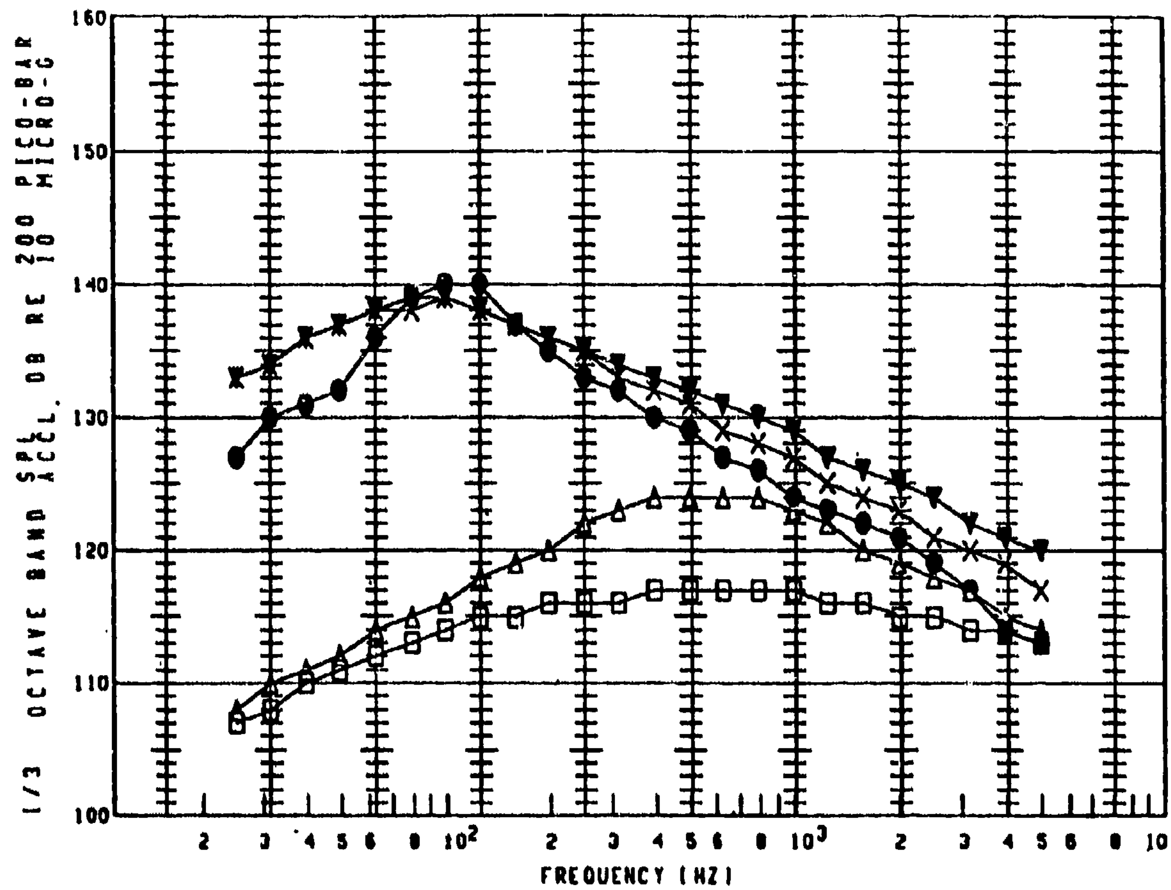

PLOT SYMBOL	X-DUCER NO.	COND. NO.	ALT. (FT)	SPEED (FPS)	N1 (RPM)	VMIX (FPS)	USBFA (DEG)	OVERALL (DB)
●	M13	7196	10000	225	2950	830	9	147
▼	M13	7196						148
⊡	M13	7196						129
◊	M13	7196						0
◊	M13	7196						102
Δ	M13	7196						134
X	M13	7196						148

NOTES

●	EXT FAIR BS875 VL220 BL102	FLAP CYCLE,VG DWN
▼	PREDICTED TOTAL NOISE,CREATED	79/07/10.
⊡	PREDICTED TBL NOISE	79/07/10.
◊	PREDICTED SEP NOISE	79/07/10.
◊	PREDICTED EDGE NOISE	79/07/10.
Δ	PREDICTED NN NOISE	79/07/10.
X	PREDICTED MIXING NOISE	79/07/10.

Figure 132. Results for M13 at Condition 7196

PREDICTION PROCEDURE DEMONSTRATION

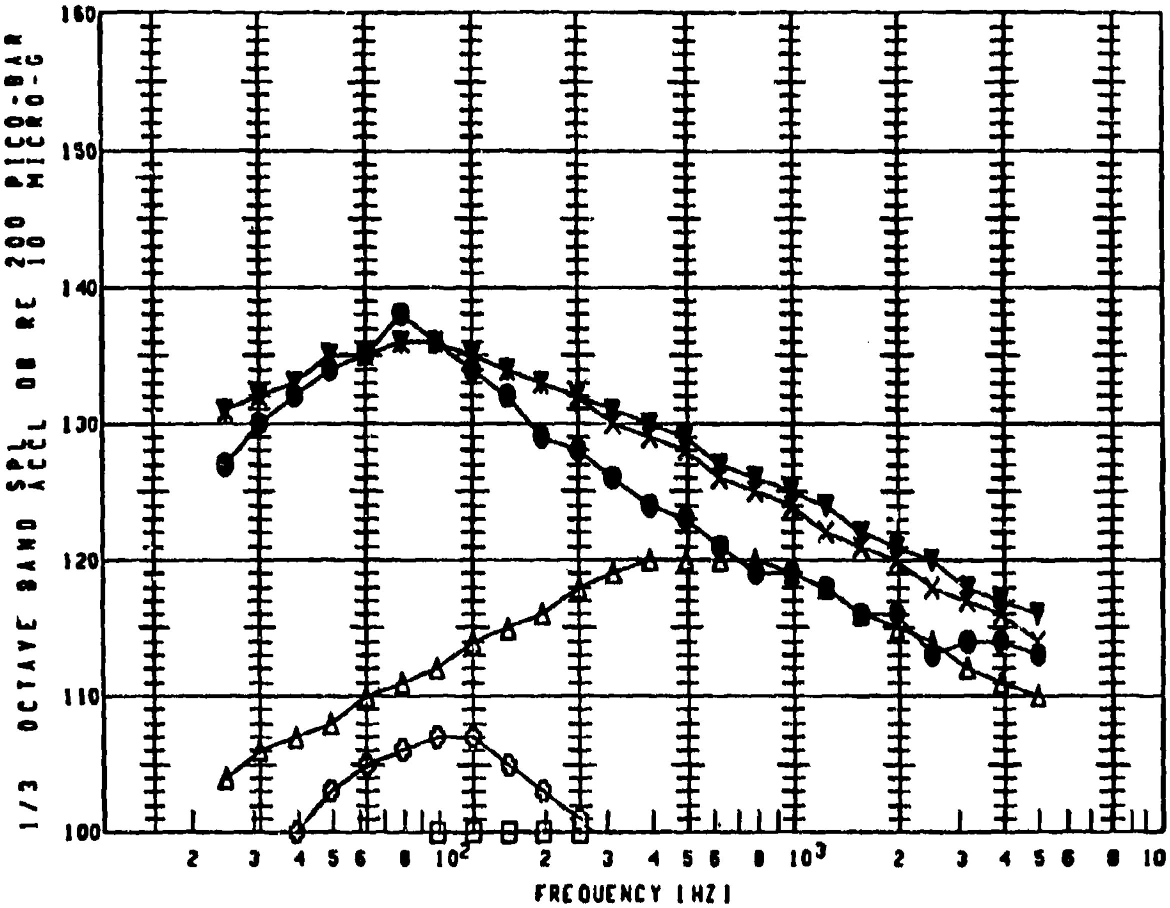

PLOT SYMBOL	X-DUCER NO.	COND. NO.	ALT. (FT)	SPEED (FPS)	NI (RPM)	VMIX (FPS)	USBFA (DEG)	OVERALL (DB)
●	M13	7193	11000	210	2950	830	29	144
▼	M13	7193						145
⊡	M13	7193						112
◊	M13	7193						102
⊙	M13	7193						115
Δ	M13	7193						130
X	M13	7193						145

NOTES

●	EXT FAIR BS875 VL220 BL102	FLAP CYCLE.VG DWN
▼	PREDICTED TOTAL NOISE.CREATED	79/07/10.
⊡	PREDICTED TBL NOISE	79/07/10.
◊	PREDICTED SEP NOISE	79/07/10.
⊙	PREDICTED EDGE NOISE	79/07/10.
Δ	PREDICTED NN NOISE	79/07/10.
X	PREDICTED MIXING NOISE	79/07/10.

Figure 133. Results for M13 at Condition 7193

PREDICTION PROCEDURE DEMONSTRATION

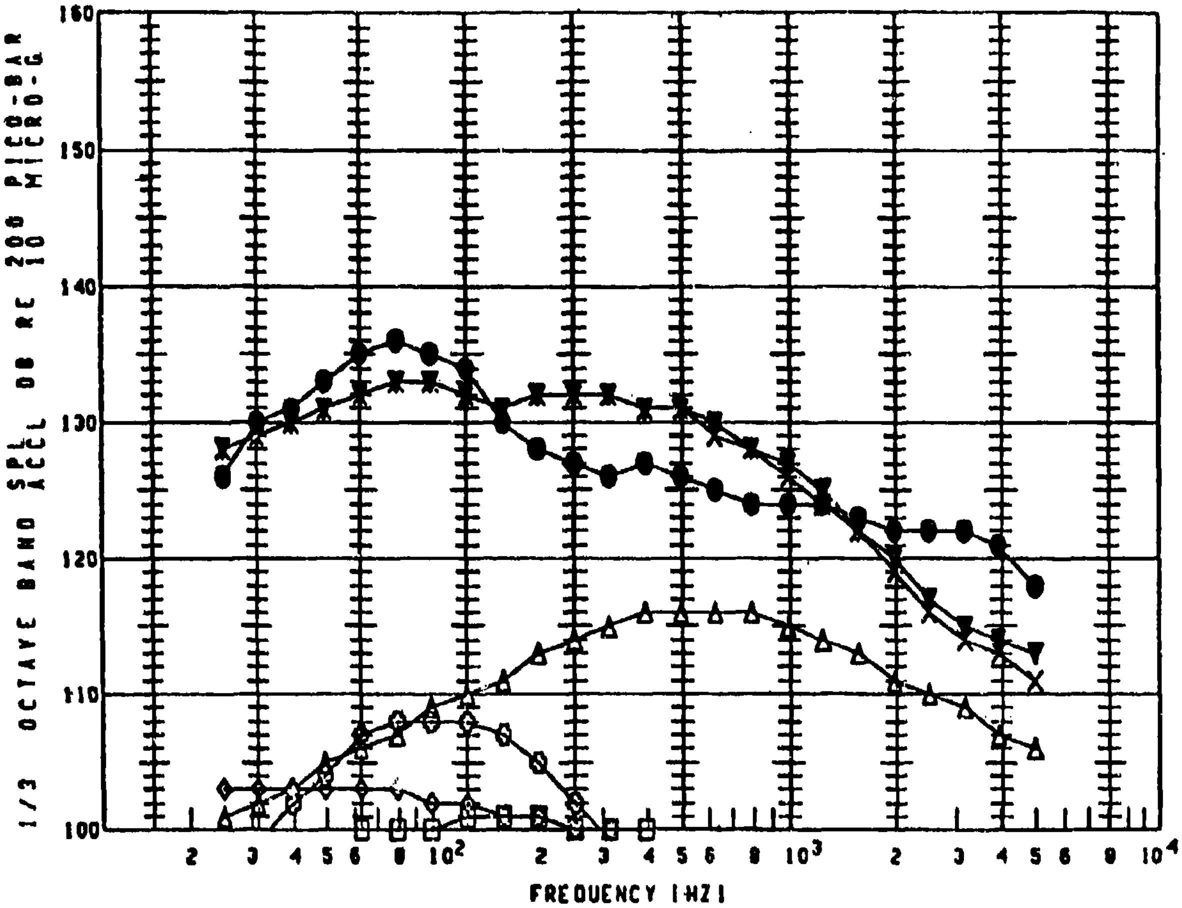

PLOT SYMBOL	X-DUCER NO.	COND NO.	ALT. (FT)	SPEED (FPS)	N1 (RPM)	VMIX (FPS)	USBFA (DEG)	OVERALL (DB)
●	M13	7195	10000	215	2950	830	41	144
▼	M13	7195						143
⊡	M13	7195						112
◊	M13	7195						114
◊	M13	7195						116
Δ	M13	7195						126
X	M13	7195						143

NOTES

●	EXT FAIR BS875 VL220 BL102	FLAP CYCLE.VG UP
▼	PREDICTED TOTAL NOISE.CREATED	79/07/10.
⊡	PREDICTED TBL NOISE	79/07/10.
◊	PREDICTED SEP NOISE	79/07/10.
◊	PREDICTED EDGE NOISE	79/07/10.
Δ	PREDICTED NN NOISE	79/07/10.
X	PREDICTED MIXING NOISE	79/07/10.

Figure 134. Results for M13 at Condition 7195

PREDICTION PROCEDURE DEMONSTRATION

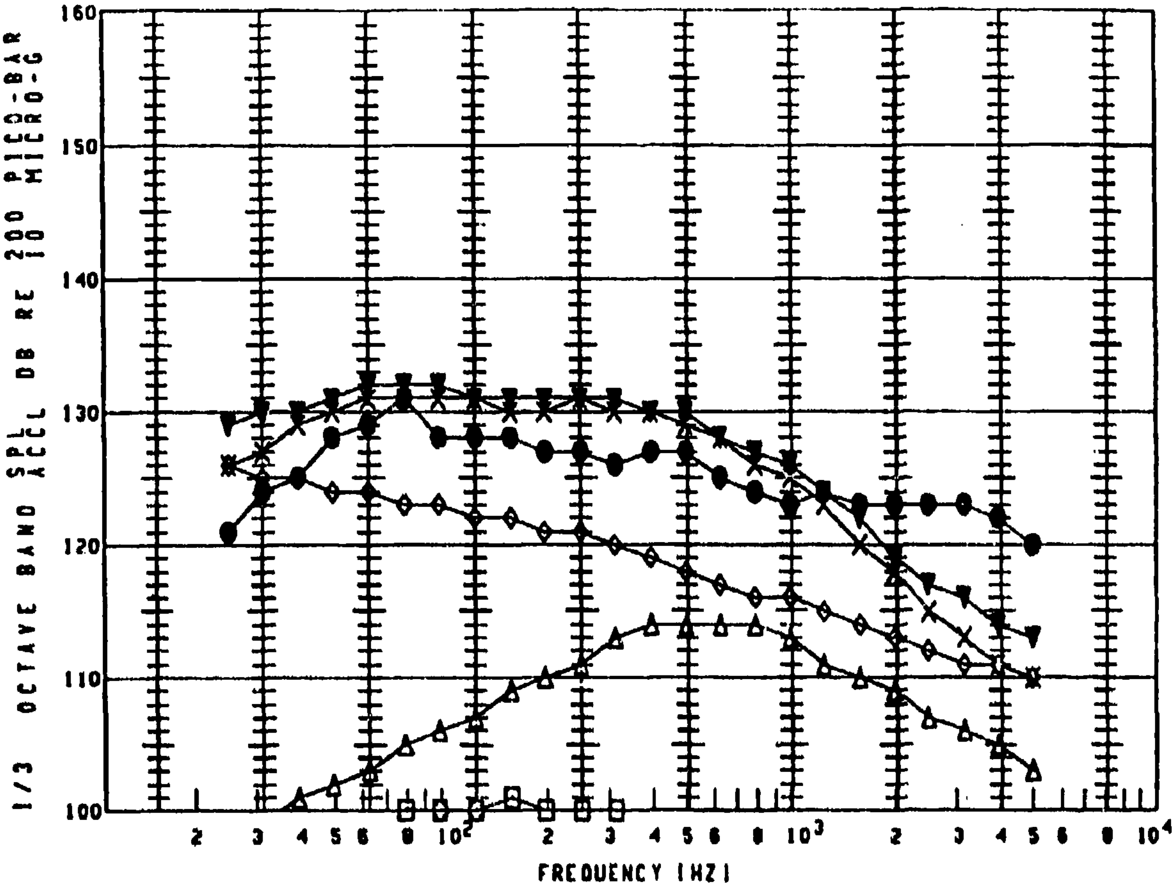

PLOT SYMBOL	X-DUCER NO.	COND. NO.	ALT. (FT)	SPEED (FPS)	N1 (RPM)	VMIX (FPS)	USBFA (DEG)	OVERALL (DB)
●	M13	7192	10700	213	2950	830	70	140
▼	M13	7192						143
⊡	M13	7192						112
◊	M13	7192						135
⊙	M13	7192						108
Δ	M13	7192						124
X	M13	7192						142

NOTES

●	EXT FAIR BS875 VL220 BL102	FLAP CYCLE,VG UP
▼	PREDICTED TOTAL NOISE,CREATED	79/07/10.
⊡	PREDICTED TBL NOISE	79/07/10.
◊	PREDICTED SEP NOISE	79/07/10.
⊙	PREDICTED EDGE NOISE	79/07/10.
Δ	PREDICTED NN NOISE	79/07/10.
X	PREDICTED MIXING NOISE	79/07/10.

Figure 135. Results for M13 at Condition 7192

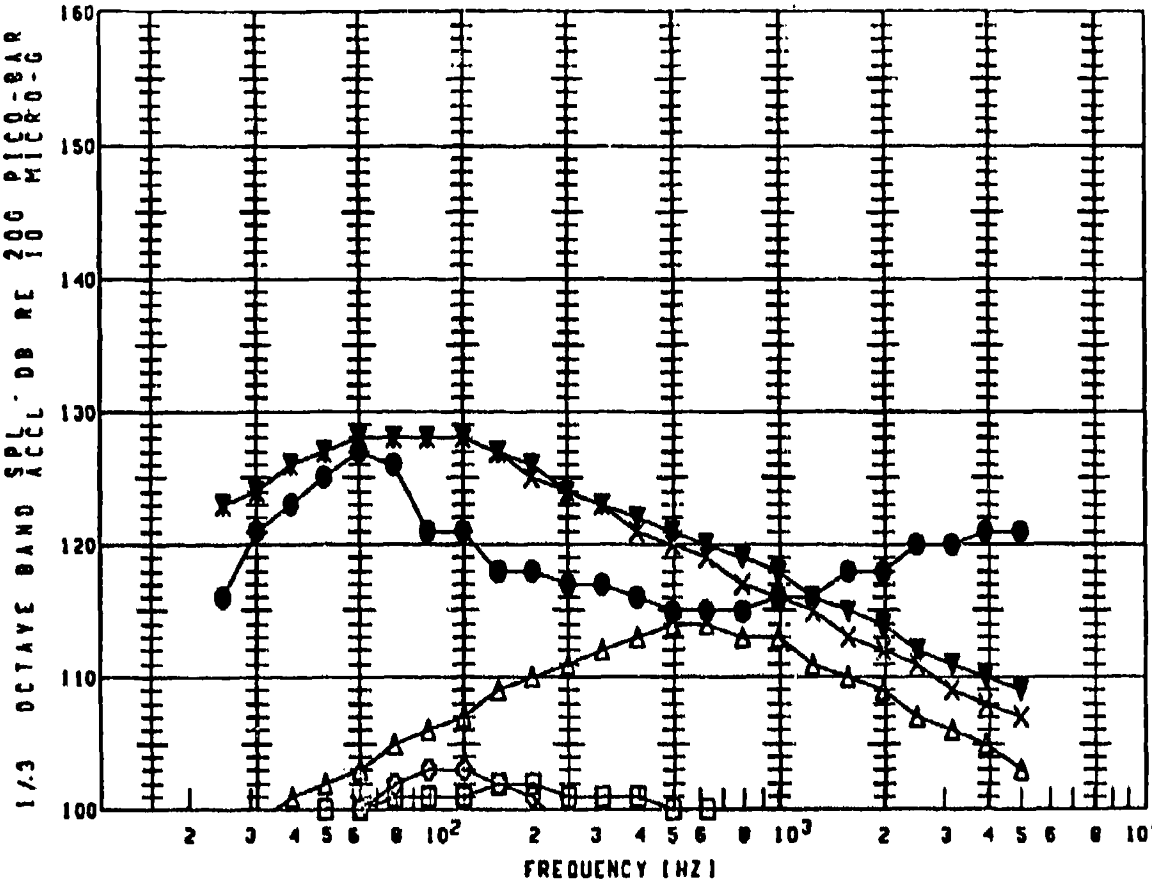

PLOT SYMBOL	X-DUCER NO.	COND. NO.	ALT. (FT)	SPEED (FPS)	NI (RPM)	VMIX (FPS)	USBFA (DEG)	OVERALL (DB)
●	M14	7196	10000	225	2950	830	9	135
▼	M14	7196						138
⊡	M14	7196						113
◊	M14	7196						0
◊	M14	7196						111
Δ	M14	7196						123
X	M14	7196						138

NOTES

●	EXT BODY BS875 WL180 BL107	FLAP CYCLE.VG DWN
▼	PREDICTED TOTAL NOISE.CREATED	79/07/10.
⊡	PREDICTED TBL NOISE	79/07/10.
◊	PREDICTED SEP NOISE	79/07/10.
◊	PREDICTED EDGE NOISE	79/07/10.
Δ	PREDICTED NN NOISE	79/07/10.
X	PREDICTED MIXING NOISE	79/07/10.

Figure 136. Results for M14 at Condition 7196

PREDICTION PROCEDURE DEMONSTRATION

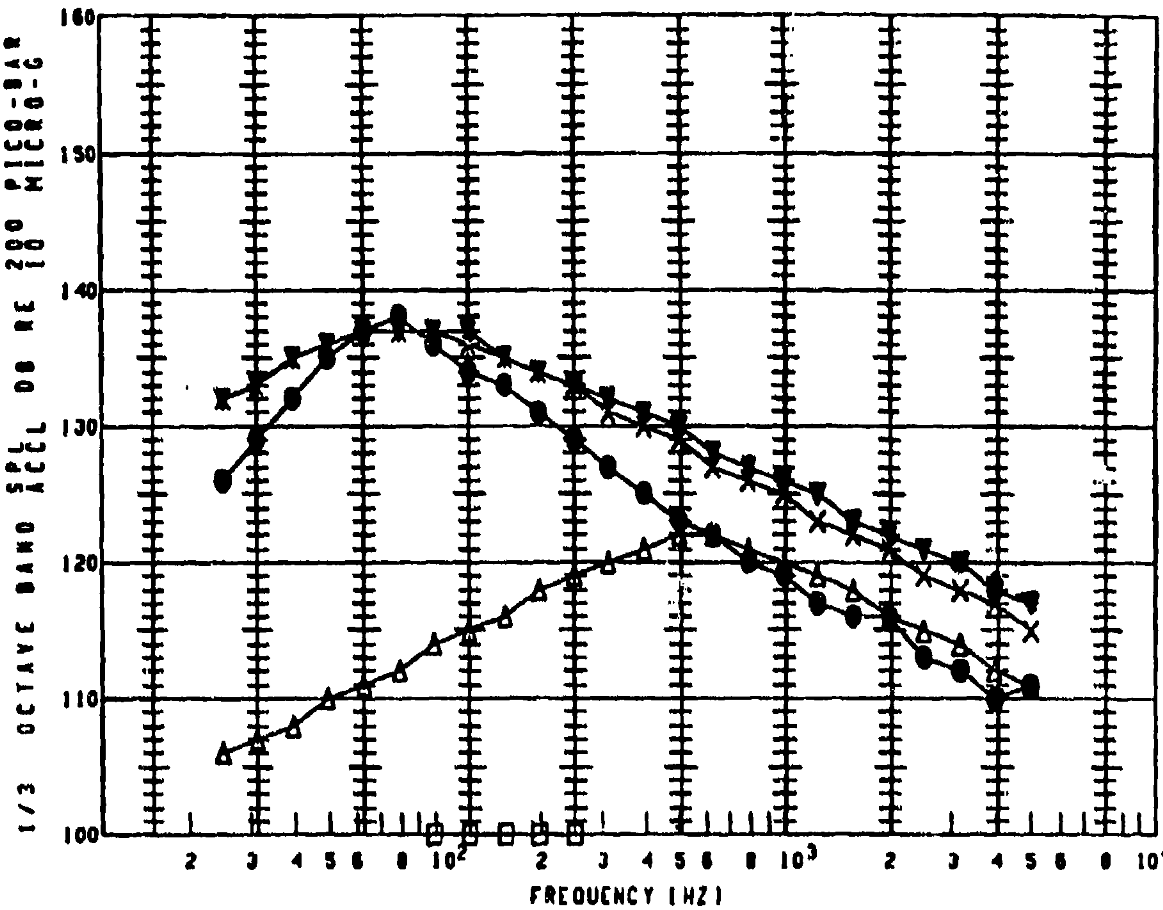

PLOT SYMBOL	X-DUCER NO.	COND. NO.	ALT. (FT)	SPEED (FPS)	N1 (RPM)	VMIX (FPS)	USBFA (DEG)	OVERALL (DB)
●	M14	7193	11000	210	2950	830	29	145
▼	M14	7193						147
⊡	M14	7193						112
◊	M14	7193						98
◊	M14	7193						100
Δ	M14	7193						131
X	M14	7193						146

NOTES

● EXT BODY BS875 VL180 BL107 FLAP CYCLE.VG DVN
▼ PREDICTED TOTAL NOISE.CREATED 79/07/10.
⊡ PREDICTED TBL NOISE 79/07/10.
◊ PREDICTED SEP NOISE 79/07/10.
◊ PREDICTED EDGE NOISE 79/07/10.
Δ PREDICTED NN NOISE 79/07/10.
X PREDICTED MIXING NOISE 79/07/10.

Figure 137. Results for M14 at Condition 7193

PREDICTION PROCEDURE DEMONSTRATION

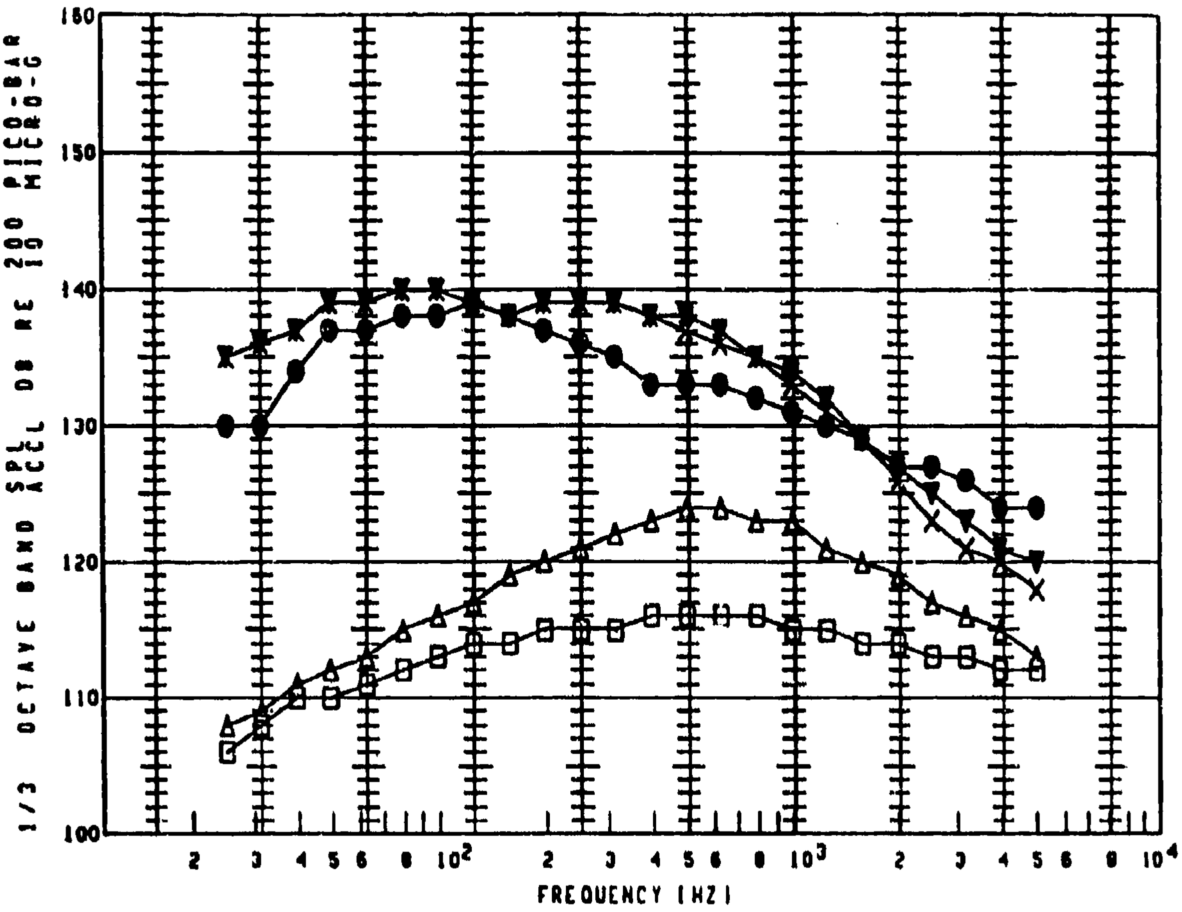

PLOT SYMBOL	X-DUCER NO.	COND. NO.	ALT. (FT)	SPEED (FPS)	N1 (RPM)	VMIX (FPS)	USBFA (DEG)	OVERALL (DB)
●	M14	7195	10000	215	2950	830	41	148
▼	M14	7195						151
⊡	M14	7195						128
◊	M14	7195						108
⊙	M14	7195						103
Δ	M14	7195						133
X	M14	7195						150

NOTES

●	EXT BODY BS875 VL180 BL107	FLAP CYCLE.VG UP
▼	PREDICTED TOTAL NOISE.CREATED	79/07/10.
⊡	PREDICTED TBL NOISE	79/07/10.
◊	PREDICTED SEP NOISE	79/07/10.
⊙	PREDICTED EDGE NOISE	79/07/10.
Δ	PREDICTED NN NOISE	79/07/10.
X	PREDICTED MIXING NOISE	79/07/10.

Figure 138. Results for M14 at Condition 7195

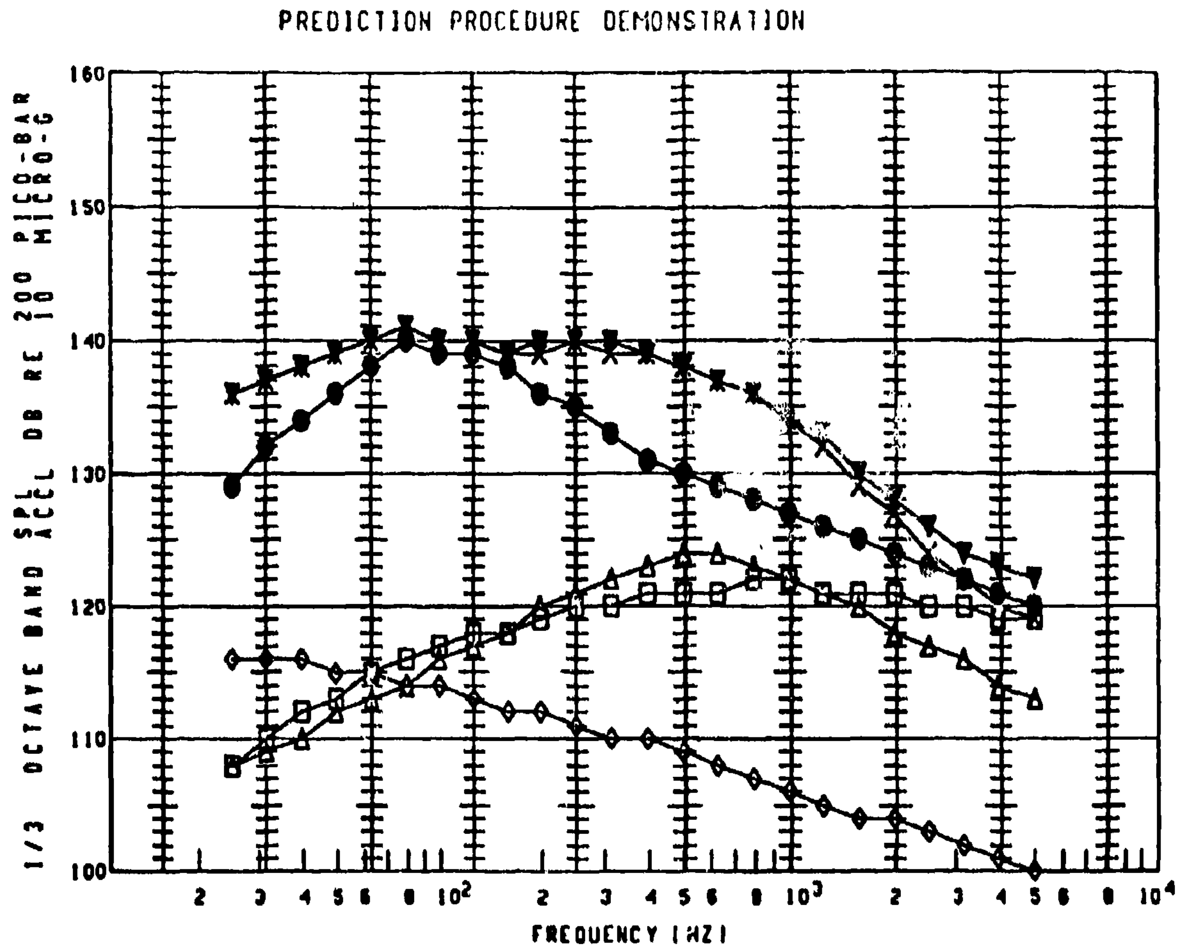

PLOT SYMBOL	X-DUCER NO.	COND. NO.	ALT. (FT)	SPEED (FPS)	N1 (RPM)	VMIX (FPS)	USBFA (DEG)	OVERALL (DB)
●	M14	7192	10700	213	2950	830	70	148
▼	M14	7192						151
⊡	M14	7192						133
◊	M14	7192						125
◊	M14	7192						106
Δ	M14	7192						133
X	M14	7192						151

NOTES

●	EXT BODY BS875 VL180 BLIQ,	FLAP CYCLE,VG UP
▼	PREDICTED TOTAL NOISE,CREATED	79/07/10.
⊡	PREDICTED TBL NOISE	79/07/10.
◊	PREDICTED SEP NOISE	79/07/10.
◊	PREDICTED EDGE NOISE	79/07/10.
Δ	PREDICTED NN NOISE	79/07/10.
X	PREDICTED MIXING NOISE	79/07/10.

Figure 139. Results for M14 at Condition 7192

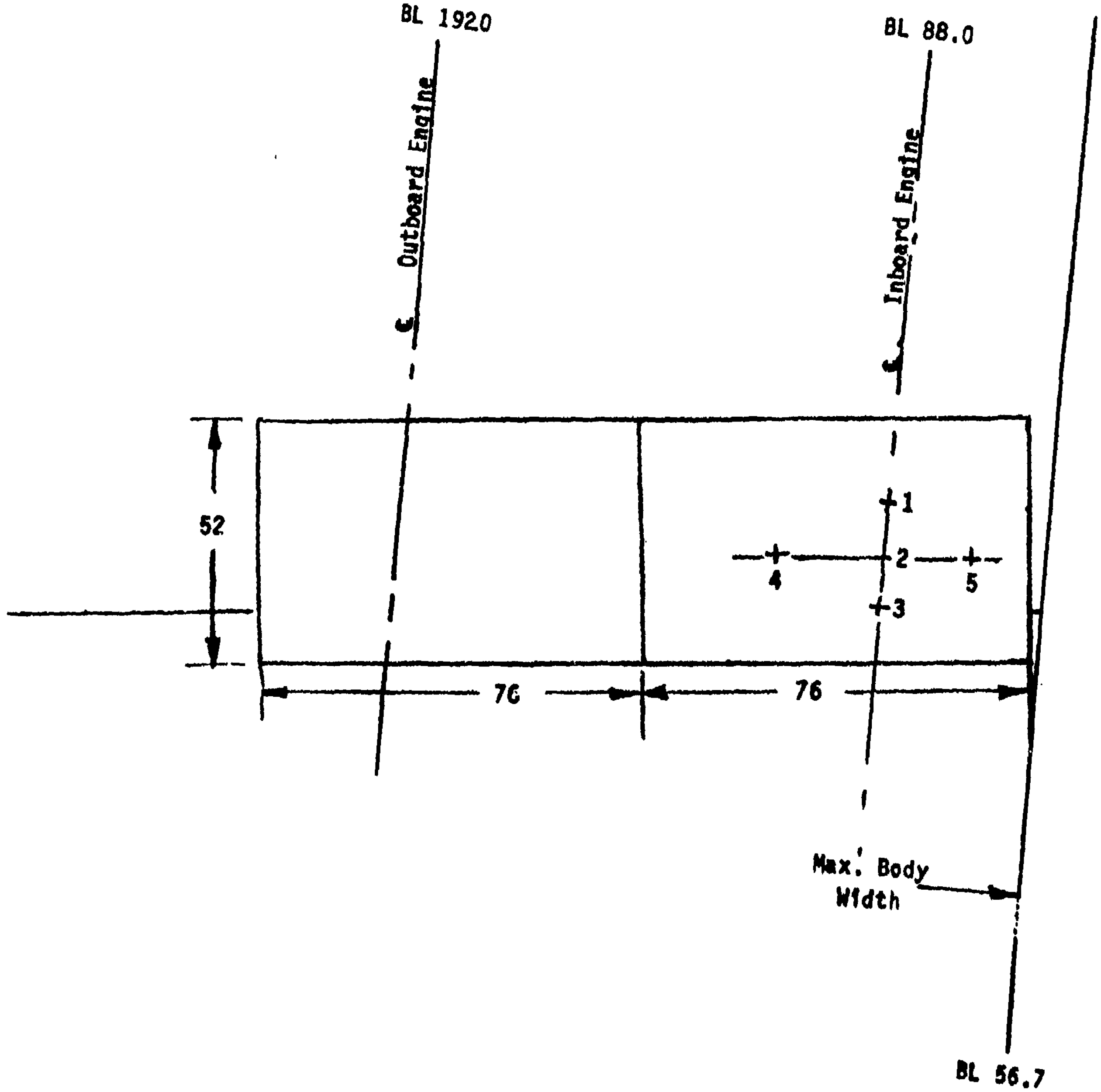

Figure 140. QSRA USB Flap Dimensions

QSRA USB FLAP

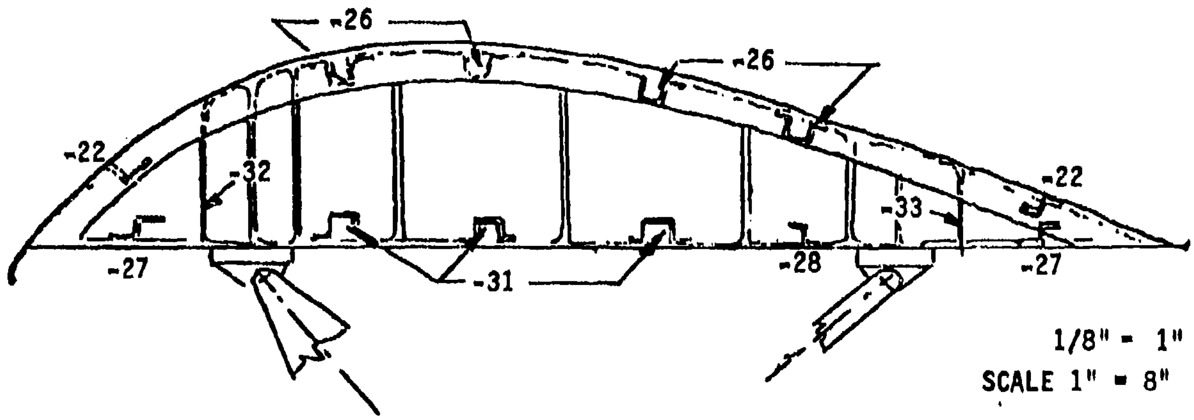

1/8" = 1"
SCALE 1" = 8"

-22	STR. UPPER	.071 x 2.70 x 17.2	AL 301 1/2 HARD
-26	STR. UPPER	.071 x 5.20 x 5.80	AL 301 1/2 HARD
-27	STR. LOWER	.071 x 3.70 x 17.2	AL 2024 -0
-28	STGR LOWER	.071 x 2.70 x 18.0	AL 2024 -0
-31	STGR LOWER	.071 x 5.20 x 18.0	AL 2024 -0
-4	SKIN LWR	.071 x 52.0 x 76.0	AL 2024 - T3 SHEET
-3	SKIN UPPER AFT	.071 x 12.0 x 76.0	AL 301 1/2 HARD
-2	SKIN UPPER CTR	.071 x 32.5 x 76.0	AL 301 1/2 HARD
-32	SPAR FRONT	.071 x 11.3 x 76.0	AL 301 1/2 HARD
-33	SPAR REAR	.071 x 8.60 x 76.0	AL 301 1/2 HARD

Figure 141. QSRA USB Flap Schematic

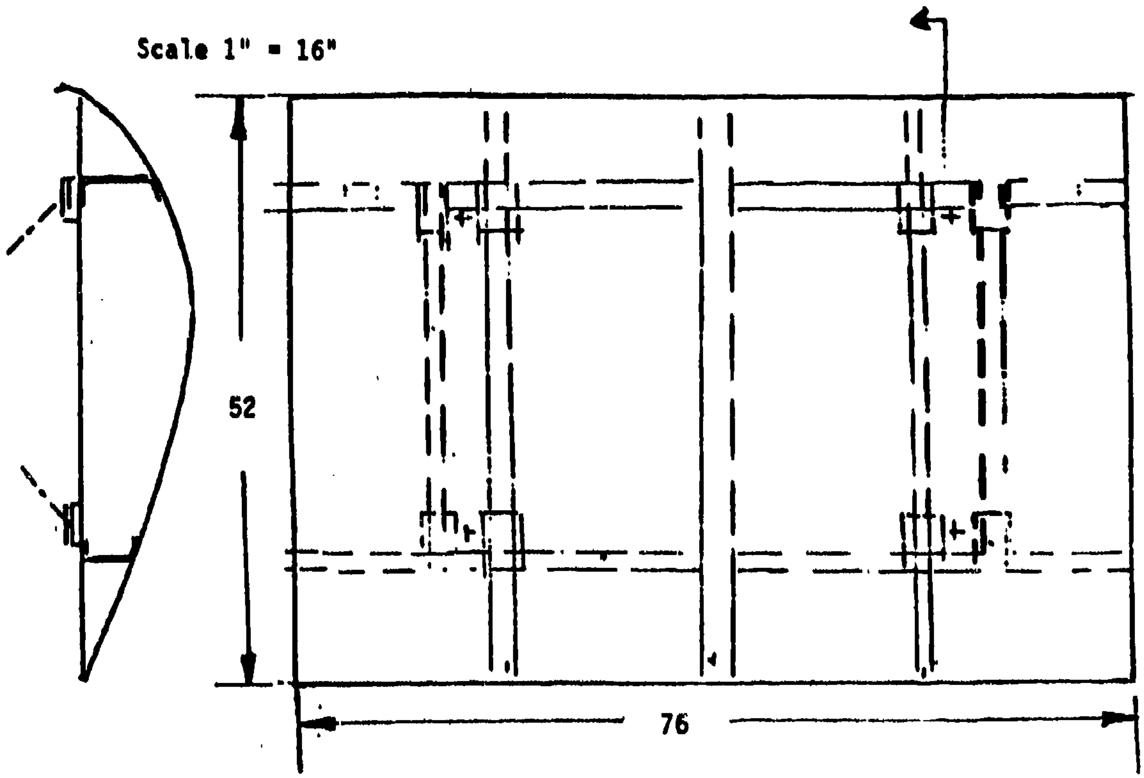

Figure 142. QSRA USB Flap Representation

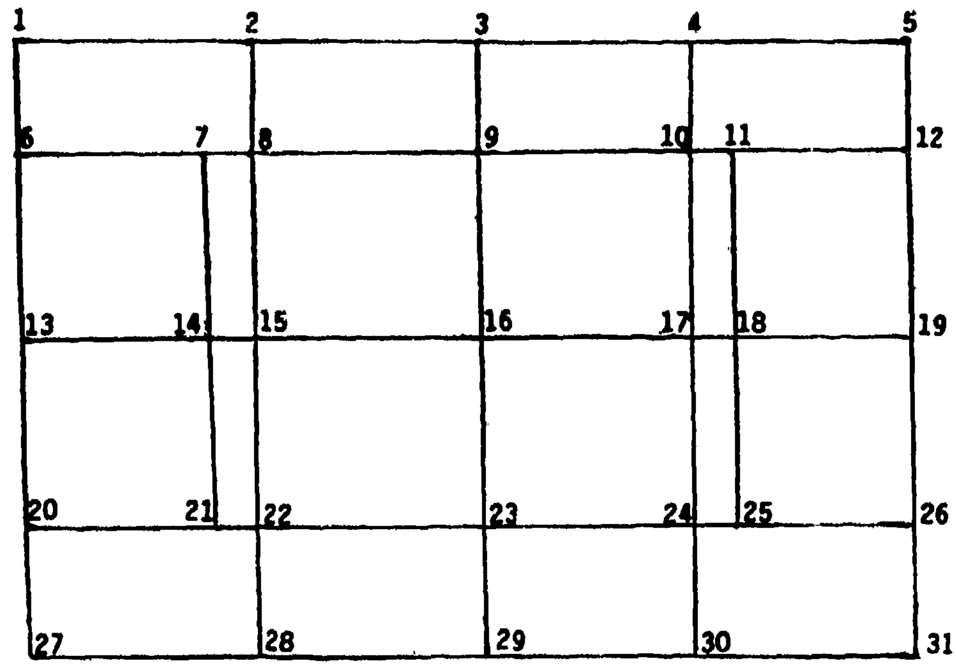

Figure 143. QSRA USB Flap Nodal Points

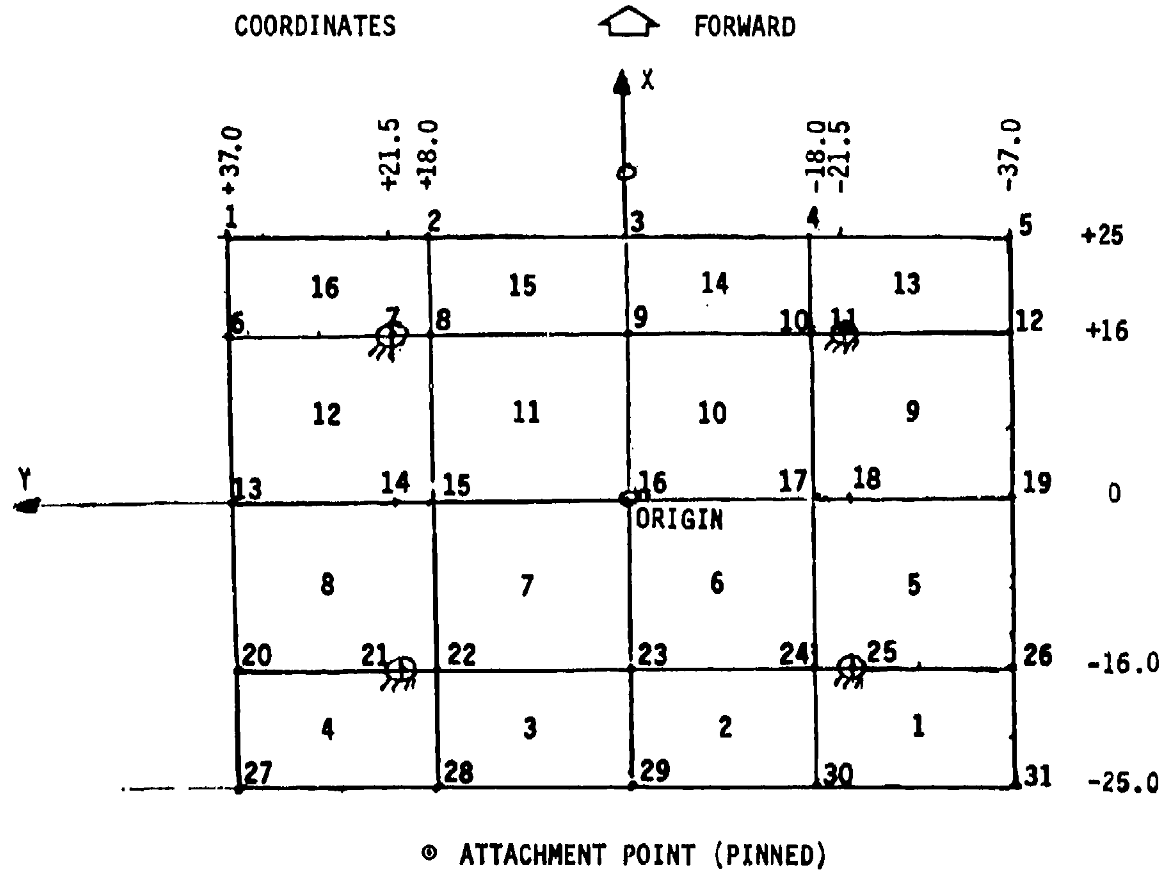

NODE	1	2	3	4	5	6	7	8	9	10	11	12	13	14	
X	+25	←		→	+25	+16.0	←				→	+16.0	0	0	
Y	-37.0	-18.0	0	+18.0	37.0	-37.0	-21.5	-18.0	0	18	21.5	37.0	+37.0	+21.5	
NODE	15	16	17	18	19	20	21	22	23	24	25	26	27	28	29
X	0	0	0	0	0	-16	←				→	-16	-25.0	←	—
Y	+18.0	0	-18.0	-21.5	-37.0	+37.0	+21.5	+18.0	0	-18.0	-21.5	-37.0	+37.0	+18.0	0

Figure 144. QSRA USB Flap Finite Elements

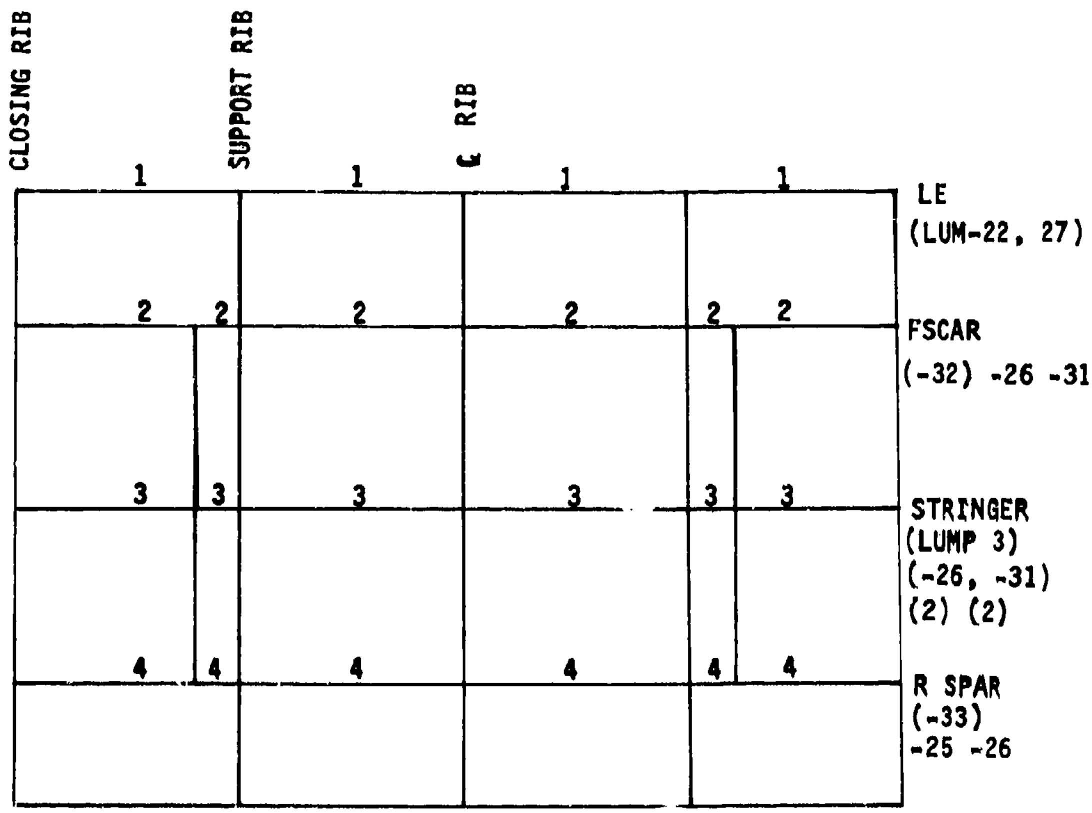

GEOM	DESCRIPTION	MAT'L	A_{AX}	A_{S2}	A_{S3}	I	I_2	I_3
1	LE △	AL	1.5194	0.3834	1.1360	0.0026	3.0726	10.9755
2	FS [	↓	0.8023	0.4615	0.3408	0.0888	10.0992	0.6682
3	STRINGER		1.4768	0.5680	0.9088	1.2423	0.2022	0.0811
4	RS]		0.6106	0.2698	0.3408	.001027	1.5717	1.0428
5	TE ◺		1.5194	0.3834	1.1360	0.0028	2.9358	7.9337

Figure 145. QSRA USB Flap Element Properties

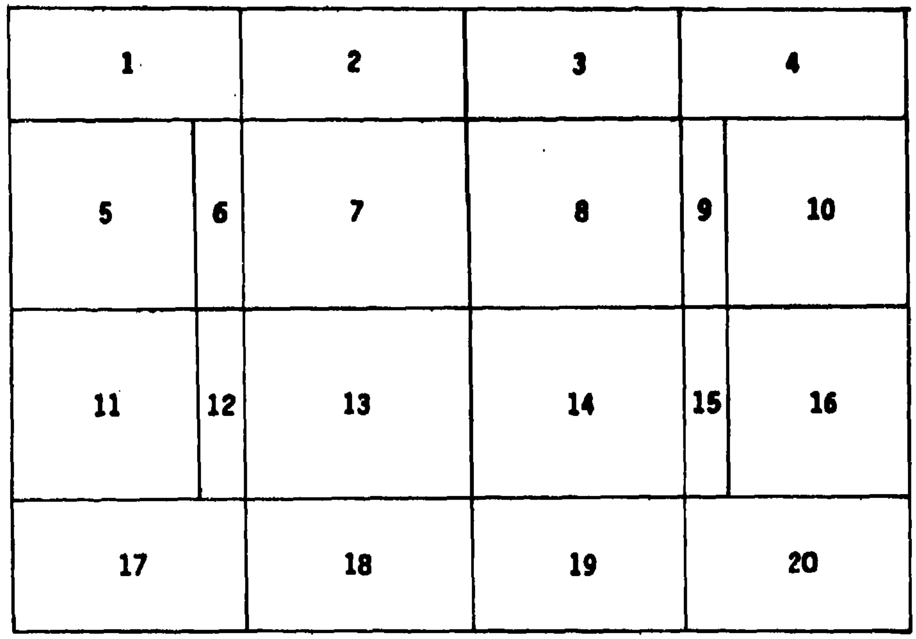

Figure 146. QSRA USB Flap Model Plate Elements

MODE NUMBER	CIRCULAR FREQUENCY (RAD/SEC)	FREQUENCY (CYCLES/SEC)	PERIOD (SEC)
1	9.4527E+02	1.5044E+02	.00665
2	1.2557E+03	1.9985E+02	.00500
3	1.4049E+03	2.2360E+02	.00447
4	1.6957E+03	2.6987E+02	.00371
5	1.9251E+03	3.0638E+02	.00326
6	2.3061E+03	3.6703E+02	.00272
7	2.3756E+03	3.7809E+02	.00264
8	2.4802E+03	3.9474E+02	.00253
9	2.8154E+03	4.4808E+02	.00223
10	3.4389E+03	5.4732E+02	.00183
11	3.8801E+03	6.1754E+02	.00162
12	4.1419E+03	6.5921E+02	.00152
13	4.5525E+03	7.2456E+02	.00138
14	4.9084E+03	7.8119E+02	.00128
15	5.0220E+03	7.9927E+02	.00125
16	5.1144E+03	8.1398E+02	.00123
17	5.2241E+03	8.3144E+02	.00120
18	6.0220E+03	9.5843E+02	.00104
19	6.5468E+03	1.0420E+03	.00096
20	6.5860E+03	1.0483E+03	.00095

Figure 147. Print of Frequencies for Small Airplane QSRA Flap Model 31 Nodes, No Camber

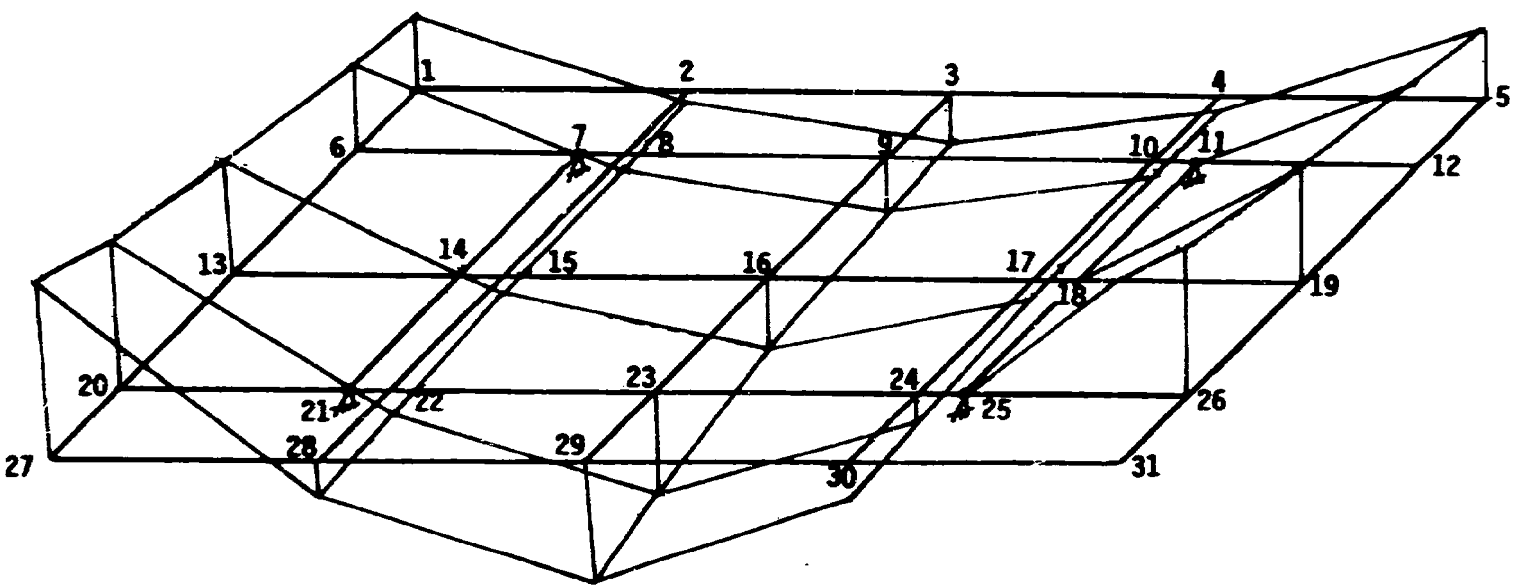

Figure 148. Small USB Flap Model, Modal Plot Frequency = 150.44 Hz.

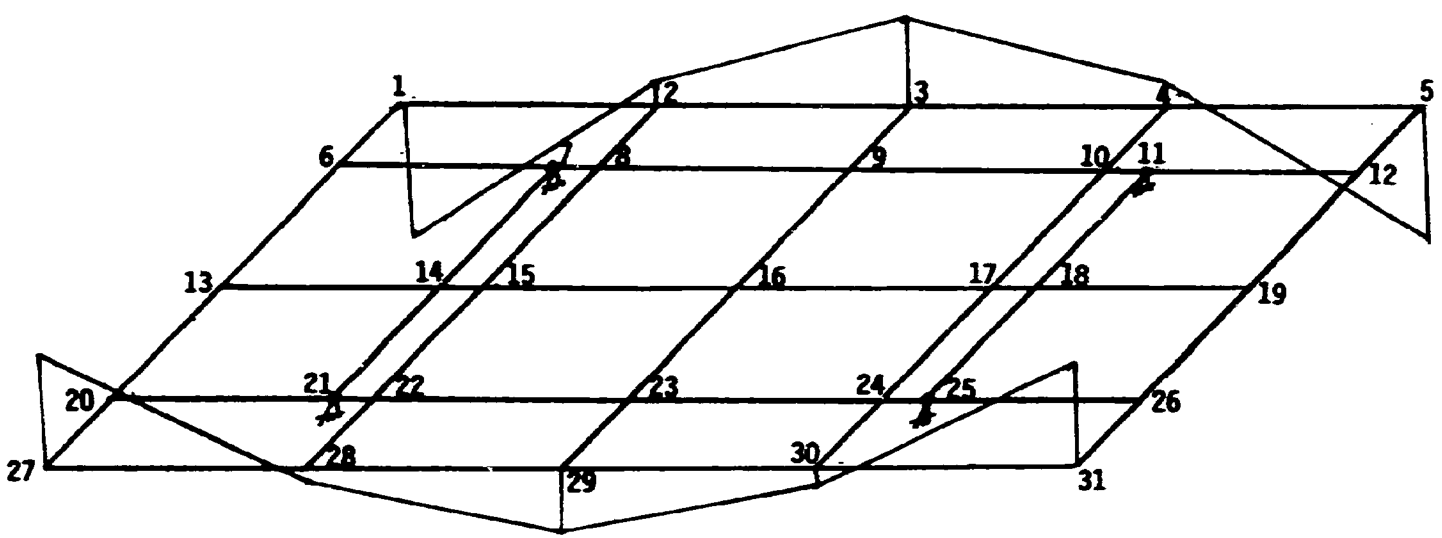

Figure 149. Small USB Flap, Modal Plot, Frequency = 199.85 Hz.

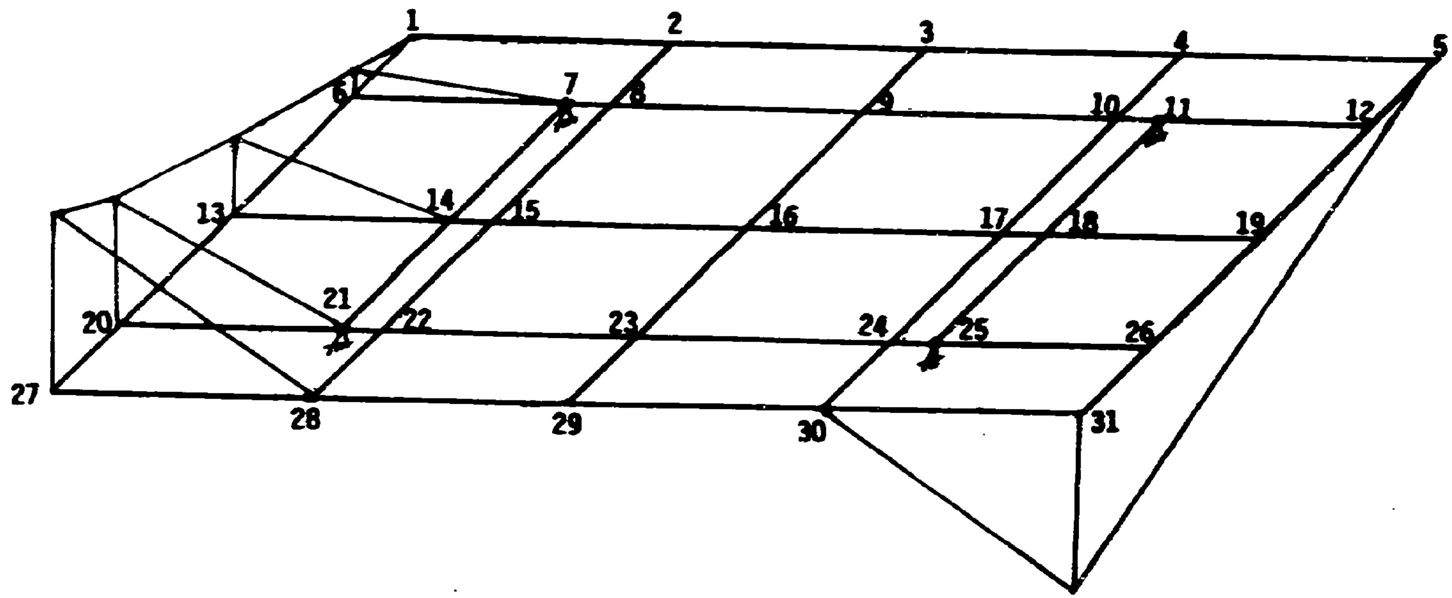

Figure 150. Small USB Flap, Modal Plot, Frequency = 223.85 Hz.

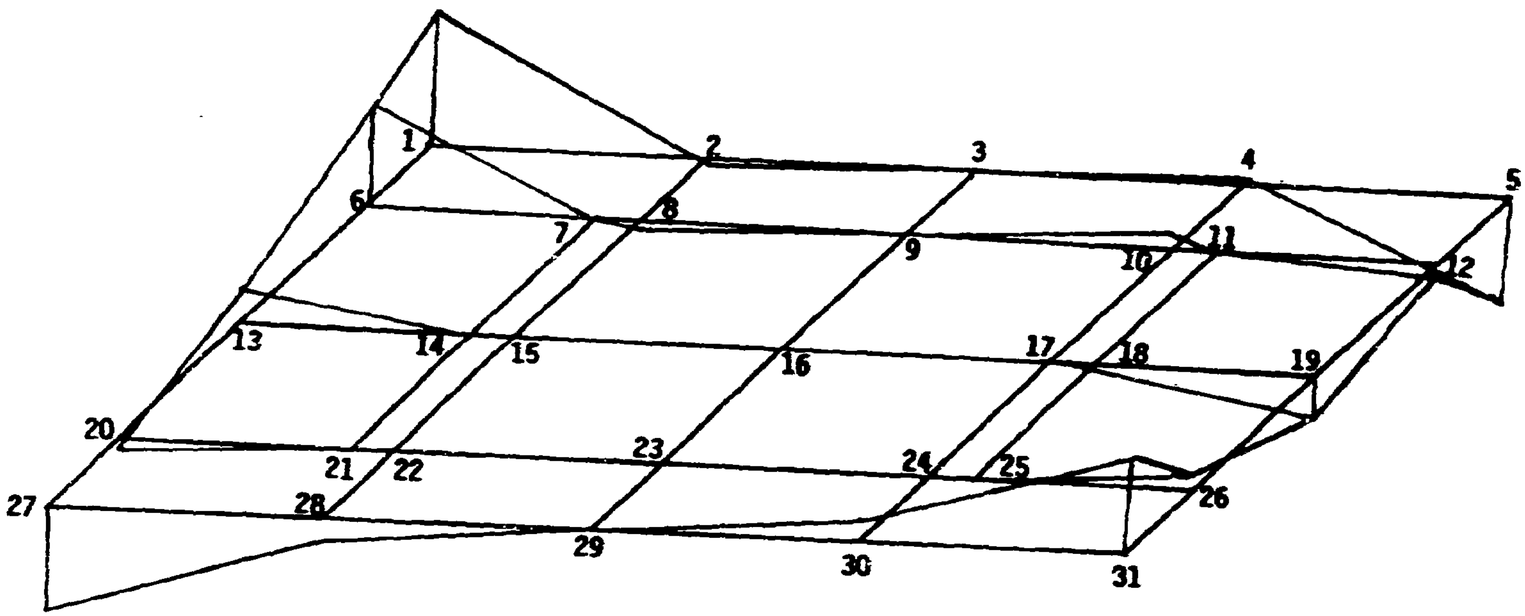

Figure 151. Small USB Flap, Modal Plot, Frequency = 269.87 Hz.

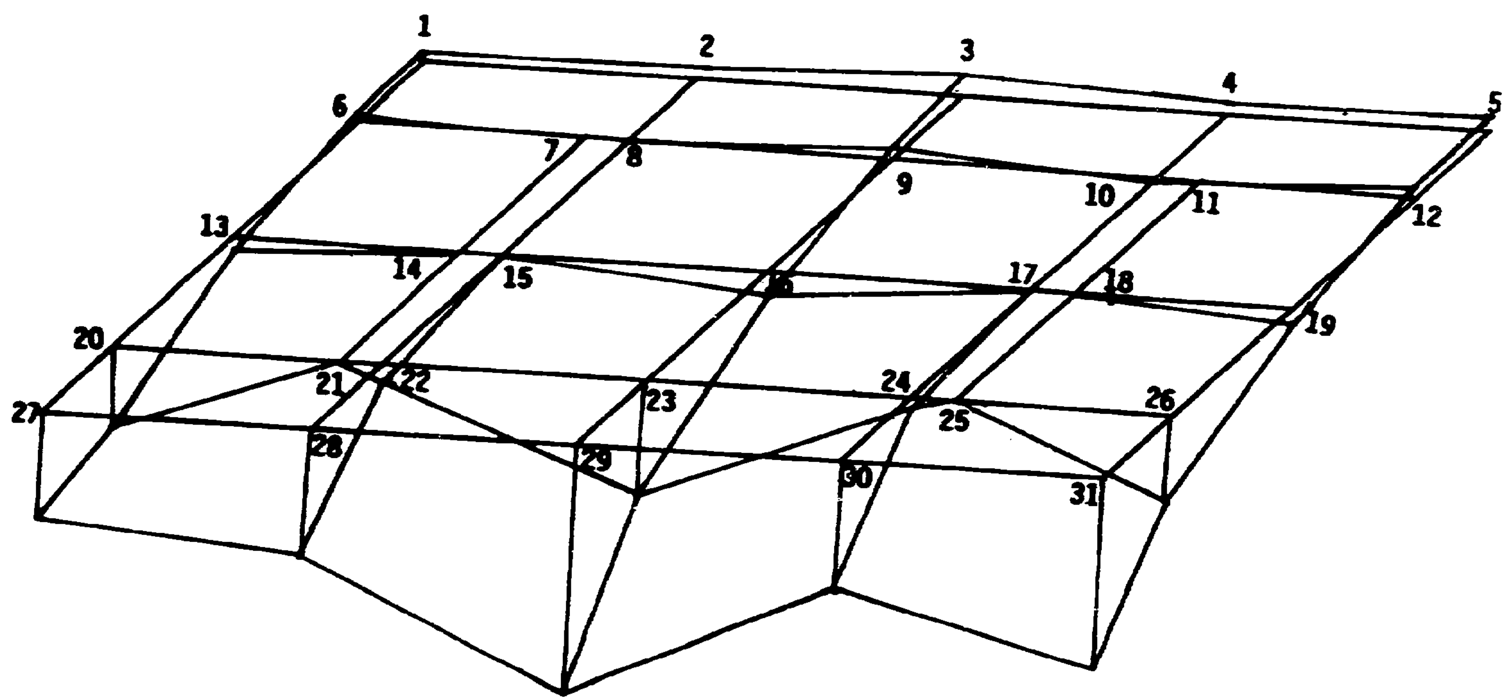

Figure 152. Small USB Flap, Modal Plot, Frequency = 306.38 Hz.

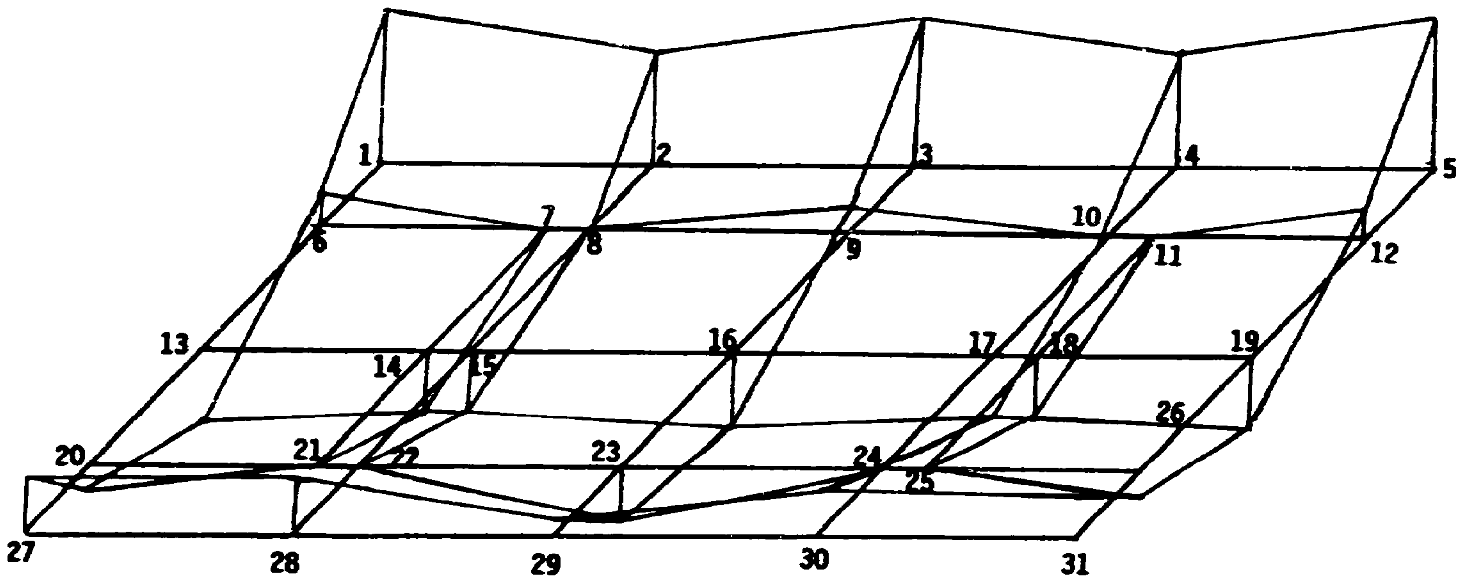

Figure 153. Small USB Flap, Modal Plot, Frequency = 367.03 Hz.

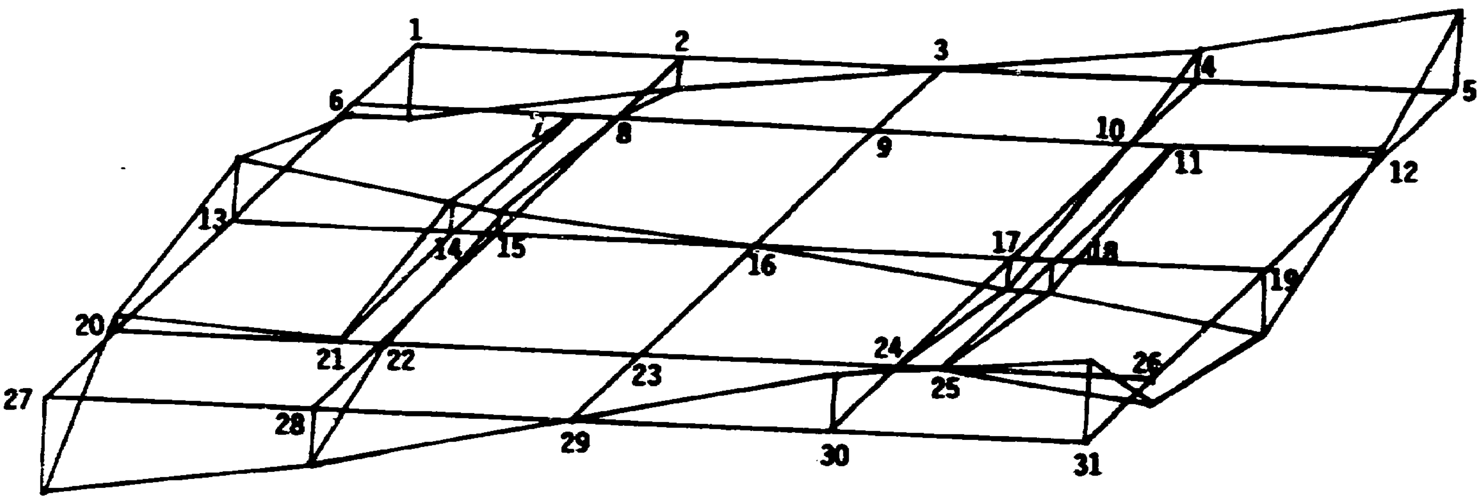

Figure 154. Small USB Flap, Modal Plot, Frequency = 378.09 Hz.

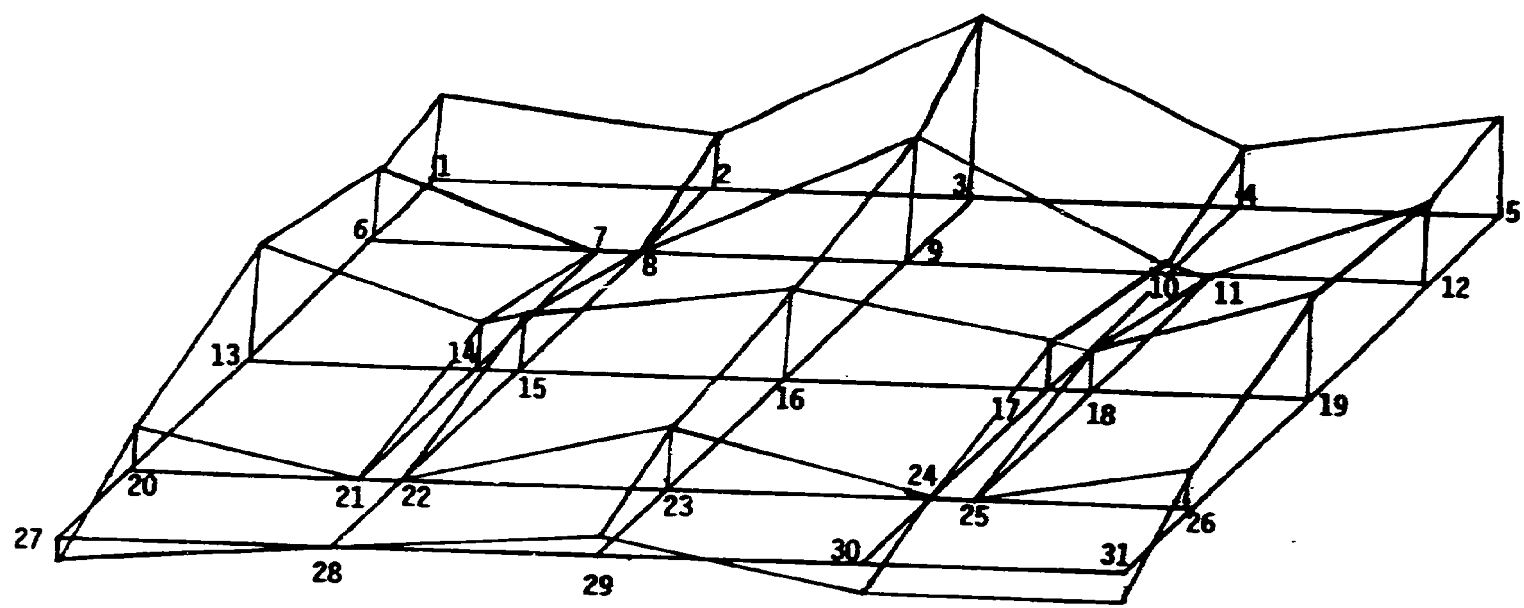

Figure 155. Small USB Flap, Modal Plot, Frequency = 394.74 Hz.

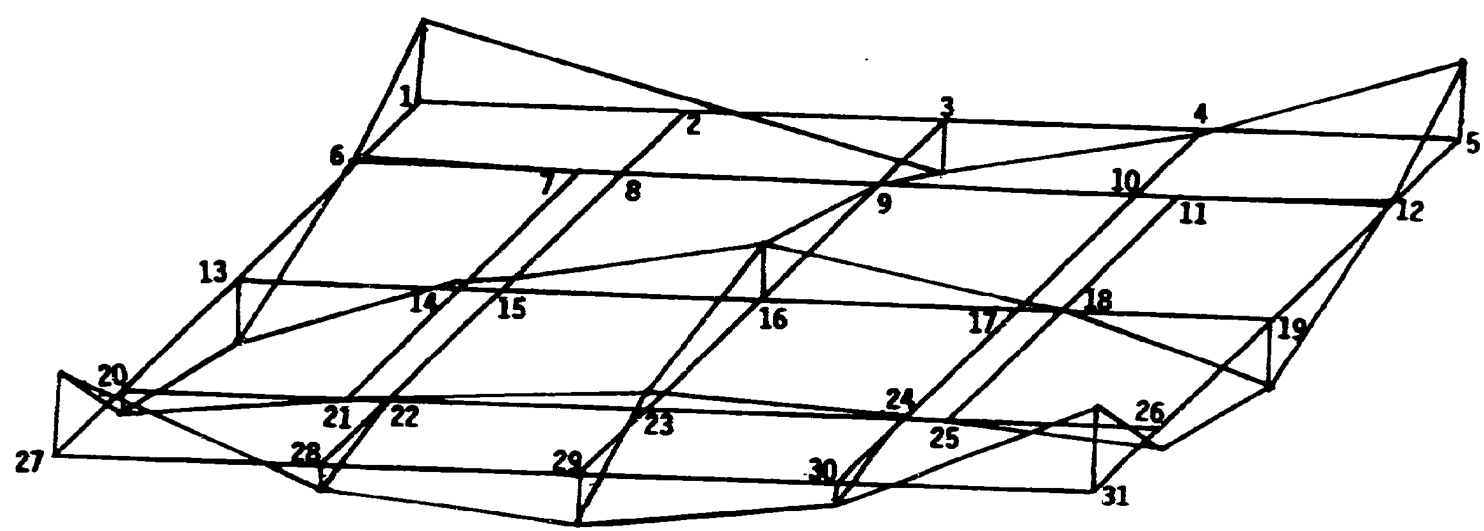

Figure 156. Small USB Flap, Modal Plot, Frequency = 448.08 Hz.

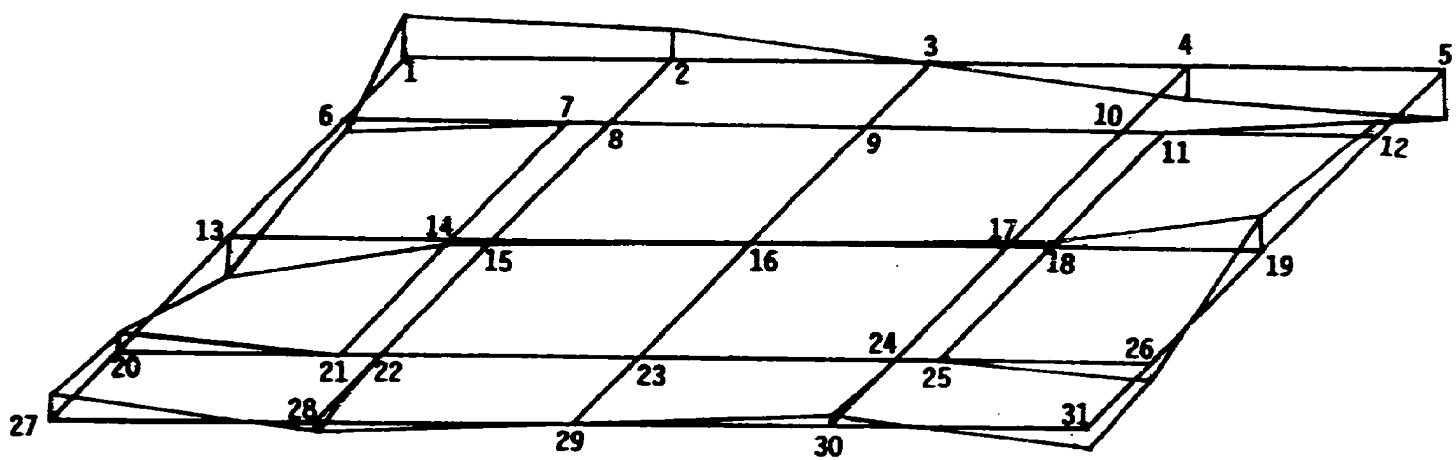

Figure 157. Small USB Flap, Modal Plot, Frequency = 547.32 Hz.

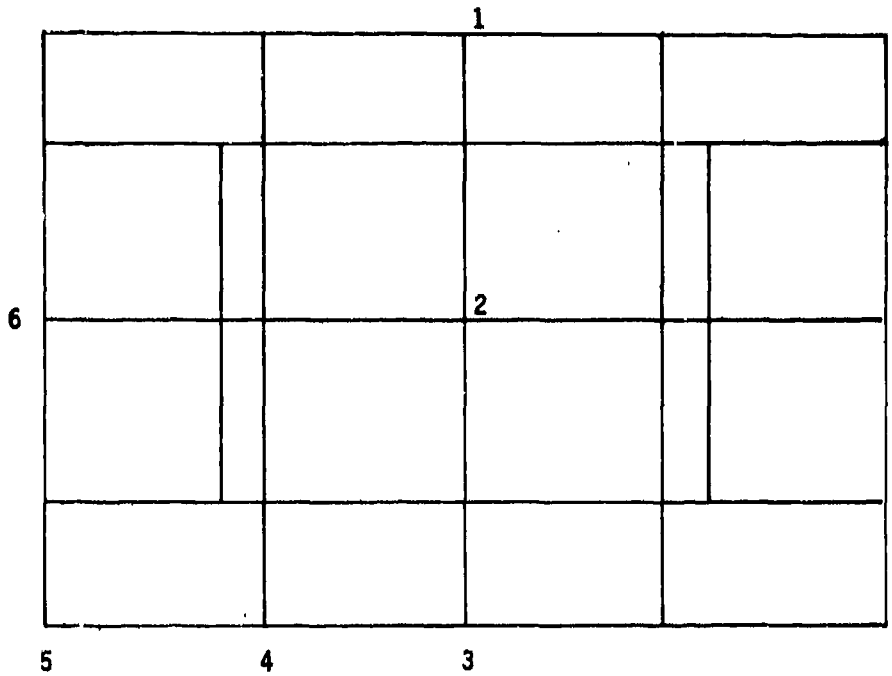

Figure 158. QSRA Flap Structural Response Prediction Locations

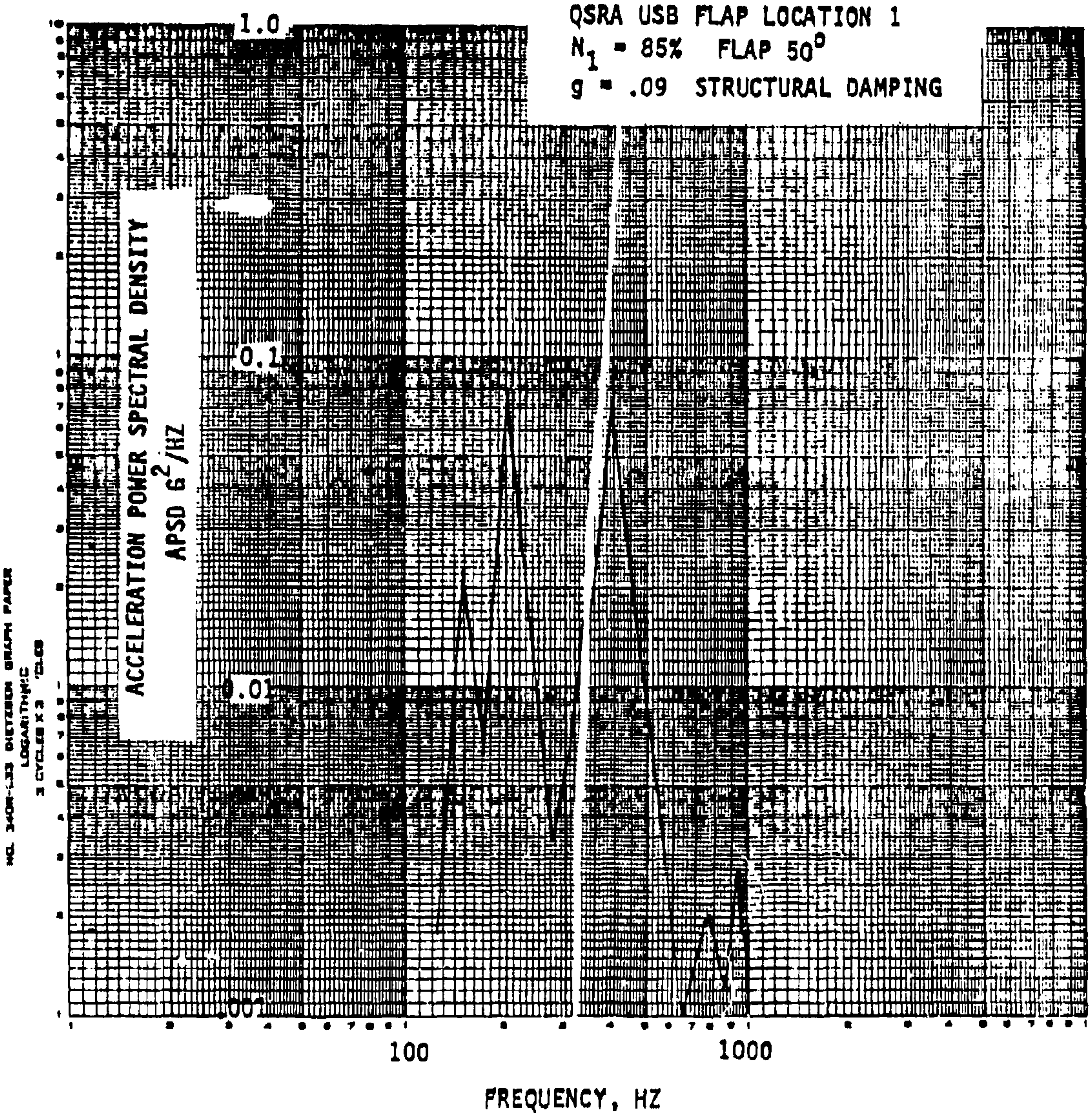

Figure 159. Vibration Environment on QSRA USB Flap, Location 1

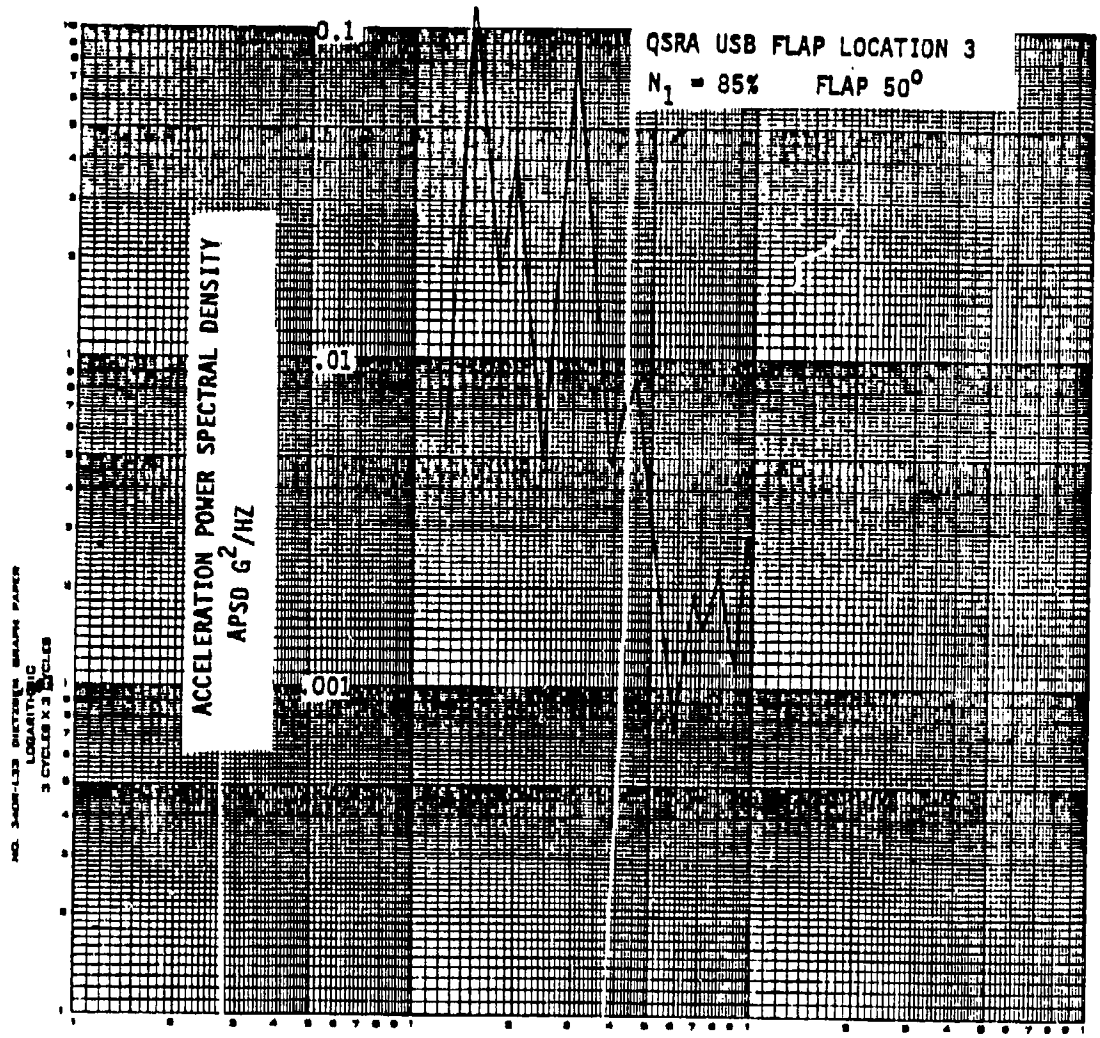

Figure 160. Vibration Environment on QSRA USB Flap, Location 3

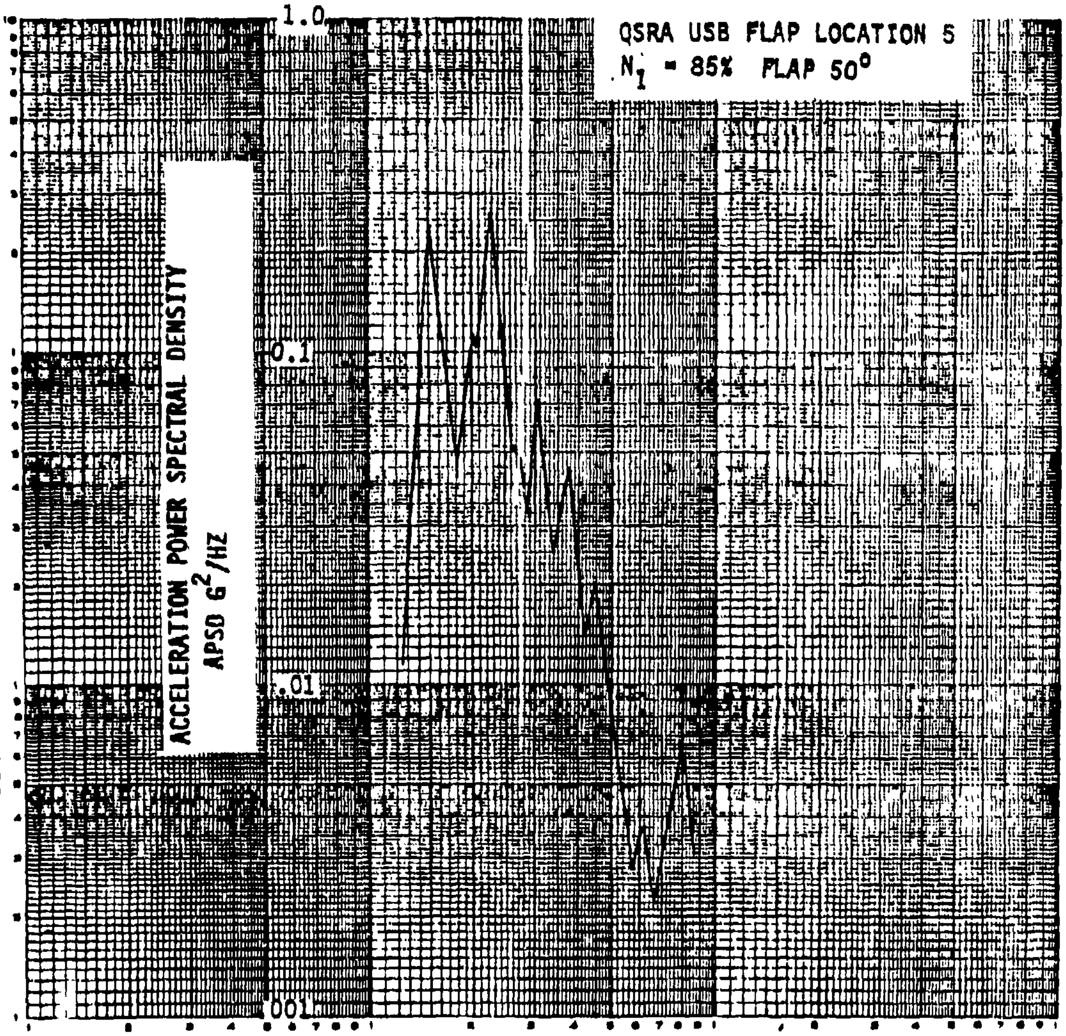

Figure 161. Vibration Environment on QSRA USB Flap, Location 5

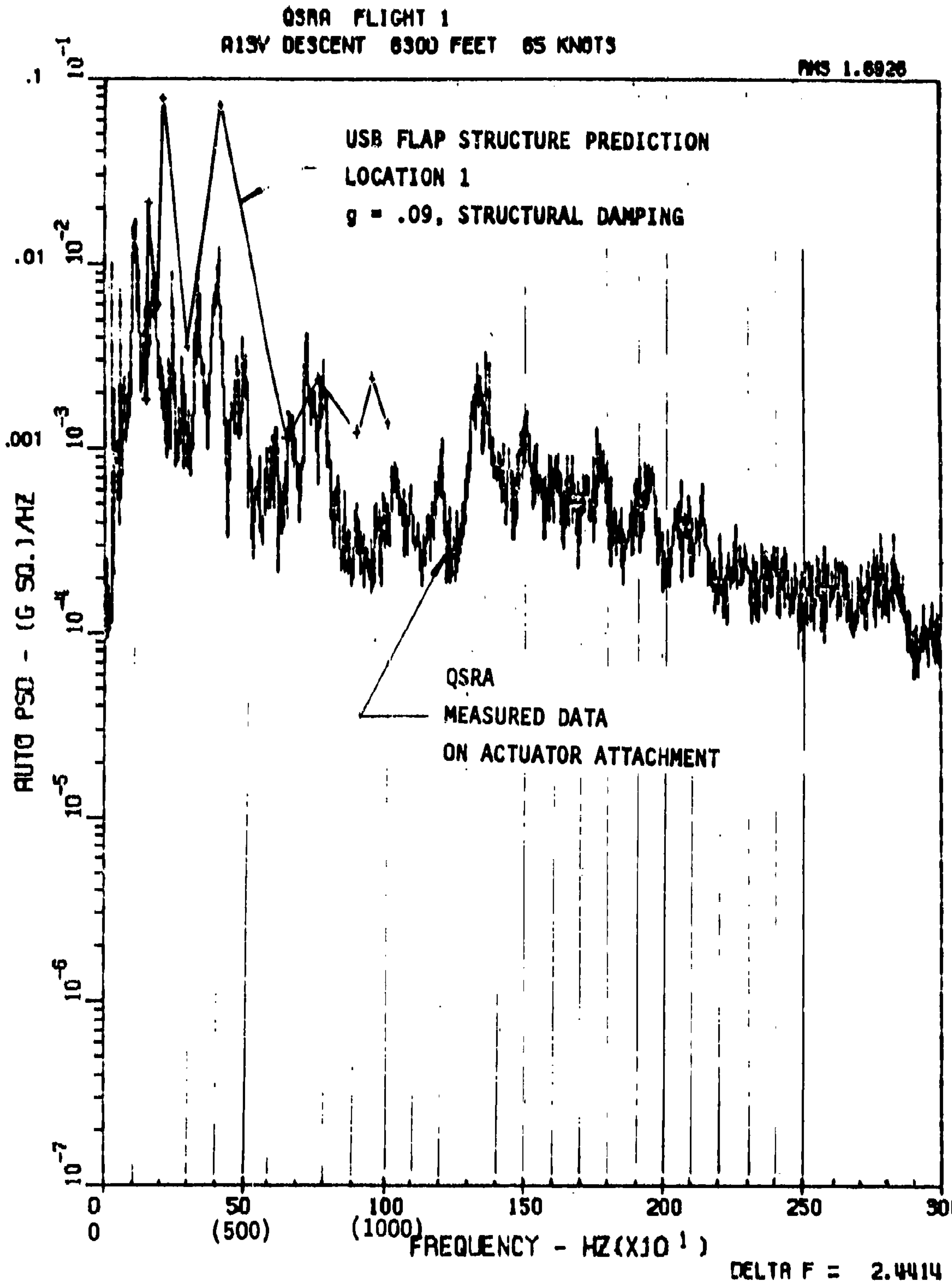

Figure 162. Comparison of USB Flap Prediction to Flight Test Data

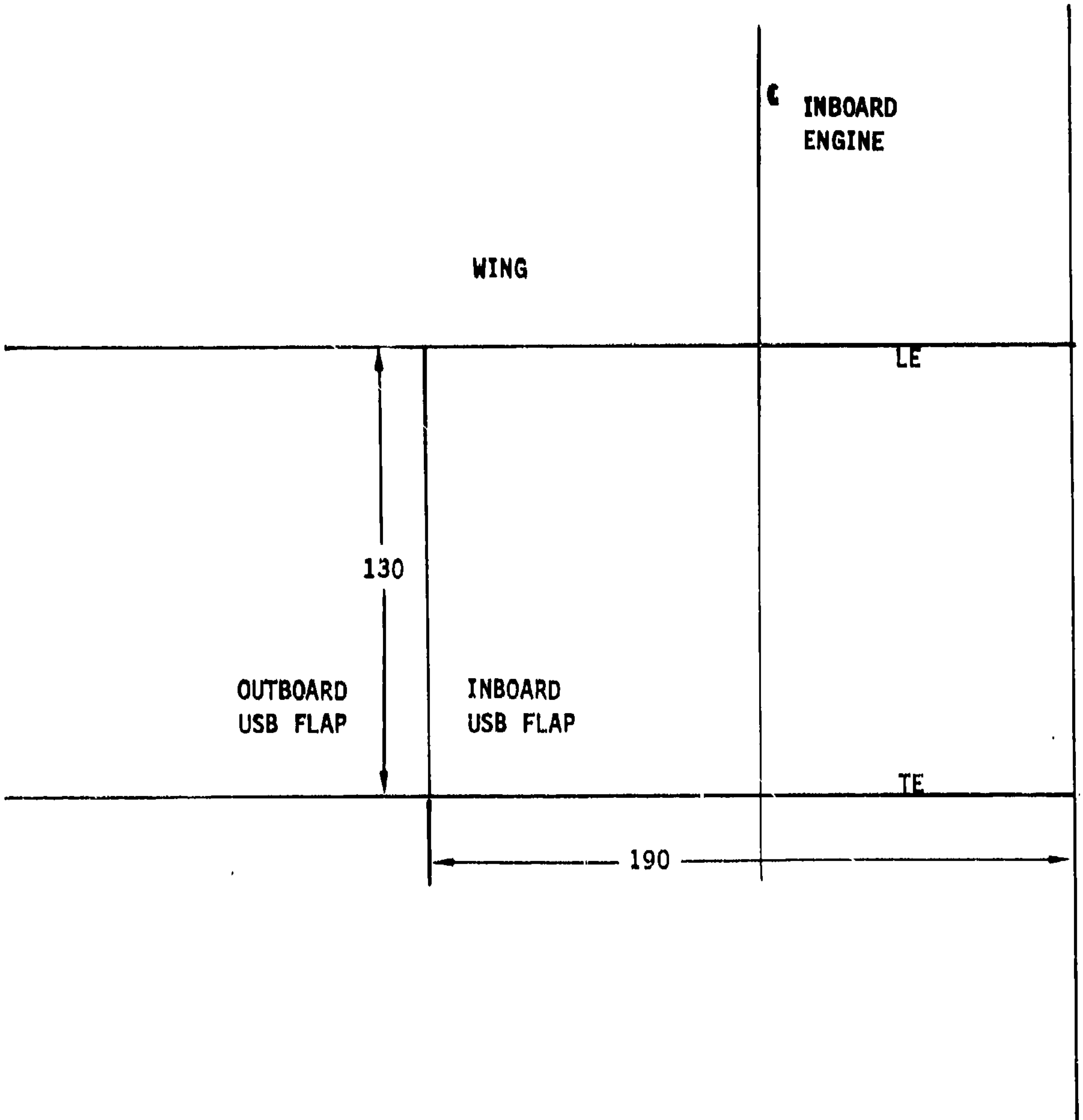

Figure 163. Large STOL Airplane USB Inboard Flap

LARGE AIRPLANE USB FLAP

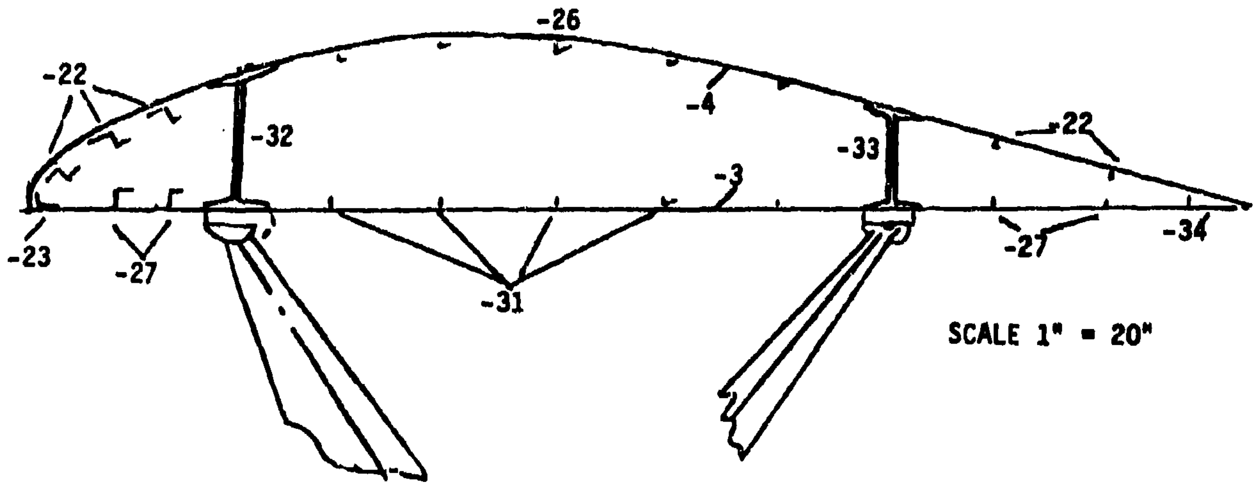

PART

-3	SKIN, UPPER
-4	SKIN, LOWER
-22	STRINGER, UPPER (Z)
-23	STRINGER, NOSE (L)
-26	STRINGER, UPPER (HAT)
-27	STRINGER, LOWER (Z)
-31	STRINGER, LOWER (HAT)
-32	SPAR, FRONT
-33	SPAR, REAR

Figure 164. Large STOL USB Flap Schematic

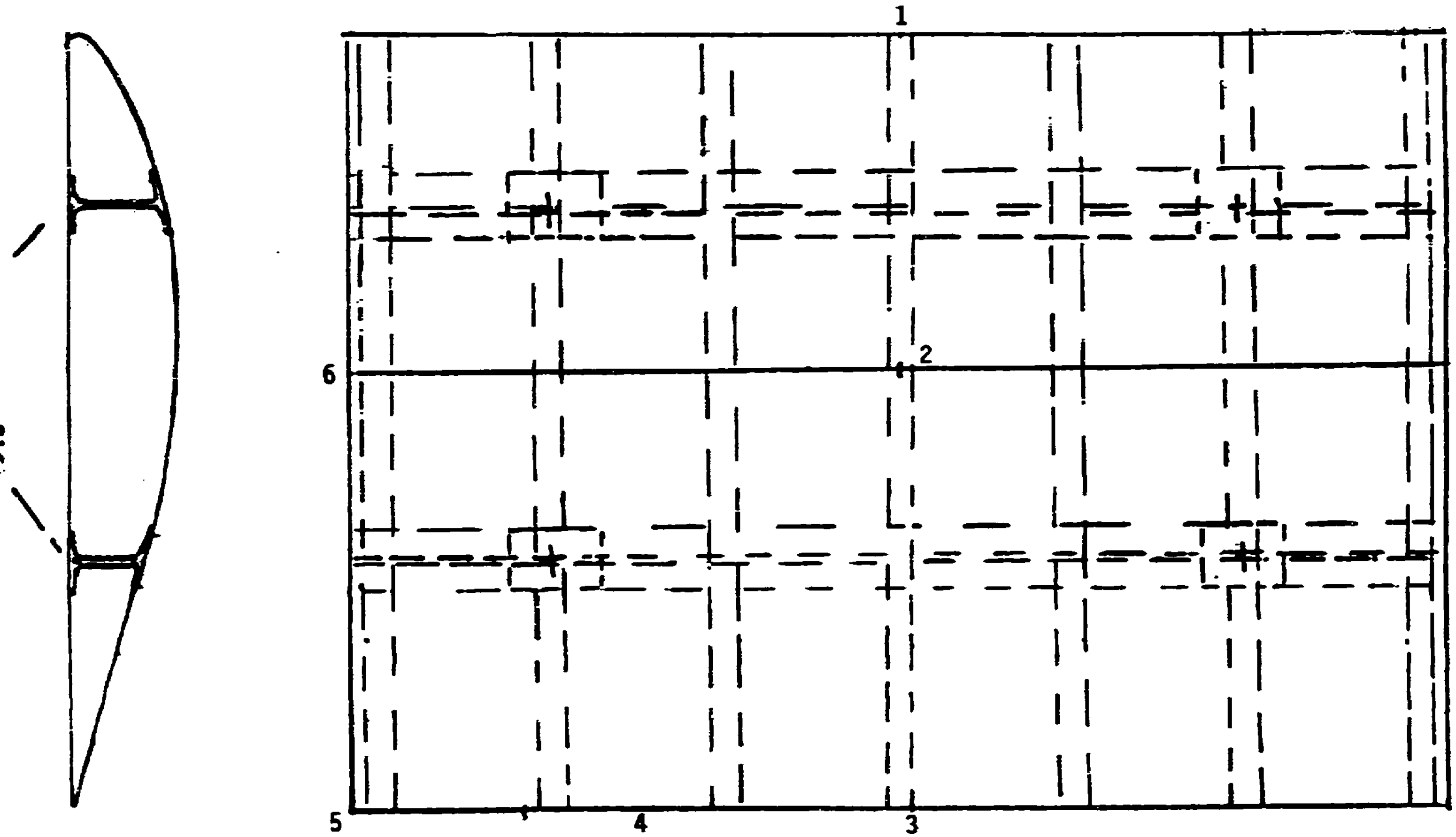

1" = 30"

Figure 165. Large STOL USB Flap

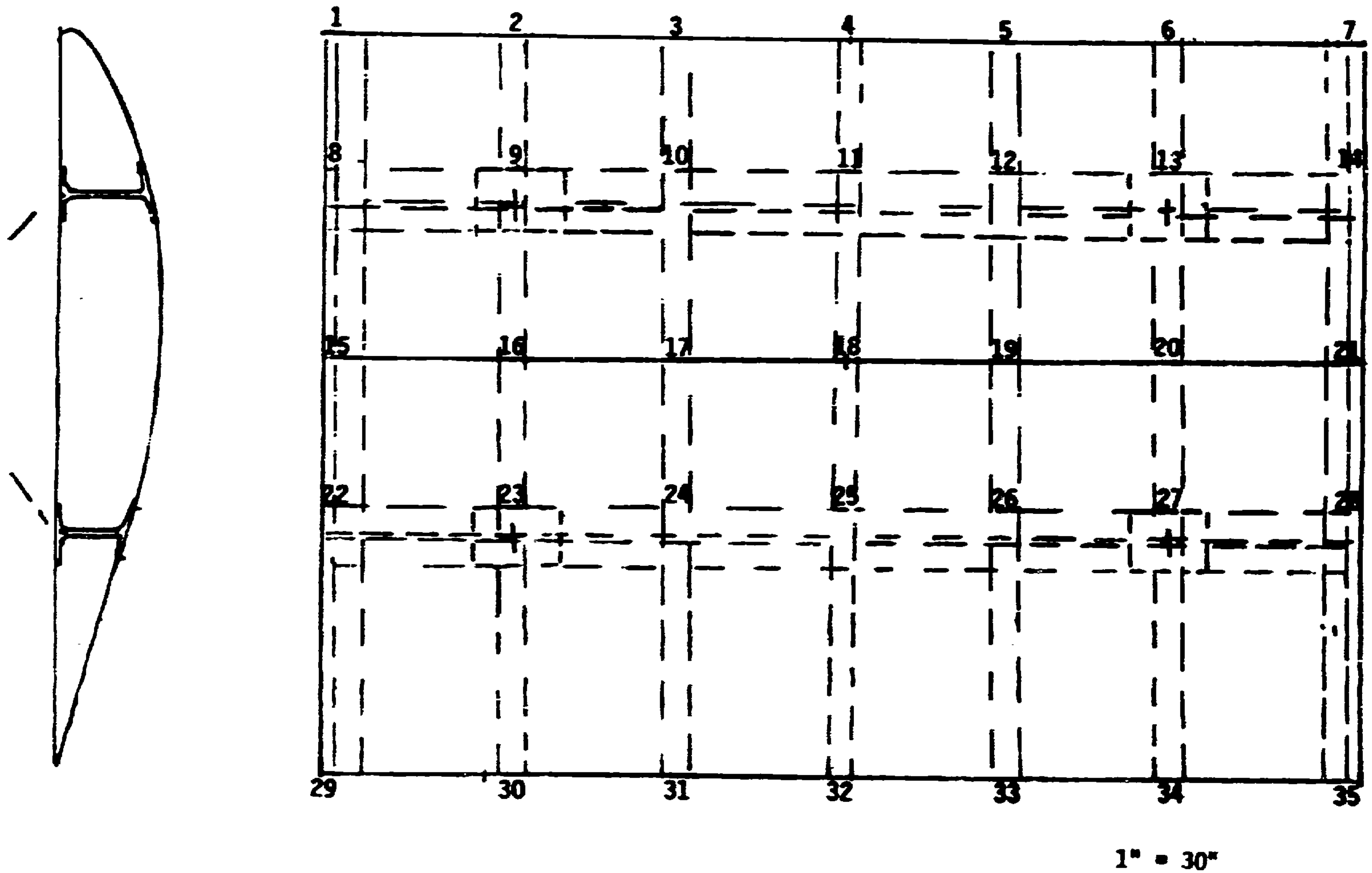

Figure 166. Large STOL USB Flap Finite Element Model Node Points

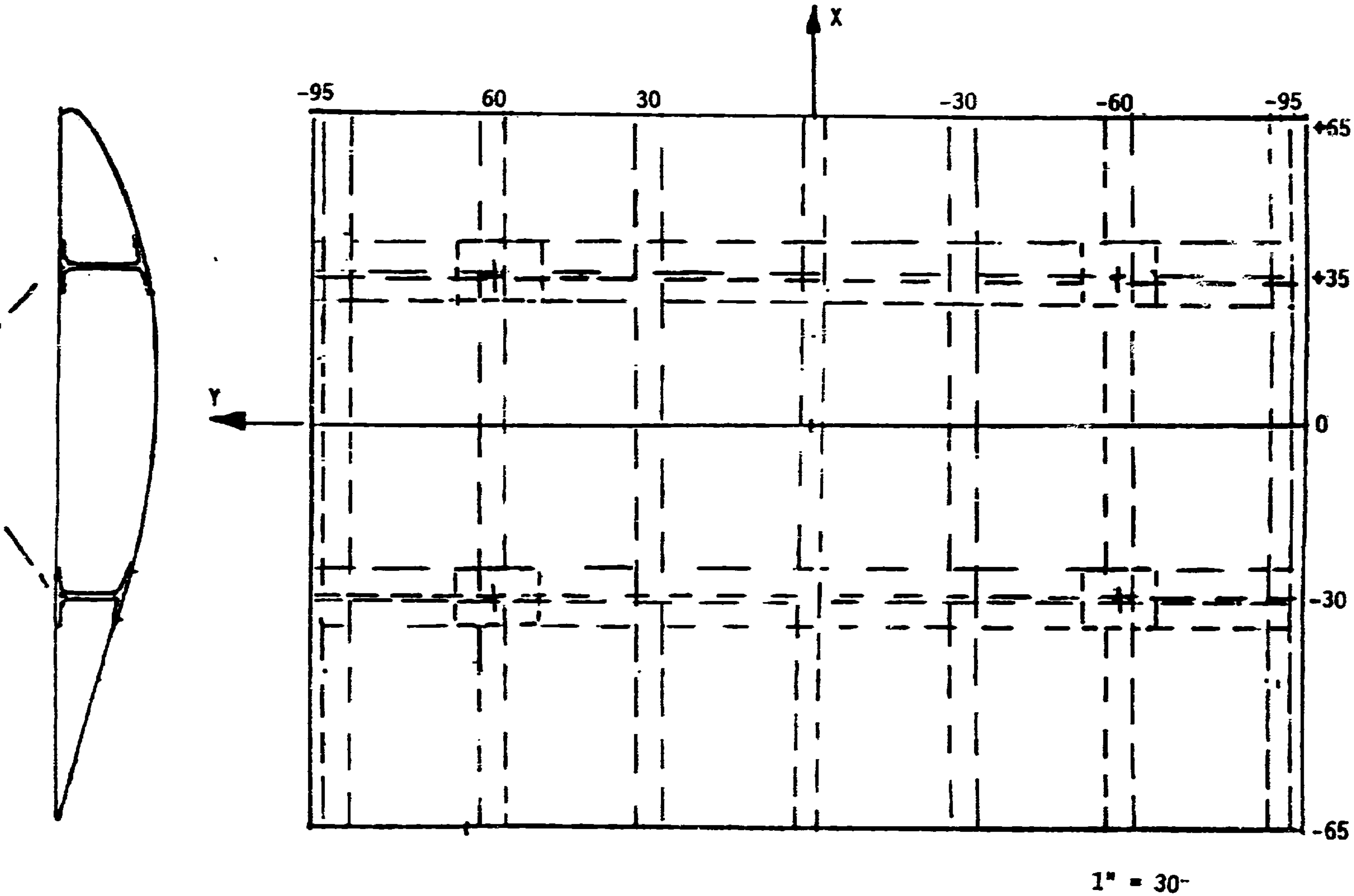

Figure 167. Large STOL USB Flap Finite Element Model Coordinates

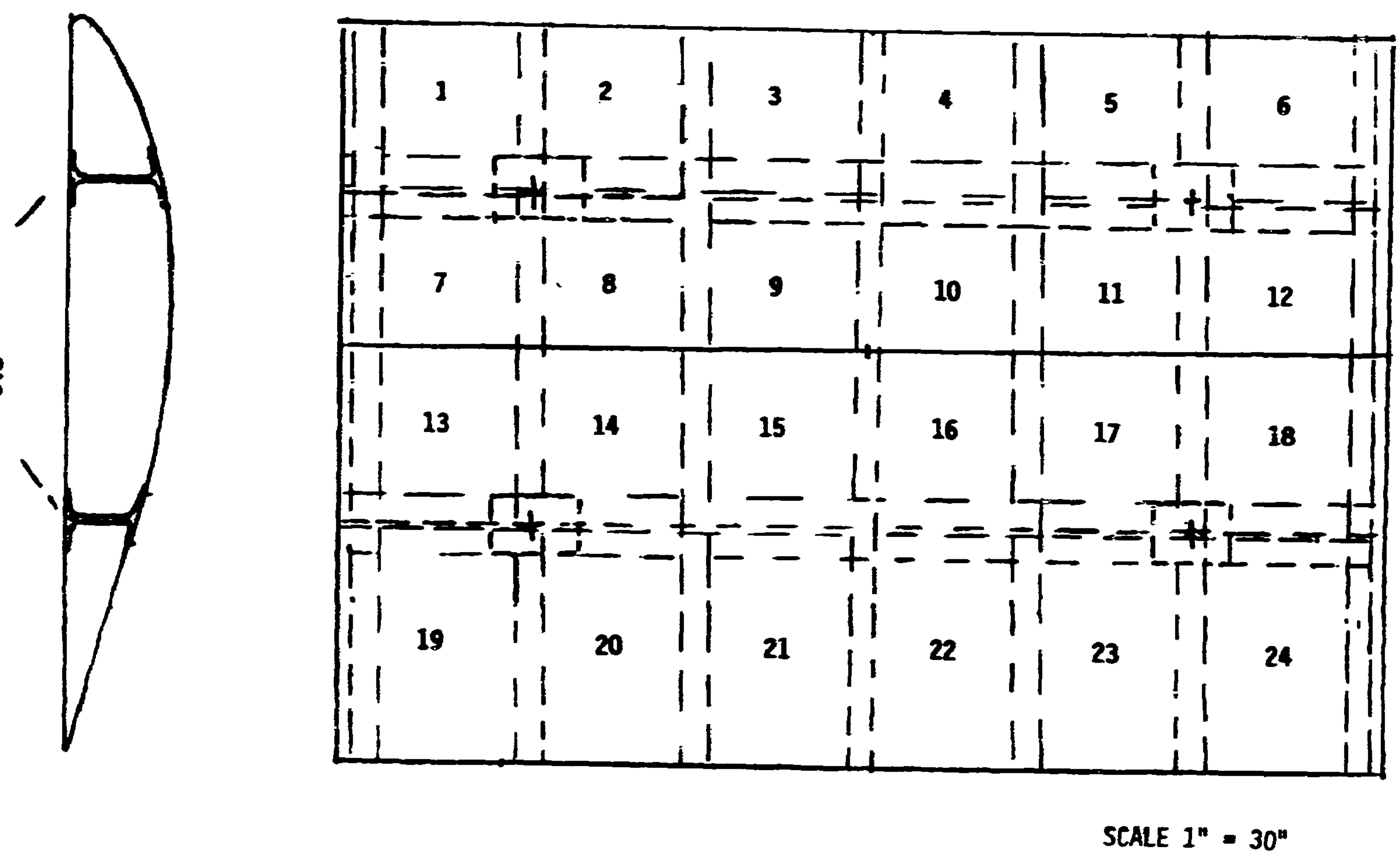

Figure 168. Large STOL USB Flap Finite Element Plate Elements

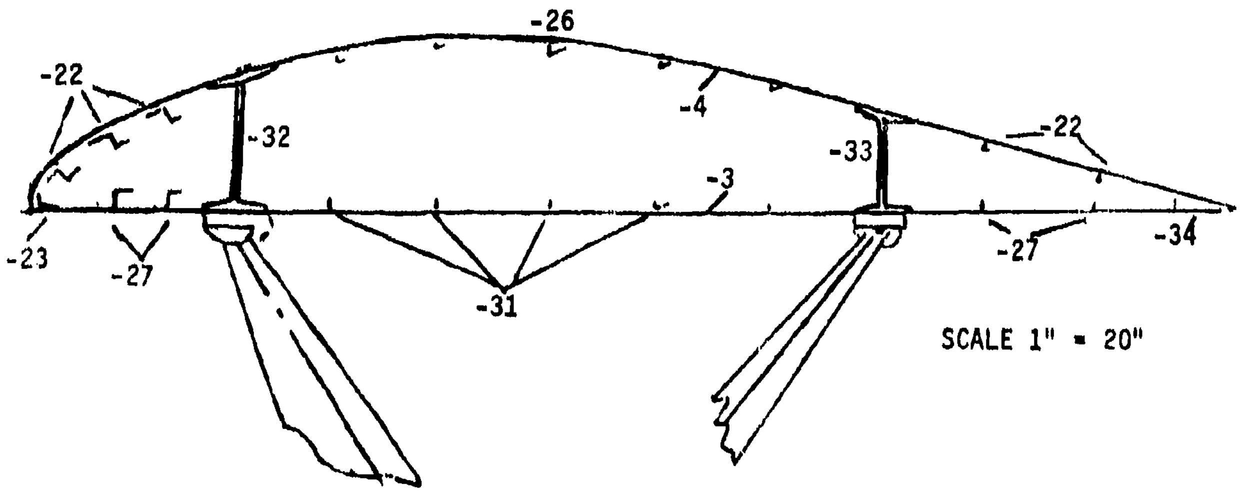

PART		
-3	SKIN, UPPER	.250 x 140 x 190
-4	SKIN, LOWER	.250 x 130 x 190
-22	STRINGER, UPPER (Z)	.1875 x 4.0 x 190
-23	STRINGER, NOSE (L)	.1875 x 2.0 x 190
-26	STRINGER, UPPER (HAT)	.1875 x 6.0 x 190
-27	STRINGER, LOWER (Z)	.1875 x 4.0 x 190
-31	STRINGER, LOWER (HAT)	.1875 x 6.0 x 190
-32	SPAR, FRONT	.375 x 14.0 x 190
-33	SPAR, REAR	.375 x 10.0 x 190

Figure 169. Structural Components of Large Airplane USB Flap

MODE NUMBER	CIRCULAR FREQUENCY (RAD/SEC)	FREQUENCY (CYCLES/SEC)	PERIOD (SEC)
1	4.0274E+02	6.4097E+01	.01560
2	5.6229E+02	8.9491E+01	.01117
3	6.2980E+02	1.0024E+02	.00998
4	7.2411E+02	1.1525E+02	.00868
5	8.4670E+02	1.3476E+02	.00742
6	1.0622E+03	1.6905E+02	.00592
7	1.2013E+03	1.9120E+02	.00523
8	1.2247E+03	1.9492E+02	.00513
9	1.2739E+03	2.0274E+02	.00493
10	1.4137E+03	2.2499E+02	.00444
11	1.5527E+03	2.4712E+02	.00405
12	1.8277E+03	2.9088E+02	.00344
13	1.9557E+03	3.1125E+02	.00321
14	2.0858E+03	3.3197E+02	.00301
15	2.3194E+03	3.6915E+02	.00271
16	2.5835E+03	4.1117E+02	.00243
17	2.6554E+03	4.2262E+02	.00237
18	2.7125E+03	4.3170E+02	.00232
19	2.9539E+03	4.7013E+02	.00213
20	3.2129E+03	5.1134E+02	.00196

Figure 170. Print of Frequencies for Large Airplane USB Flap Model, 35 Nodes, No Camber

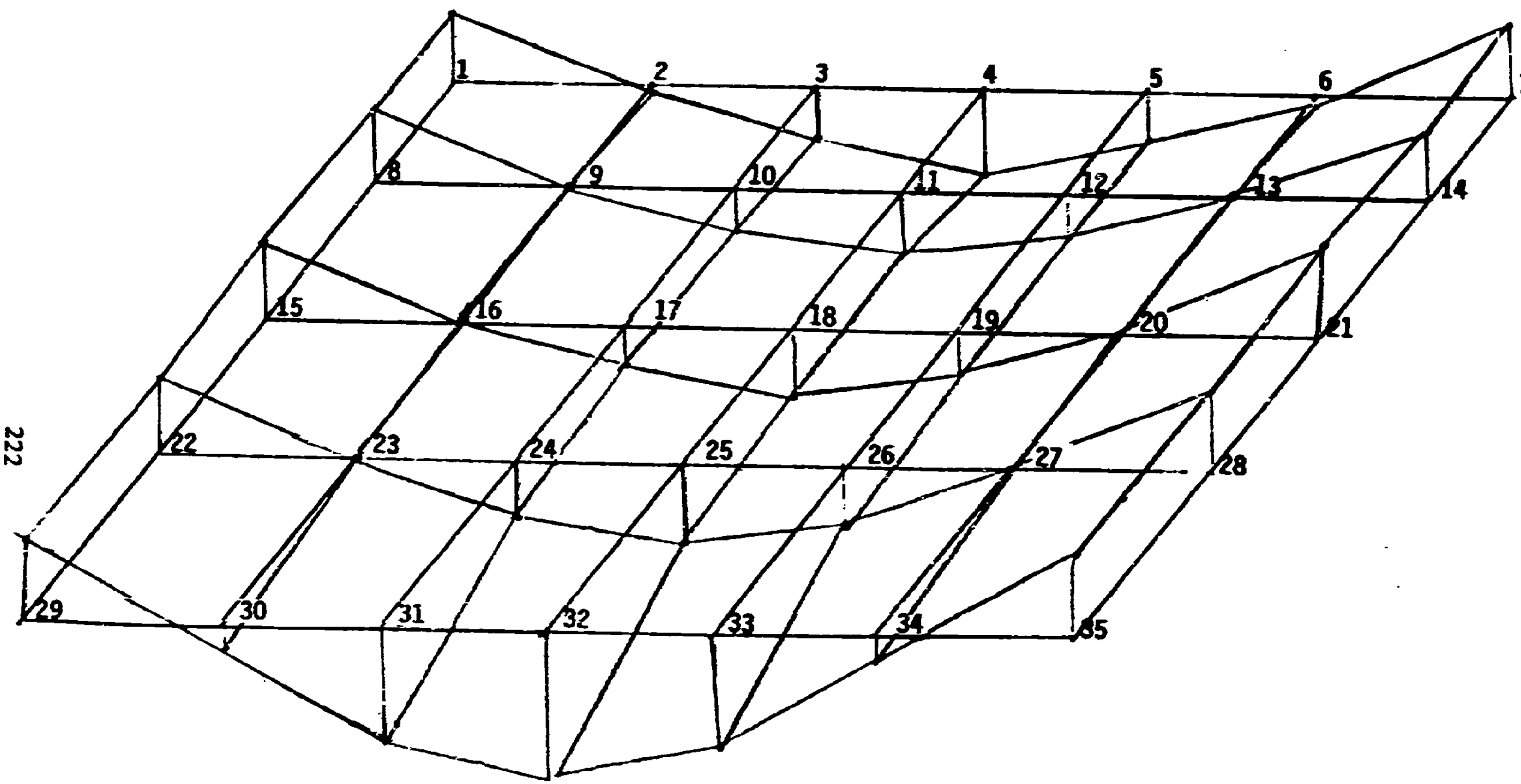

Figure 171. Large STOL USB Flap Modal Plot, Frequency = 64.097 Hz.

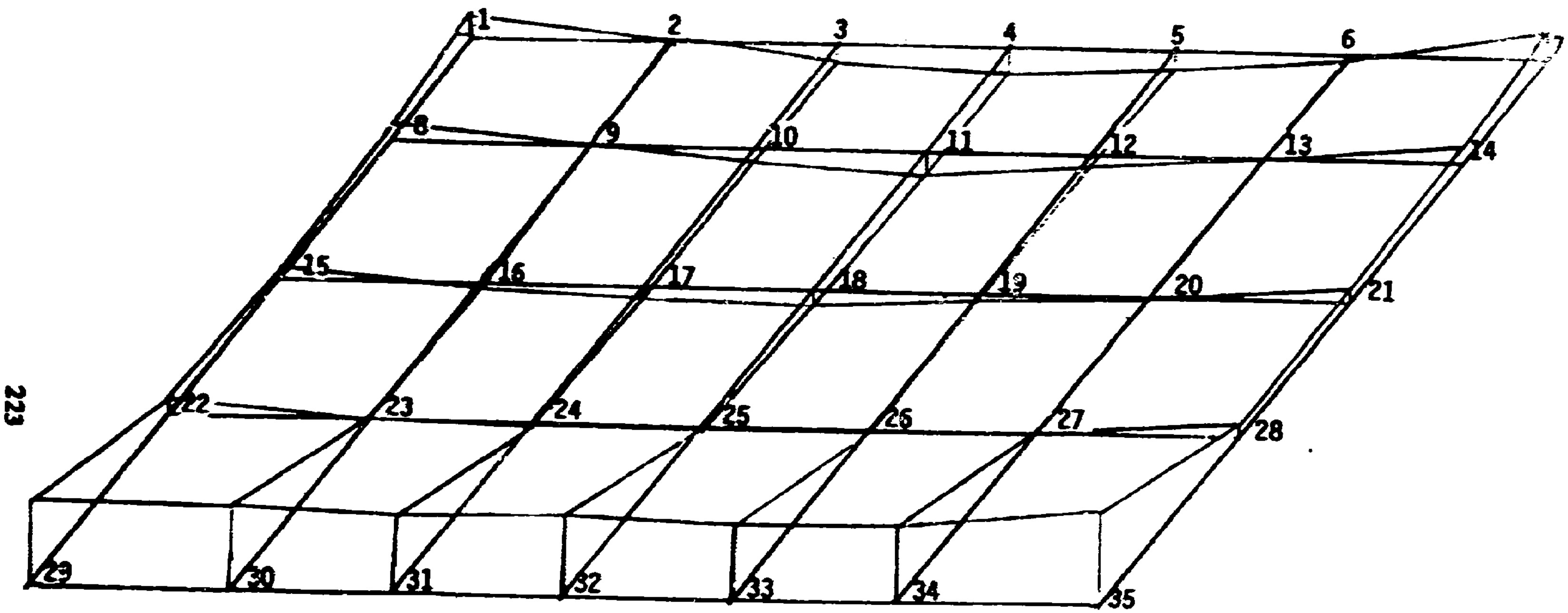

Figure 172. Large STOL USB Flap Modal Plot, Frequency = 89.49 Hz.

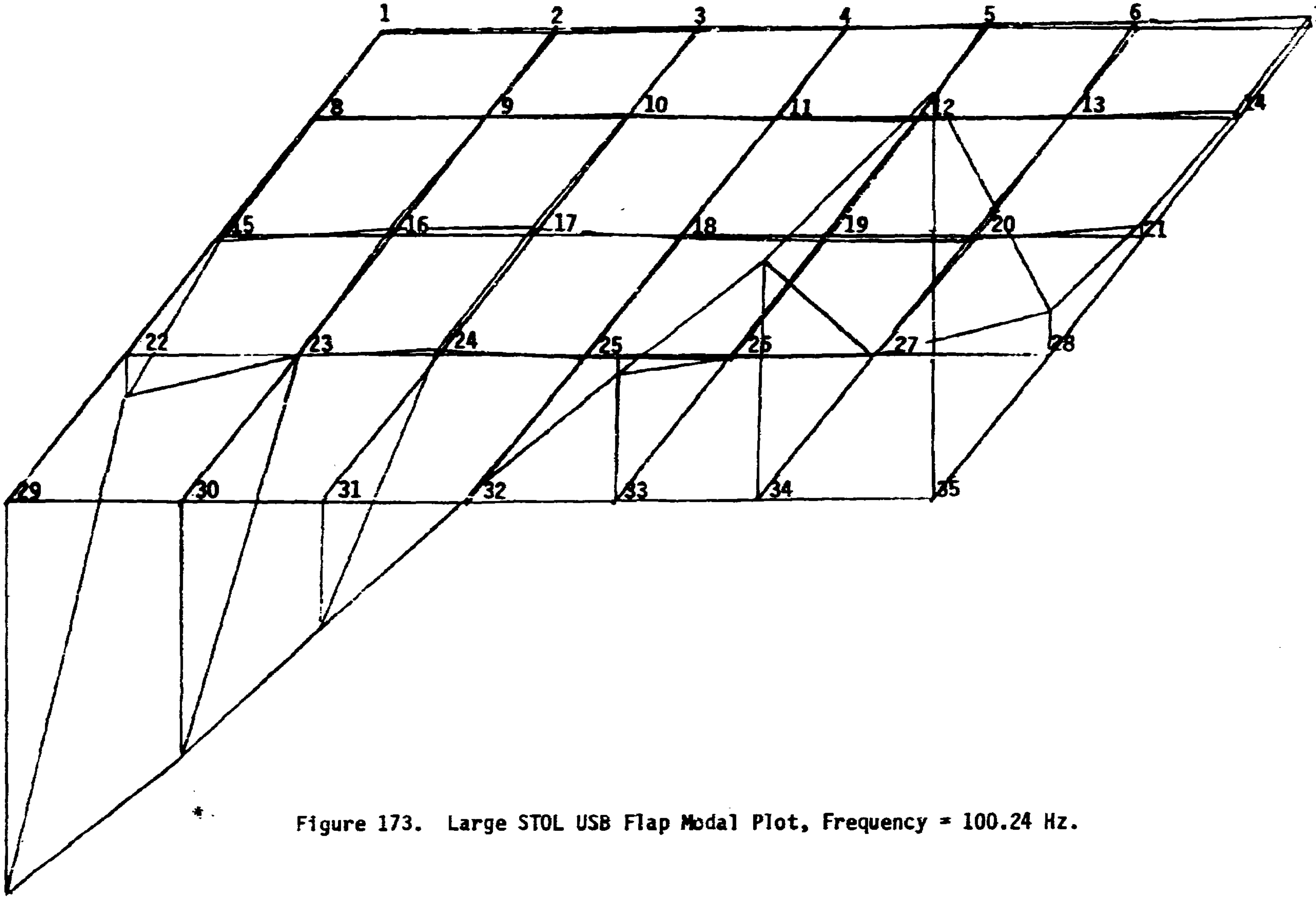

Figure 173. Large STOL USB Flap Modal Plot, Frequency = 100.24 Hz.

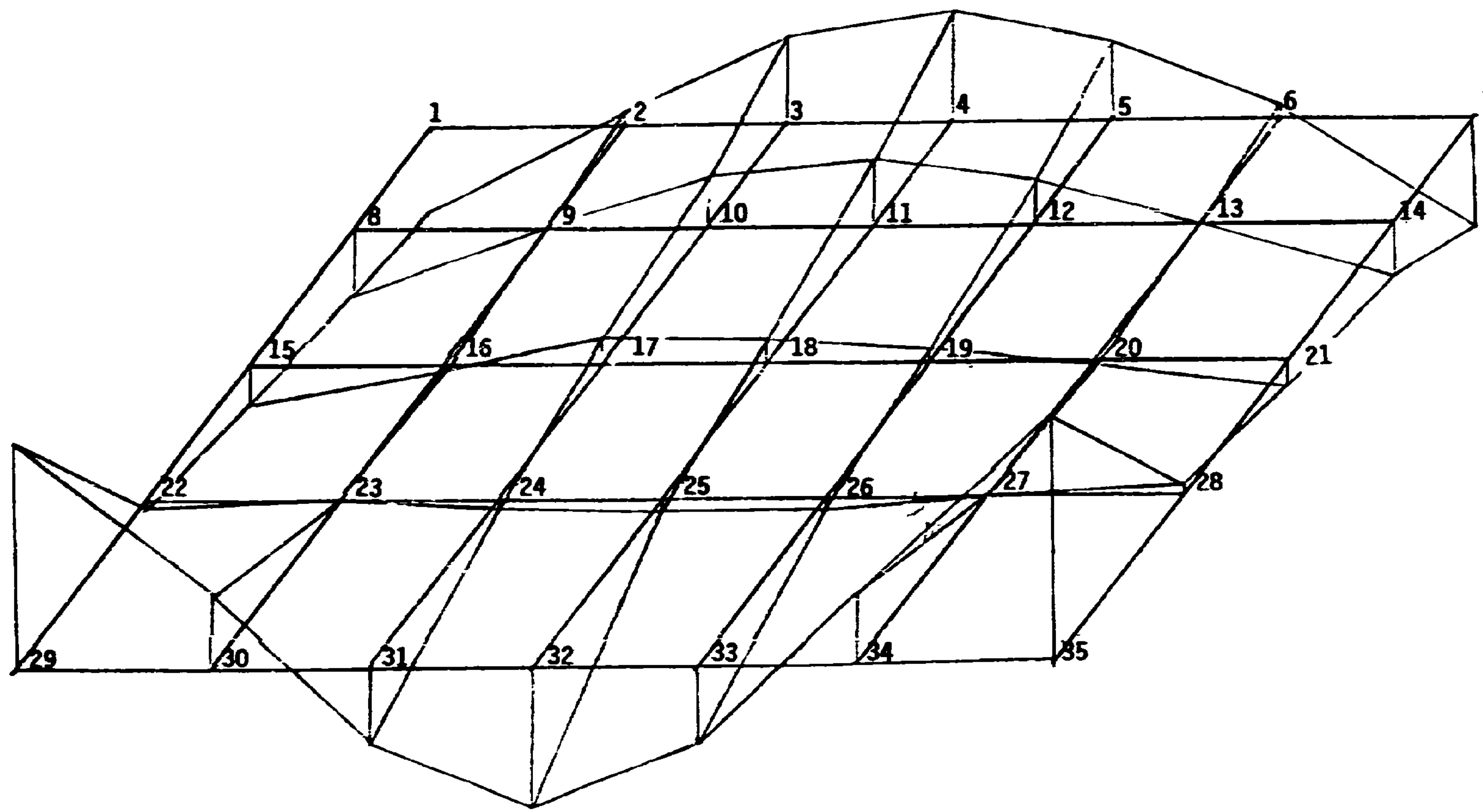

Figure 174. Large STOL USB Flap Modal Plot, Frequency = 115.25 Hz.

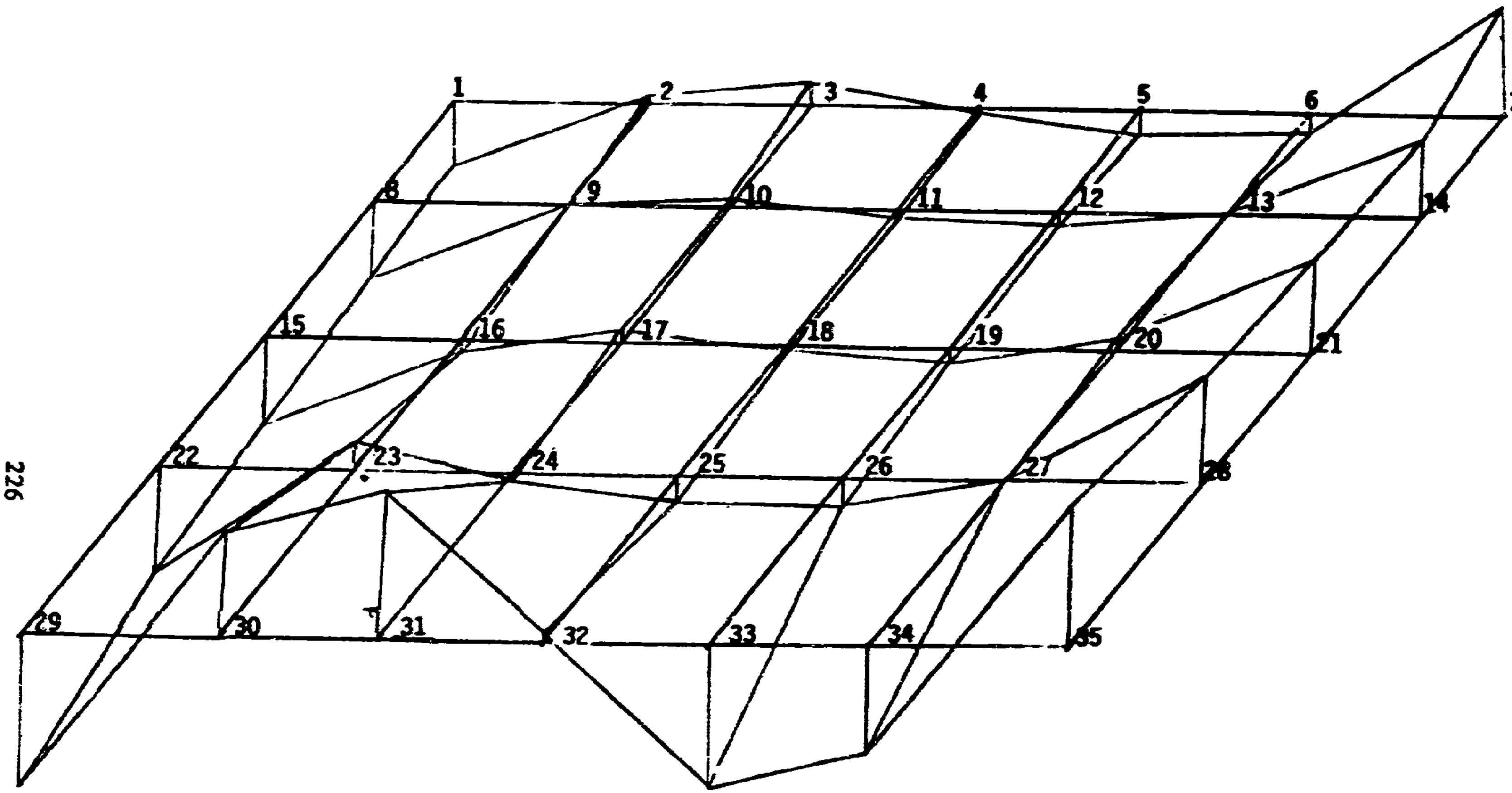

Figure 175. Large STOL USB Flap Modal Plot, Frequency = 134.76 Hz.

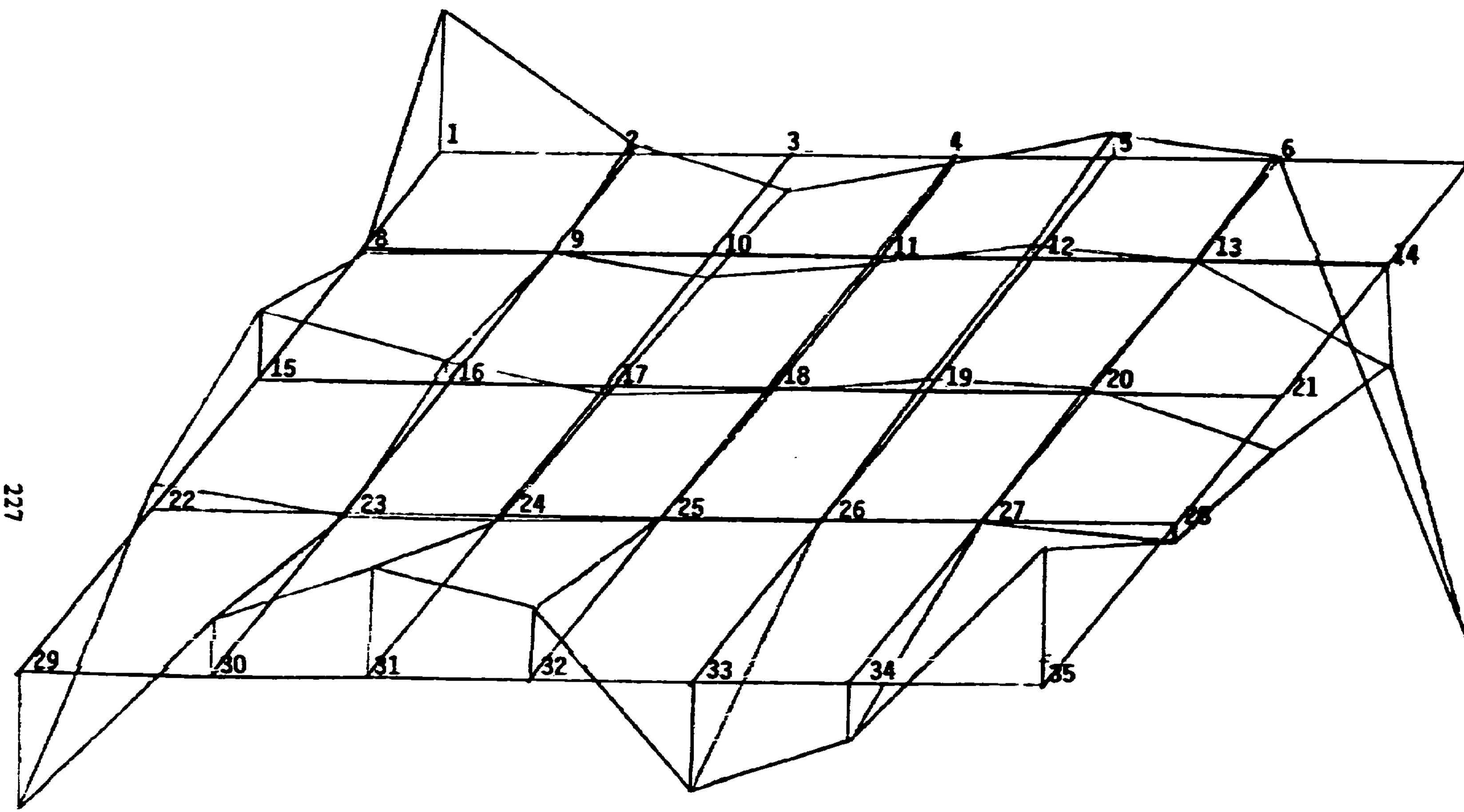

Figure 176. Large STOL USB Flap Modal Plot, Frequency = 169.05 Hz.

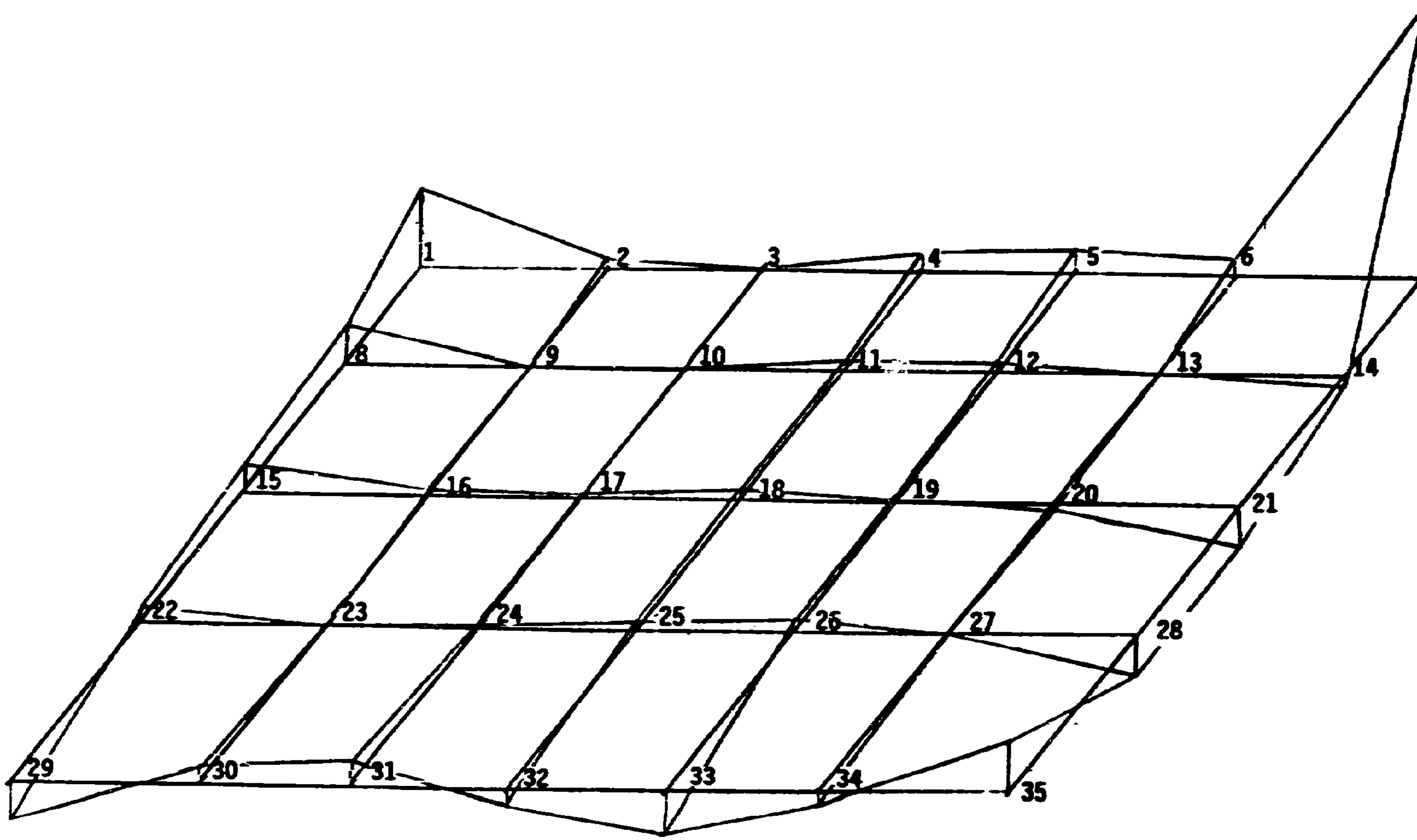

Figure 177. Large STOL Airplane USB Flap Modal Plot, Frequency = 191.2 Hz.

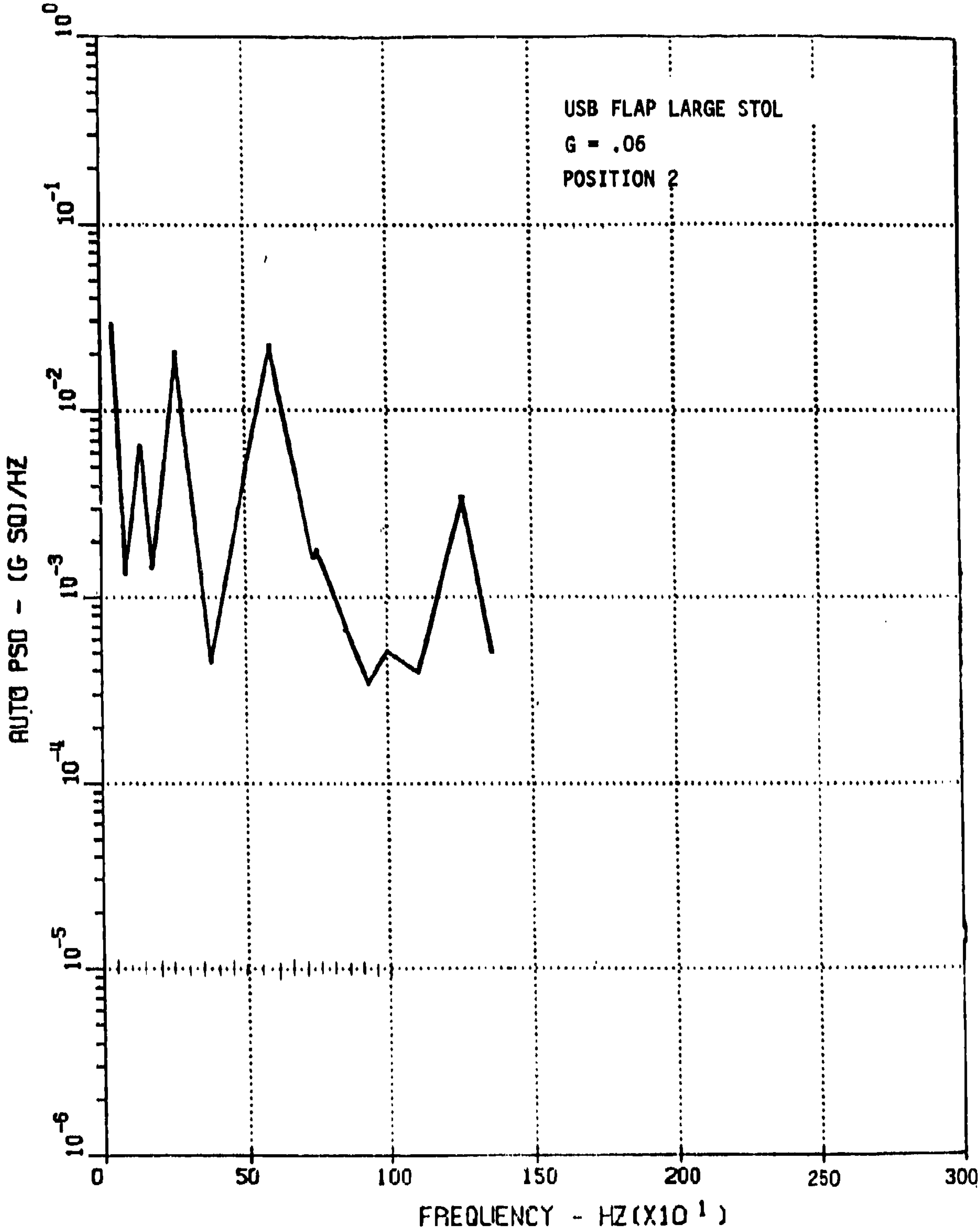

Figure 178. Response Prediction of Large STOL USB Flap Position 2, Damping G=.06

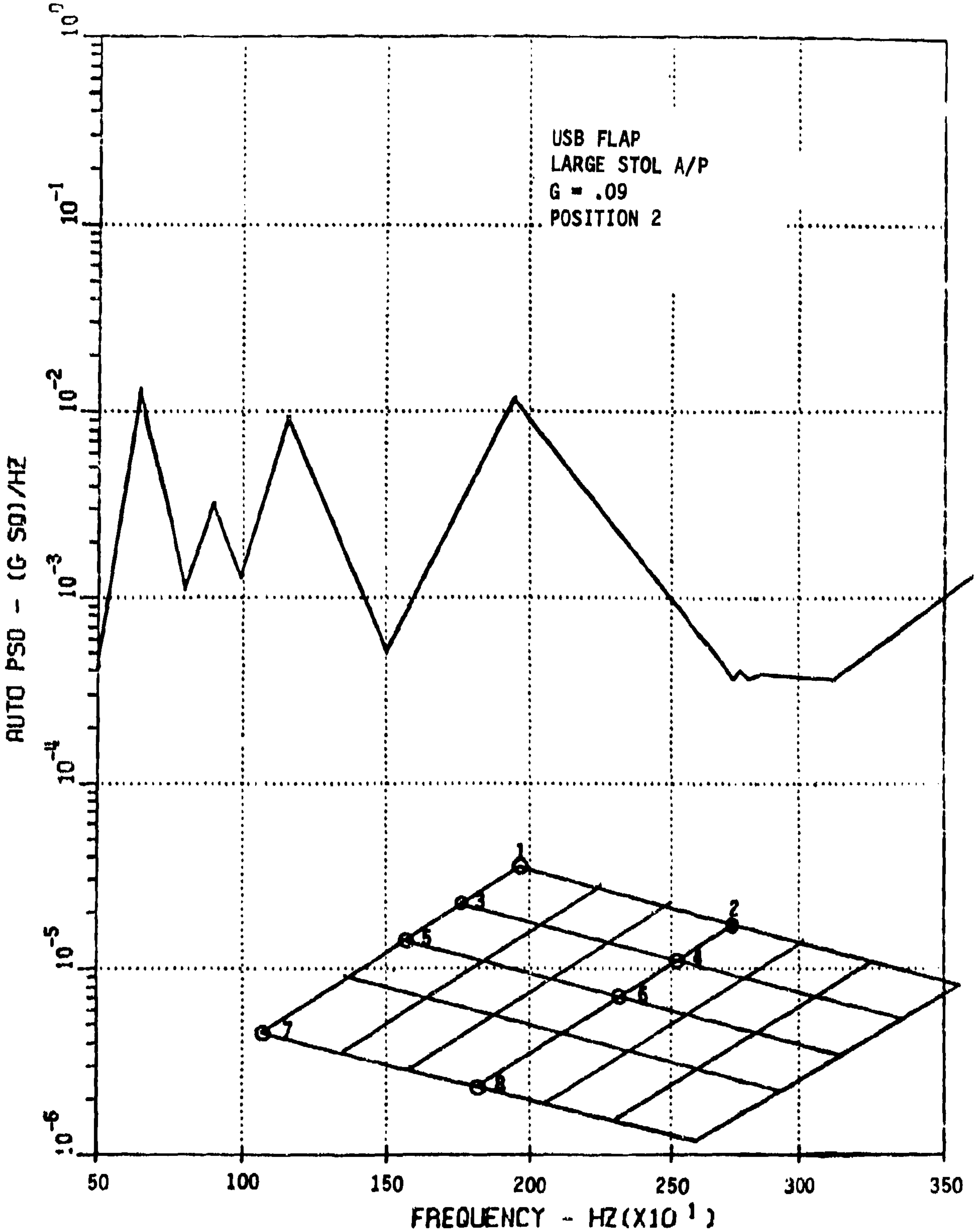

Figure 179. Response Prediction of Large STOL USB Flap Position 2, Damping G=.09

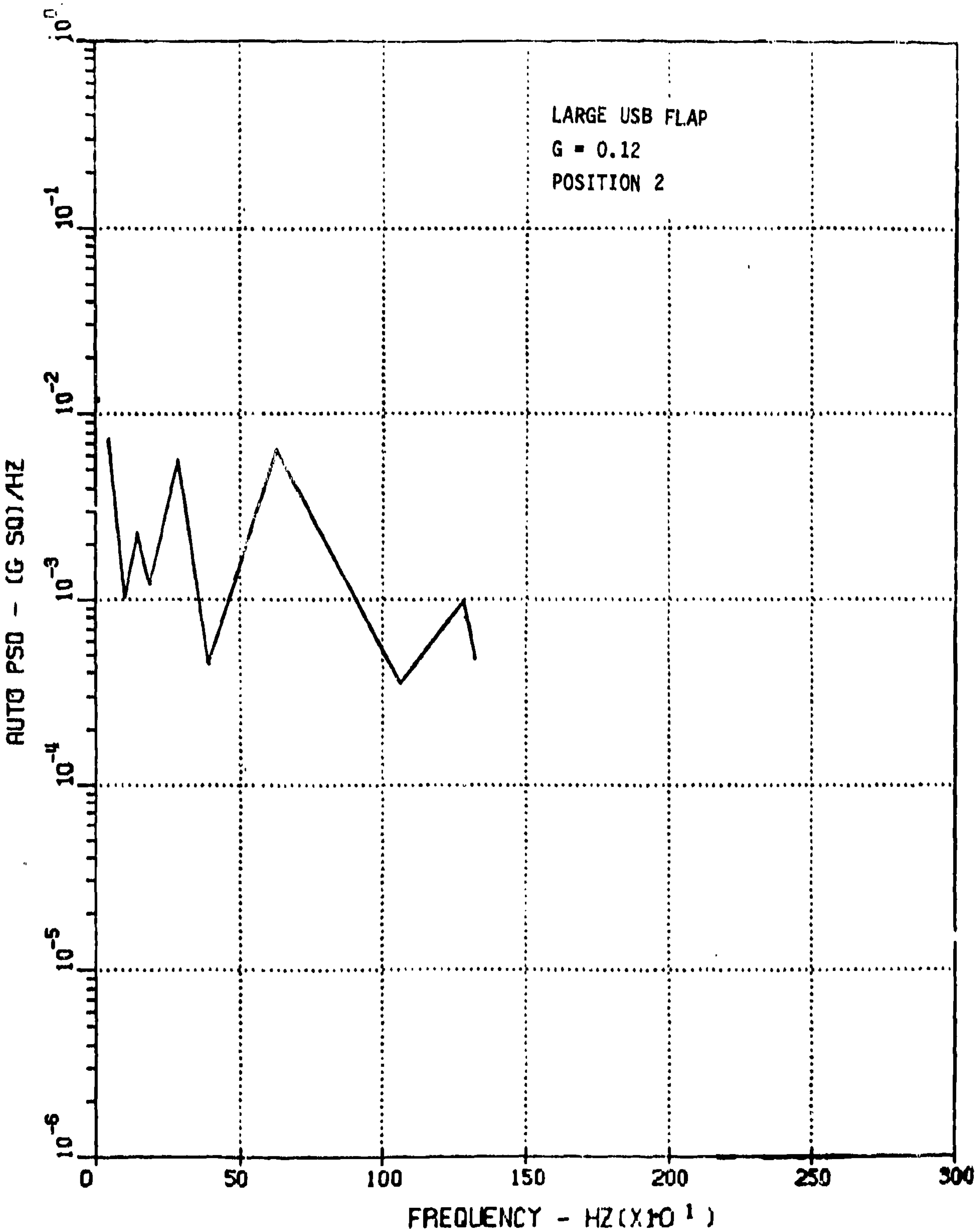

Figure 180. Response Prediction of Large STOL USB Flap Position 2, Damping G=.12

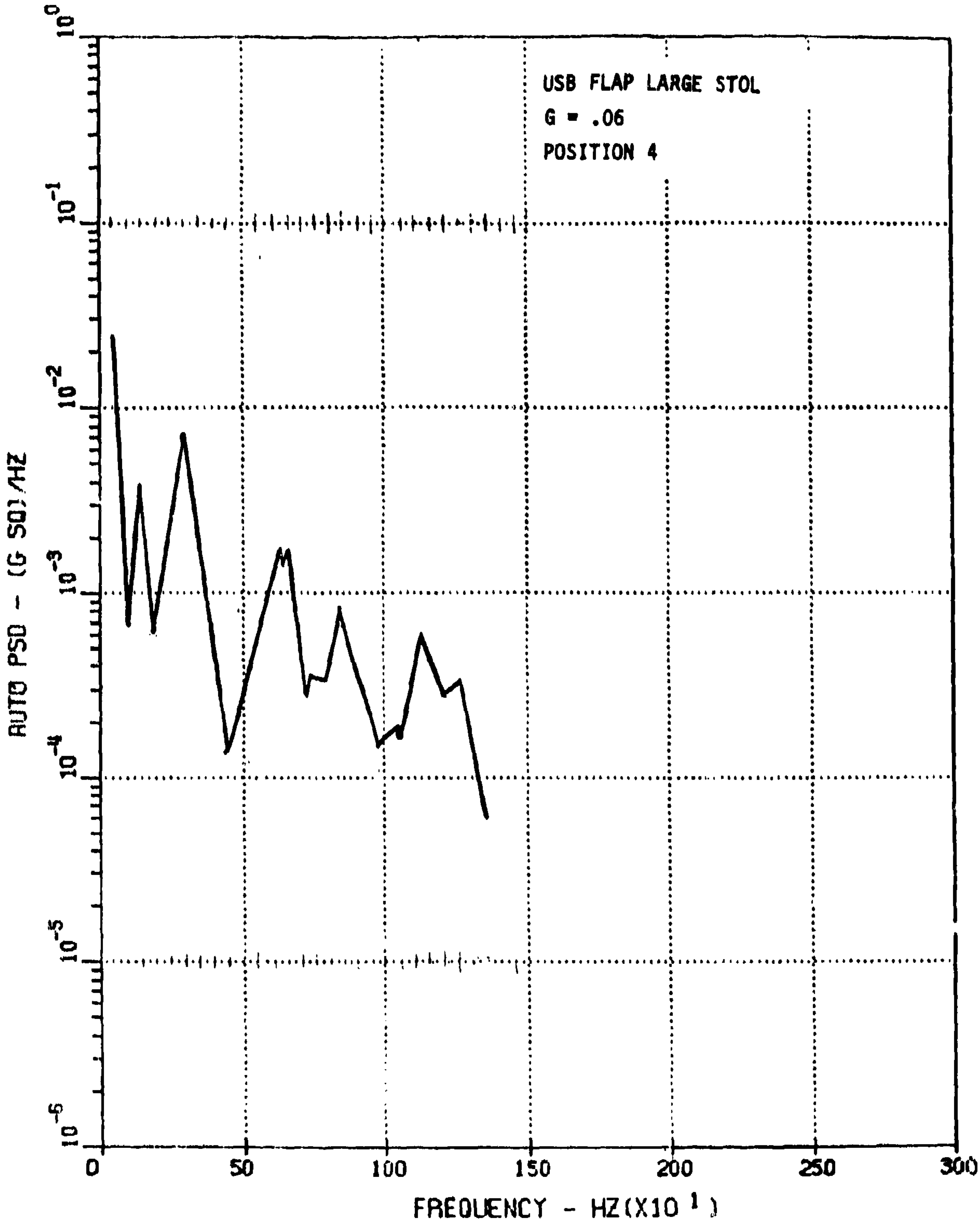

Figure 181. Response Prediction of Large STOL USB Flap Position 4, Damping G=.06

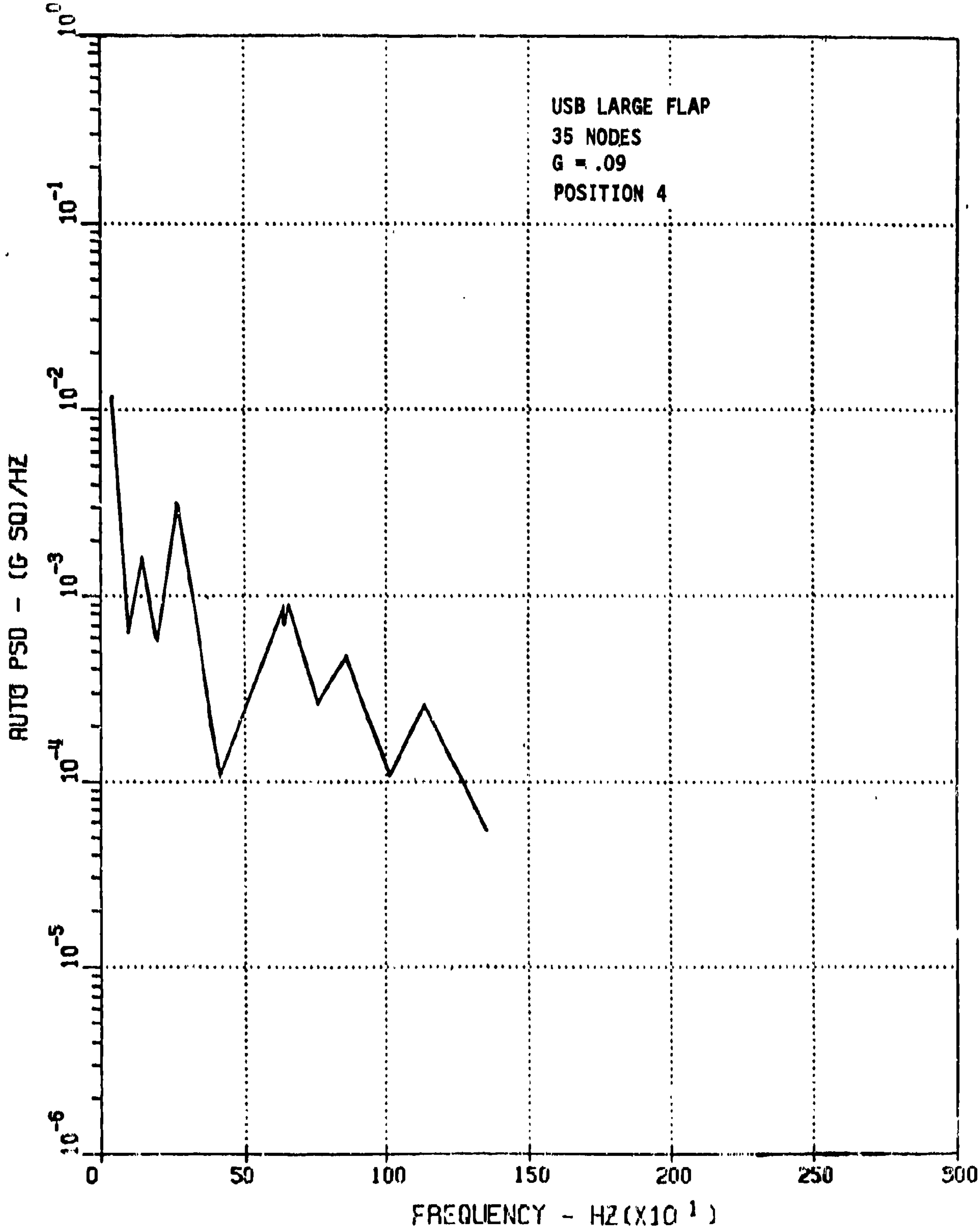

Figure 182. Response Prediction of Large STOL USB Flap Position 4, Damping G=.09

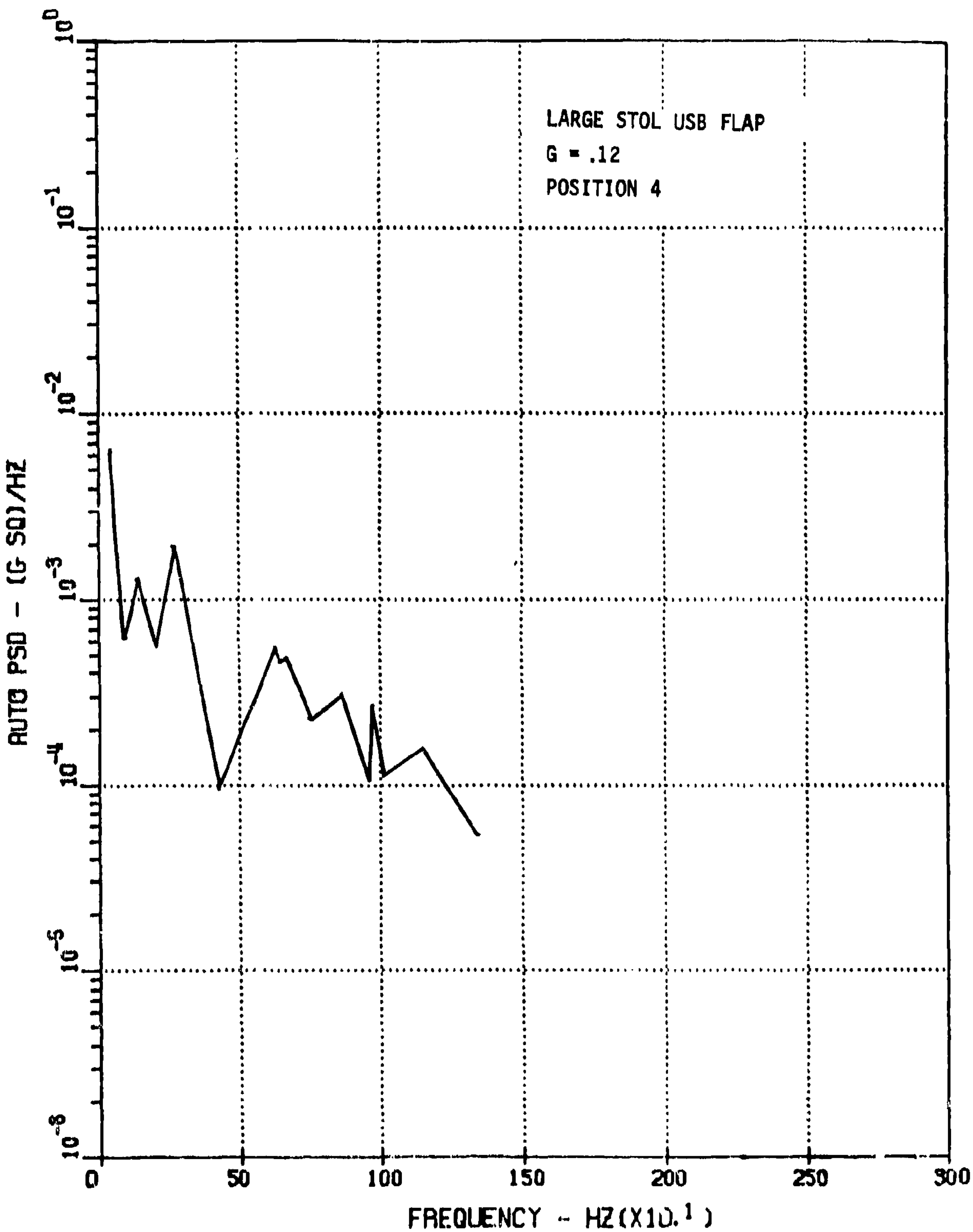

Figure 183. Response Prediction of Large STOL USB Flap Position 4, Damping G=.12

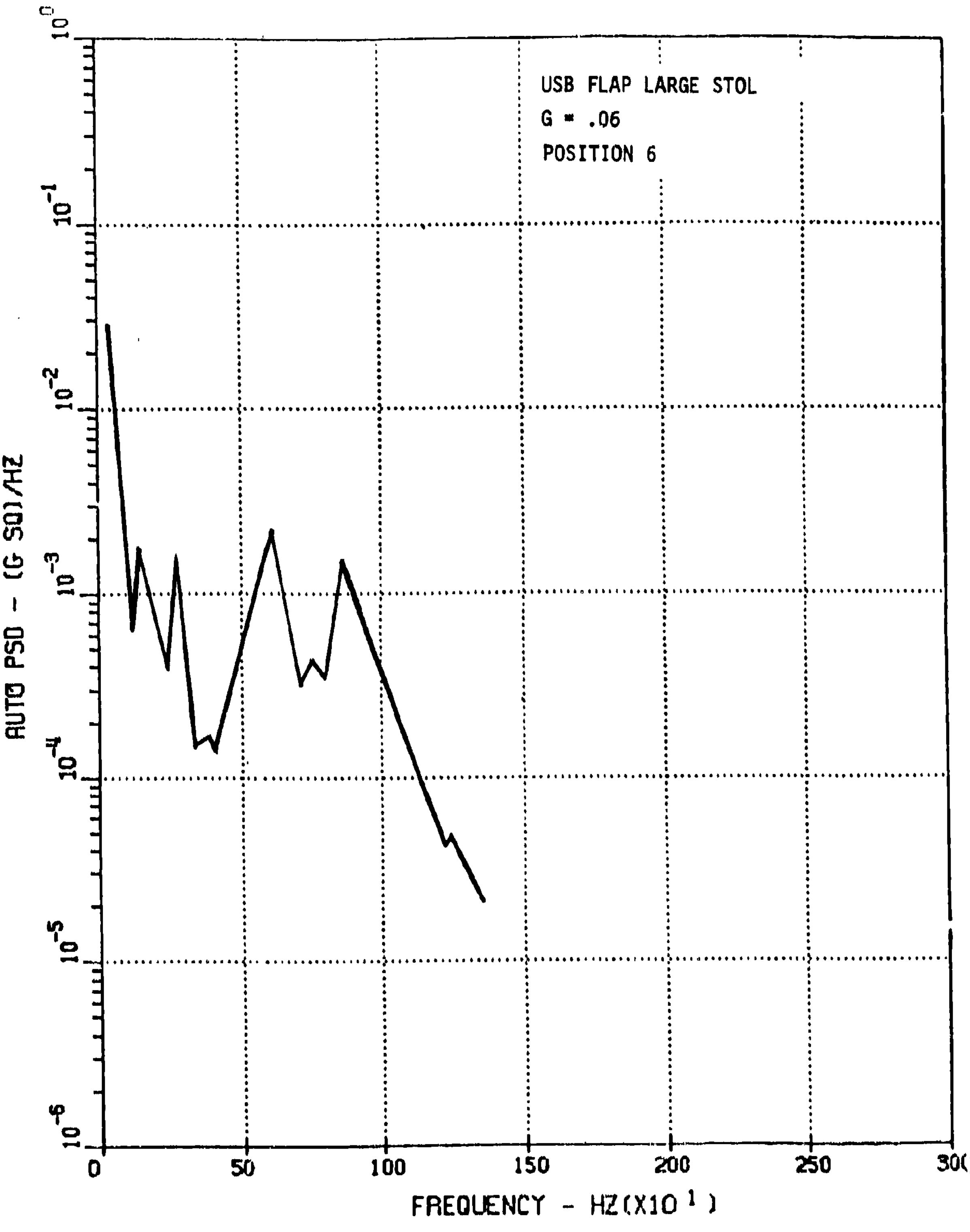

Figure 184. Response Prediction of Large STOL USB Flap Position 6, Damping G=.06

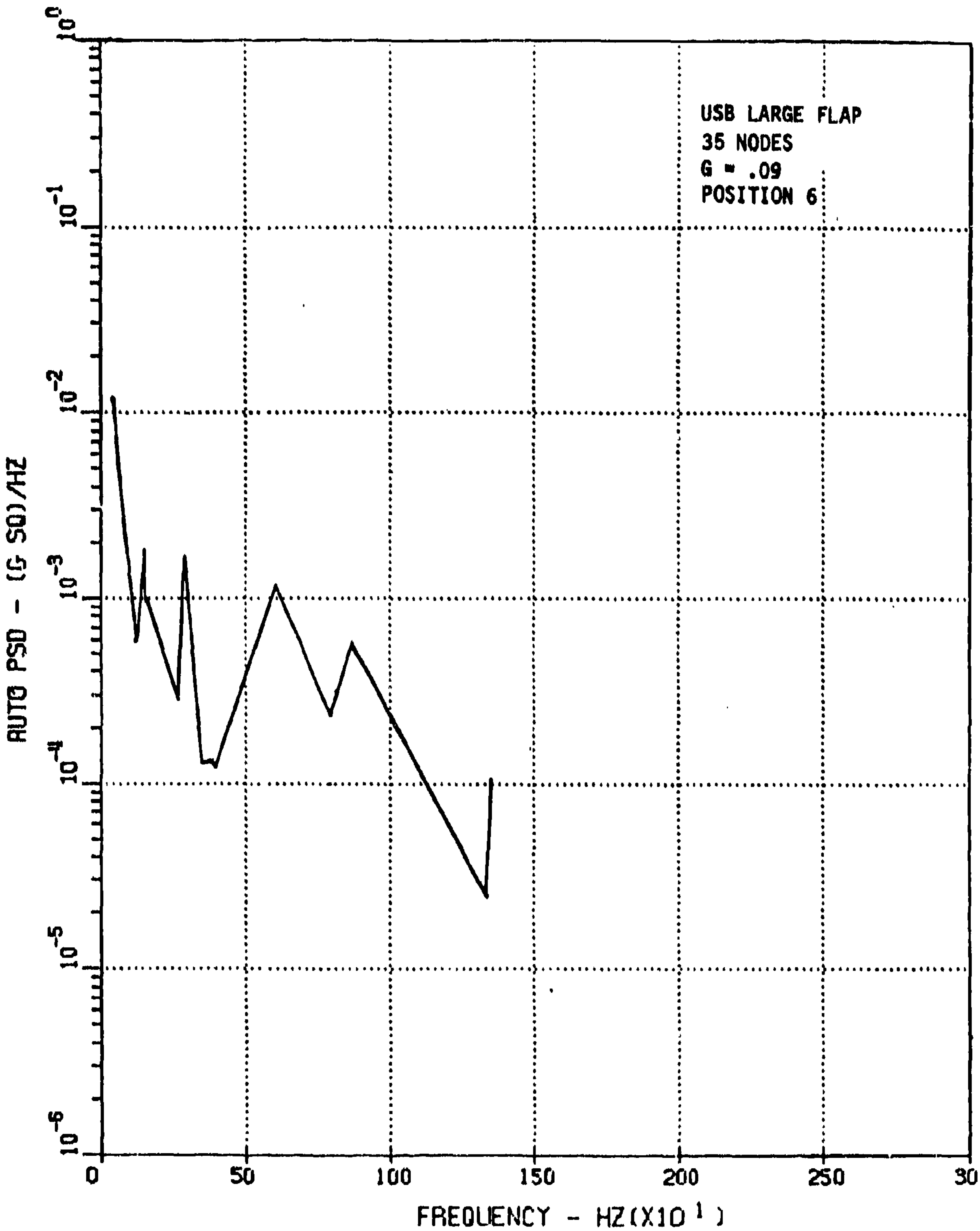

Figure 185. Response Prediction of Large STOL USB Flap Position 6, Damping G=.09

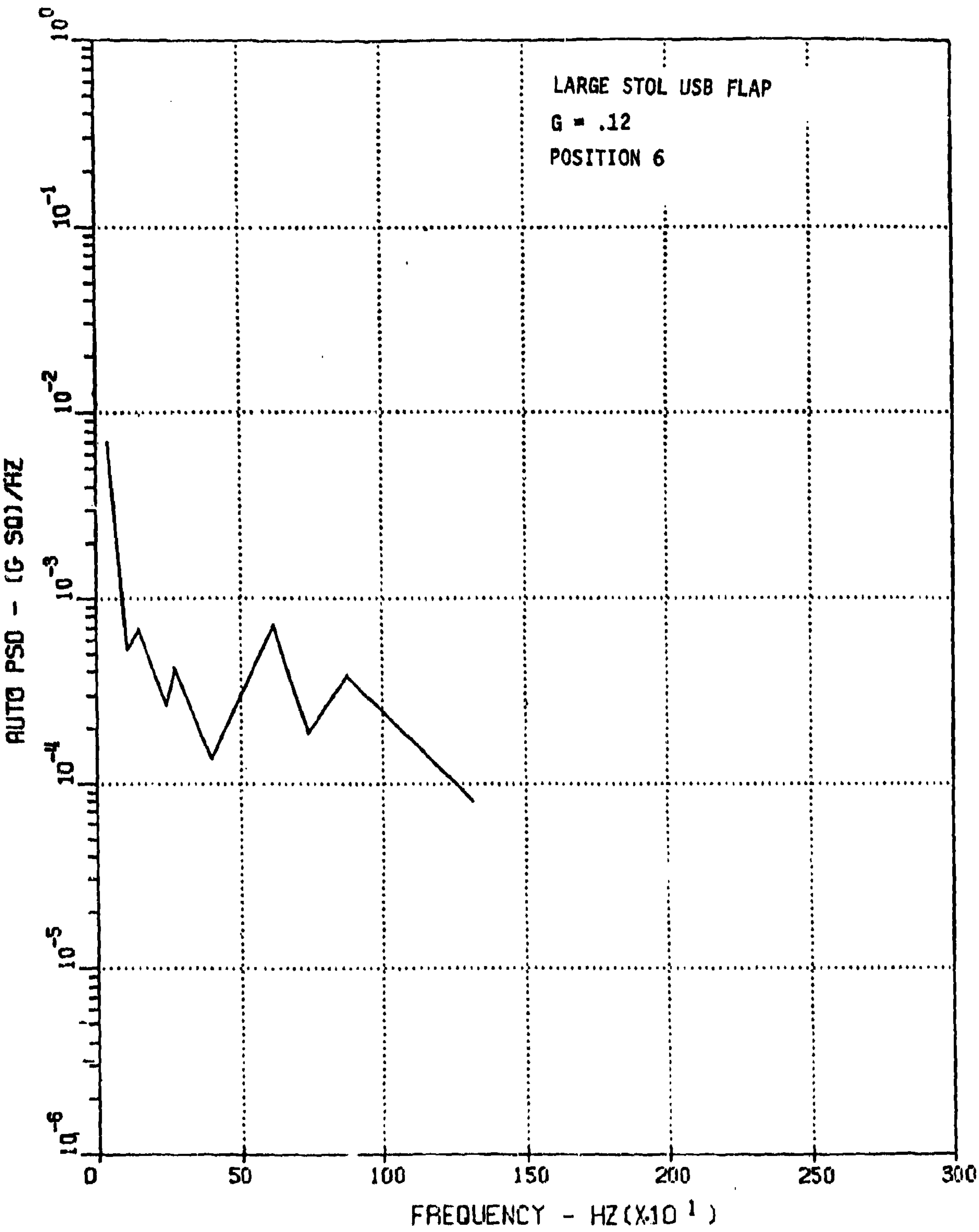

Figure 186. Response Prediction of Large STOL USB Flap Position 6, Damping G=.12

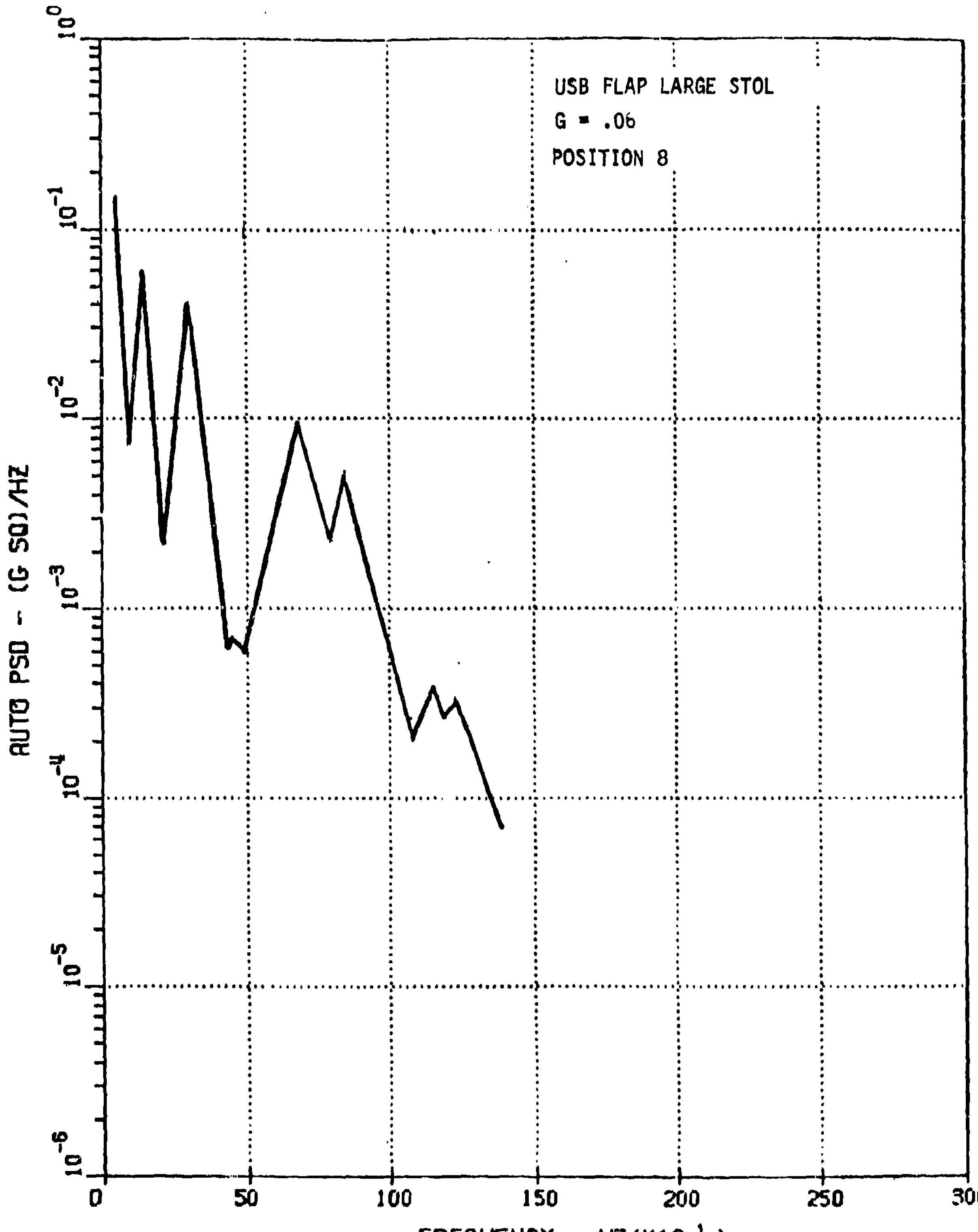

Figure 187. Response Prediction of Large STOL USB Flap Position 8, Damping G=.06

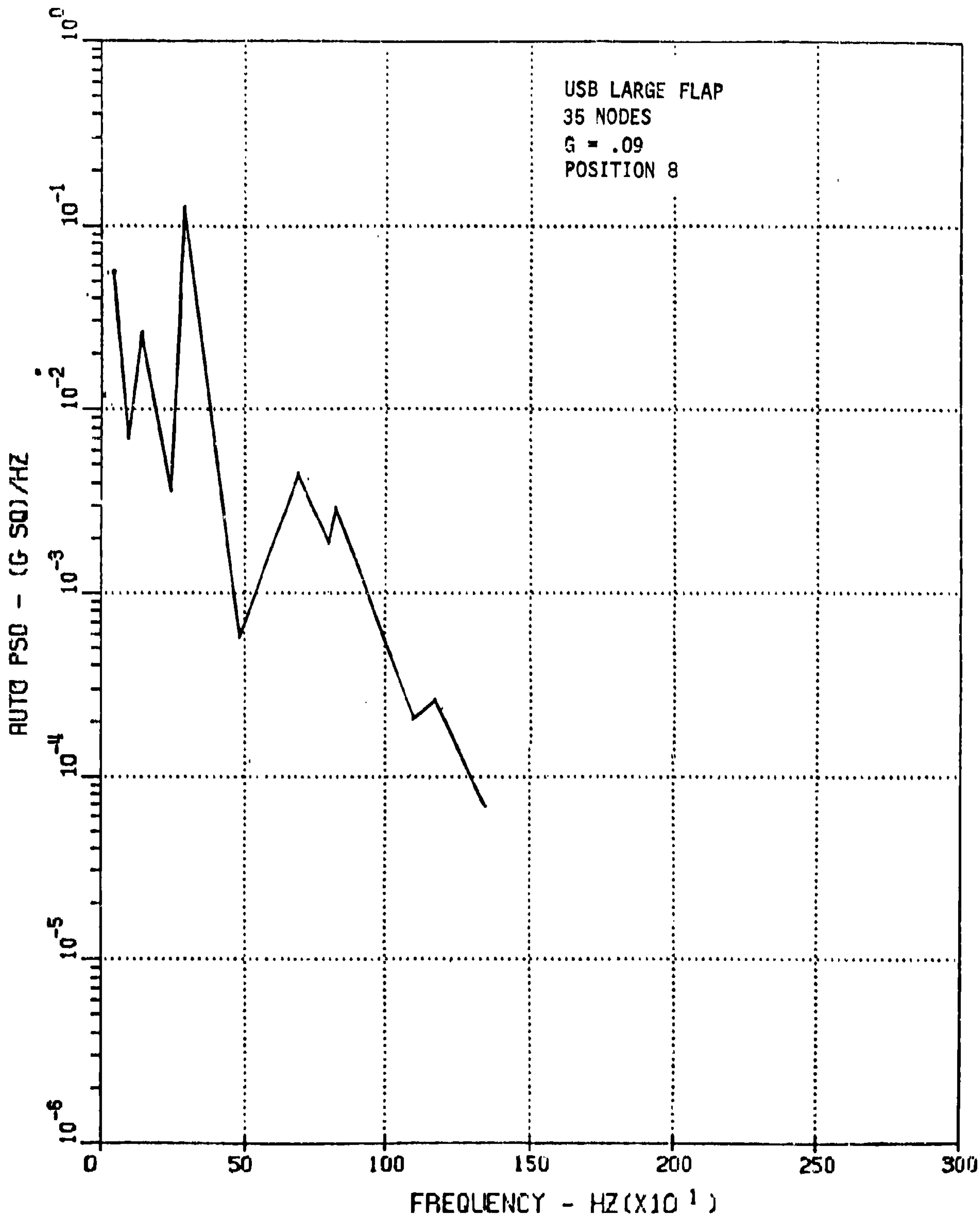

Figure 188. Response Prediction of Large STOL USB Flap Position 8, Damping G=.09

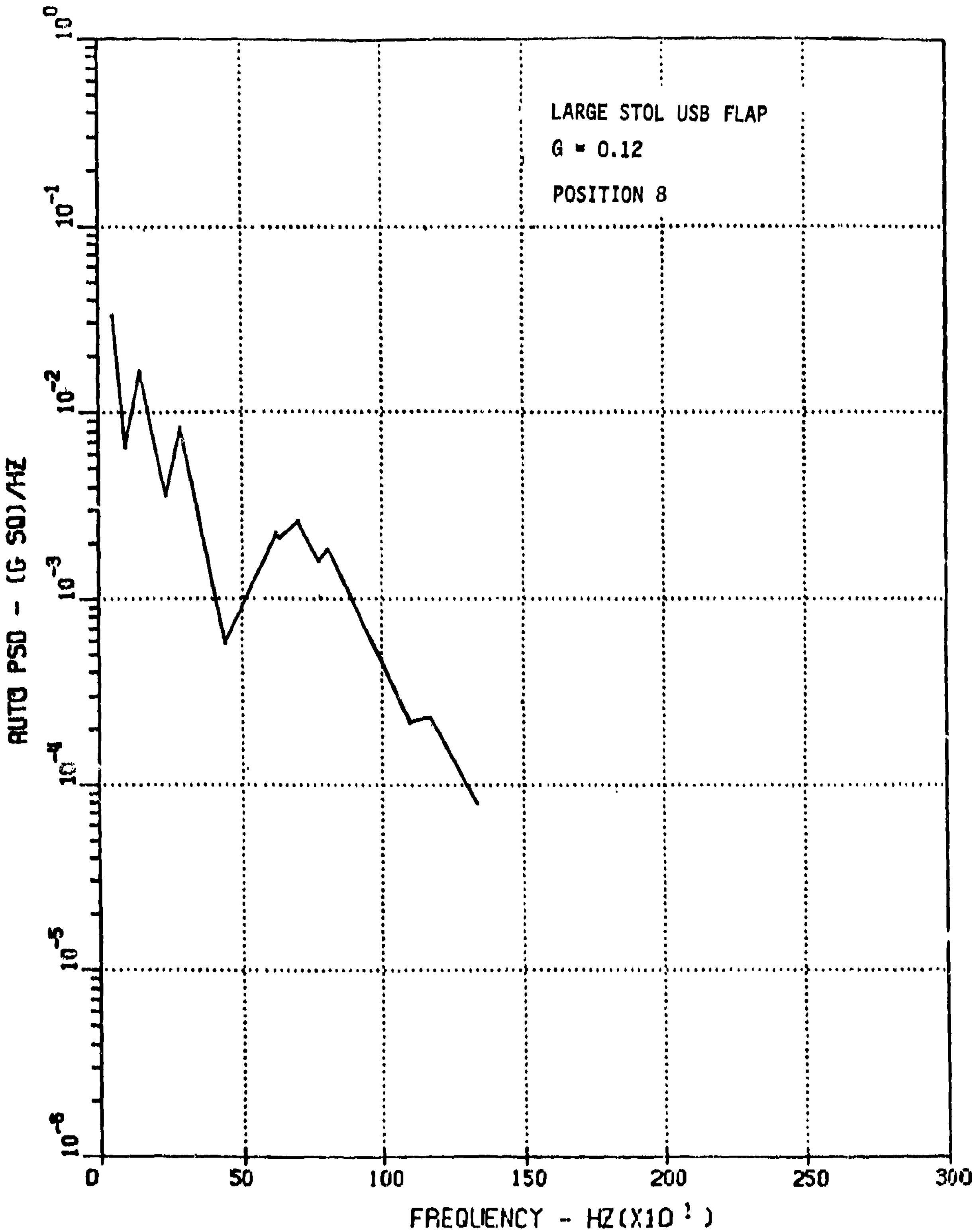

Figure 189. Response Prediction of Large STOL USB Flap Position 8, Damping G=.12

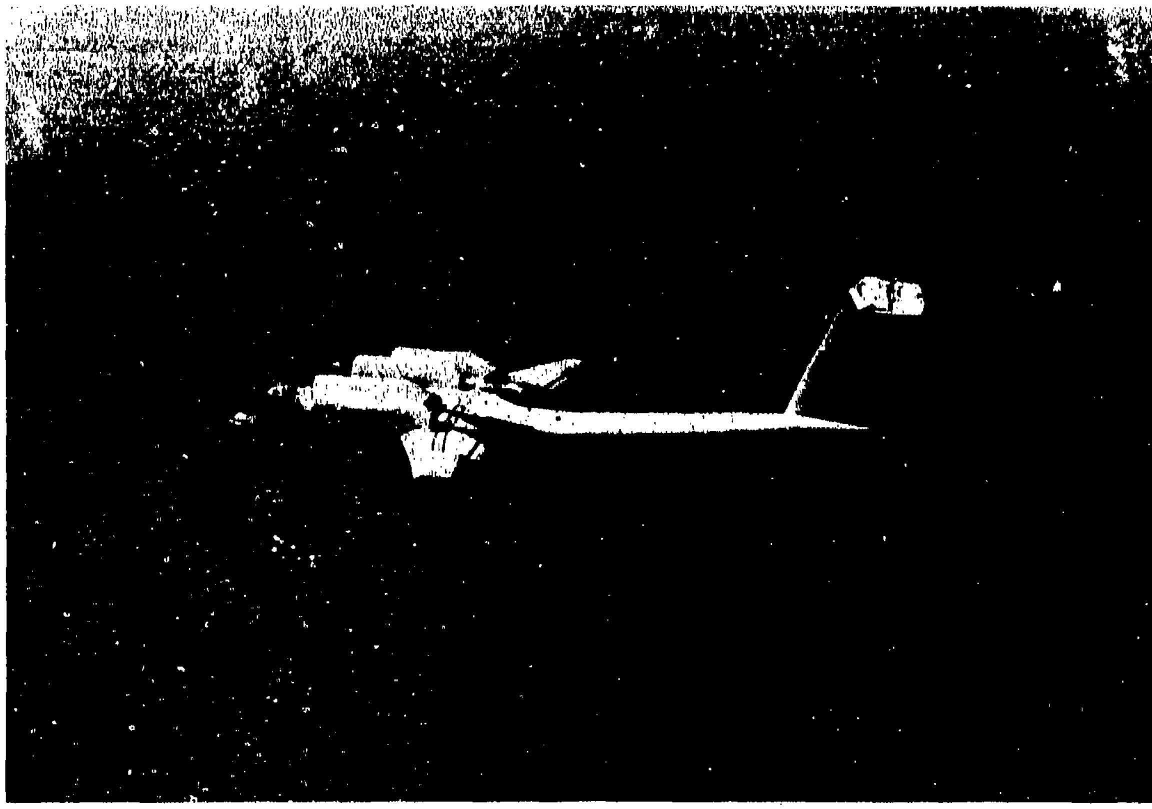

Figure 190. QSRA Aircraft in Flight

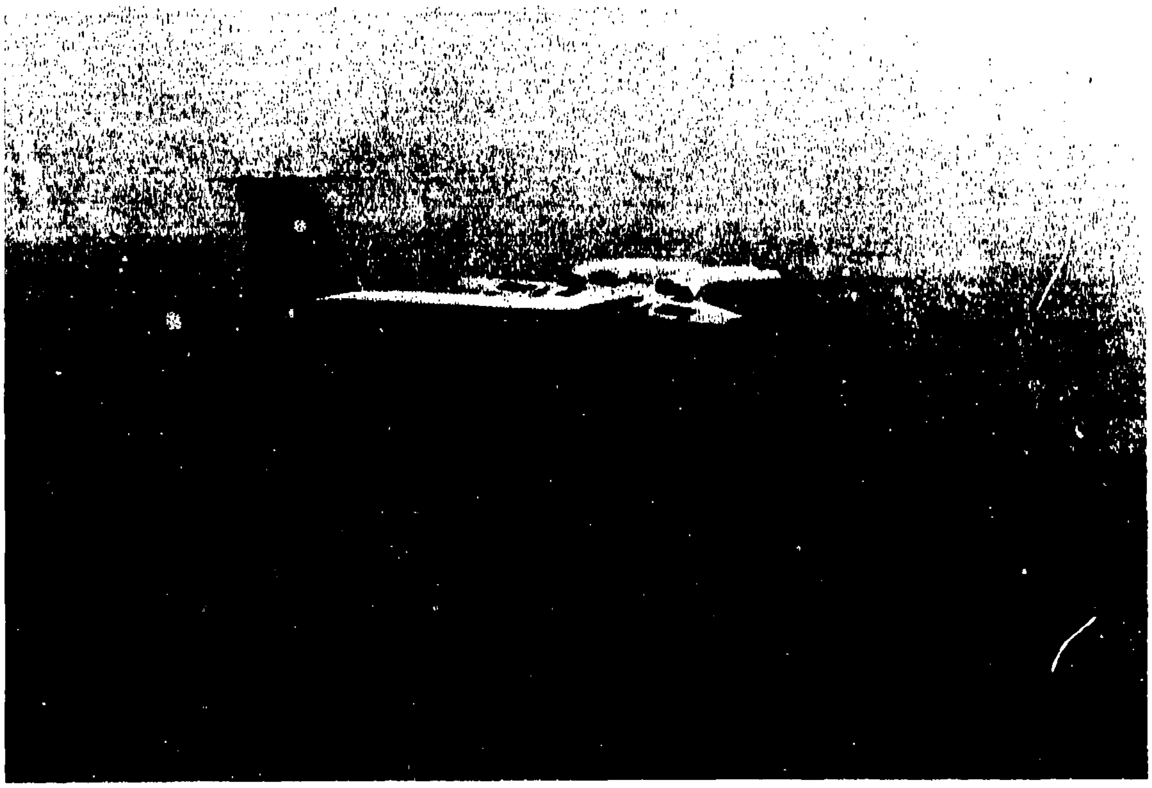

Figure 191. QSRA Aircraft in Flight

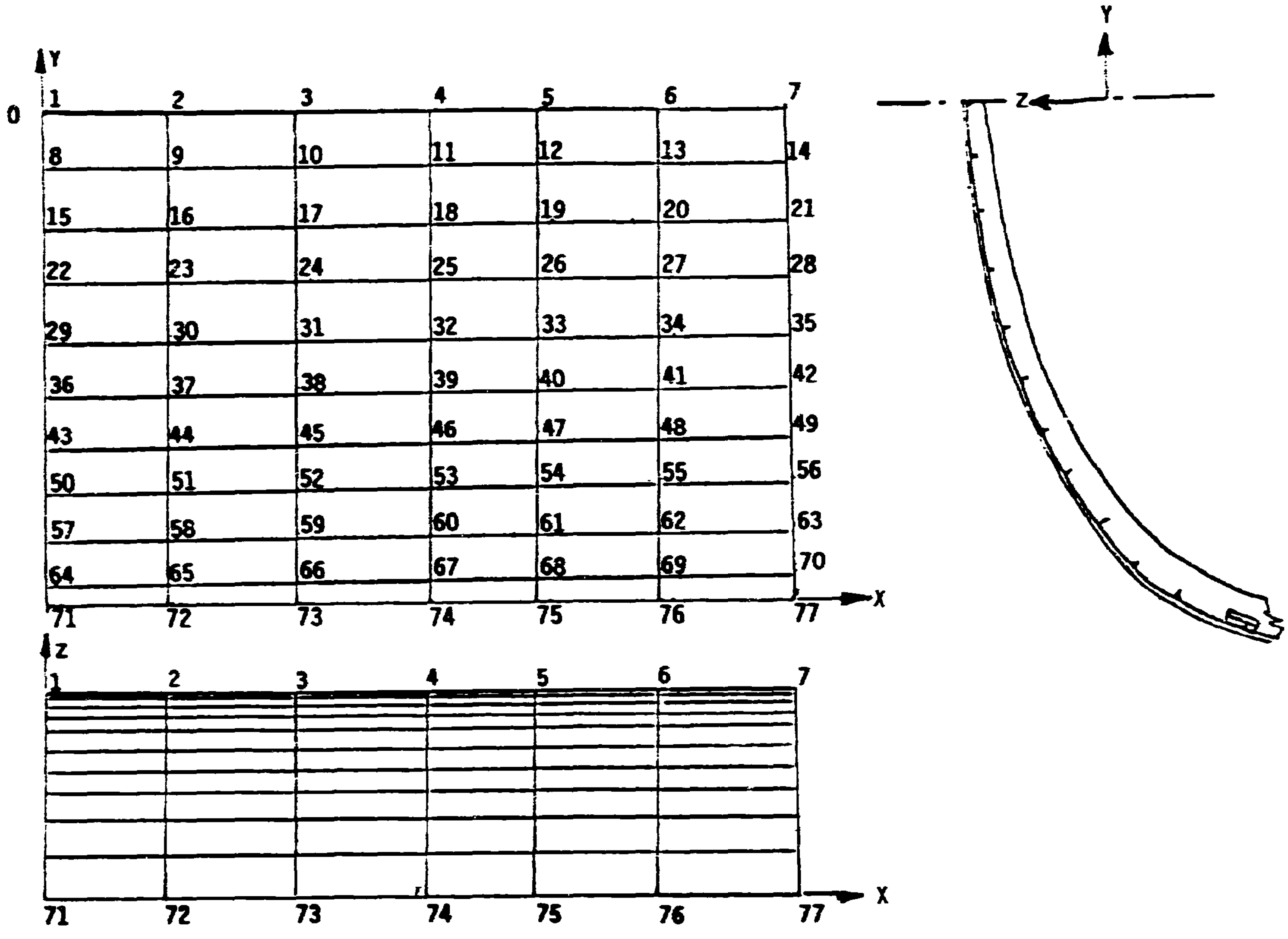

Figure 192. Fuselage Structure Finite Element Model Node Points

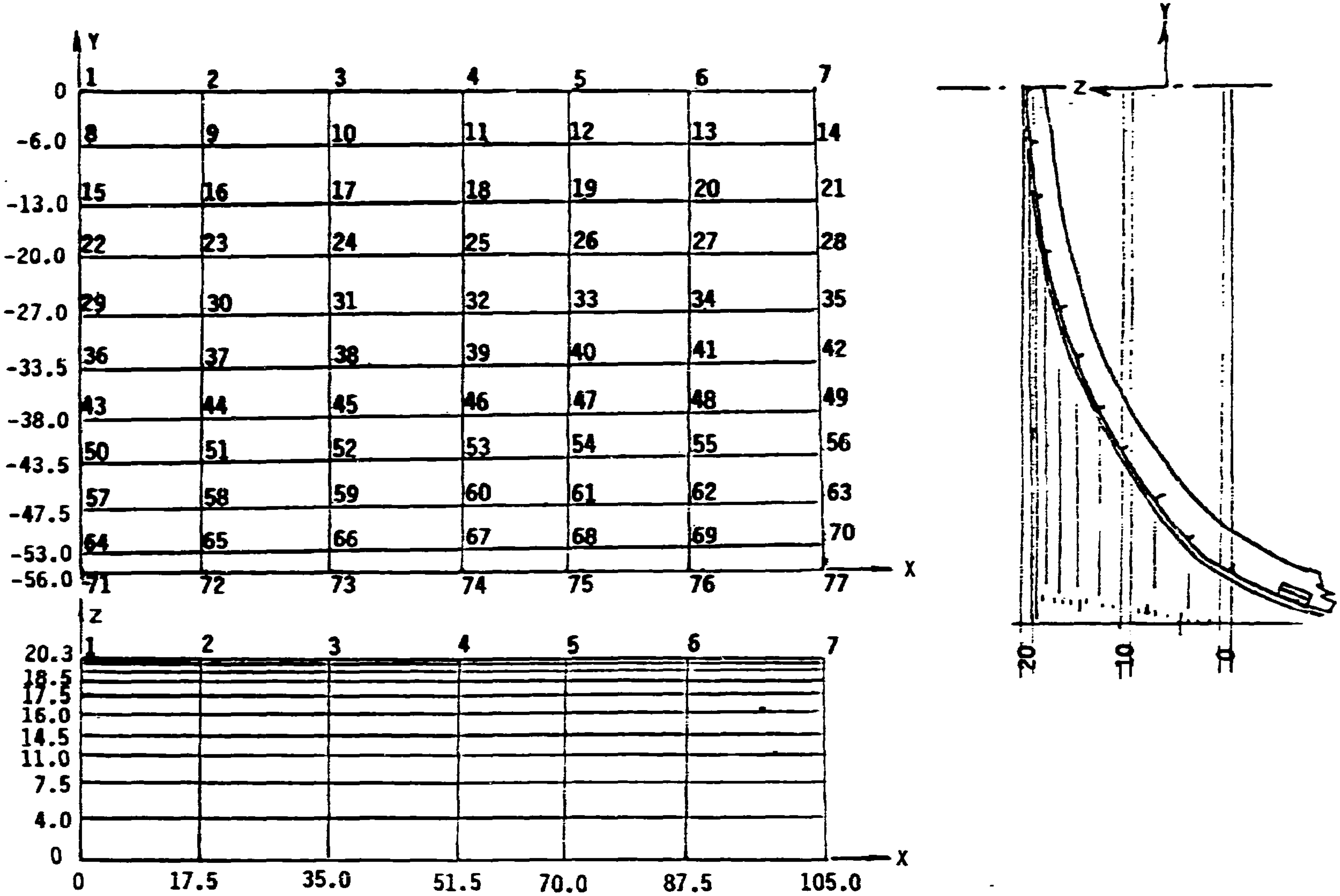

Figure 193. QSRA Fuselage Structure Model Coordinates

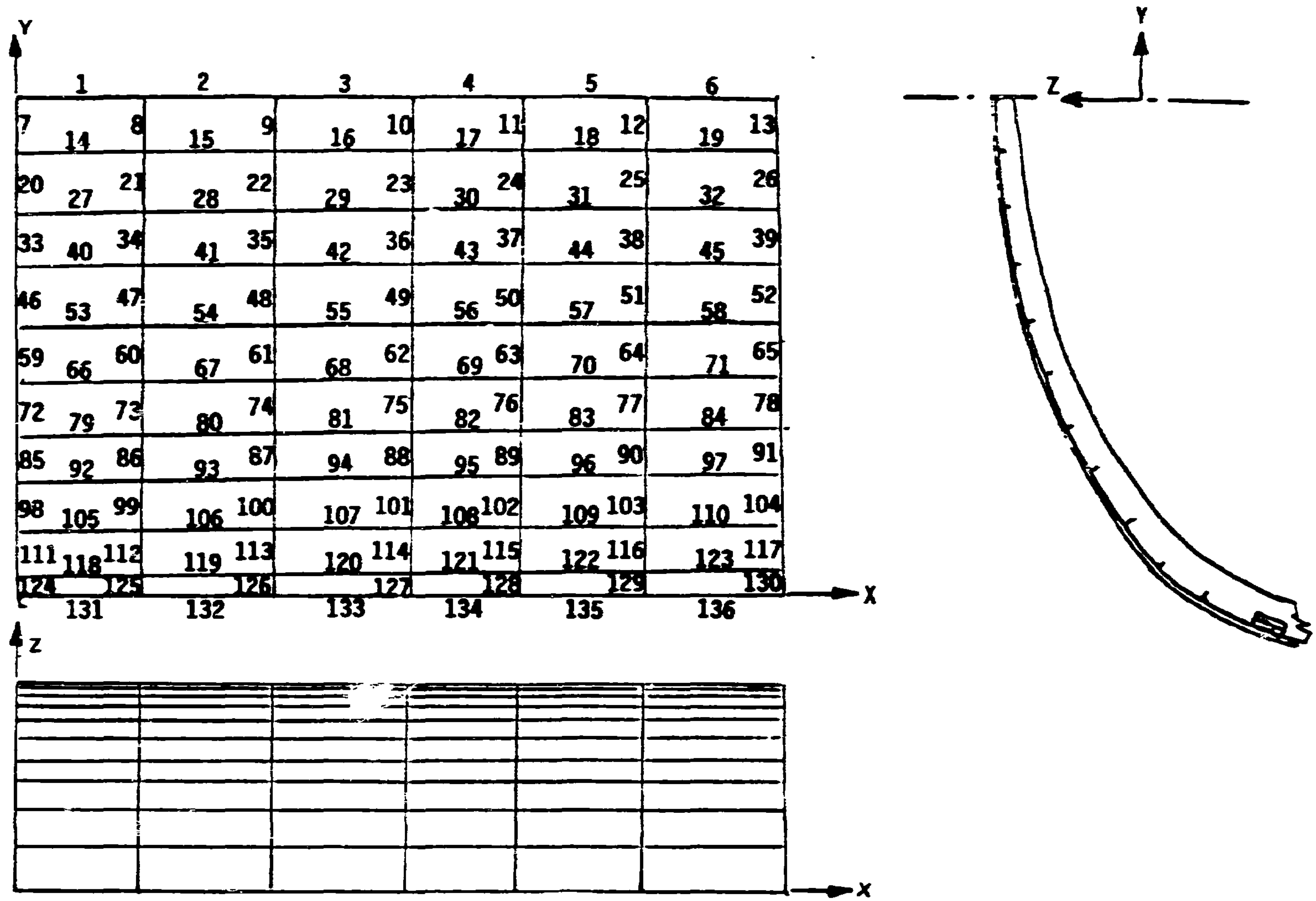

Figure 194. QSRA Fuselage Structure Model Beam Elements

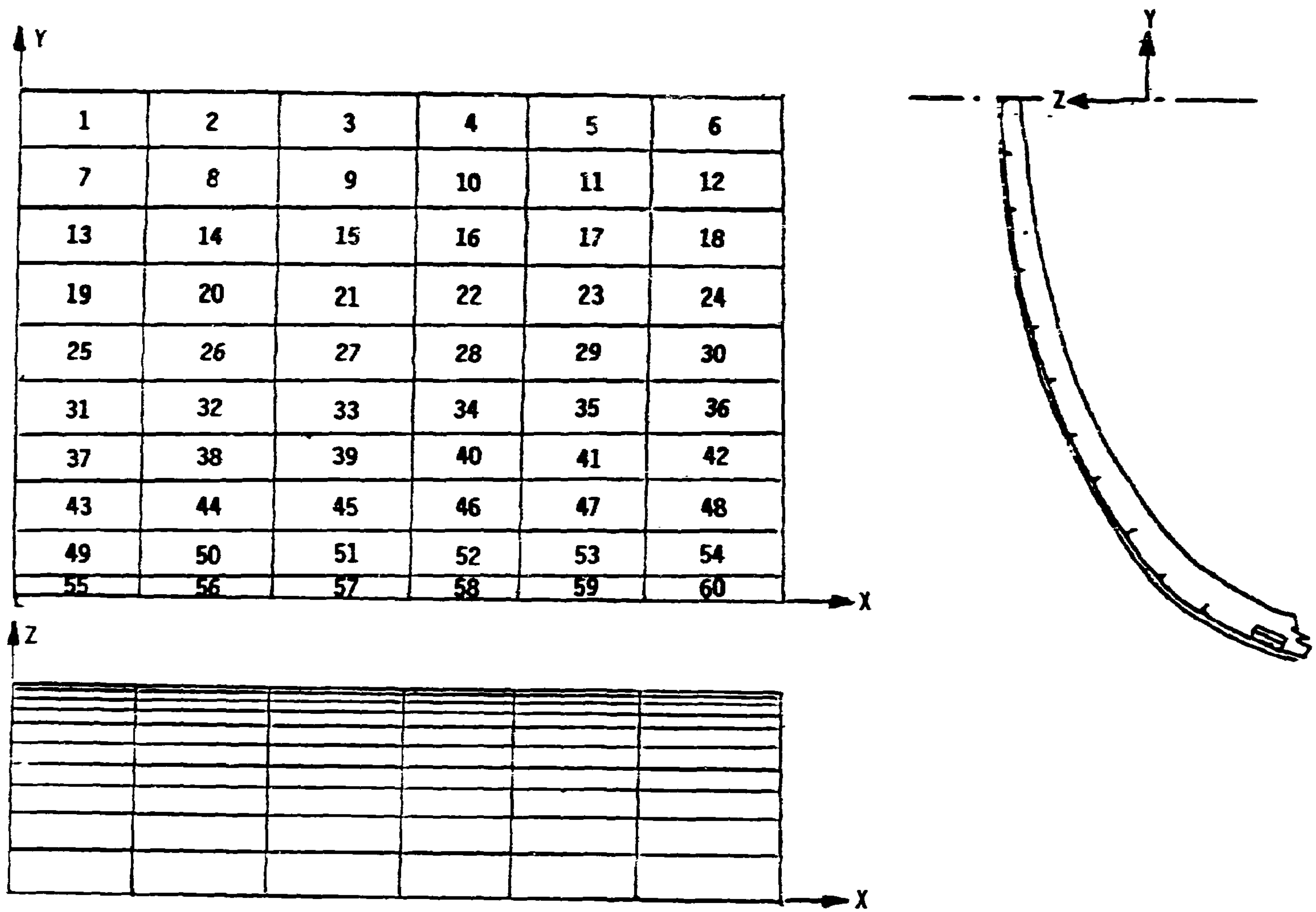

Figure 195. QSRA Fuselage Structure Model Plate Elements

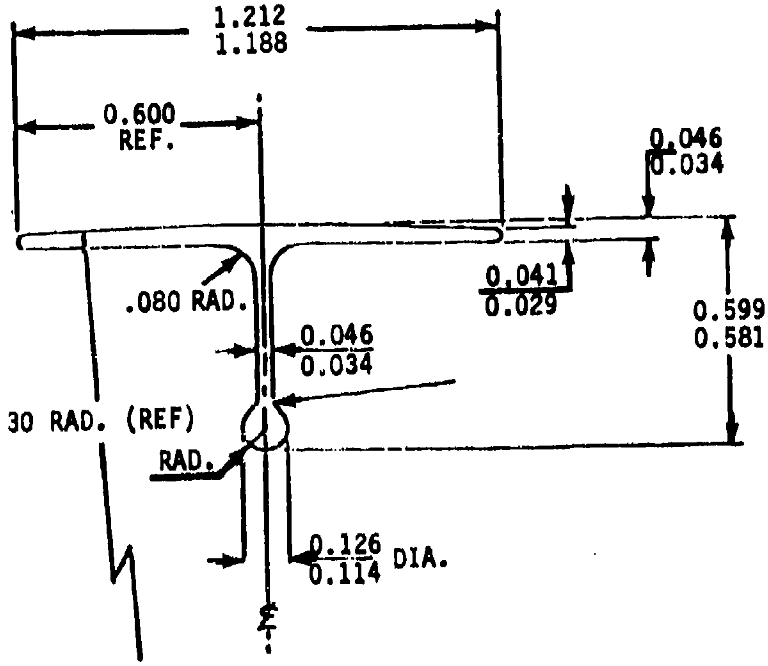

ACTUAL SIZE

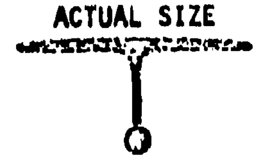

SCALE: TWICE SIZE
MATERIAL: AL ALLOY 2024-T4
SPECIFICATION: QQ-A-267 TEMPER T4

Figure 196. Skin Stringers for QSRA Fuselage Model

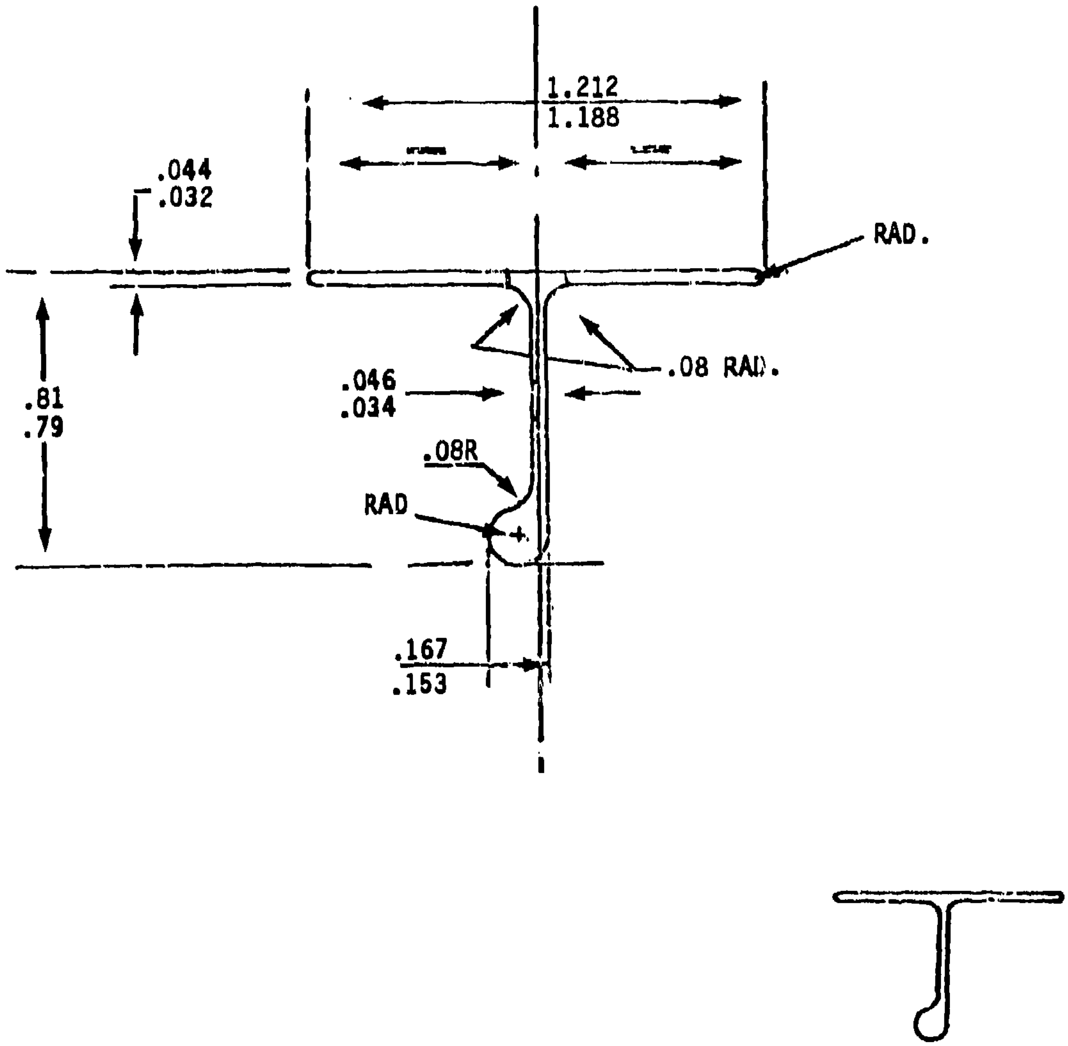

SCALE: TWICE SIZE

MATERIAL: AL. ALLOY 2024-T4

SPECIFICATION: QQ-A-267 TEMPER T4

Figure 197. Skin Stringer for QSRA Fuselage Model

1A STRINGERS 1 THROUGH 5

1B STRINGERS 6 THROUGH 10

GEOM.	ELEMENT	MATERIAL	A_{AX}	AS_2	AS_3	J	I_2	I_3	t_{EQ}	P
1 A/B	STRINGER	AL	.072 / .102	.048 / .048	.024 / .054	3×10^{-5} / 5×10^{-5}	.0060 / .0040	.0058 / .0058	—	—
2	FRAME	AL	.320	.128	.192	.0001	1.728	.0213	—	—
3	SKIN PANEL (BONDED)	AL & HONEYCOMB	—	—	—	—	—	—	.064	—

Figure 198. Values for QSRA Fuselage Model

MODE NUMBER	CIRCULAR FREQUENCY (RAD/SEC)	FREQUENCY (CYCLES/SEC)	PERIOD (SEC)	TOLERANCE
1	1.0379E+03	1.6518E+02	.00605	6.9168E-15
2	1.7352E+03	2.7616E+02	.00362	9.8986E-15
3	1.7906E+03	2.8498E+02	.00351	4.6508E-15
4	2.1008E+03	3.3436E+02	.00299	0.
5	2.1818E+03	3.4724E+02	.00288	1.8783E-14
6	2.1925E+03	3.4894E+02	.00287	1.8599E-14
7	2.2558E+03	3.5902E+02	.00279	1.7570E-14
8	2.5219E+03	4.0137E+02	.00249	9.3718E-15
9	2.6281E+03	4.1827E+02	.00239	1.2945E-14
10	2.7109E+03	4.3145E+02	.00232	3.6498E-14
11	2.7746E+03	4.4159E+02	.00226	1.1614E-14
12	2.8942E+03	4.6062E+02	.00217	7.1158E-15
13	3.4452E+03	5.4833E+02	.00182	1.5065E-14
14	4.2255E+03	6.7251E+02	.00149	5.1978E-10
15	4.4347E+03	7.0581E+02	.00142	5.1598E-09
16	4.5100E+03	7.1779E+02	.00139	1.6054E-09
17	4.6202E+03	7.3532E+02	.00136	1.2061E-07
18	4.6772E+03	7.4439E+02	.00134	2.2859E-06
19	4.6994E+03	7.4801E+02	.00134	1.0639E-10
20	4.7799E+03	7.6074E+02	.00131	8.0063E-07

UPPER BOUNDS ON EIGENVALUE CLUSTERS

.10879365150396E+07	.30408742393295E+07	.32360424194540E+07
.64235878049331E+07	.69758364376031E+07	.74224949712489E+07
.16033196442174E+08	.19863381525223E+08	.20543841357851E+08

Figure 199. Print of Frequencies for QSRA Fuselage Model

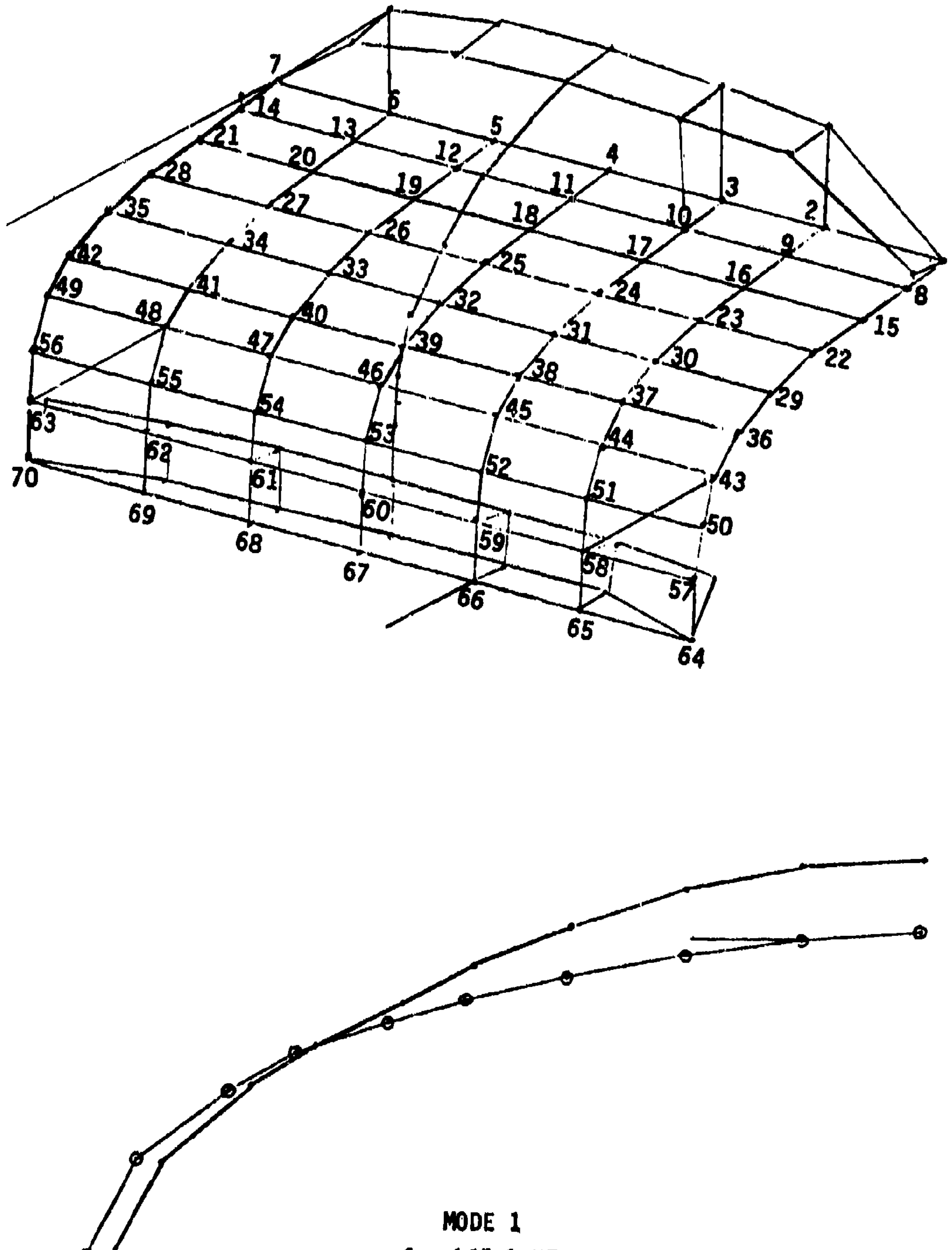

MODE 1
f = 165.1 HZ

Figure 200. QSRA Fuselage Modal Plot

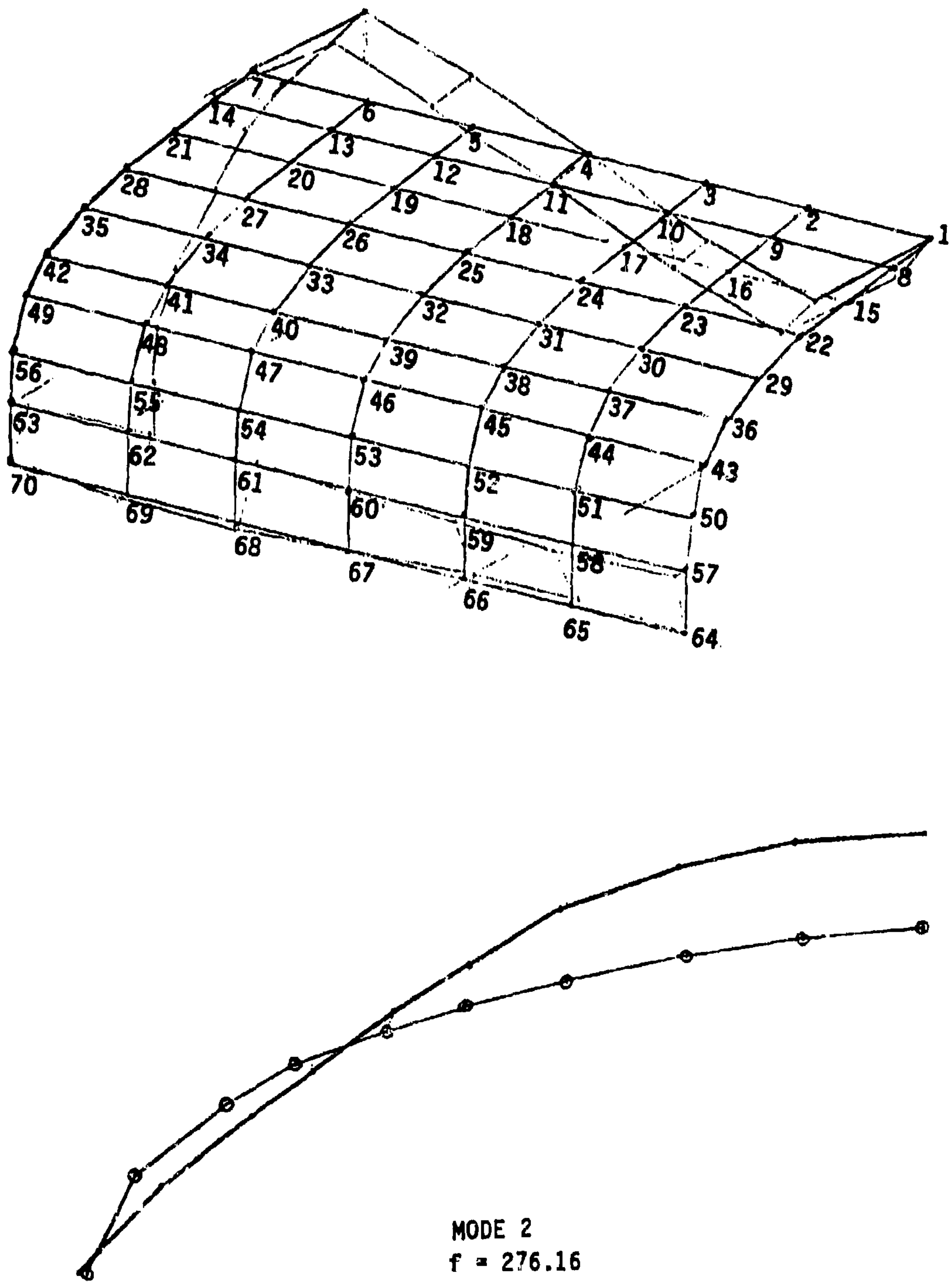

Figure 201. QSRA Fuselage Modal Plot

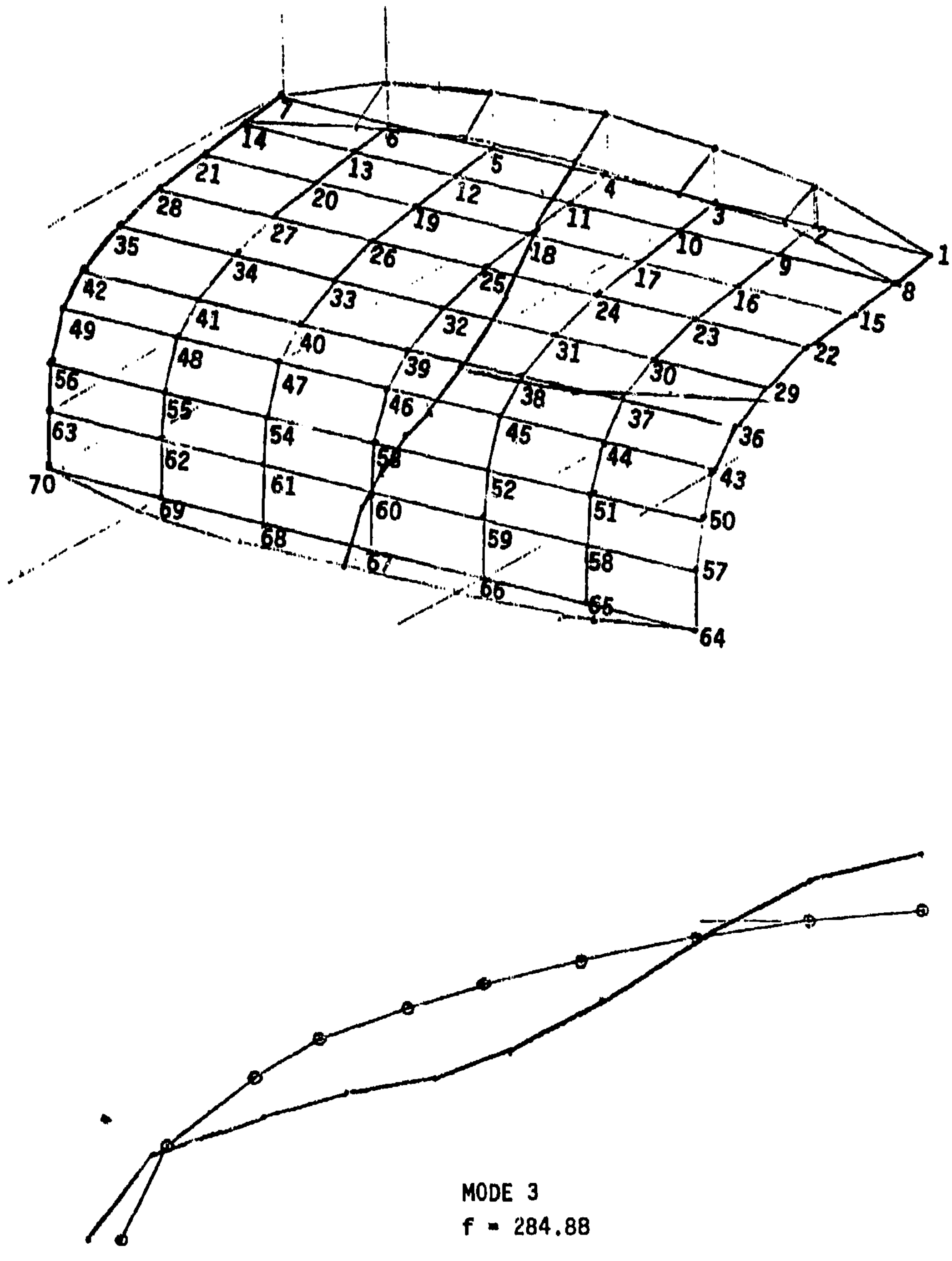

Figure 202. QSRA Fuselage Modal Plot

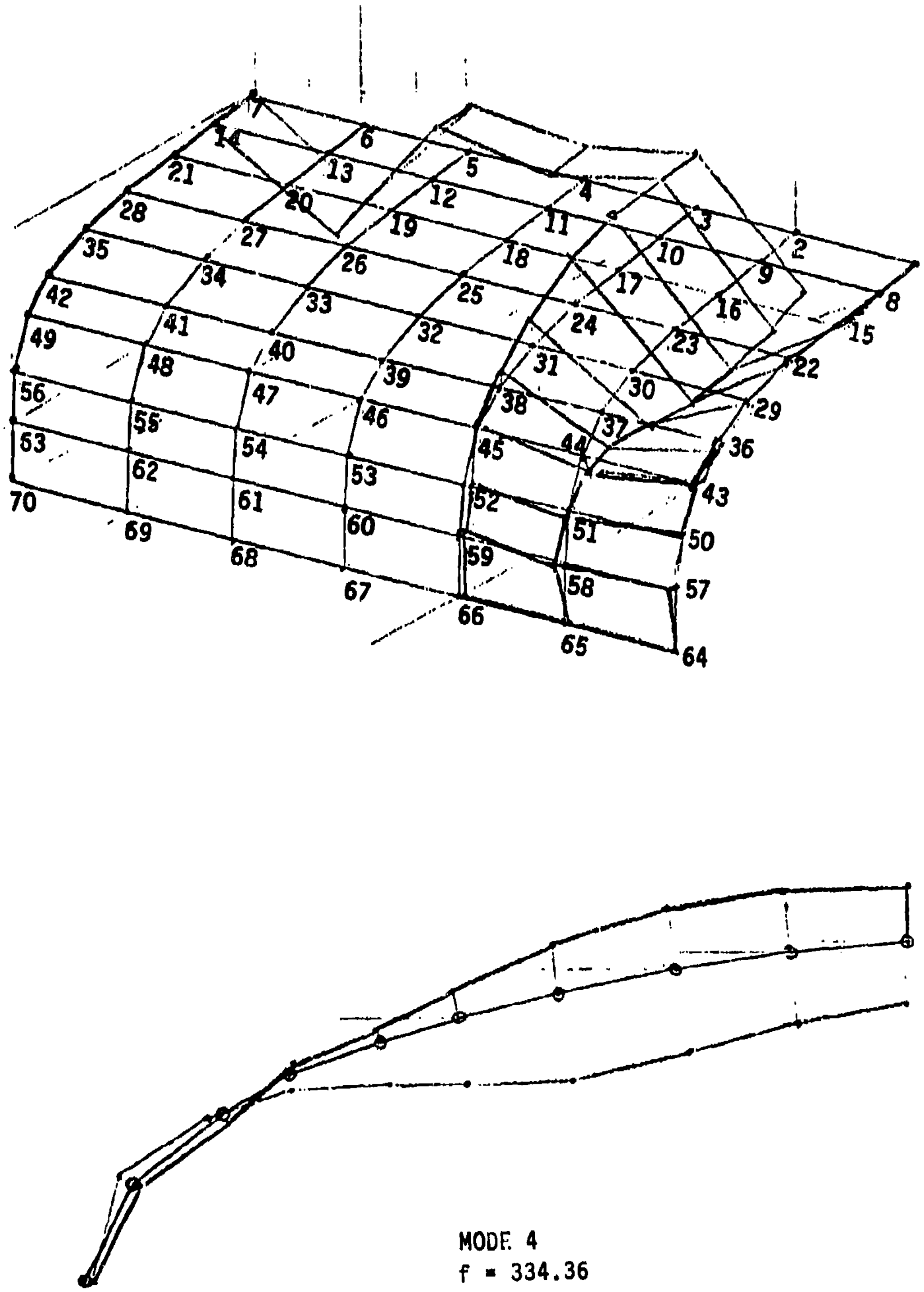

Figure 203. QSRA Fuselage Modal Plot

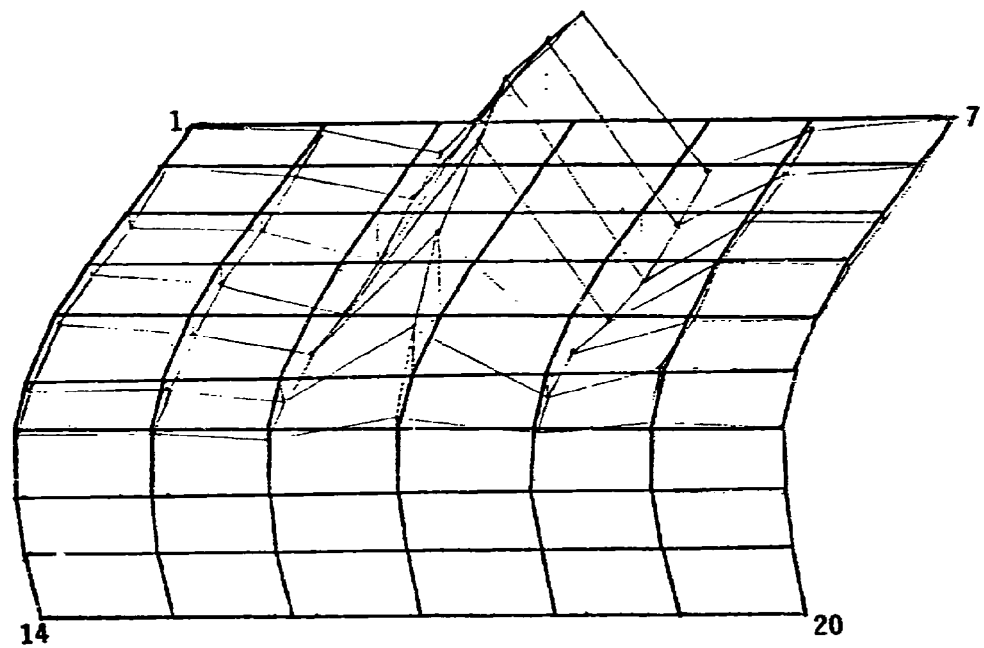

Figure 204. QSRA Fuselage Modal Plot
Mode 5
f = 347.24 Hz.

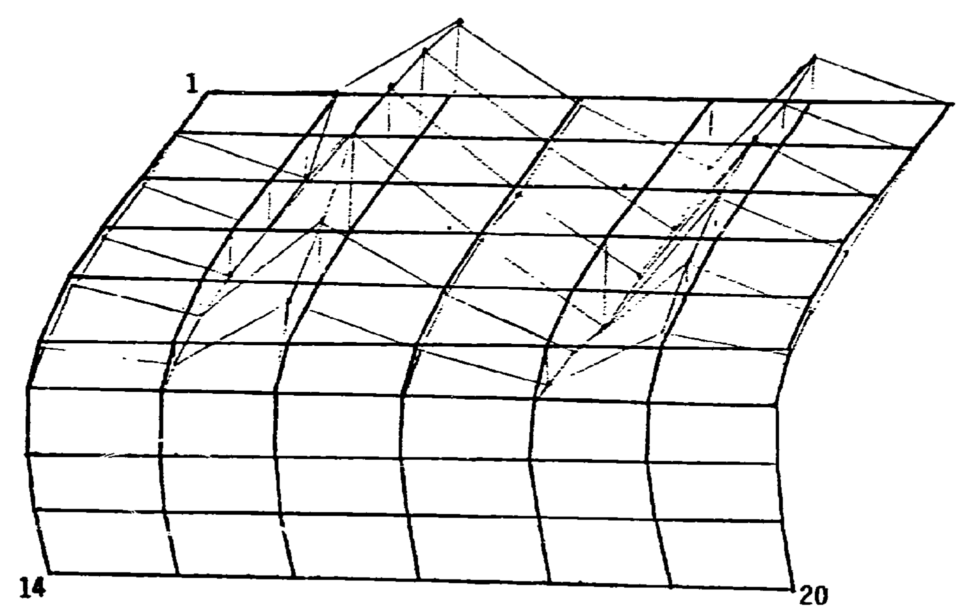

Figure 205. QSRA Fuselage Modal Plot
Mode 6
f = 348.94 Hz.

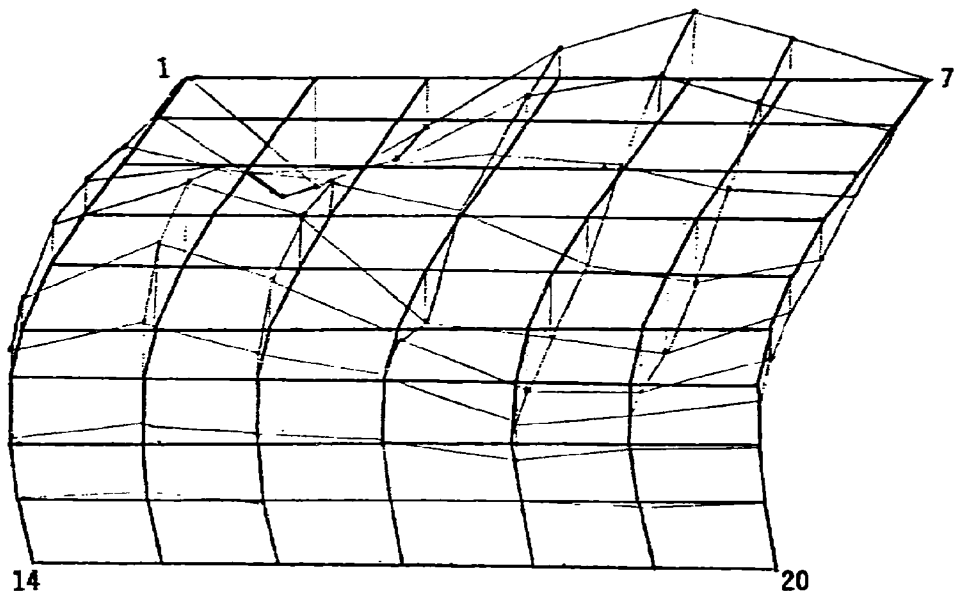

Figure 206. QSRA Fuselage Modal Plot
Mode 7
f = 359.02 Hz.

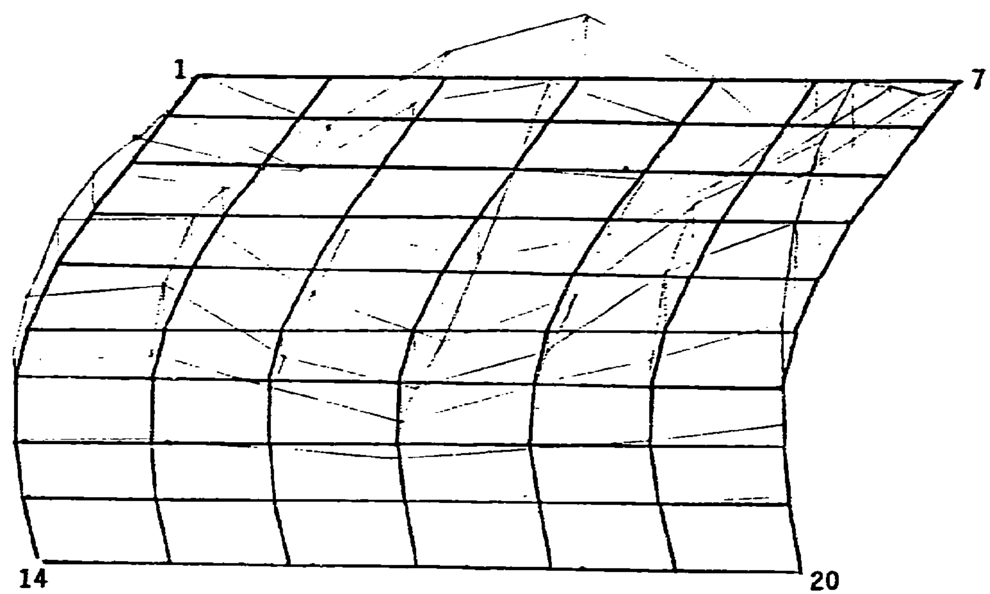

Figure 207. QSRA Fuselage Modal Plot
Mode 8
f = 401.37 Hz.

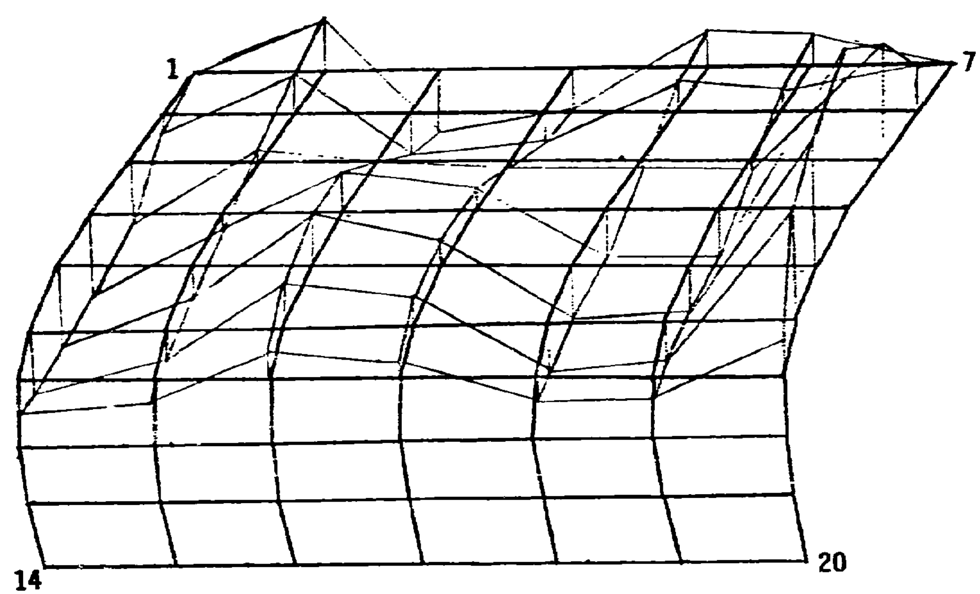

Figure 208. QSRA Fuselage Modal Plot
Mode 9
f = 418.27 Hz.

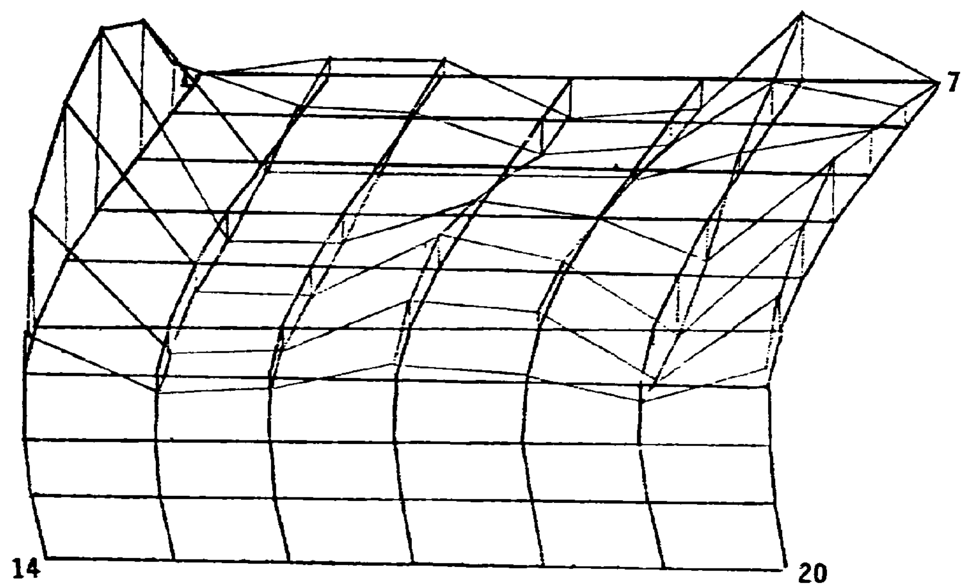

Figure 209. QSRA Fuselage Modal Plot
Mode 10
f = 431.45 Hz.

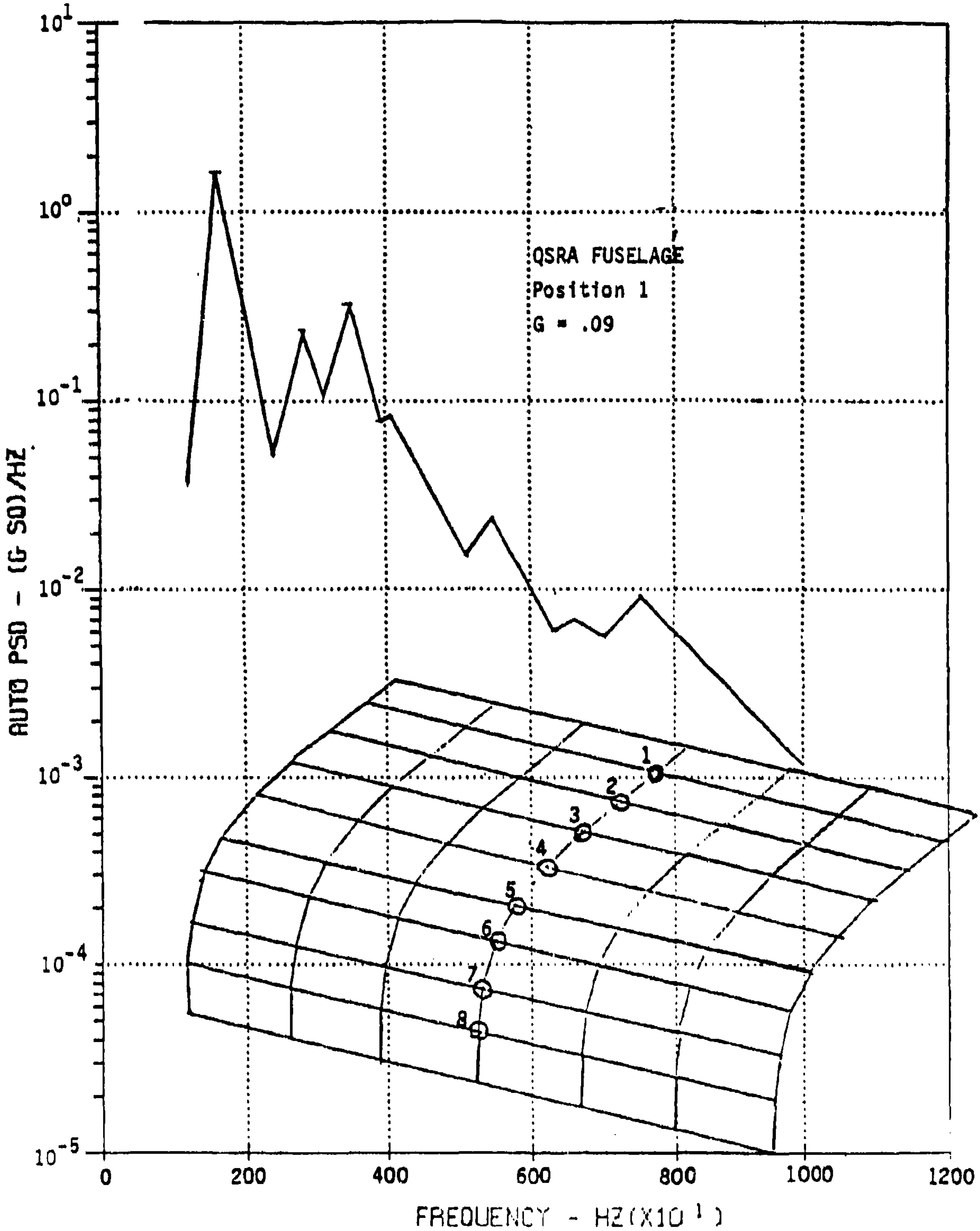

Figure 210. PSD Plot of QSRA Fuselage, Position 1

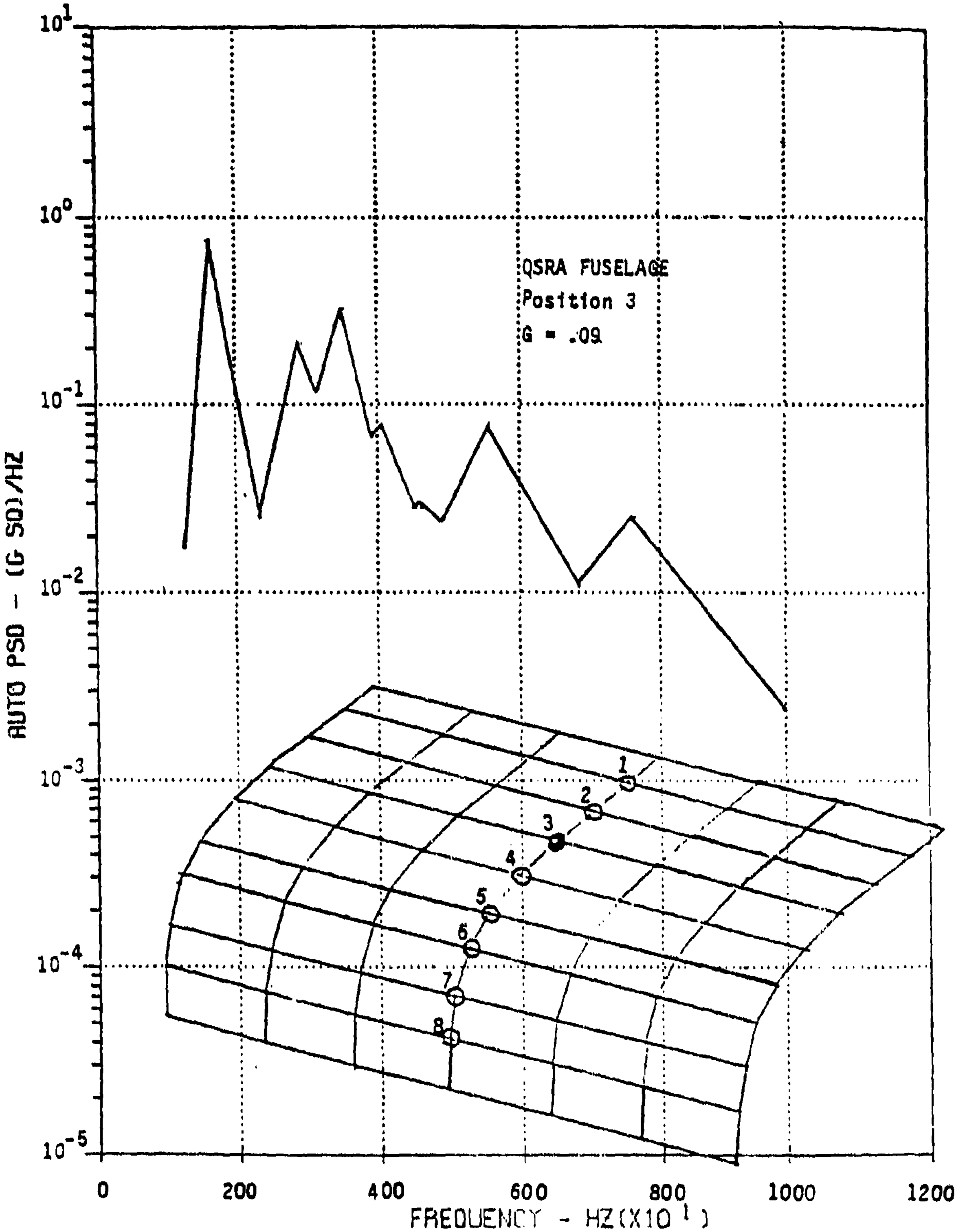

Figure 211. PSD Plot of QSRA Fuselage, Position 3

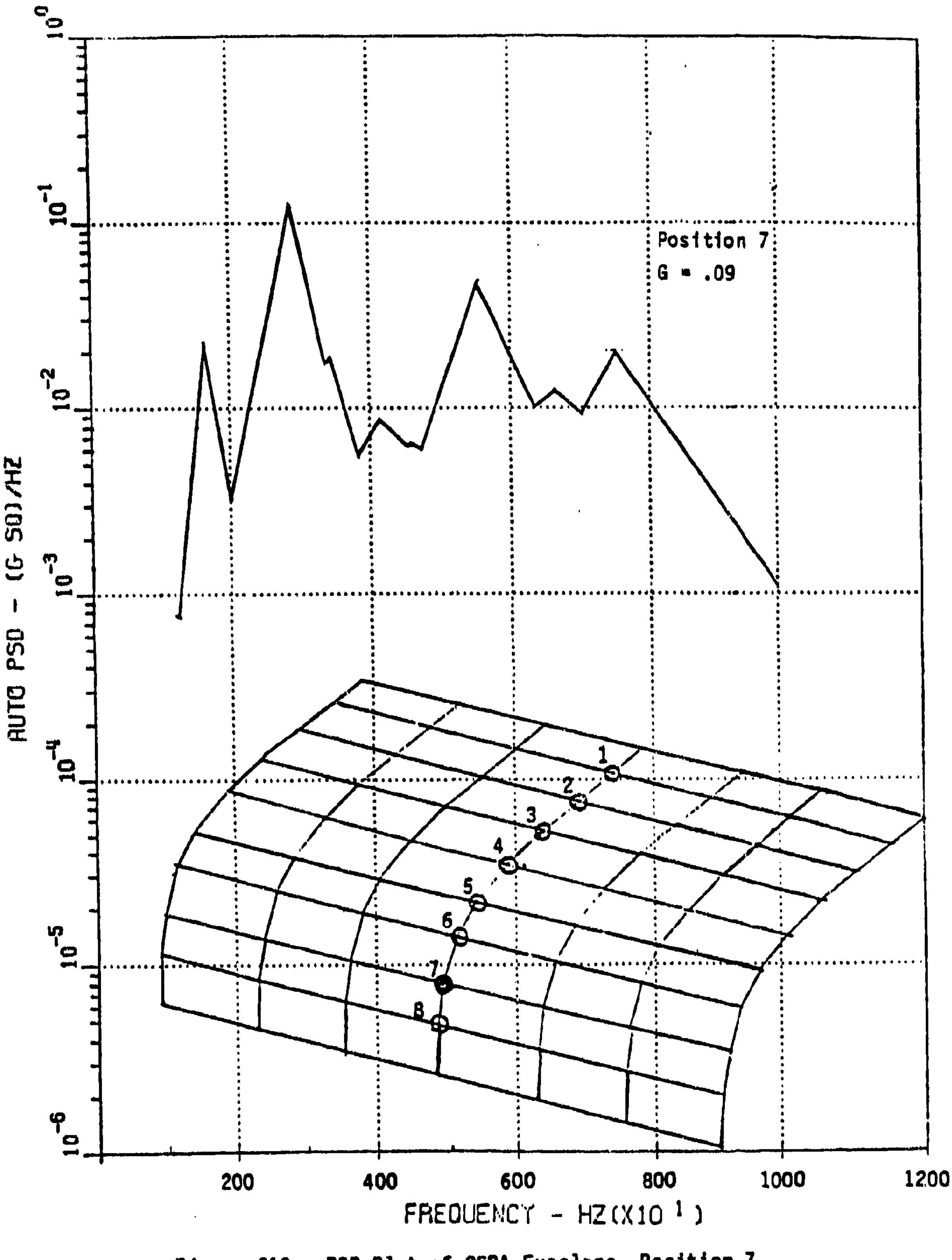

Figure 212. PSD Plot of QSRA Fuselage, Position 7

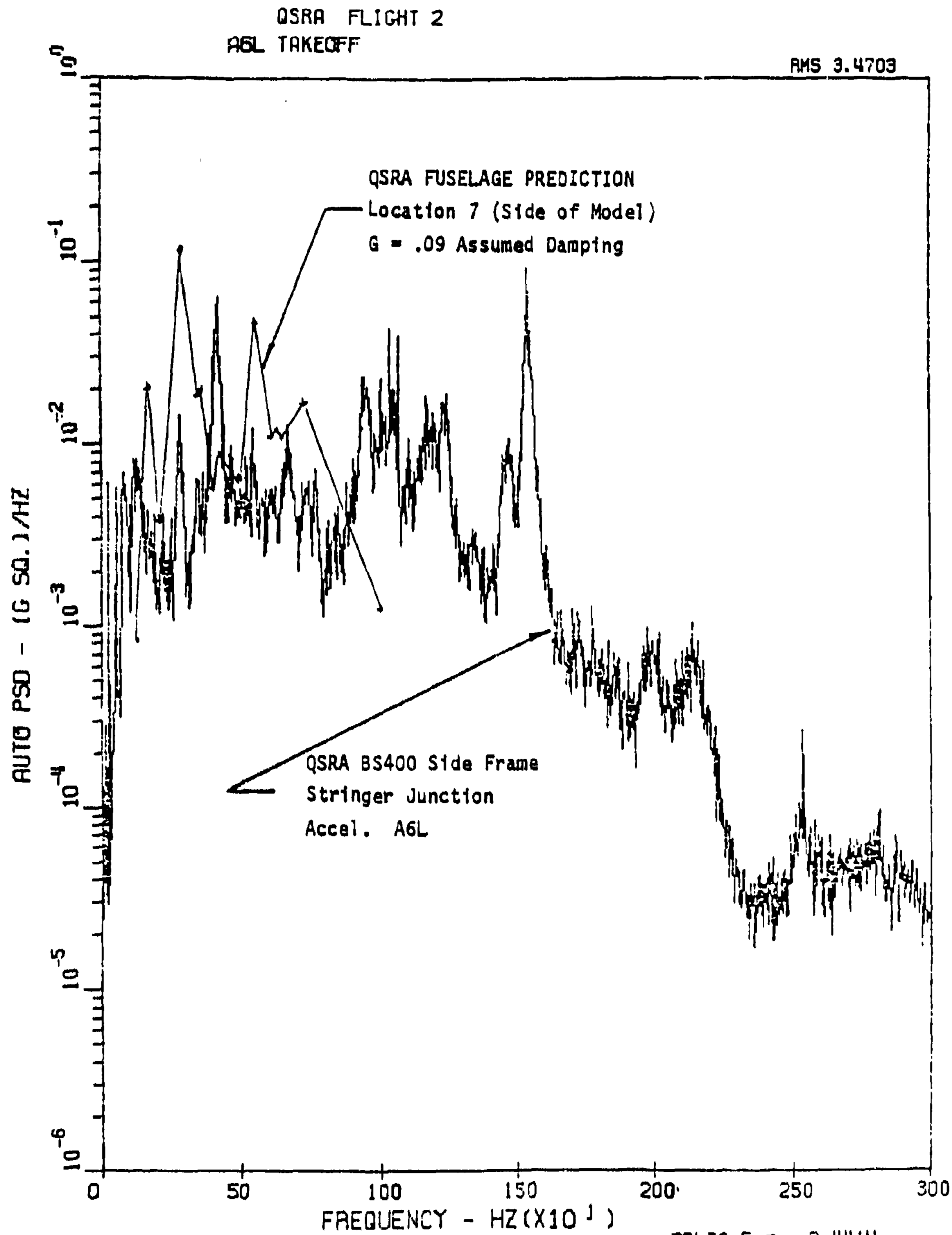

Figure 213. Comparison of QSRA Fuselage Response with Predicted Values, Location 7

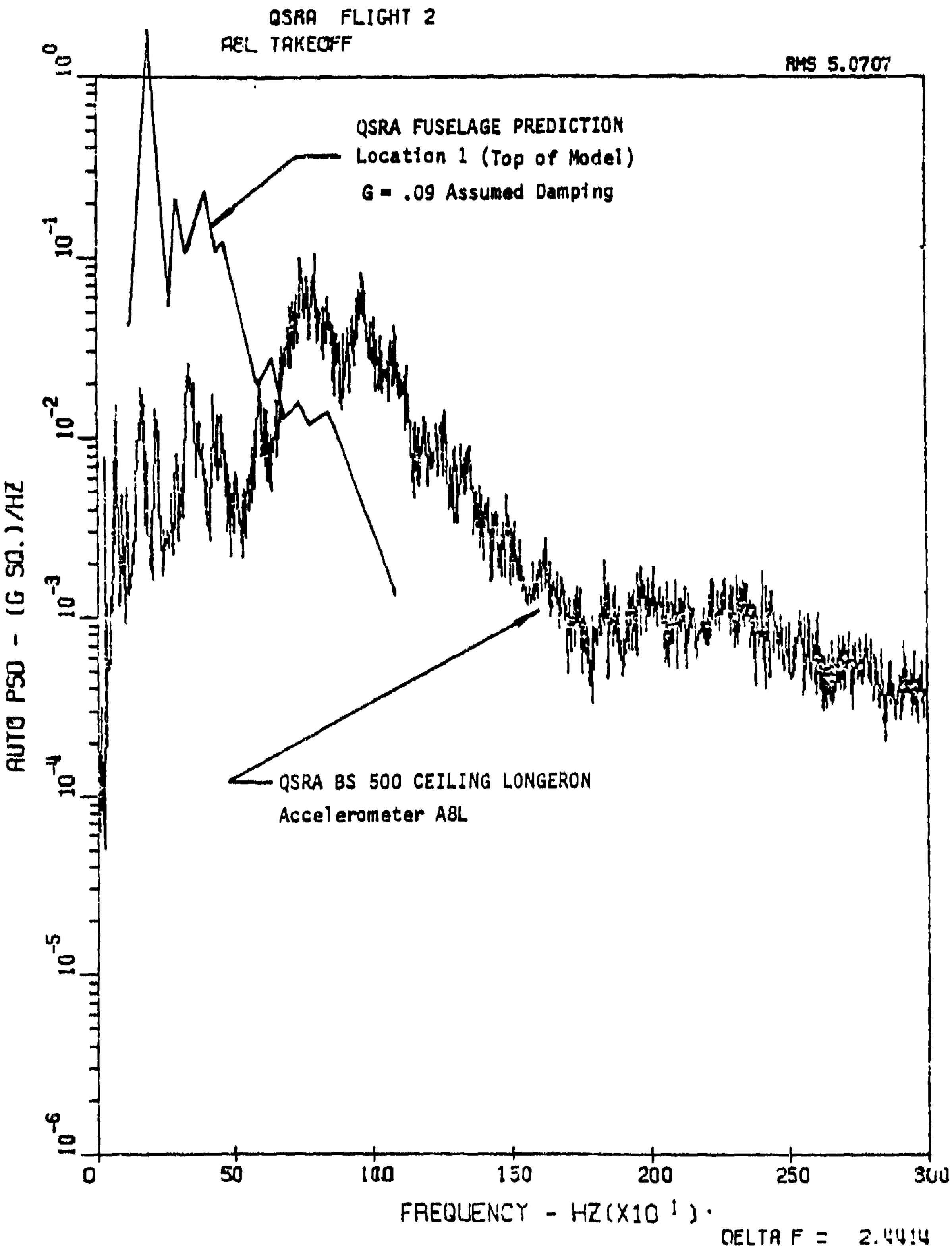

Figure 214. Comparison of QSRA Fuselage Response with Predicted Values, Location 1

MODE NUMBER	CIRCULAR FREQUENCIES (RAD/SEC)	FREQUENCY (CYCLES/SEC)	PERIOD (SEC)	TOLERANCE
1	3.6872E+02	5.8683E+01	.01704	6.8504E-15
2	6.6913E+02	1.0649E+02	.00939	8.3204E-15
3	7.4792E+02	1.1904E+02	.00840	6.6596E-15
4	9.0907E+02	1.4468E+02	.00691	9.0156E-15
5	9.1744E+02	1.4602E+02	.00685	2.2130E-14
6	9.6984E+02	1.5435E+02	.00648	0.
7	9.9956E+02	1.5908E+02	.00629	7.4572E-15
8	1.0572E+03	1.6826E+02	.00594	6.6662E-15
9	1.1775E+03	1.8741E+02	.00534	1.0747E-14
10	1.5061E+03	2.3970E+02	.00417	4.9599E-12
11	1.6294E+03	2.5933E+02	.00386	1.1168E-10
12	1.6450E+03	2.6181E+02	.00382	2.1294E-11
13	1.6846E+03	2.6811E+02	.00373	1.2010E-10
14	1.7498E+03	2.7842E+02	.00359	1.1820E-09
15	1.8074E+03	2.8765E+02	.00348	4.1996E-10
16	1.9543E+03	3.1104E+02	.00321	1.6936E-09
17	2.0475E+03	3.2587E+02	.00307	6.6344E-07
18	2.2130E+03	3.5221E+02	.00284	1.1237E-07
19	2.2646E+03	3.6042E+02	.00277	3.5902E-06
20	2.3190E+03	3.6908E+02	.00271	2.1697E-06

UPPER BOUNDS ON EIGENVALUE CLUSTERS

.13731046886417E+06	.45220743032504E+06	.56498229346720E+06
.11288442288671E+07	.14004374755522E+07	.22909381740913E+07
.32992792149974E+07	.38576710319038E+07	.42340561342655E+07

Figure 215. Print of Frequencies for Large STOL Airplane Fuselage Model

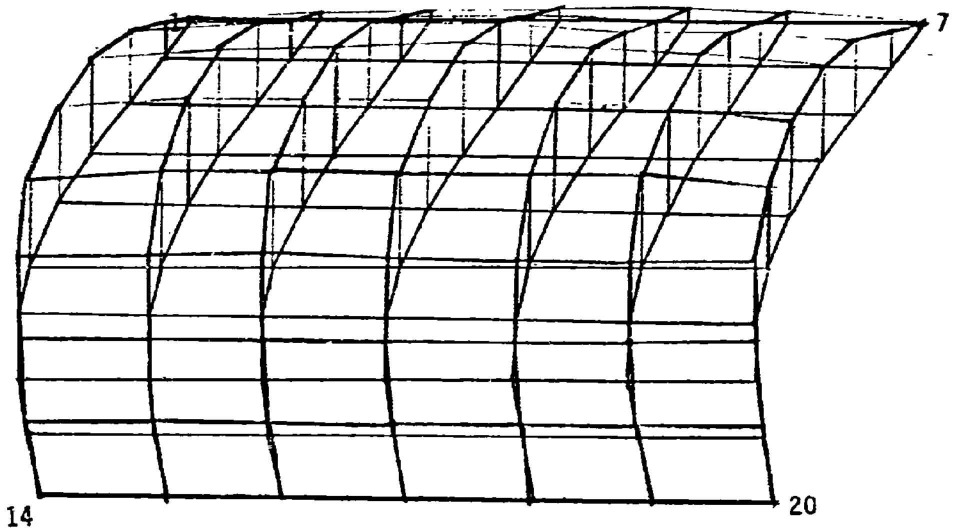

Figure 216. Large STOL Fuselage Modal Plot
Mode 1 f = 58.68 Hz.

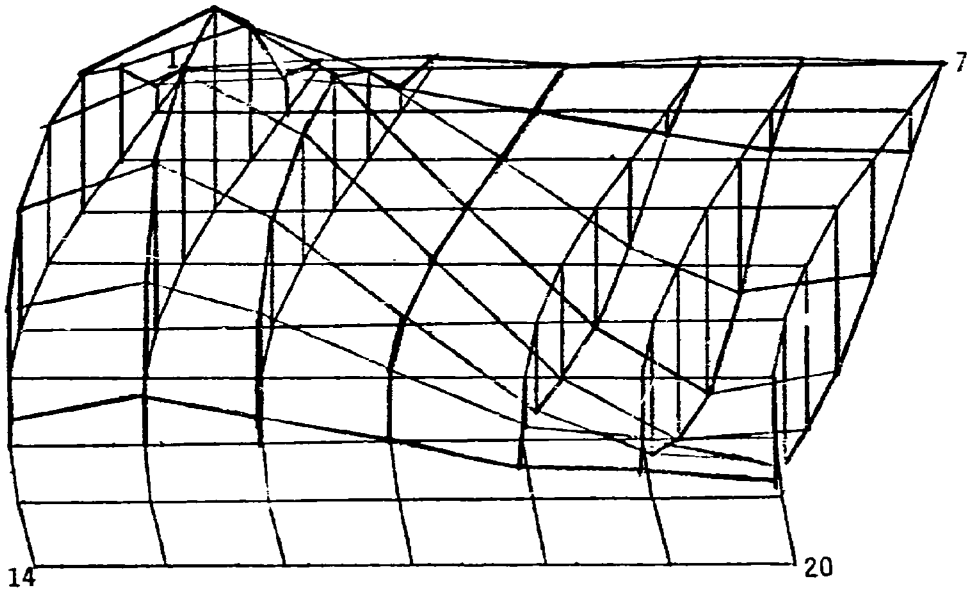

Figure 217. Large STOL Fuselage Modal Plot
Mode 2 f = 106.49 Hz.

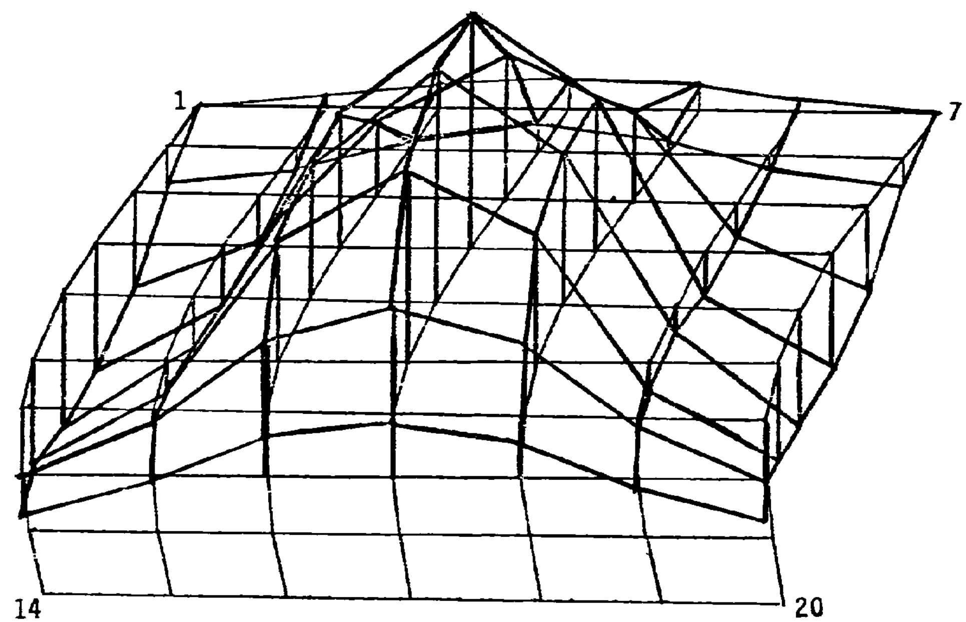

Figure 218. Large STOL Fuselage Modal Plot
Mode 3 f = 119.04 Hz.

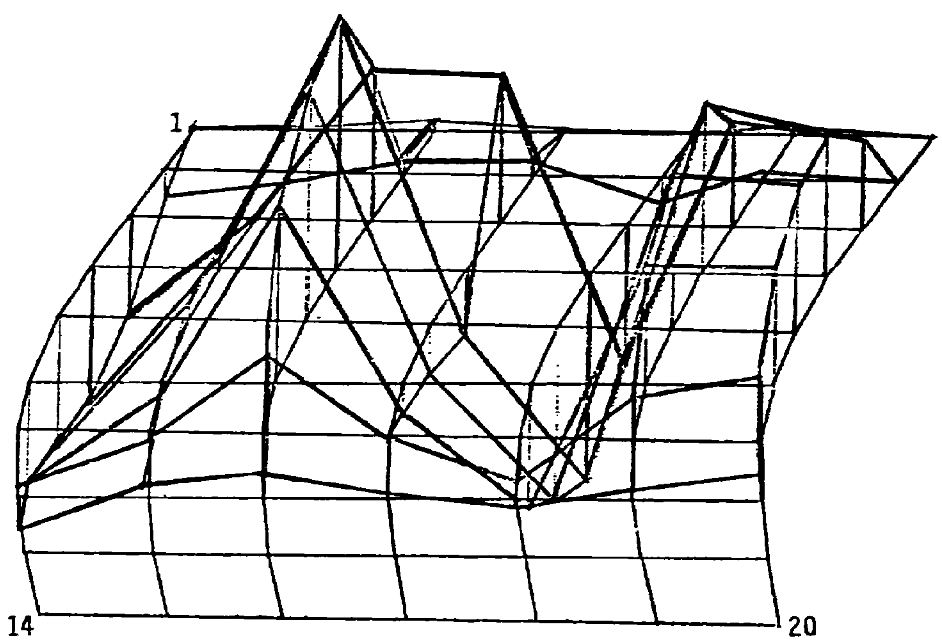

Figure 219. Large STOL Fuselage Modal Plot
Mode 4 f = 144.68 Hz.

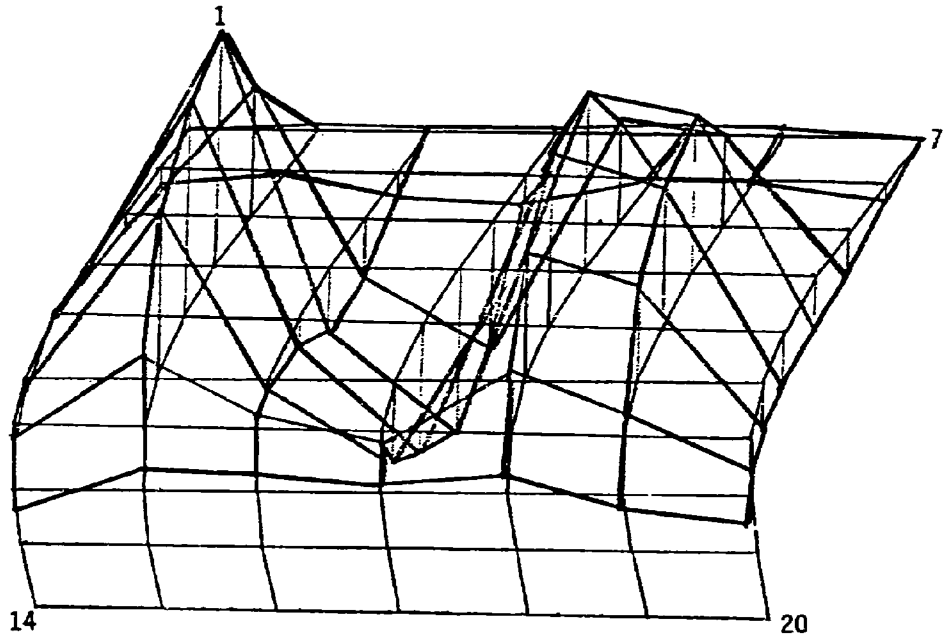

Figure 220. Large STOL Fuselage Modal Plot
Mode 5 f = 146.02 Hz.

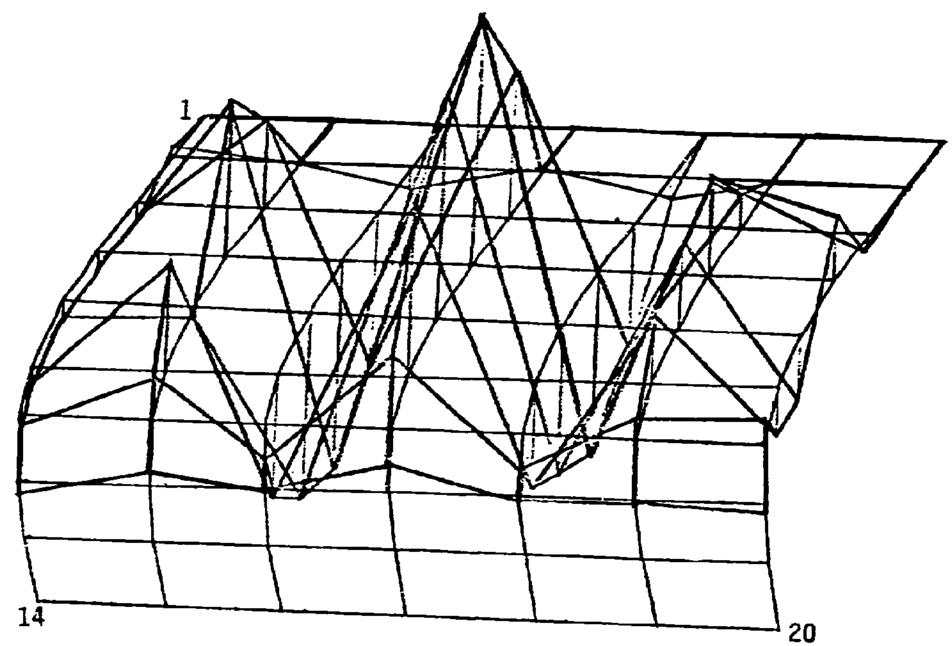

Figure 221. Large STOL Fuselage Modal Plot
Mode 6 f = 154.35 Hz.

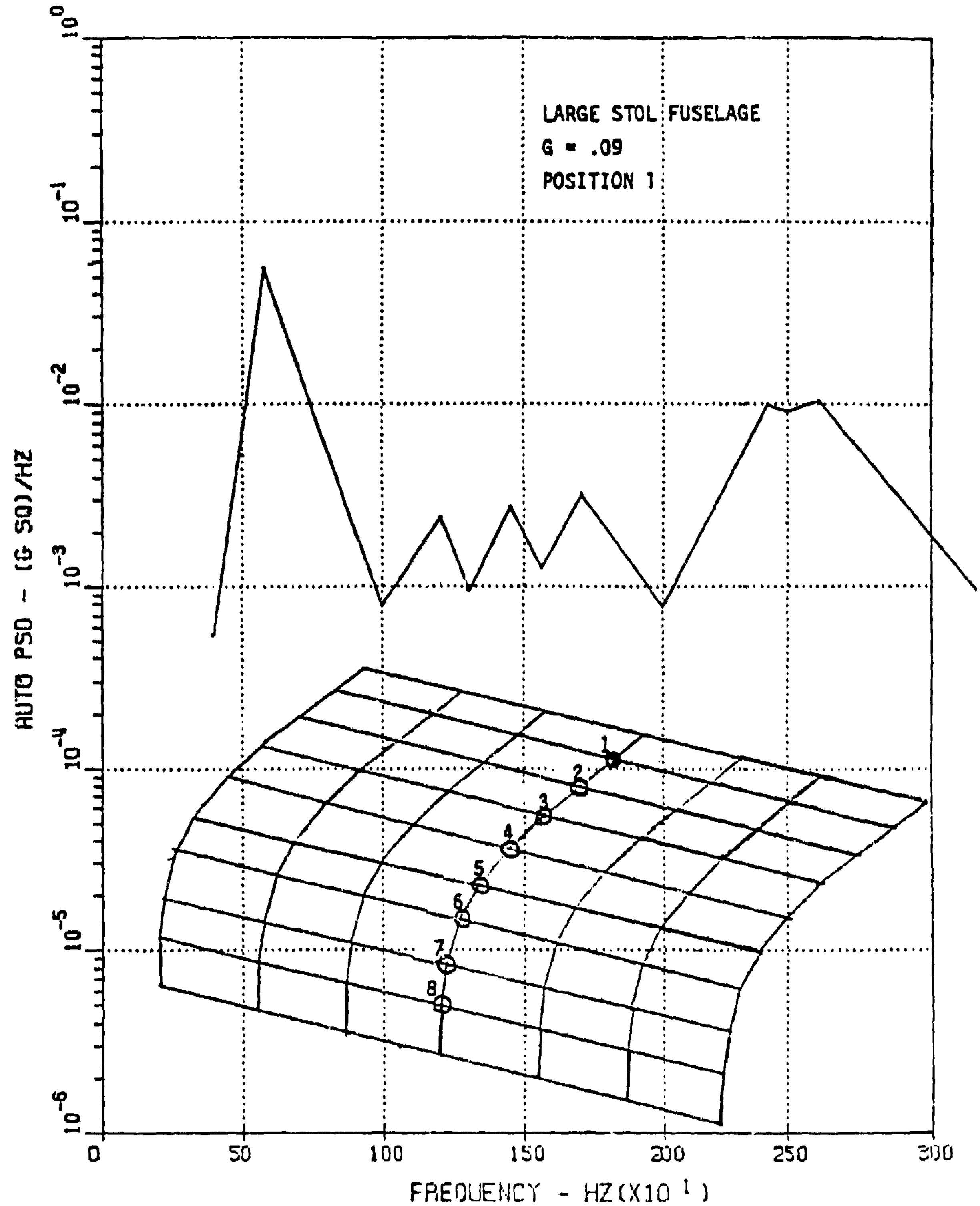

Figure 222. PSD Plot of Large STOL Airplane Fuselage, Position 1

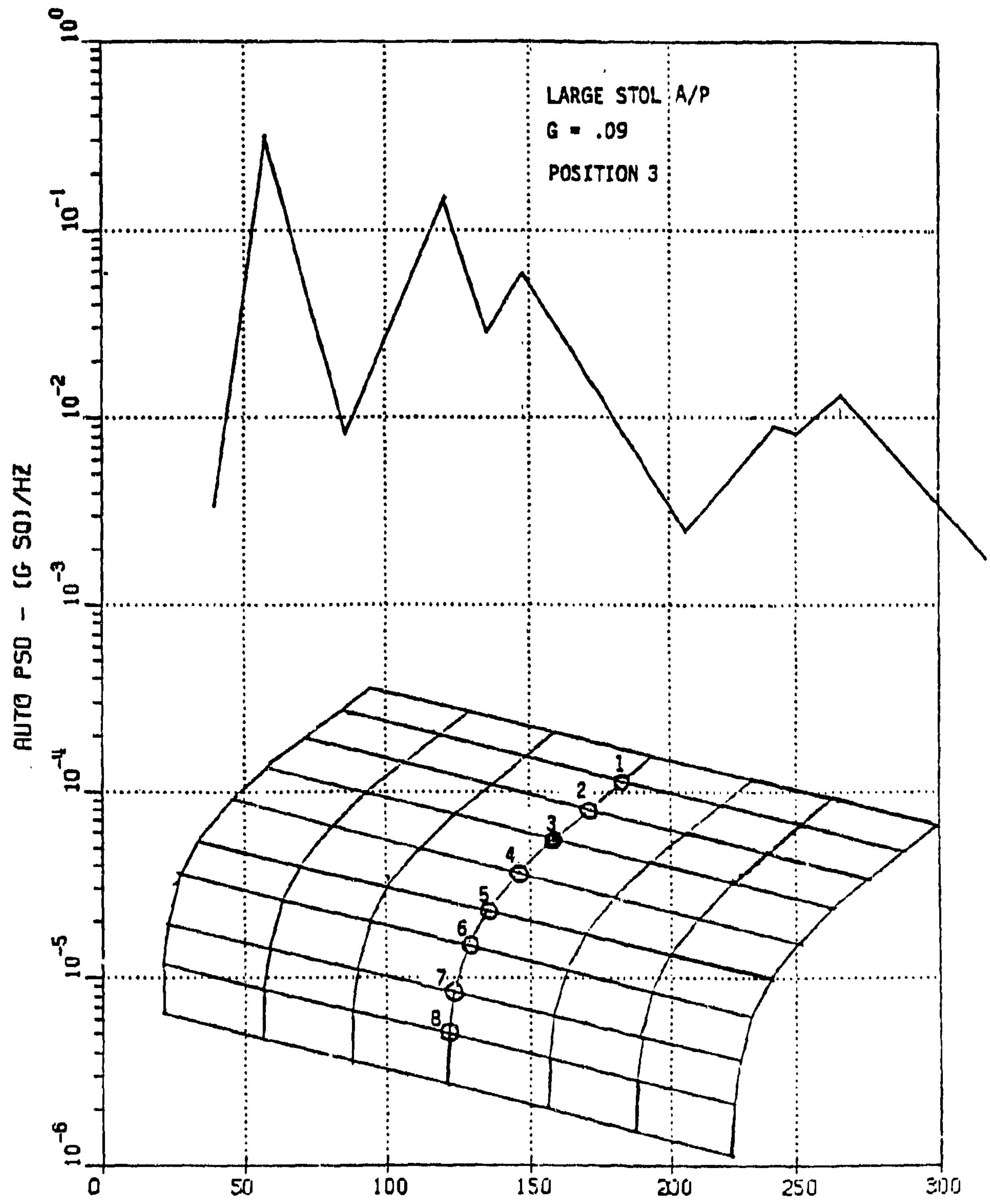

Figure 223. PSD Plot of Large STOL Airplane Fuselage, Position 3

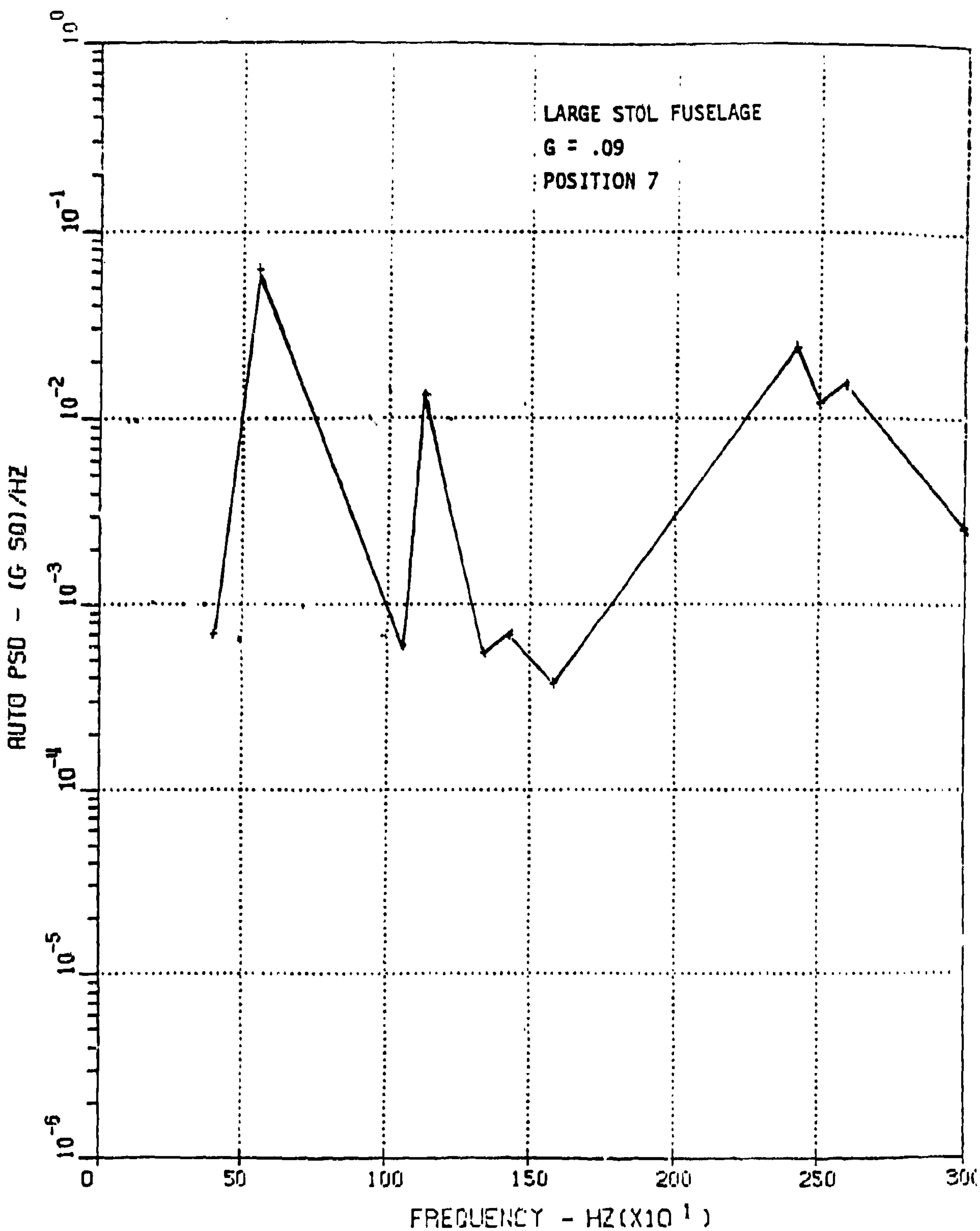

Figure 224. PSD Plot of Large STOL Airplane Fuselage, Position 7

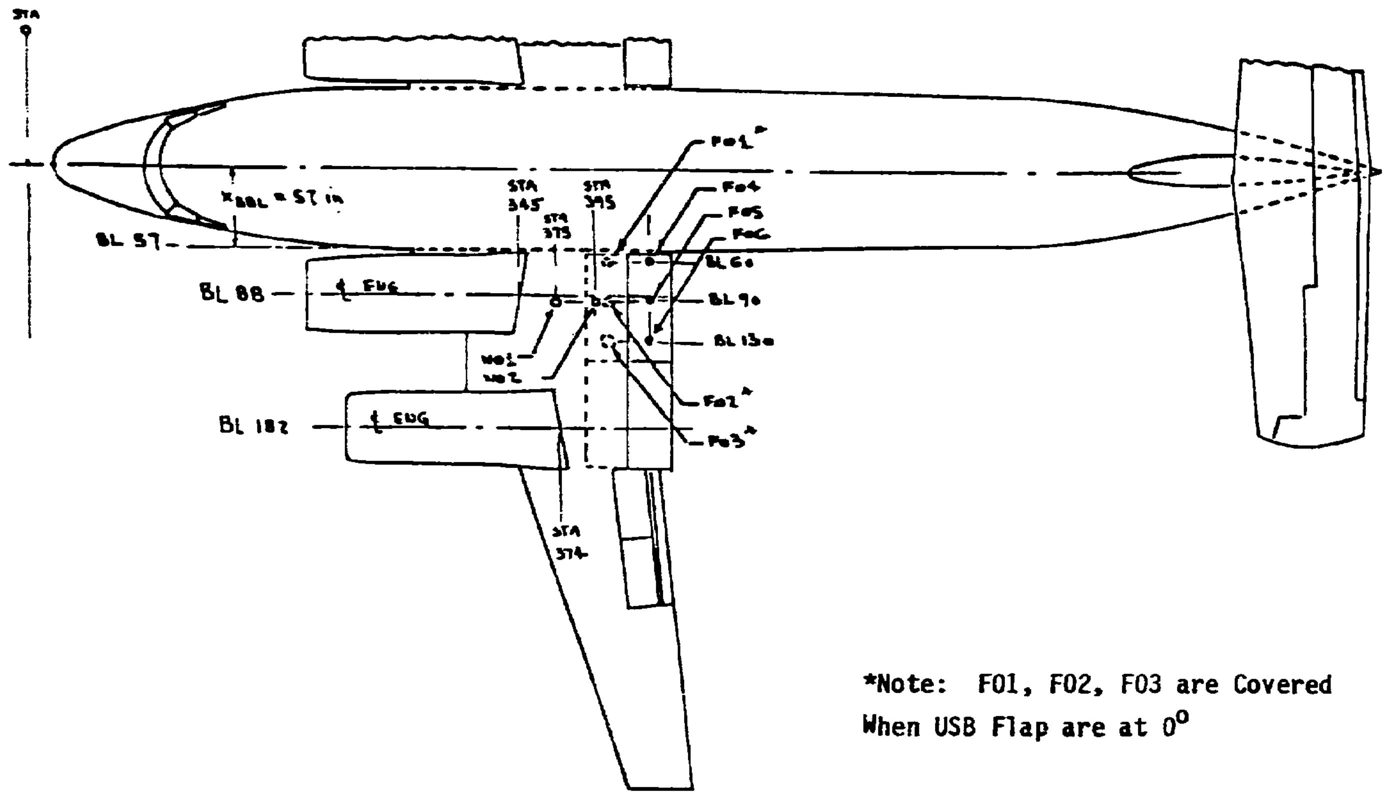

*Note: F01, F02, F03 are Covered
When USB Flap are at 0^{o}

Figure 225. QSRA Type Airplane - Top View -

Maximum Weight = 50,000 lbs

SLST = 4 x 7500 = 30,000 lbs

Length = 76.6 ft

Height to Top of Stabilizer = 27.8 ft

Height to Top of Wing = 17.75 ft

Dihedral = 0

Wing Area = 600 ft^2

Span = 73.5 ft

Horiz. Stab. Area = 232 ft^2

Vert Stab Area = 152 ft^2

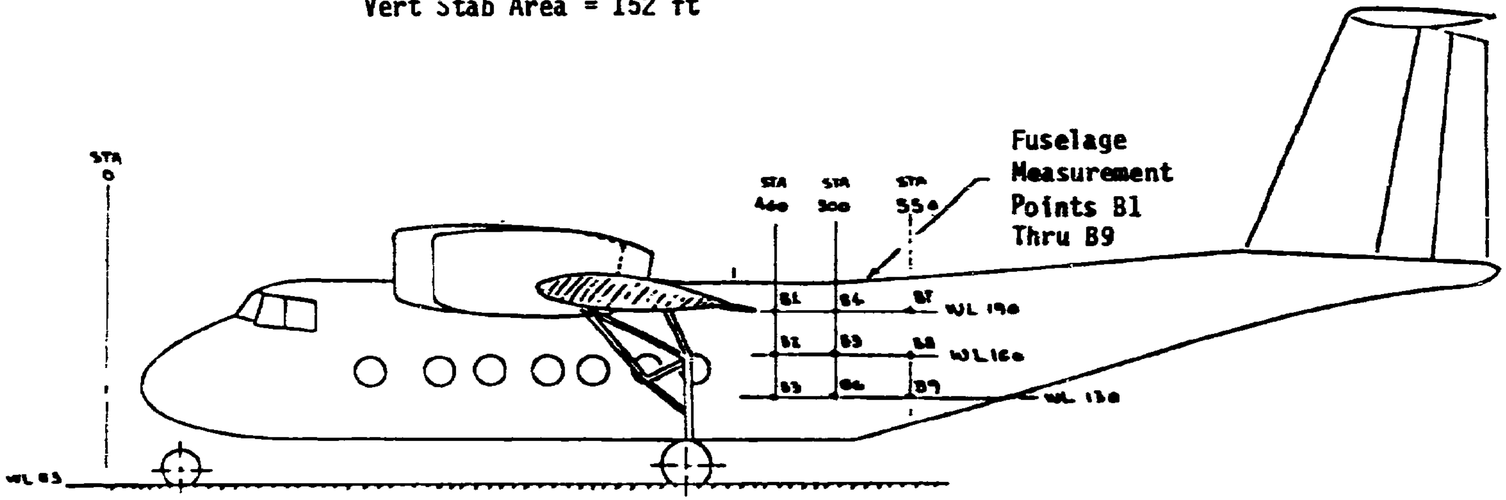

Figure 226. QSRA Type Airplane - Side View -

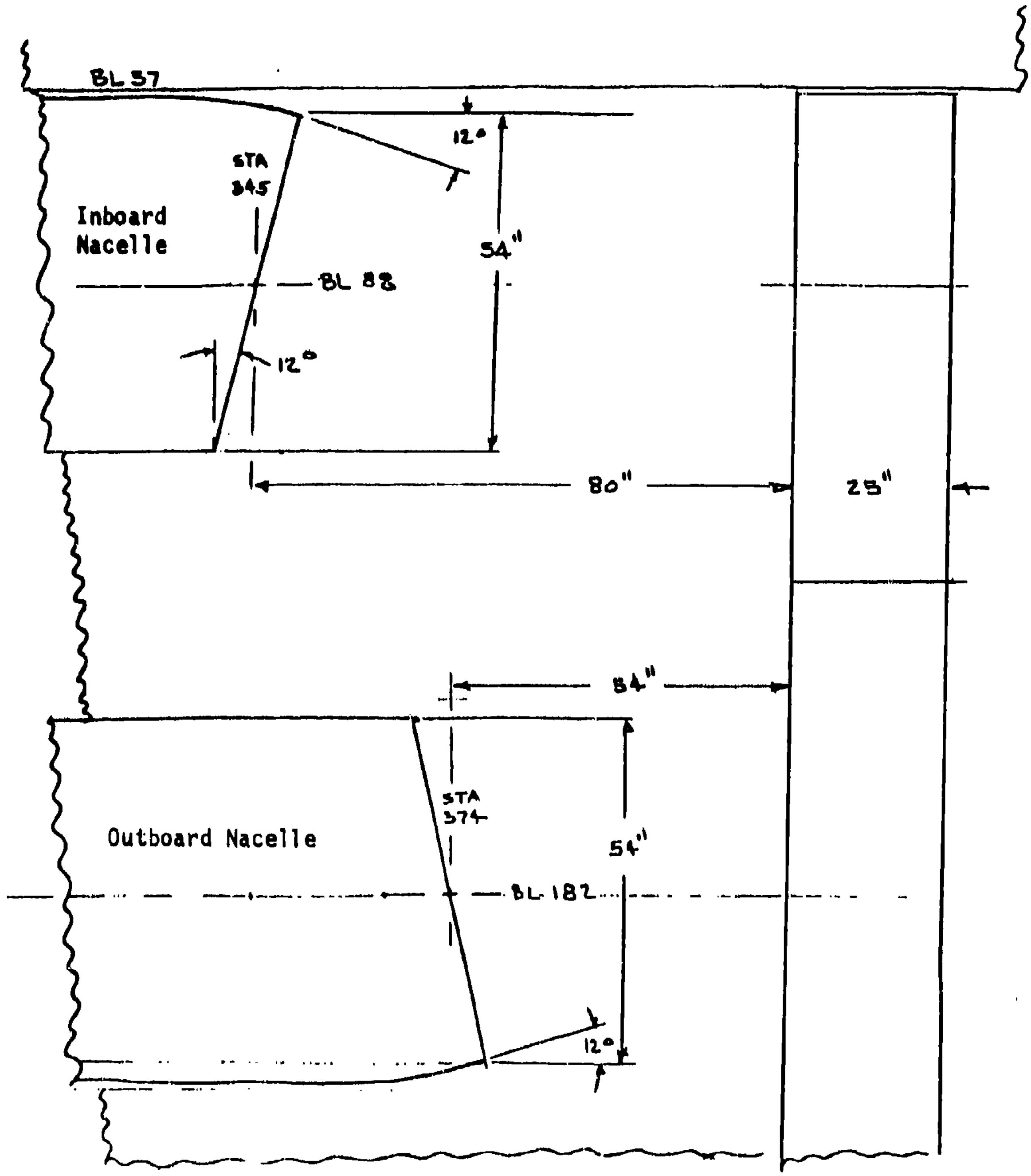

Note: Geometry Shown for USB Flaps at 0^{0}

Figure 227. QSRA Wing-Flap-Nacelle Geometry

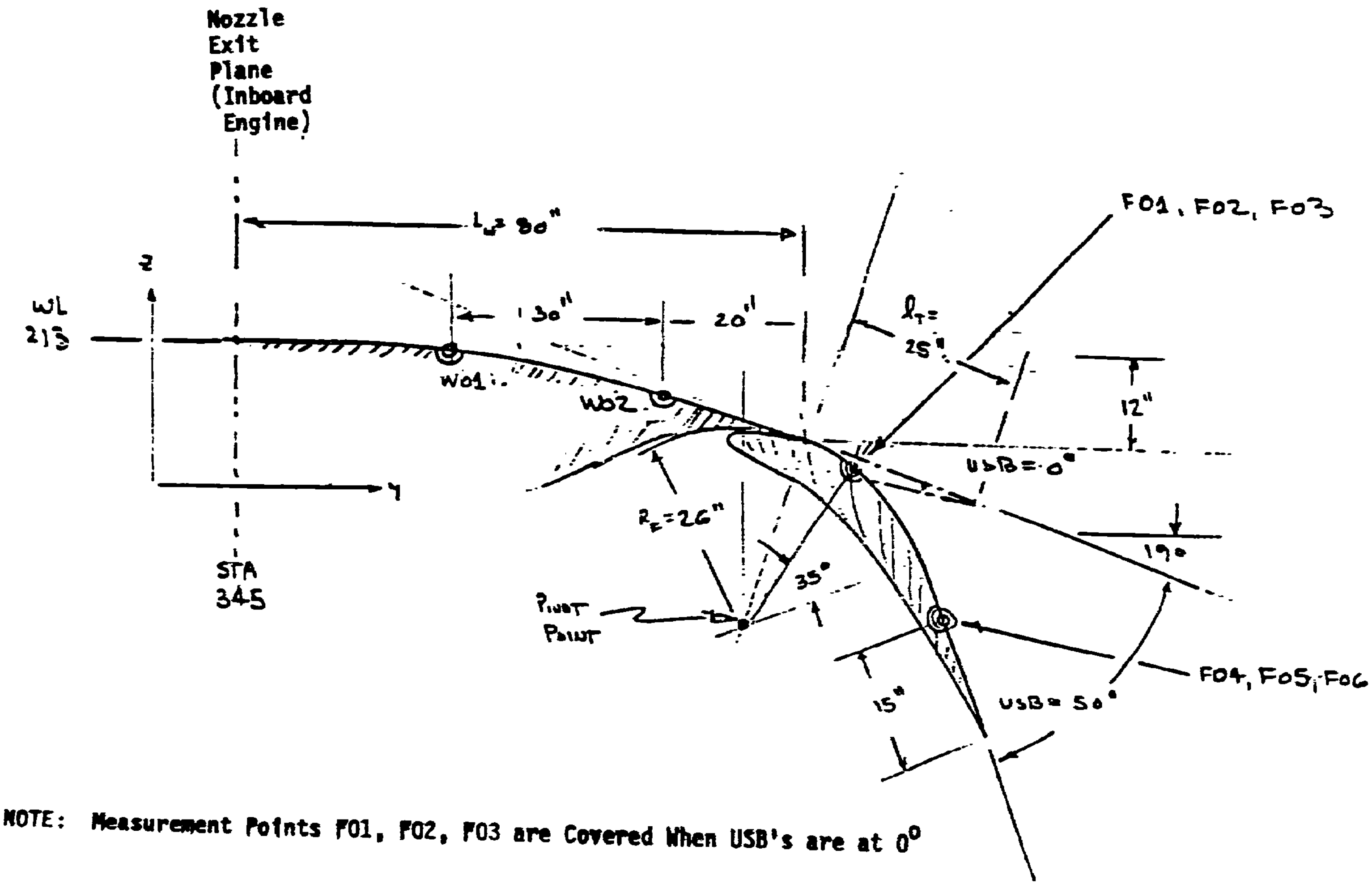

NOTE: Measurement Points F01, F02, F03 are Covered When USB's are at 0°

Figure 228. Side View-Wing/Flap Geometry (Inboard Engine)

POINT	STA	WL	BL
B01	460	190	57
B02	460	160	
B03	460	130	
B04	500	190	
B05	500	160	
B06	500	130	
B07	550	190	
B08	550	160	
B09	550	130	57

Figure 229. Body Measurement Locations

POINT	STA		WL		BL
	USB = 0^0	USB = 50^0	USB = 0^0	USB = 50^0	
F02	COVERED	432	COVERED	199	60
F01	COVERED	432	COVERED	199	90
F03	COVERED	432	COVERED	199	130
F04	433	445	199	177	6C
F05	433	445	199	177	90
F06	433	445	199	177	130
W01	375	375	212	212	90
W02	395	375	206	206	90

Figure 230. USB Flap and Wing Measurement Locations

CASE 11,F05,ST50 (STOL FLAPS=50)

ALT= 6500. FT	USB =50. DEG	R/RO = .848
VA = 110. FT/S	DOOR= CLOSED	THETAS= 5. DEG
VJ = 680. FT/S	VGS = UP	THETAP=33. DEG

RIBBON	STA	WL	BL(IN)	BL(OUT)
AT NOZ EX	345.	213.	61.	115.
AT WNG TE	425.	201.	57.	133.
AT TR OFF	431.	198.	57.	133.
AT TR EDG	460.	179.	57.	133.
TRAIL EDGE	450.	162.	57.	133.
FIELD POINT	445.	177.	90.	

FIELD POINT IN ZONE 3 AND IS
ABOVE,ON OR UNDER FLOW RIBBON
S= 109.9 DELTA = 10.0

PEAK JET MIX LEVEL= 137. DB AT 116. HZ
CORRECTION FOR VGS APPLIED
DSPL= 5. DB F1= 2190. HZ
PEAK NEAR NOZ LEVEL= 117. DB AT 938. HZ
STE= 122. ,DELTATE= 20.
PEAK TRAIL EDGE LEVEL= 103. DB AT 110. HZ
PEAK SEP LEVEL= 135. DB AT 33. HZ
PEAK TBL LEVEL= 90. DB AT 118. HZ

SPL-IN DB RE 200 PICOBAR (BY COMP AND SUM)

HZ	MIX	NN	TE	SEP	TBL	SUM
25.	131.	98.	90.	134.	88.	135.9
31.	132.	99.	92.	135.	88.	136.5
40.	133.	100.	95.	134.	89.	136.9
50.	135.	102.	98.	134.	89.	137.4
63.	136.	103.	100.	134.	89.	138.0
80.	137.	104.	102.	133.	90.	138.5
100.	137.	106.	103.	133.	90.	138.6
125.	137.	107.	103.	132.	90.	138.5
160.	137.	108.	102.	132.	90.	138.1
200.	136.	110.	100.	131.	89.	137.4
250.	135.	111.	97.	131.	89.	136.4
315.	134.	112.	95.	130.	89.	135.3
400.	132.	114.	92.	129.	88.	134.1
500.	131.	115.	89.	129.	88.	133.1
630.	131.	116.	87.	128.	87.	132.8
800.	131.	116.	84.	127.	87.	132.4
1000.	130.	117.	81.	126.	86.	132.0
1250.	130.	116.	79.	125.	85.	131.3
1600.	129.	115.	76.	125.	85.	130.4
2000.	128.	114.	73.	124.	84.	129.4
2500.	127.	113.	71.	123.	83.	128.3
3150.	125.	112.	68.	122.	82.	126.9
4000.	123.	110.	65.	121.	81.	125.4
5000.	121.	109.	63.	120.	81.	123.9
OASPL	147.2	126.0	110.6	144.5	101.5	149.1

Figure 231. Computer Prediction of Noise for QSRA Type STOL Airplane.

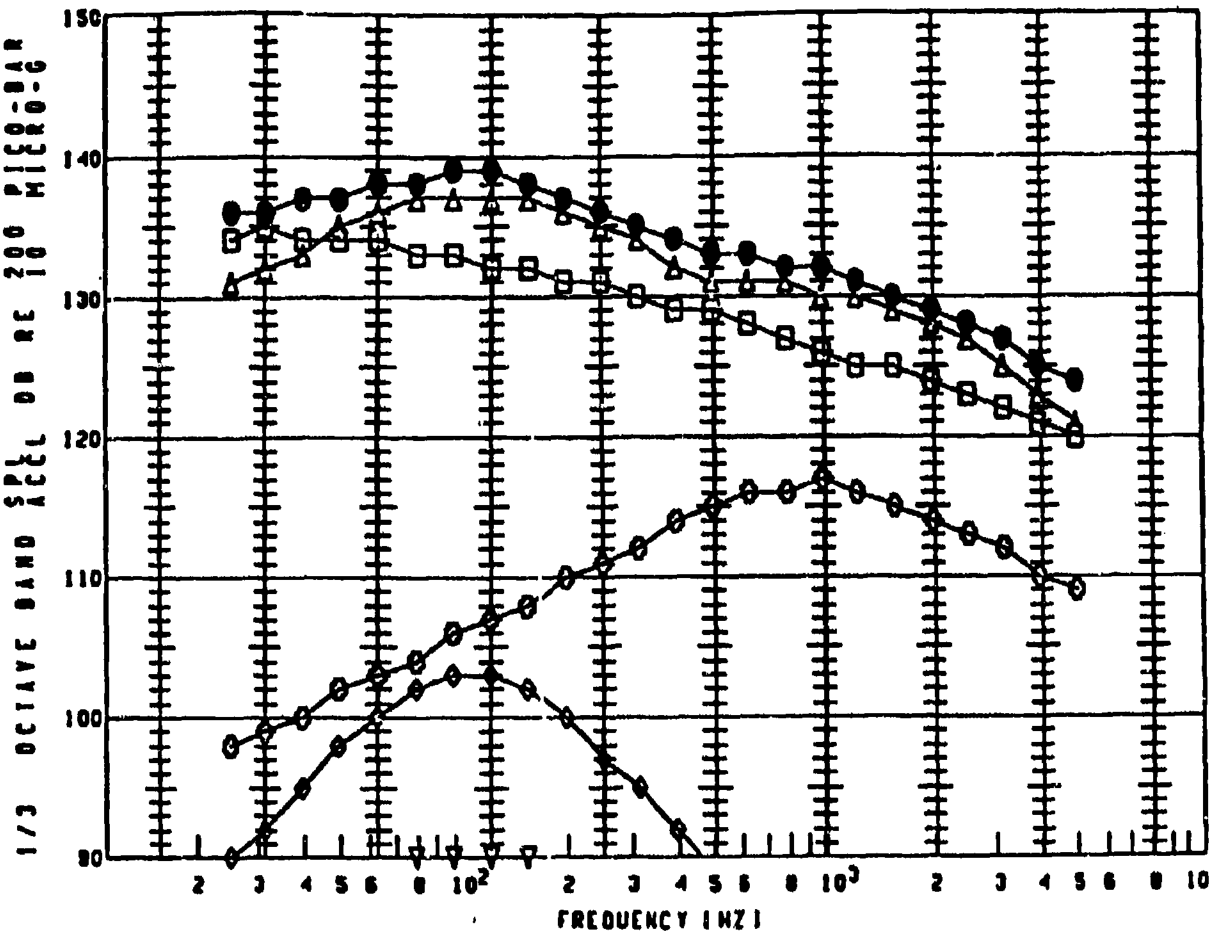

PLOT SYMBOL	X-DUCER NO.	COND. NO.	ALT. (FT)	SPEED (FPS)	N1 (RPM)	VMIX (FPS)	USBFA (DEG)	OVERALL (DB)
●	F05	ST50						149
▽	F05	ST50						102
⊡	F05	ST50						145
◊	F05	ST50						111
⊙	F05	ST50						126
△	F05	ST50						147

NOTES

●	PREDICTED TOTAL NOISE.CREATED	79/03/21.
▽	PREDICTED TBL NOISE	79/03/21.
⊡	PREDICTED SEP NOISE	79/03/21.
◊	PREDICTED EDGE NOISE	79/03/21.
⊙	PREDICTED NN NOISE	79/03/21.
△	PREDICTED MIXING NOISE	79/03/21.

Figure 232. Prediction for QSRA Type Airplane. USB=50 - Inboard Engine

FIELD POINT	BRAKE RELEASE		USB FLAPS = 50°	
	INBOARD	OUTBOARD	INBOARD	OUTBOARD
B01	158 dB	135 dB	149 dB	129 dB
B02	142	134	141	128
B03	137	132	131	126
B04	147	133	133	126
B05	145	132	148	125
B06	136	131	133	123
B07	137	130	125	121
B08	153	130	128	121
B09	137	129	142	121
F04	158	136	148	128
F05	158	139	149	132
F06	158	152	150	146
W01	150	137	142	128
W02	152	132	143	124
F01	—	—	150	127
F02	—	—	150	131
F03	—	—	150	142

Figure 233. Comparison of Field Point OASPL From Inboard and Outboard Engines

Table 514.2-II. Test Procedure and Time Schedule Chart for Equipment Installed in Propeller Airplanes - Equipment Category b.1

A. Procedure Selection and Time Schedule Chart

Equipment mounting configuration	Procedure number	Procedure part number	Applicable tests (see 4 for test procedures) Resonance search (4.5.1.1)	Resonance dwell (4.5.1.2)	Sinusoidal cycling (4.5.1.3)	Test time schedule (per axis) Dwell time at each resonance (4.5.1.2)	Sinusoidal cycling time	Sweep time 5-500-5 Hz	Sweep time 5-2000-5 Hz	Fig. 514.2-2 Curve 1/
Without vibration isolators	1	1	X	X	X	30 min	3 hrs less dwell time	15 min	20 min	C, D, E, F G, H, J, or L
With vibration isolators 2/	1	1	X	X	X	30 min	3 hrs less dwell time	15 min	20 min	C, D, E, F, G, J, H, or L
		2	X	X	X	10 min	30 min	15 min	20 min	B, AR
Normally with vibration isolators but tested without isolators	1	2	X	X	X	30 min	3 hrs less dwell time	15 min	20 min	B, AR

1/ For sinusoidal vibration resonance tests and cycling tests of item mounted in airplanes and weighing more than 80 pounds, the vibratory accelerations shall be reduced by 1g for each 20-pound increment of weight over 80 pounds. Acceleration derating shall apply only to the highest test level of the selected test curve, however, the vibratory acceleration shall in no case be less than 50 percent of the specified curve level.

2/ Test items of equipment normally provided with vibration isolators first shall be tested with the isolators in place (part 1). The isolators then shall be removed, and test item rigidly mounted and subjected to the test level indicated (part 2).

B. Curve Selection Chart for Category b.1 Equipment

Selection criteria	Fig. 514.2-2 Curve (for freq. to 500 Hz)	Fig. 514.2-2 Curve (for freq. to 2000 Hz for jet engines)
Equipment installed on vibration isolated panels or racks when the panel or rack is not available for test or when the equipment is tested with isolators removed as specified by the applicable procedure.	B	AR
Equipment in forward half of fuselage or equipment in wing areas of airplanes with engines at rear of fuselage.	C	J
Equipment in rear half of fuselage or equipment in wing areas of airplanes with wing or front mounted engines or other equipment of engine locations not specifically mentioned for other curves.	D	H
Equipment located in the engine compartments or engine pylons of airplanes.	E	G
Equipment mounted directly on airplane engines.	F	L

Figure 234. Mil-Std 810C Test Procedures

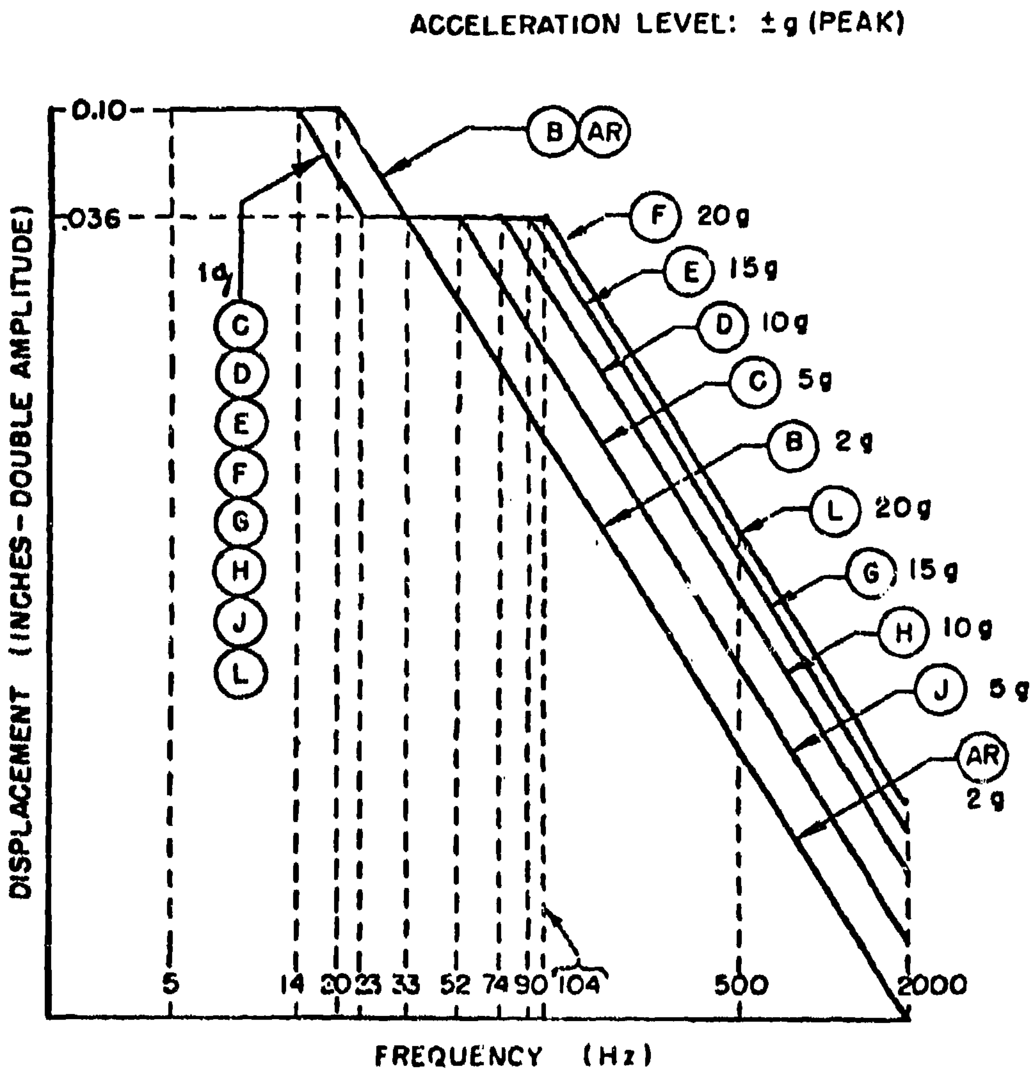

Figure 235. Mil-Std 810C Vibration Test Levels

Table 514.2-IIA. Random Vibration Test Criteria for Jet Aircraft Equipment, Category b.2

Criteria

Aerodynamic induced vibration (curve A, figure 514.2-2A)

Functional test level 1/, 5/ $W_o = K(q)^2$

Endurance test level 2/, 3/, 5/ $W_o = K(q)^2 \; (N/3T)^{1/4}$

Jet engine noise induced vibration (curve A, figure 514.2-2A)

Functional test level 1/, 3/, 4/, 7/, 5/ $W_o = (0.48 \cos^2\theta/R)[D_c(V_c/1850)^3 + D_f(V_f/1850)^3]$

Endurance test level 2/, 3/, 4/, 6/, 7/, 8/ $W_o = (0.48 \cos^2\theta/R)[D_c(V_c/1850)^3 + D_f(V_f/1850)^3] \; (N/10T)^{1/4}$

Gunblast induced vibration (see method 519)

Definitions

$K = 2.7 \times 10^{-8}$ for cockpit equipment and equipment attached to structure in compartments adjacent to external surfaces that are smooth, free from discontinuities.

$K = 14 \times 10^{-8}$ for equipment attached to structure in compartments adjacent to or immediately aft of external surfaces having discontinuities (cavities, chins, blade antennas, speed brakes, etc.) and equipments in wings, pylons, stabilizers, and fuselage aft of trailing edge wing root.

q = 1200 psf or maximum aircraft q, whichever is less.

N = maximum number of anticipated service missions for equipment or carrying aircraft ($N \geq 3$).

T = test time per axis, hours ($T \geq 1$).

D_c = engine core exhaust diameter, feet (for engines without fans, use maximum exhaust diameter).

D_f = engine fan exhaust diameter, feet.

R = minimum distance between center of engine aft exhaust plane and the center of gravity of installed equipment, feet.

V_c = engine core exhaust velocity, feet per sec (for engines without fans, use maximum exhaust velocity without afterburner).

V_f = engine fan exhaust velocity, feet per sec.

θ = angle between R line and engine exhaust axis, degrees, aft vectored.

Notes

1. Functional test time shall be 1 hour per axis.
2. Use $W_o = 0.04 \; g^2/Hz$ if calculated endurance test level values are less than 0.04 g2/Hz, T = 1.
3. If one hour (T = 1) endurance test level is $\leq$ functional test level, no endurance test is required except according to Note 2.
4. If aircraft has more than one engine, W_o shall be the sum of the individually computed values for each engine.
5. For equipment weighing more than 30 pounds, the vibration W_o level may be reduced according to Curve B, Figure 514.2-2A.
6. For $70° < \theta \leq 180°$, use $\theta = 70°$ to compute W_o.
7. For engines with afterburners use W_o which is 4 times larger than W_o computed using maximum V_c and V_f without afterburner.

Figure 236. Mil-Std 810C Random Test Level Calculation

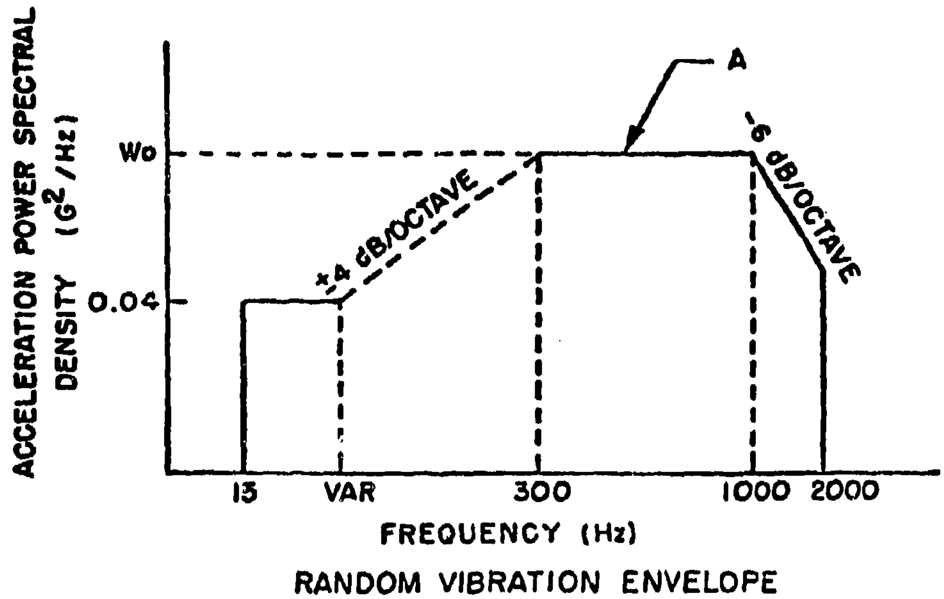

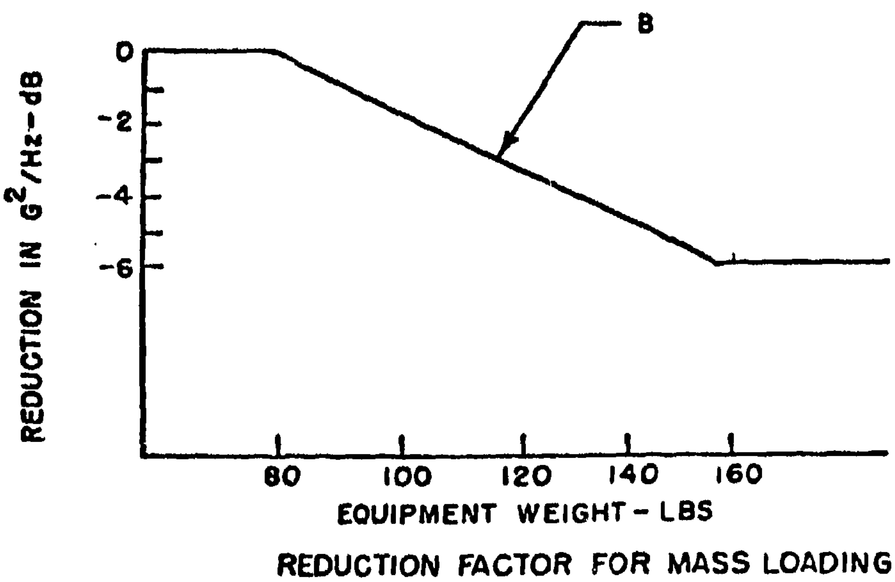

Figure 237. Mil-Std 810C Random Test Levels

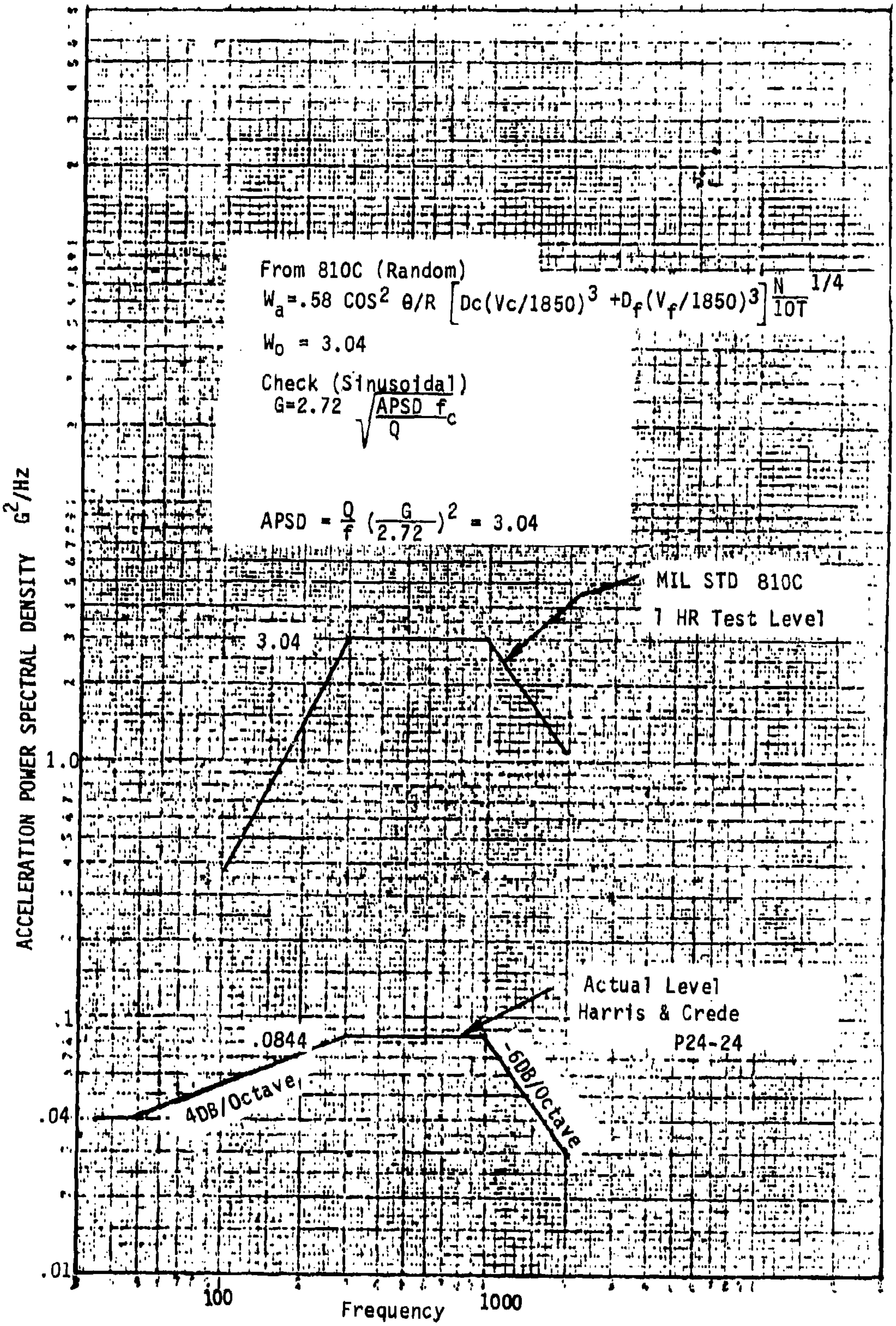

Figure 238. MIL-STD 810C Environmental Vibration Levels

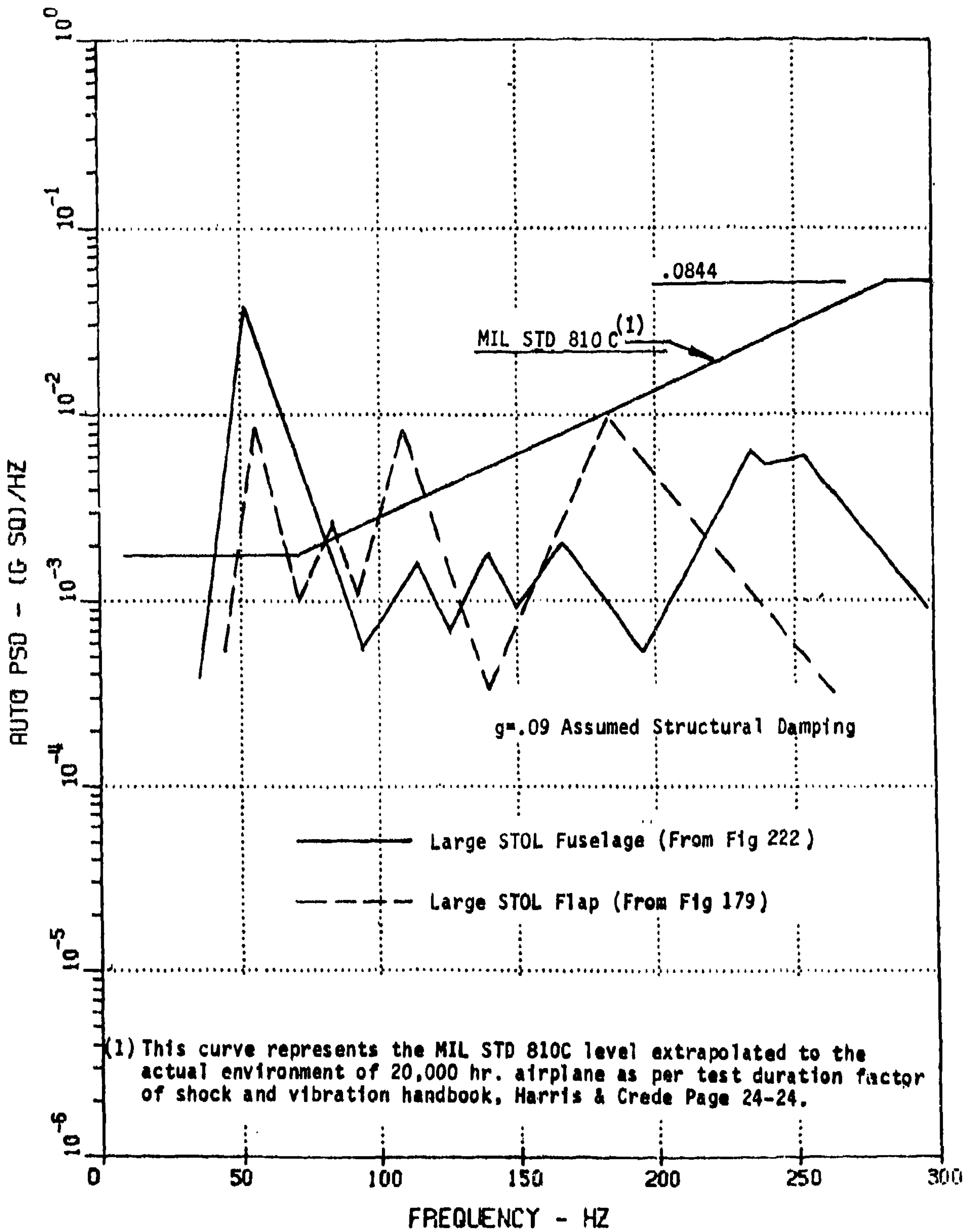

Figure 239. Comparison of Large STOL Response to Predicted MIL-STD 810C Environmental Vibration Levels

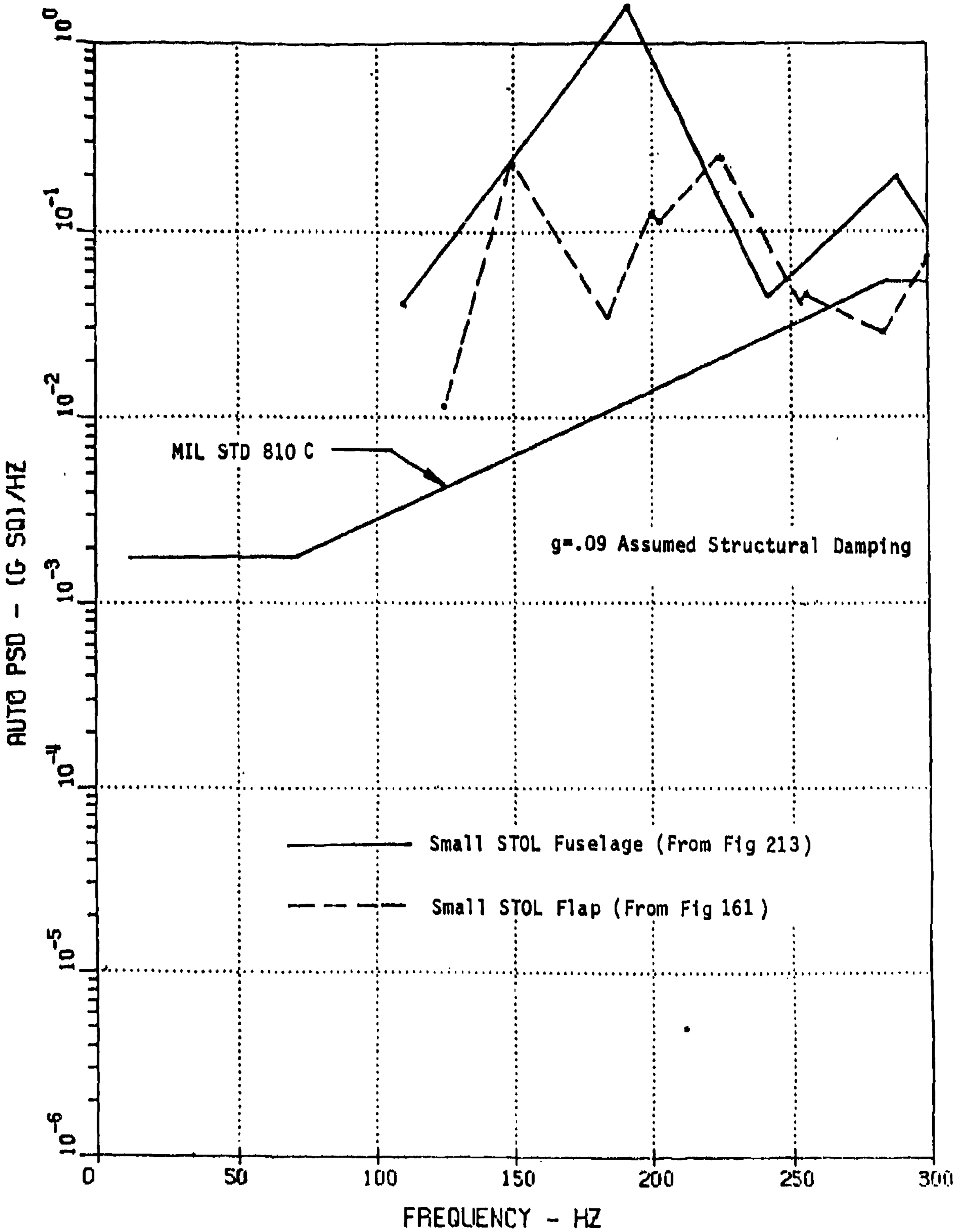

Figure 240. Comparison of Small STOL Response to Predicted MIL-STD 810C Environmental Vibration Levels

☆U.S.Government Printing Office: 1980 — 657-084/782